UNIVERSITÀ DEGLI STUDI DI PALERMO

PhD Course in Chemical, Environmental, Biomedical, Hydraulic and Materials Engineering
Dipartimento di Ingegneria
Settore Scientifico Disciplinare (ICAR/03)

Innovative solar greenhouses for sewage sludge drying: study of the application at prototype and open field scale

PhD Candidate:
Ing. Alice Sorrenti

Phd Course Coordinator:
Prof. Ing. Giorgio Domenico Maria Micale

Supervisors:
Prof. Ing. Michele Torregrossa

Co-Supervisors:
Prof. Ing. Santo Fabio Corsino

XXXVII CYCLE
GRADUATION YEAR 2025

Programma Operativo Nazionale Ricerca e Innovazione 2014-2020 (CCI2014IT16M2OP005), risorse FSE REACT-EU, Azione IV.4 "Dottorati e contratti di ricerca su tematiche dell'innovazione" e Azione IV.5 "Dottorati su tematiche Green"

Index

Index of Figures

Index of Table

Acronyms

Dry solids	**DS**
Dry matters	**DM**
Total solids	**TS**
Volatil solids	**VS**
Total Suspended Solid	**TSS**
Sludge volume index	**SVI**
Lower Calorific Value	**LCV**
Higher Calorific Value	**HCV**
Differential Thermal Analysis	**DTA**
Extracellular Polymeric Substances	**EPS**
Moisture Ratio	**MR**
Indirect Drying	**ISD**
Solar thermal Drying plant	**STDP**
Greenhouse Gas	**GHG**
Wastewater treatment plant	**WWTP**
Fiel Water Capacity	**FWC**
Humidity	**U**
Net Present Value	**NPV**
Actual Cash Flow	**ACF**
Global Warming Potential	**GWP**

1 Summary

Within wastewater treatment plants, the treatment of wastewater takes place. These processes yield treated effluent that will be released into the environment and sewage sludge. Proper management of the latter, in accordance with the principles of the circular economy, is essential for achieving environmental sustainability goals In recent years, the continuous growth of the urban population, the improvement of the quality of human life and the development of agriculture and industry have made the topic of sludge treatment and disposal the subject of considerable and growing interest. Today it represents one of the major critical issues in the wastewater treatment cycle and is assuming growing importance at both a national and international level.

According to Ispra data, in 2023 (ISPRA, 2023) Italy produced approximately 3.4 million tons of sludge deriving from the treatment of urban wastewater, with a growth of 10 % in recent years, which suggests that the figure has now exceeded 4 million of tons per year. The purification activities have generated over 3.23 million tons of sludge, with a rather stable trend in recent years: the over 18 thousand urban wastewater purification plants are not sufficient to satisfy the needs of the entire population, and still today 1.6 million citizens live in areas without a purification plant. According to ISPRA, Lombardy is the region with the largest quantity produced, over 487 thousand tons (16 % of the sludge produced in Italy), followed by Emilia-Romagna with 372 thousand tons (11.4%).

In per capita terms, however, the region with the highest quantity of sludge produced is Trentino-Alto Adige (63 kg/equivalent inhabitant).

In terms of management, the tons of sludge resulting from urban wastewater treatment managed in 2021 were just over 2.9 million. As a management method, disposal (52.3 % of managed) prevails over recovery (45.6 %), demonstrating that there is ample space for the valorisation of sewage sludge. Furthermore, every year more than 1.6 million tons of sludge are disposed of which could instead be sent for treatment for the recovery of material or energy.

The doctoral research was, therefore, aimed at the development of efficient drying systems to carry out a dehydration phase aimed at increasing the dry content and reducing the quantity of water present in the sludge leaving the plants with a consequent reduction in the costs of transport and disposal.

The problem of sludge disposal is one of the most critical issues in the wastewater treatment cycle and is becoming increasingly important in many countries. In fact, the cost of treatment and disposal varies from 100 to 400 euros per ton, and this value is expected to grow soon mainly due to the growth of urban population and the intensification of treatment due to the increase of environmental quality standards (Bao et al., 2024). In sewage treatment plants, much of the energy demand is consumed in the sludge dewatering process, which requires a large amount of energy, accounting for about 30-35% of the total operating costs. Therefore, efficient drying systems need to be developed to increase the dry content and reduce the amount of water in the sludge, thereby decreasing transportation and disposal costs.

In the past two decades, numerous studies have focused on developing techniques and exploring the mechanisms of various sludge dewatering processes (Bao et al., 2024).
As can be seen in the Figure 1.1, there has indeed been an exponential increase in studies related to the issues of sludge dewatering.

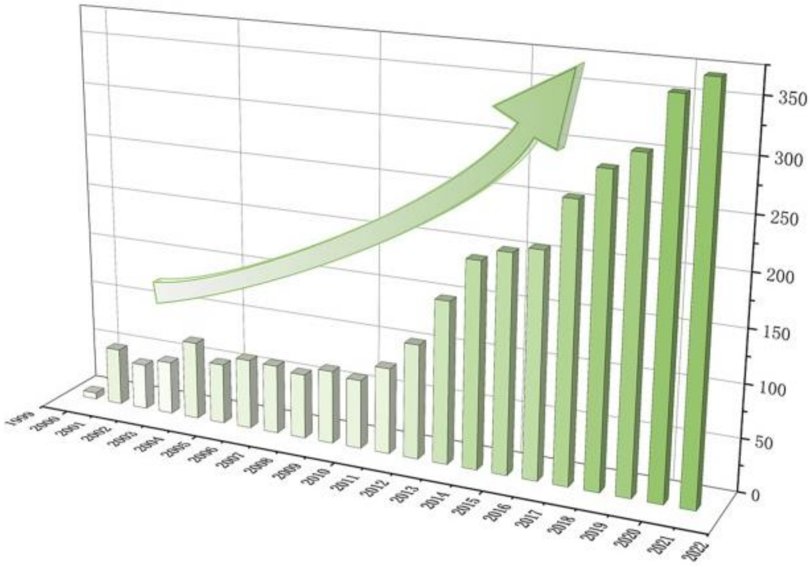

Figure 1.1 - Research on sludge dehydration (adapted from Bao et al., 2024)

A key issue in the operation of wastewater treatment plants is sludge management. Mechanical dewatering is a crucial step in reducing sludge disposal volumes and costs.
However, because it is a delicate process and dependent on many factors, such as the type of biologic treatment, stabilization method and conditioning operation, the choice of the most suitable dewatering technology is always complex. In fact, the characteristics of the sludge greatly influence the dewatering efficiency, in terms of final dry solids content (DS), and it is often unclear what the discriminating parameters are when choosing which machine to install.
In addition, models that exploit the principle of electro dehumidification, which are already available in the market, are presented, and, finally, some dewatering methods with a low level of technology, but which need large available areas, such as drying beds, solar drying, tubular geofilters, lagoons, and reed beds. To better understand dewatering technologies, the characteristics of the sludge that mag-most affect the dewatering stage are given.
The objective was to design and implement several solar greenhouse prototypes to achieve greater sludge drying powered by panels to produce hot air. The innovation of the research lies in the delivery of hot air directly under the sludge layer. In particular, the air is heated by a solar panel and inserted under the sludge layer. These are therefore prototypes that exploit green and renewable energies, allowing not only to obtain environmental benefits in terms of reducing the quantity of

sludge sent for disposal, but also to exploit a totally free source of energy with almost no environmental impact. Thanks to the configurations adopted, various advantages will be obtained such as: obtain the maximum evaporation rate, optimize the conversion of solar energy into thermal energy, control ventilation to manage the relative humidity of the air inside the greenhouse and obtain particularly dried sludge. The first step of the study was to investigate both the effect of the thickness of the sludge and the drying kinetics of the sludge subjected to blowing compressed air into the drainage layer and to a specific air flow through the design and construction of a benchtop system, consisting of five cylindrical PVC units. This benchtop system allowed essential tests to be carried out for the selection of the optimal solution and the definition of the operating variables. The next phase of the research focused on the creation and configuration of solar greenhouse prototypes that work differently.

Finally, the results of the different tests were used to define the optimal values of the sizing parameters for this type of systems. At the Caltanissetta wastewater treatment plant (Caltaqua) a drying bed was set up as a solar greenhouse to carry out full-scale demonstration tests.

Therefore, the objective of this thesis was to define the design criteria for a new type of solar greenhouse, using the results obtained from various configurations of prototype greenhouses in order to achieve the highest possible drying of the sludge. These new types of solar greenhouses are connected to solar panels to produce hot air. Thus, these are prototypes that takes advantage of green and renewable energies, allowing not only a significant environmental benefit in terms of sludge reduction, but also the exploitation of a totally free source of energy with a very low environmental impact.

The energy and environmental benefits from the reduction in water content that will be found will be:

- Drying treatment of not dewatered sludge, with possibility to treat sludge just thickened.
- Reduction of the weight of the sludge quantity in the range of 3 to 4 times with consequent reduction of impacts from sludge transportation.
- Possibility of sludge storage before final disposal.
- Use of renewable energy (solar radiation).
- Process with low carbon footprint.
- Structural system easily integrated into the surrounding environment in relation to its greenhouse configuration.
- Effective Odor control.
- Sanitization of sludge: the sanitization process, carried out at high temperature thanks to solar radiation, ensures the destruction of pathogens and a strong reduction in moisture content, excluding the potential subsequent occurrence of putrefactive phenomena. Sanitized sludge can have several uses, including reuse to produce quality compost.
- Sludge stabilization: the stabilization of sludge allows for the reduction of volatile solids content within it, thereby reducing the potential for putrefaction of the sludge, making them easier to manage, transport, and dispose of.

Thanksgivings

2 Sludge management and environmental regulations: Approaches, Regulations, and Sustainability

2.1 Introduction

Both in the domestic and industrial fields, wastewater purification processes almost always involve the production of sludge made up of concentrated suspensions of the materials removed during treatments. In fact, it is rare to find the case in which purification can be achieved by gasification of pollutants or by their dissolution into a form compatible with correct disposal. Generally, the treatment can be seen as a concentration in the sludge of substances initially dispersed in suspended and dissolved form and removed with processes that end with a sedimentation phase or with another solid-liquid separation process such as flotation, filtration and centrifugation. This is one of the reasons that makes sludge treatment delicate: being the result of a concentration process, the sludge contains large amounts part of the substances responsible for the pollution of the sewage influent to the plant; if not treated and disposed of correctly it can therefore give rise to new pollution phenomena. The quality and quantity of sludge produced in a water treatment plant depends on the treatment units present in the plant's supply chain. The main sources of sludge production are primary sedimentation, biological treatment and tertiary treatments (filtration or sedimentation) in which chemical precipitation is often carried out.
Sewage sludge is an organic by-product of global wastewater treatment (Sackey et al., 2023). With global development and population growth, waste, and sewage production increases year after year. Figure 2.1 shows a complete schematic of the system.

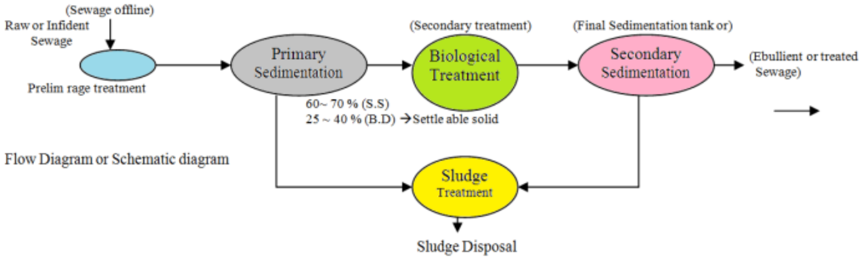

Figure 2.1 - Basic flow diagram for conventional wastewater treatment plant

The sludge resulting from purification processes has a water content between 95 % and 99.5 %. Primary sludge is that which derives from a physical sedimentation treatment (primary sedimentation), while secondary sludge is that which derives from the biological sedimentation treatment applied to the mixture of purified water and activated sludge (secondary sedimentation).
Primary sludge has the following characteristics: inert inorganic substances (sand, carbonates, metal oxides); organic substances that are difficult to degrade (fibres, seeds, and gums); organic substances (carbohydrates, proteins, fats), biologically unstable and easily attacked by anaerobic microorganisms with the production of

smelly gases. They are highly putrescible, a source of unpleasant Odor, thickened and dehydratable and contain a percentage of solids equal to 3 – 4 %. Secondary sludge, on the other hand, has a flaky consistency and low Odor. They consist predominantly of microorganisms and cellular debris. They also have biological activity, are more difficult to dehydrate and contain a percentage of solids equal to 1 %. The main treatment processes of the sludge line are:

- thickening: thickening by gravity, thickening by flotation and dynamic thickening by centrifugation or filtration.
- stabilization: stabilization by anaerobic digestion, stabilization by aerobic digestion, stabilization with lime and composting.
- dehydration: with centrifuge or with belt press or with filter press and in medium-small wwtps and in emergency, with drying beds;
- thermal drying at high temperature: with direct or indirect dryer;
- thermal drying at low temperature: with solar greenhouses.

Thickening, dehydration, and thermal drying are separation processes, i.e. processes which have the aim of removing part of the liquid phase from the solid phase of the sludge. On the other hand, stabilization by digestion, conditioning and lime stabilization are conversion processes, i.e. which have the aim of determining changes to the characteristics of the sludge to facilitate subsequent final recovery treatments.

Both primary and secondary sludge can contain pathogenic microorganisms and sludge be managed and disposed of without causing inconvenience or damage to operators.

In the overall, sludge treatment are aimed to obtain:

- break down pathogenic bacteria;
- reduce the concentration of biodegradable organic matter;
- remove most of the water present;

2.2 The issues in sewage sludge management

A fundamental problem in the operation of wastewater treatment plants is the efficient and environmentally friendly management of sludge (Cintoli et al., 2017). The crucial phase for reducing the volumes and costs of sludge disposal is the dehydration phase (Iswa et al., 1997).

The disposal of this by-product of the purification process is one of the main problems in terms of plant management and one of the most expensive cost items (in some cases the disposal cost can be equal to 50% of the total operating costs).

The choice of the most suitable dehydration technique appears increasingly complex as it depends on various factors such as: the type of biological treatment, the stabilization method, and the conditioning operation. Therefore, the choice of the most suitable treatment cycle must be made based on the type of wastewater line treatment, the characteristics of the sludge, different for each wwtps, the limits of acceptability and the environmental conditions, and requires a preliminary examination of the alternatives for final disposal.

The increase in sludge production, regulations on waste management (management priorities) and limitations on the disposal of organic waste recoverable in landfill, as well as economic evaluations lead to considering with greater attention

the possibilities of reuse/recovery of sludge. This increase is mainly due to the significant increase in connections/discharges to public sewers and the greater efficiency of wastewater treatment plants. Faced with this situation, the importance of correct management of the sludge to be treated and for which finding a destination, possibly aimed at the recovery of resources, which reduces its environmental impact is evident. Equally important is the search for the optimization of existing technologies. In the case of smaller plants, where soil availability is generally not a problem, drying beds or lagoons are still used today.
On the contrary, for larger plants or those located on sites where space is limited, mechanical dewatering unit (filter presses, centrifuges or belt presses) are installed. Different solutions at European level are available for the end use of sludge, such as landfill disposal, agricultural use, composting, or thermal drying (Figure 2.2).

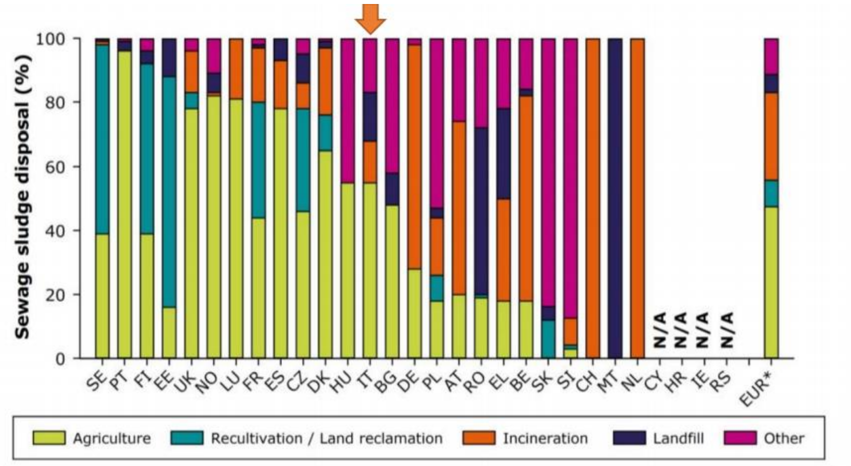

Figure 2.2 - Destination of the sludge in different countries (adapted from Cintoli et al., 2017)

For decades, sludge has been used as fertilizer in agriculture, depending on whether its composition is suitable or not. Otherwise, they are sent to landfill as solid waste. The advantage of drying the sludge is that not only is the mass reduced, but the calorific value increases. By comparing the calorific value of dried sewage sludge with that of other energy resources, it is demonstrated that dried sewage sludge can be an interesting energy alternative (Figure 2.3). This means that sewage sludge, once dried to 90 % DS, is not waste, but an interesting alternative energy. Solar drying, particular drying solution alternative to high temperature thermal processes, allows the sludge to be dehydrated by solar radiation in specially designed greenhouses, obtaining final DM (Dry Matters) contents of approximately 85% (Figure 2.4). This process is an eco-friendly and environmentally friendly solution (Osvaldo Garanto, 2016).

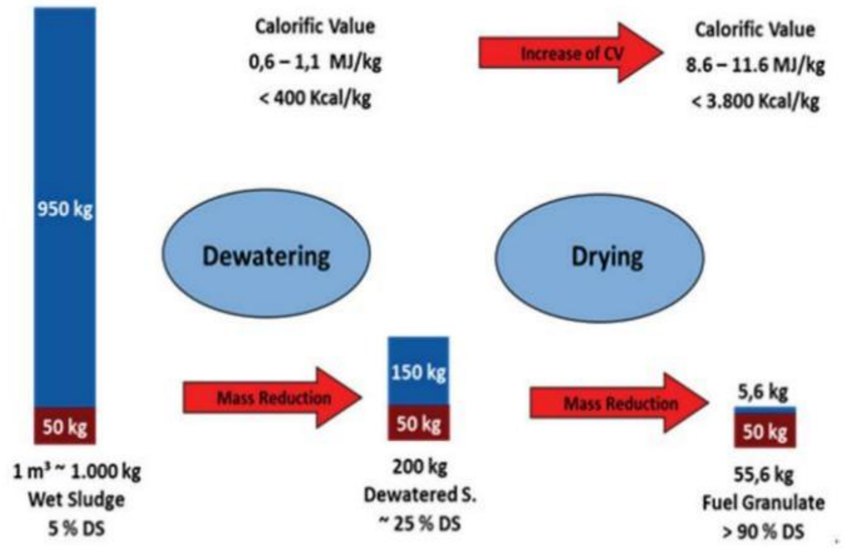

Figure 2.3 - Mass reduction and increase in calorific value (adapted from Osvaldo Garanto, 2016)

Figure 2.4 - Solar sludge drying system (adapted from Osvaldo Garanto, 2016)

2.3 The regulatory environment in sludge management

The fundamental principle on which all the regulations regarding sewage sludge should be based is set out in art. 127 of Legislative Decree 152/06 (sludge deriving from wastewater treatment).

"1. Without prejudice to the provisions of Legislative Decree 27 January 1992, n. 99, the sludge deriving from wastewater treatment (Legislative Decree 152/06, part III, art. 74: domestic wastewater, industrial wastewater, urban wastewater) are subject to waste regulation (Legislative Decree 152 /06, part IV), where applicable (and at the end of the overall treatment process carried out in the purification plant). The sludge must be reused as often as possible reuse is appropriate.
2. The disposal of sludge in fresh and brackish surface waters is prohibited."

The management of sewage sludge is a central element for closing the entire water cycle, both from an environmental and economic point of view. A sustainable approach involves multiple sectors (water, waste management, agriculture, energy) and aims to transform sludge management from a cost to an opportunity in a circular economy perspective(Marangoni Alessandro, 2021).

Through technological development and the improvement of management and planning, adequate solutions produce multiple benefits, allowing the supply chain to reach a balance with the territories served. To obtain these results, however, a clear and stable regulatory framework is needed, predictable authorization procedures and an integrated water-waste-agriculture vision capable of defining a medium-long term national strategy. The closing phase of the water cycle is, in fact, strictly linked to the structure and operating methods of the entire sector and cannot be considered an independent or stand-alone activity. At the origin there are a series of factors that affect the entire cycle and management of the sludge. The sector is still fragmented, with ATO agreements still unfinished, complex governance influenced by local public administrations often reluctant to make choices that could be contested, and which require huge infrastructure investments.

2.3.1 European Framework

Since 2010, the EU-27 countries have been estimated to produce between 6 and 9 million tonnes of dry sewage sludge each year. In comparison, the average annual sewage sludge production in the EU, the USA, and China ranges from 18 to 33 million tonnes. The Sewage Sludge Directive (86/278/EEC) is the main EU regulation governing sewage sludge recovery for agricultural use, setting limits on heavy metal concentrations and operational conditions. Complementary directives, including the Water Framework Directive (2000/60/EC), Landfill Directive (1999/31/EC) and Waste Framework Directive (2008/98/EC), provide additional definitions and rules for water and waste management. The Waste Framework Directive also establishes a waste hierarchy that emphasizes environmentally sustainable circular economy strategies. Overall, EU legislation primarily targets agricultural use of sewage sludge while promoting alternative valorisation methods through stricter renewable energy and landfill regulations (Figure 2.5) (Neri et al., 2024).

Directive	Reference	Main contributions to sewage sludge management
Sewage Sludge Directive	86/278/EEC	The use of sewage sludge in agriculture is encouraged. Sludge must be treated before use, but Member States may authorise the use of untreated sludge if it is injected or incorporated into the soil. The Directive sets limit values for heavy metals in soil and important operational conditions for its use.
Urban Wastewater Treatment Directive	91/271/EEC	The Directive requires collection and primary, secondary and more stringent treatment for agglomerations depending on their size. Sludge from wastewater treatments must be reused where appropriate.
Landfill Directive	1999/31/EC	The Directive bans the landfilling of liquid and untreated waste and sets restrictions and targets for biodegradable and solid waste (including sewage sludge) that is landfilled. The amendment 2018/850 imposes further restrictions on the landfilling of biodegradable waste.
Waste Framework Directive	2008/98/EC	The Directive defines the concept of the waste hierarchy: prevention, reuse, recycling and energy recovery. It allows the transport of waste for incineration between European countries.
Renewable Energy Directive	2009/28/EC	The Directive sets targets for the amount of energy to be produced from renewable sources, including biogas and sewage sludge.
Fertilisers Regulation	2003/2003/EC; 2009/1009/EC	The Directive regulates the characteristics of the market for organic carbon products used as fertilisers or soil improvers.

Figure 2.5 - Overview of the main EU regulations related to sewage sludge management (adapted from Neri et al., 2024)

2.3.2 National Framework

In 2022, the quantities of sludge produced from the treatment of urban wastewater (EER Code 190805) across the national territory amounted to nearly 3.2 million tons. Lombardy and Veneto are the leading regions, producing almost 542,000 and

405,000 tons respectively, which corresponds to 16.9 % and 12.7 % of the national total. Emilia-Romagna follows with approximately 373,000 tons, or 11.4% of the national total.
Compared to 2021, national production shows a decrease of just over 40,000 tons (1.3 %), primarily due to a decline observed in the Central-Southern regions (Figure 2.6), which follows a reduction of over 150,000 tons (4.5 %) noted between 2020 and 2021 (ISPRA, 2024).

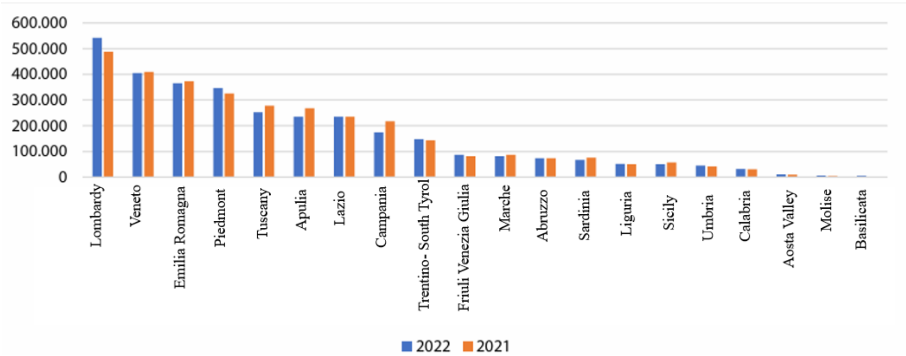

Figure 2.6 - Quantity of sludge produced by urban wastewater treatment by region, years 2022-2021 (adapted from ISPRA, 2024)

Among the disposal operations, "Biological Treatment" (D8) is the most prevalent, accounting for just over 1 million tons, which is 39.0 % of the total managed and 72.0 % of the total sent for disposal. This is followed by "Physical-Chemical Treatment" (D9), which, with over 230,000 tons, represents 7.7 % of the total managed and 14.3 % of the total disposed of. Incineration (D10) accounts for nearly 145,000 tons, or 4.9 % of the total managed and 9.0% of the total sent for disposal. This figure includes the quantities of special waste treated in dedicated energy recovery incineration plants, primarily for urban waste and classified as R1 under Annex II of Directive 2008/98/EC. Landfilling (D1) involves over 63,000 tons, which is 2.1 % of the total managed and 3.9 % of the total sent for disposal.
Regarding recovery, the predominant operation is "Recycling/Recovery of Other Organic Substances" (R3), which involves more than 939,000 tons; this operation accounts for 31.5% of the total managed and 72.6 % of the total recovered. Following this, "Waste Exchange for Operations R1-R11" (R12) includes nearly 236,000 tons, representing 7.9 % of the total managed and 18.2 % of the total waste recovered. "Energy Recovery" (R1) involves over 20,000 tons, or 0.7 % of the total managed and 1.6 % of the total recovered, while the quantity sent for "Land Treatment for Agricultural or Ecological Benefit" (R10) amounts to over 85,000 tons, which is 2.9 % of the total managed and 6.6% of the total sent for recovery.
Finally, as of December 31, 2022, nearly 71,000 tons of sludge remained stored in "Reserve" (R13), "Preliminary Storage" (D15), and at the producers, representing

2.4 % of the total managed. Figure 2.7 summarizes all forms of management used in 2022 for EER Code 190805 (ISPRA, 2024).

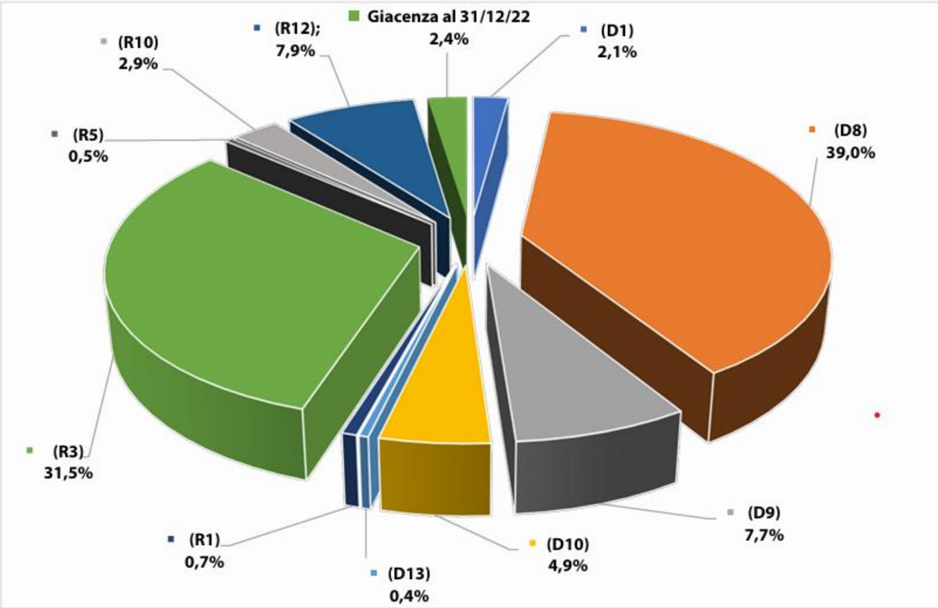

Figure 2.7 - Percentage of management methods for sludge produced from urban wastewater treatment relative to the total managed (EER Code 190805), year 2022 (adapted from ISPRA, 2024)

The difficulties in managing and valorising sludge also depend on rather complex and detailed legislation: at the centre is the Legislative Decree. 152/2006 Consolidated Environmental Law, according to which, if the sludge remains inside the purification plant, water regulations apply, while once they leave it, waste regulations apply. This decree aims to harmonize Italian environmental legislation with European directives and establishes the fundamental principles for the management of industrial wastewater. The Consolidated Law on the Environment establishes detailed requirements for the treatment of industrial wastewater, including emission limits for specific pollutants, authorization procedures and control measures. The use of sludge in agriculture (only from civil or similar wastewater) is still regulated by Legislative Decree. n. 99/92. Furthermore, the sludge must still be "treated" before being used. Regulatory uncertainty, aggravated by the interventions of the judiciary and some Regions, has thrown the system into crisis, resulting in a decline in sludge in agriculture in 2017, creating difficulties for purifiers and causing an increase in costs. And the possible alternative solutions have also been limited: few Waste to Energy plants for sludge, limited use in cement factories and strong restrictions on landfill disposal. The entire supply chain thus had to look for he more expensive destinations, with consequences both for the managers of the treatment-recovery plants and for the agricultural companies, which were no longer able to use the fertilizer.

2.3.3 Regional Framework

"In Sicily we are experiencing, as often happens in other fields, a profound delay with respect to a correct and effective purification of wastewater which, however,

has now been started and accelerated by the EU infringement procedures against Sicily, producing a significant increase in sludge. to be disposed of. The interest of purification plant managers in applying reliable technological solutions that allow the production of excess sludge to be minimized is therefore obvious". The Sicilian legislation for the treatment of industrial water is largely aligned with national laws and European directives. For example, the European Union's Water Framework Directive (2000/60/EC) provides a general framework for water management and establishes environmental objectives. This directive was implemented at regional level through Legislative Decree no. 152/2006 which also regulates the management of industrial wastewater in Sicily and is known as the "Consolidated Law on the Environment". This decree aims to harmonize Italian environmental legislation with European directives and establishes the fundamental principles for the management of industrial wastewater. The Consolidated Law on the Environment establishes detailed requirements for the treatment of industrial wastewater, including emission limits for specific pollutants, authorization procedures and control measures. As stated in the Special Waste Report, 2024 quantity with EER code 190805, in the year 2021, 49.738 tons. The total for the South is 636.945 tons (ISPRA, 2024).

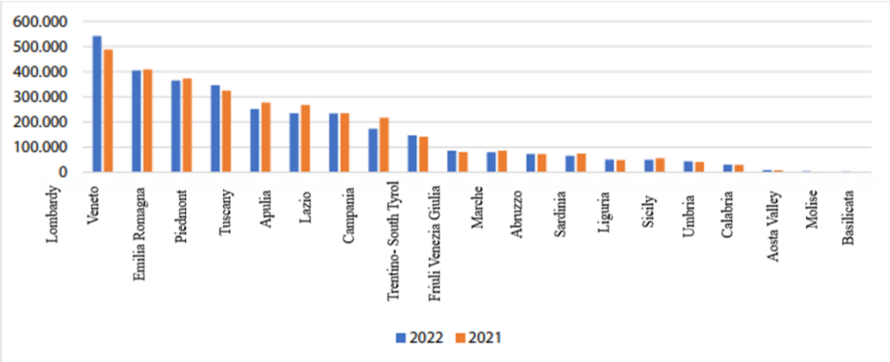

Figure 2.8 - Production of sewage sludge for the Italian regions (adapted from ISPRA, 2024)

The operations for the management of sludge produced from the treatment of urban wastewater by region (EER 190805) in tons, year 2022 in Sicily are: D1:6003 t, D8: 2162 t, D9: 988 t,D10*:193 t,D13: 370 t,R3:121124 t, R13/D15: 326 and total is 130 973 t (Figure 2.9) (ISPRA, 2024).

REGIONE	D1	D8	D9	D10*	D13	D14	R1	R3	R5	R10	R12	R13/D15 al 31/12/22	Totale 2022
Piemonte	17	164.940	10.365	12.923	409	30	167	50.820	0	0	0	4.014	243.685
Valle d'Aosta	0	1.171	3.389	0	0	0	0	0	0	0	0	0	4.560
Lombardia	4.321	109.712	22.136	102.755	759	189	15.319	405.026	111	0	183.970	14.027	858.325
Trentino-Alto Adige	76	33.814	23.745	0	0	0	4.719	0	435	0	15.532	67	78.388
Veneto	1.805	144.483	15.723	1.888	2.404	458	0	95.040	0	4.631	25.848	23.682	315.962
Friuli-Venezia Giulia	2.070	43.506	101	0	0	0	0	655	0	10.103	3.485	35	59.955
Liguria	4.829	6.230	6.782	0	0	0	0	0	0	0	0	60	17.901
Emilia-Romagna	3.092	245.560	26.423	11.319	0	0	0	125.607	0	0	868	23.623	436.492
Nord	**16.210**	**749.416**	**108.664**	**128.885**	**3.572**	**677**	**20.205**	**677.148**	**546**	**14.734**	**229.703**	**65.508**	**2.015.268**
Toscana	558	119.415	25.720	15.715	8.479	0	0	34.177	0	7.759	328	540	212.691
Umbria	13	21.028	155	0	0	0	0	11.936	0	0	0	76	33.208
Marche	18.042	30.275	9.163	0	11	0	0	11.700	0	0	4	51	69.246
Lazio	0	140.509	10.591	0	414	1	0	28.435	0	0	18	51	180.019
Centro	**18.613**	**311.227**	**45.629**	**15.715**	**8.904**	**1**	**0**	**86.248**	**0**	**7.759**	**350**	**718**	**495.164**
Abruzzo	0	20.922	892	0	19	0	0	7.192	0	0	0	1.360	30.385
Molise	1.623	9.235	0	0	0	0	0	950	0	0	0	68	11.876
Campania	0	1.631	2.201	0	64	0	0	16.848	13.090	19.702	7	1.948	55.491
Puglia	16.846	56.482	71.916	0	100	27	0	15.712	0	0	88	108	161.279
Basilicata	0	0	0	0	0	0	0	375	0	0	0	39	414
Calabria	0	390	313	22	0	0	0	13.443	0	0	181	591	14.940
Sicilia	6.003	2.162	988	370	0	0	0	121.124	0	0	0	326	130.973
Sardegna	4.229	10.644	0	0	0	0	0	243	0	43.329	5.666	322	64.433
SUD	**28.701**	**101.466**	**76.310**	**392**	**183**	**27**	**0**	**175.887**	**13.090**	**63.031**	**5.942**	**4.762**	**469.791**
TOTALE	**63.524**	**1.162.109**	**230.603**	**144.992**	**12.659**	**705**	**20.205**	**939.283**	**13.636**	**85.524**	**235.995**	**70.988**	**2.980.223**

Figure 2.9 - Operations for the management of sludge produced from the treatment of urban wastewater by region (EER 190805) in tons, year 2022 (adapted from ISPRA, 2024).

2.3.4 On roadmap a 2030

The foreseeable evolution of sludge management will be driven by a series of opposing factors: on the one hand technological innovations, which will tend to reduce production; on the other, more thorough purification and sewerage-purification adaptation, which will compensate for the reductions. The 2030 scenario estimates production of 4.2 million tons, with a decline in landfill, stability in direct agricultural uses with increasingly higher quality sludge and significant increases in incineration. Hence the need to provide a long-term strategy that goes beyond the management of periodic emergencies and to be implemented through a roadmap to 2030. This must provide a clearer and more stable framework of rules for use in agriculture, capable of balancing the needs of water managers and treatment companies with environmental and health protection. At the centre of the strategy there must be the improvement of the quality of the sludge, a fundamental aspect for its agricultural outlet; an integrated water-waste-agriculture vision to aim for a controlled supply chain and allow the safe use of sludge. It is fundamental to create a network of stakeholders that must include producers, operators, users,

and agricultural processing companies, also in view of quality brands. Likewise, the establishment of a permanent coordination table between national and territorial institutions is necessary.
We will then need more options for the destinations of the sludge, which will allow the territories to equip themselves with the best techniques available. Waste-to-energy with plants dedicated to or also intended for other waste is, for example, very widespread in some European countries, also due to the potential recovery of phosphorus. The set of solutions must be harmonized within the scope of a national plant plan that guarantees adequate self-sufficiency at a national level and by territorial areas based on a planning of plant needs (purification and destination), based on the current and future forecast of supply and demand for treatment.

2.4 Objective of the study

This doctoral thesis involved a pilot-scale study of the sewage sludge drying process using solar greenhouses powered by photovoltaic panels. The term drying refers to a procedure that aims to remove the water present in the product, in this case from the sludge. The use of solar greenhouses and photovoltaic panels for sludge drying within wastewater treatment plants is in principle an interesting solution to obtain superior drying than that normally obtained with other types of thermal drying treatments. The choice to study different configurations was made to evaluate how the air introduced affects the effectiveness of the drying process. This effectiveness was evaluated by monitoring the process parameters of the pilot plants and of the different configurations studied. The application of free solar energy can be an alternative solution to reduce the costs of the drying process since solar radiation represents the main energy source for drying. The prototype greenhouses used represent an evolution of traditional greenhouses. The innovation of the research lies in introducing hot air inside the solar greenhouses. It is an economical and ecologically sustainable solution which, through solar drying, reduces the water content in the sludge to around 85-90 % dryness, thus reducing the quantity of sludge to be removed and, consequently, simultaneously reducing associated costs.

3 Physical, chemical, and biological properties of wastewater sludge

3.1 Characteristics municipal wastewater sewage sludge

It is always quite difficult to have precise knowledge of the qualitative characteristics of wastewater purification sludge. They do not appear as a homogeneous product, as their chemical and physical properties essentially depend on the characteristics of the water of origin and the treatment operations to which they are subjected. In fact, one of the consequences of the technological processes implemented is the transfer and concentration in the sludge of the polluting substances initially contained in the treated wastewater. The minimization of the quantities produced is one of the priorities to be pursued in sludge disposal, but the achievement of this objective must naturally not compromise the final quality of the liquid effluents.

The most suitable treatment is chosen based on various factors, and mainly on the physical and chemical characteristics of the sludge (degree of residual humidity, content of heavy metals and toxic substances) and the availability of disposal sites and plants. The quality characteristics of the sludge depend on the quality of the incoming wastewater, both for industrial and urban wastewater. In the latter, in fact, in addition to domestic wastewater, there may be wastewater from commercial, artisanal, and industrial establishments. Many pollutants, including metals and fat-soluble organic compounds, condense in sludge, resulting in high concentrations in the solid phase (De Feo et al., 2013). The qualitative characteristics of the sludge are also strongly influenced by the type of wastewater treatment, possible addition of chemicals, biological activity, etc.

Some parameters that characterize the sludge (such as total and volatile solids) are specifically linked to the ways in which they are produced (for example, presence of primary sludge and age of the biological excess sludge). The microelement content (organic carbon, total nitrogen, and total phosphorus) also derives from the treatments undergone by the sewage, as well as from the nature of the original wastewater; just think of the plants with chemical or biological diphosphatase phases which accumulate higher quantities of phosphorus in the sludge than those of plants without such phases.

A sludge is normally defined as solid when it becomes "shovel able sludge", that is, it must be collected in piles, collected with a shovel (manual or mechanical), and be easily loaded onto means of transport. To be solid and shovel able, a sludge must have a water content of no more than 60 % through a dehydration process (Kusturin Mauro, 2007).

A distinction can be made between:

- raw sludge, which is extracted during the water treatment phases and does not undergo any subsequent transformation. They are divided into primary sludge (deriving from primary sedimentation), secondary or active sludge (deriving from the biological oxidation unit) and chemical sludge (deriving from a treatment with the addition of chemical substances).

- treated sludge, which originates during the treatments to which the raw sludge is subjected (mechanical dehydration, evaporative drying, composting).

The different nature of the sludge significantly influences the treatment cycle to which it is subjected (Table 3.1). The treatments are aimed at reducing the water content (with consequent reduction in volume), stabilizing the organic material, and destroying the pathogenic organisms present.
Although raw sludge treatment operations are possible (for example incineration and composting), their characteristics of putrescibles and potential pathogenicity recommend that they be previously subjected to stabilization of the organic material and the destruction of the organisms present, i.e. an operation aimed at reducing the causes of sludge instability, which allows its final disposal without causing damage to human health and the environment.
Biological stabilization occurs by microorganisms (anaerobic or aerobic) which eliminate unstable and putrescible organic substances by using them for the synthesis of their own cellular material (metabolism) and/or transforming them into gaseous products. The main difference consists in the fact that the Anaerobic digestion results in the production of a "biological gas" consisting mainly of methane (which can be used as fuel), while in aerobic digestion only simple gaseous products are obtained which are no longer degradable and mostly inorganic (water and carbon dioxide).

Table 3.1 - Characteristics of sludge of urban origin (adapted from Dellacqua Luisella, 2020)

	Raw Primary	**Digested Primary**	**Biological raw**	**Digested biological**	**Raw mixed (primary and biological)**	**Digested Mixed (primary and biological)**
Quantity (l/ab/ day)	0.9÷2.2	0.3÷0.5	0.2÷7.3	1.5÷2.0	0. 1÷2.8	0.04÷1.o
Total Solids (% SS)	3÷7	6÷11	1÷2		3÷6	3÷10
Ashes (%)	20÷35	40÷65	28÷37		20÷50	45÷65
Total Carbon	43÷60		30÷60	54*	35÷60	20÷35
Volatil Solid (% VS)	59÷79	33÷60	62÷74		55÷77	43÷56
Nitrogen (%)	2÷4	1	4÷9	1.5÷5	4÷5	2÷5
C/N ratio	10÷30		4÷15	18*	9÷15	8÷14
Phosphorus	1÷3	1	3÷6	1÷3.5	1÷3	1
Potassium	0÷0.09	0.1÷0.5	0.1÷0.9	0.2÷0.4	0.2÷0.6	0. 1÷0.6
PH	5÷7	7÷8	6÷8		6.5÷7	6.5÷7.5
Lower Calorific Value	3700÷5000	1500÷3800	3600*		3500÷4000	

Numerous differences can be found between the characteristics of a digested sludge compared to those of a raw sludge, in particular:

- volatile solids (putrescible organic substances) decrease in digested sludge because they are transformed into gas, water, or inorganic products.

- the total solids increase, in percentage, mainly due to the removal of the solvation water, with a consequent reduction in the volume and overall mass of the digested sludge.
- total carbon decreases because of the gasification of a certain amount of carbon with the production of methane and/or carbon dioxide.
- the calorific value, linked to the presence of combustible products (in the sludge represented almost exclusively by volatile organic substance), is reduced by approximately half.
- the dehydration improves compared to a raw sludge and is useful for choosing the dehydration system to be adopted.
- the grain size is more uniform than that of raw sludge.
- the stability of the sludge improves significantly due to the almost complete reduction of biodegradable organic substances; as parameters to evaluate the degree of stability of the sludge we can consider the content of pathogenic organisms (which decrease due to the creation of an environment unfavourable to their survival), the reduction of faecal pollution indices and the almost total absence of unpleasant Odors (putrescible substances have been transformed into inert substances during digestion).

The main physical and chemical properties of sludge are therefore the following (Dellacqua Luisella, 2020):

1. Putrescibility and pathogenic organisms.
2. Humidity and characteristics of solids.
3. Sedimentability of the sludge.
4. Dehydration of a sludge.

3.2 Putrescibility and pathogenic organisms

The primary raw sludge has a grey-brown colour, is highly putrescible and a source of rather unpleasant odors (the concentration in solids is around 3 %). In fact, they contain many inert inorganic substances (sand, carbonates, metal oxides) and organic substances that are not easily degradable (seeds, fibres, rubbers), but also organic substances that are biologically unstable and therefore potentially attackable by anaerobic microorganisms, with the formation of smelly gaseous compounds (methane, mercaptans, hydrogen sulphide, ammonia). Activated sludge, on the other hand, is much more diluted (the concentration in solids is approximately 0.5÷1 %) and is essentially brown or yellow brown in colour: it has a floppy consistency and is largely made up of microorganisms. and cellular residues that are still biologically active, so they too can be subject to putrefactive phenomena. All raw sludge of urban origin contains both non-pathogenic microorganisms of faecal origin (fecal coliforms, streptococci), which are very resistant and can be taken as a measure of the degree of pollution of the sludge, and pathogenic microorganisms (viruses, bacteria, protozoa), which can constitute a significant source of danger for humans and the environment in general.

Even if raw sludge treatment operations are possible (incineration, composting, etc.), their characteristics of putrescibility and potential pathogenicity recommend that they be subjected to "stabilisation" beforehand, an operation which serves to reduce the causes of instability of the sludge and is achieved by transforming all putrescible substances into gas (carbon gasification), so that the manipulation and final disposal of the sludge occurs without causing discomfort or damage.

3.3 Humidity and characteristics of solids

Both raw and digested sludge contain a high percentage of water: it is therefore convenient to carry out treatments that have the aim of removing humidity from the sludge, with a consequent notable reduction in costs and complexity of subsequent processing and disposal operations to which the sludge will be subjected.
The removal of water in fact corresponds to a reduction in volume or weight of the sludge and the main consequence is seen in the increase in solid concentration, based on the relationships:

$$C_2 = \frac{C_1 * V_1}{V_2}$$

$$C_2 = \frac{C_1 * P_1}{P_2}$$

- C1, C2 = initial and final concentration in solids.
- V1, V2 = initial and final volume of the sludge.
- P1, P2 = initial and final weight of the sludge.

In the sludge we can differentiate total solids and volatile solids.

a) The ***total solids*** or the organic and inorganic solid substances that constitute the solid residue (dry matter or TS) after the removal of the water by drying in an oven at 105°C. The determination is carried out by exactly weighing a portion of sludge (about 10 g.) in a calibrated porcelain capsule; the sample is then placed for about an hour in a thermostatic oven at 105°C, cooled first in a desiccator and then at room temperature and finally weighed again. The number of total solids present in the sample, expressed as % by weight of solids in the wet sludge, is given by:

$$TS\ [\%] = \frac{Dry\ residual\ weight}{Initial\ sample\ weight} \cdot 100$$

At the same time, the percentage humidity of the same sample can be defined as:

$$U\ [\%] = \frac{initial\ sample\ weight - dry\ residual\ weight}{initial\ sample\ weight} \cdot 100$$

A fraction of the total solids is represented by ***volatile solids (VS)***, which are identified by incinerating the dry residue obtained from the determination of the total solids, by calcination in a muffle at 600-700°C, for a period of time adequate to allow the volatilization of the organic substance (not less than 30 minutes); the sample, after cooling first in a desiccator and then at room temperature, is weighed again. The difference between the values obtained at 105°C and 700°C, i.e. the loss due to calcination, provides the volatile solids content, expressed as a % by weight on the dry basis based on the relationship:

$$VS\ [\%] = \frac{Dry\ rsidual\ weight - calcined\ sample\ weight}{dry\ residual\ weight} \cdot 100$$

This parameter is often used to evaluate the quantity of organic substance present in the sludge (although it is possible that both the zinc oxide and other inorganic substances have volatilized during the calcination); at the same time the ash content can be expressed, always as a % of dry weight, as:

$$Ash\ [\%] = \frac{Calcined\ sample\ weight}{Dry\ residual\ weight} \cdot 100$$

Quantitatively we have:

TS (total solids) = SSV + Ash

b) filterable solids, i.e. particles with a very small grain size that are not retained by a filter and remain dissolved or dispersed in the aqueous phase of the sludge.
c) suspended solids or larger particles which, remaining suspended in the liquid phase, cause turbidity of the sludge. In this case, the sedimentability characteristics of the sludge are decisive: in fact, the particles with very large granulometry, after an adequate residence time, can settle due to the effect of gravity on the bottom of special sedimentation tanks (this is called sedimentable suspended solids), thus separating an aqueous liquid phase and a "thickened" sludge, with a higher solid content than the feed one (this operation is not feasible in the case of activated sludge, which settles very poorly, being light and flaky). Quantitatively the following relationship is valid:

TSS = suspended solids (sedimentable and non-sedimentable) + filterable solids

Quantities directly linked to the moisture content and the characteristics of the solids in the sludge are the sedimentability and dehydration of the same (Dellacqua Luisella, 2020).

3.4 Sedimentability and thickening of a sludge

Settleability is the ability of the sludge to separate the sedimentable suspended solids during a sedimentation operation. A measure of this attitude of the sludge is the Sludge Volume Index (SVI), i.e. the ratio between the volume, in ml, occupied by the settled suspended solids in a 1,000 ml graduated cylinder, after a sedimentation period of 30 minutes, and the concentration of biomass (in mg or g of TSS). Sometimes it can also be useful to have the sedimentation curve of the sludge as a function of time, constructed by recording the height of the sludge at regular time inter-vals interface between suspension and supernatant).
The analytical procedure includes a measure of sedimentability and a measure of total suspended solids, which allow us to define:

$$\text{SVI} = \frac{volume\ of\ sedimented\ sludge\ (\frac{ml}{l})}{suspended\ solids\ in\ the\ initial\ sample\ (\frac{g}{l})}$$

The lower the SVI value, the better the sedimentability characteristics of the sludge: for example, the gravity thickening operation can be carried out optimally when the sludge volume index is low (< 100 mg/l). Thickening is the process that causes the removal of the interparticle water contained in the sludge, i.e. the water that we find free between the solid particles.
The main consequence is the increase in the concentration of solids: the thickened sludge, however, still has the characteristics of a liquid since the dry substance content reaches a maximum of 10 ÷ 12 %.
The main objective of carrying out the thickening is to reduce the volume and weight of the sludge, to reduce the costs of the subsequent operations to which it will be subjected.
More in detail, the main objective of thickening is to increase the solids content of the sludge, thereby reducing its moisture. The sludge undergoes sedimentation in specific basins called "thickeners." However, the thickening effect does not result in substantial changes in the moisture of the sludge, which remains, after this operation, still not "dewatered" (i.e., not suitable for being treated as solid waste in terms of physical state) due to its extremely high-water content. Nevertheless, the modest reduction in moisture achieved through this treatment allows for a significant decrease in the volumetric flow rate directed to the downstream units, thus reducing their size.
For example, if we consider feeding a thickener with a sludge flow rate of 100 m^3/day (QF2), having a moisture content of 99% (u1), and obtaining a sludge moisture content (u2) of 98%, the flow rate of the thickened sludge (QF2) would be 50 m^3/day:

$$Q_{F2} = Q_{F1}\frac{100 - U_1}{100 - U_2}$$

The results clearly show a significant reduction in the flow rate of the sludge achieved, even with a modest moisture reduction (1% decrease), resulting in a volume of water lost of 50 m^3.

3.5 Dehydration of a sludge

Dehydrability, on the other hand, is the ability of the sludge to release both the adhesion water (bound on the surface to the solid particles by adhesion or capillarity) and the particulate water (chemically bound inside the solid particles). Dewaterability is therefore the parameter taken into consideration for the sizing and choice of the optimal system to adopt to achieve the dehydration of the sludge. The dehydration operation allows the water to be removed from the sludge until dry contents higher than 20 ÷ 25 % are reached. The final sludge has undergone a notable reduction in volume and is easily stored and transported. They can be distinguished: *natural dehydration, which takes place on drying beds and allows only the adhesion water to be eliminated, up to a dry content of 25 ÷ 35 %.*

mechanical dehydration, which occurs thanks to mechanical means and removes particulate water, bringing the sludge to a higher degree of dehydration (in filter presses, the most effective mechanical means for dehydration, a dry content of 40 ÷ 50 %).

Dehydration, particularly mechanical dehydration, proves to be easier by carrying out the conditioning operation on the sludge beforehand, which has the aim of eliminating the surface charge (generally of a negative sign) present on the colloidal particles. This charge, in fact, prevents the particles from aggregating, as well as promoting the adsorption of a certain quantity of water which, being bound quite tenaciously, is difficult to remove. Generally, to increase the filterability of the sludge, chemical conditioning is used, which occurs through the addition of substances of an inorganic nature (aluminium or ferrous sulphate, ferric chloride, hydrated lime, ferric chlorosulphate, etc.) or of an organic nature (cationic polyelectrolytes and anionic). The choice and dosage of the suitable conditioner depend on the nature of the sludge, the dehydration system used, and the type of disposal envisaged. For example, when sludge incineration is planned, the use of organic conditioners is recommended (even if they are rather expensive), as they also participate in combustion, without however significantly increasing the quantity of residual ash. Conversely, when the final fate of the sludge is landfilling disposal, it is better to use inorganic conditioners, which have lower costs, even though they cause an increase in the mass of the sludge (Table 3.2)(B. Wu et al., 2020).

Table 3.2 - Comparative analysis of various techniques for sludge dewaterability improvement (adapted from B. Wu et al., 2020).

	Technique types	Mechanism or main hypothesis	Special technological requirements	Dosage of chemicals	Energy consumption[b]	Secondary environmental risks
Physical conditioning	Porous material addition	Enhanced compression resistance and permeability maintaining	Agitation	30-50 wt% of dry matter	/	Volume increase
	Sonication	Disintegration of colloidal bio-flocs; Cell rupture for intracellular water releasing	Specialized equipment; Difficulty of scaling-up	/	600–800 kJ/kg dry matter	/
	Thermal treatment	Disintegration of colloidal bio-flocs; Cell rupture for intracellular water releasing	Pressure-bearing heating equipment	/	Hydrothermal & thermal hydrolysis: ~1100 kJ/kg water[c]	/
	Freezing/thawing	Formation of homogeneous ice crystal; Cell swelling for intracellular water releasing	Frigid regions only	/	10000-11000 kJ/kg of target removed water[d]	/
	Electrical treatment	Electrophoresis; Electro-migration; Electro-osmosis; Electrolysis	Specialized equipment; Anti-corrosion of polar plates	/	Electro-dewatering: 180–360 kJ/kg of removed water	/
Chemical conditioning	Coagulation/flocculation	Aggregation of sludge particles	Agitation	0.1–5 wt% of dry matter[a]	/	Chlorine residues; Toxic monomer of PAM
	Acid/base treatment	Regulating surface charge; Cell rupture for intracellular water releasing	Anti-corrosion equipment	5-10 wt% of dry matter	/	Corrosion; Biological toxicity
	AOP	Lysis of water-holding EPS; Cell rupture for intracellular water releasing	Multi-step chemical dosing; pH controlling	20-50 wt% of dry matter (Oxidant+Catalyst)	/	Corrosion; Toxic persulfate; Chlorine residues; … …
	Enzymatic treatment	EPS degradation	Temperature controlling; pH controlling	1-5 wt% of dry matter	/	/

3.6 Calorific value of the sludge

The sludge can possibly be used as a fuel and its energy contribution derives from the fraction of volatile solids it contains. The calorific value is a very important parameter for the purposes of evaluating the possibility of carrying out a waste-to-energy process.

The calorific value of a solid substance is the quantity of heat generated by the complete combustion of the unit mass of the substance itself and is normally measured in kcal/kg; it is necessary to operate in standard conditions, that is:

- initial oxygen pressure from 2,000 to 4,000 kPa.
- initial and final temperature between 20 °C and 35 °C.

reaction products: solids in the form of ash; water in liquid or vapor state; carbon dioxide, sulfur oxides and nitrogen in the gaseous state considering incomplete combustion. (In a complete combustion all the carbon turns into CO_2, all the hydrogen into H_2O, all the sulfur into SO_2 and all the nitrogen into elemental nitrogen N_2). If the material contains hydrogen, water is produced which, depending on its physical state (liquid or gaseous), provides a different contribution of calories to the combustion balance, which is why it is necessary to distinguish respectively between higher calorific value, when all the water present at the end of combustion is in the liquid state and lower calorific value (LCV) when the water is in the vapor state. The difference between the two calorific values therefore corresponds to the heat of vaporization of the total water, i.e. the sum of that generated during combustion and that possibly already present in the starting fuel. Normally in industrial combustion the fumes are dispersed at a temperature such that the water is still gaseous, therefore the practical value of a fuel, also in view of its commercial evaluation, is effectively represented by its lower calorific value. There is a specific method for determining the calorific value of sludge: the UNI 15170:2009 method (which implements the European standard EN 15170 of 2008). The method involves the use of instrumental equipment such as the Mahler bomb and provides all the necessary information for the calibration of the equipment and the formulas for the calculations. Furthermore, all the corrections to be adopted to minimize temperature measurement errors are indicated, considering the degree of precision of the thermometer, and to eliminate interference in the determination due to heat of reaction and combustion independent of the calorific value of the sample. Figure 3.1 shows the LCV of the sludge dried through thermal processes. The organic characteristics of the sludge change.

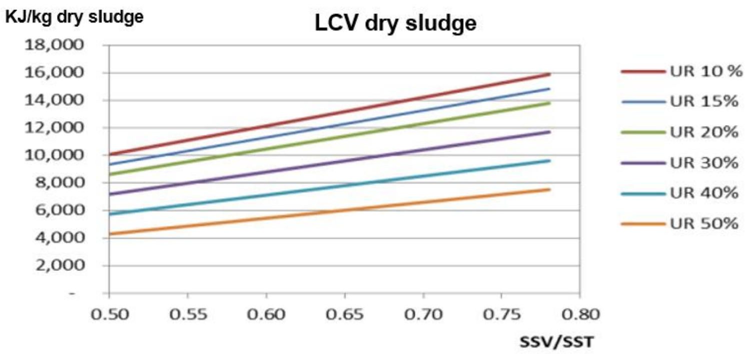

Figure 3.1- Lower calorific value of dried sludge (adapted from Canziani Roberto, 2016)

From a survey conducted by the Energy and Environment Laboratory of Piacenza (LEAP), it was estimated that mono-incineration of wet sludge, at 75 % in humidity, costs around 80-90 Euro/t (including depreciation of the plant and transport), for plants with a potential of the order of 20-25,000 t/year. The dry fraction of the sludge has a calorific value between 16 and 25 MJ/kg depending on the fraction of volatile solids and the type of stabilization process. The lower calorific value of non-stabilised sewage sludge, with a dry content of around 35% and a combustible fraction of 80% of the dry weight, is around 8 MJ/kg, a value which allows incineration without auxiliary fuels (Canziani Roberto, 2016)

3.7 Water distribution in the sludge

Water is the main constituent of sludge, and its content can fluctuate from 99 % for highly diluted sludge, such as that obtained from a biological activated sludge process, up to 88 % in the case of chemical precipitation processes (Simone Visigalli, 2019). Sewage sludge is generally difficult to dehydrate due to its gelatinous (Mahmoud et al., 2011), colloidal and compressible structure. Furthermore, due to the presence of solid particles, not all the water contained in the sludge has similar properties in terms of vapor pressure, enthalpy, entropy, viscosity, and density (Vaxelaire & Cézac, 2004).
The dewatering efficiency depends not only on the dewatering devices and chemical additives used for conditioning, but also four different types of water are classified:

1. free water not associated with solid particles.
2. interstitial/capillary water trapped within the interstitial spaces of the flakes.
3. surface water retained on the surface of solid particles for adsorption and adhesion.
4. chemically bound water to bacterial cells and sludge particles.

In general, free water represents approximately 65-85 %, capillary water 15- 25 % while surface water and bound water, which can only be removed by thermal drying at temperatures above 105 °C approximately 10 %. Certainly, the different dehydration and drying technologies can have different efficiency in removing the different types of water present within the sludge.
The estimate of the content of free water and other forms of water in the sludge is based on the different bond that exists between the water molecules and the solid particles (Figure 3.2). Since there are many characteristics that vary between the various forms of water, numerous methods have been proposed for determining the content of bound water, which exploit the various properties that differ between one form of water and another: drying tests, filtration or compression, centrifugation, dilatometric tests, Differential Thermal Analysis (DTA), Differential Scanning Calorimeters (DSC) and nuclear magnetic resonance (Vaxelaire & Cézac, 2004). This variety in methods has highlighted how the definition of free water is closely linked to the analytical procedure used for its determination.
The results reported in the scientific literature differ considerably, not only due to the different methods used, but also due to the operating conditions of execution of the individual test, which are never standardized. The literature reports values

of the bound water content, understood as the sum of interstitial, surface and hydration water, varying in the range 2.8÷10.7 g water/ g SS (Saveyn et al., 2005). *"Dehydration"* is defined as the ability of the sludge to release both adhesion water (superficially bonded to the solid particles by adhesion or capillarity) and particulate water (chemically bonded inside the solid particles). Dewaterability is therefore the parameter taken into consideration for the sizing and choice of the optimal system to adopt to achieve the dehydration of the sludge.

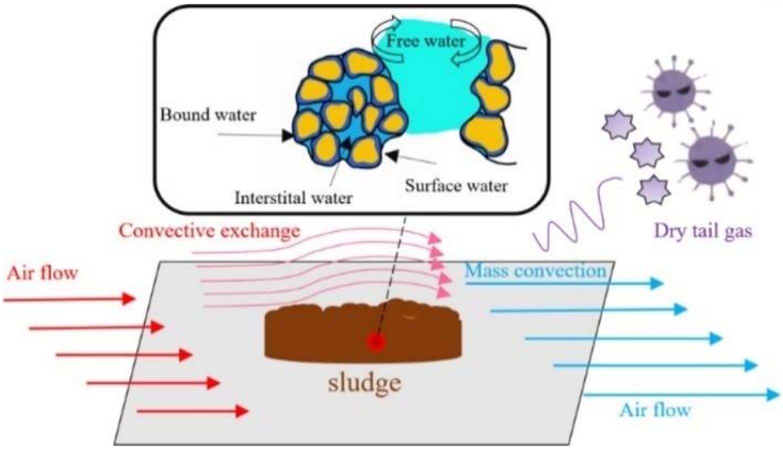

Figure 3.2 - Drying mechanisms (adapted from Ling et al., 2022)

The evaluation of dewatering efficiency is a complex task due to the extremely variable nature of sludge. Among the parameters that most influence the dewaterability of the sludge are the pH, the charge of the particles, the content of bound water, the content of organic substance and EPS (extracellular polymeric substances), the granulometry of the suspended solids, the type of sludge, the type of chemical additives used and the degree of mixing of the conditioning phase, the mechanical resistance of the aggregates and the porosity (Figure 3.3) (R. M. Wu et al., 2001).

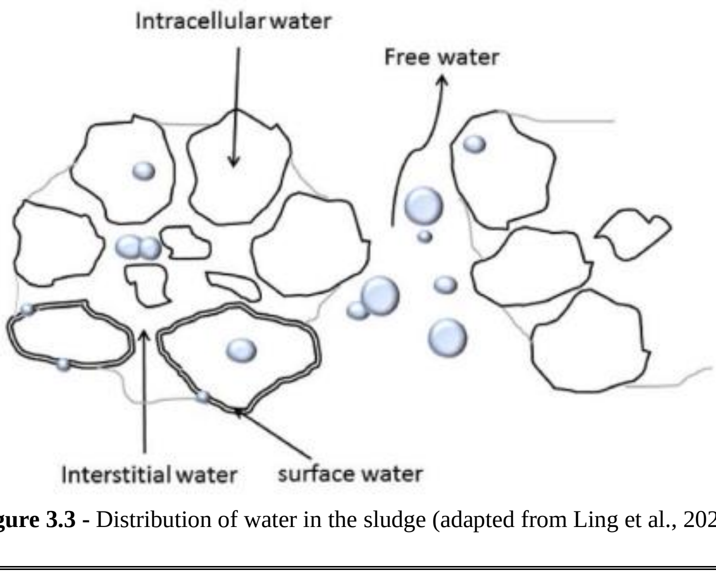

Figure 3.3 - Distribution of water in the sludge (adapted from Ling et al., 2022)

Water migration from the interior to the surface is a complex process. A conceptual visualization of the moisture distribution in the sludge is shown in Figure 3.3. The moisture content of the sludge can be calculated as follows (Zhou & Jin, 2016).

$$M_t = \frac{(w_o - w_t) - W_d}{W_d}$$

Where:

- w_0 mass of the initial sludge sample.
- w_t mass of moisture evaporated at time t.
- w_d dry mass of the sludge sample.

The moisture ratio (MR), on the other hand, is calculated from the mass loss of the sludge:

$$MR = \frac{(M_t - M_e)}{(M_o - M_e)}$$

Where:

- Mo represents the initial moisture content.
- M_t represent the moisture content.
- M_e represent the final moisture content.

Moisture diffusion in sludge is mainly controlled by internal diffusion in the drying process. The analytical solution of Fick's second law can be expressed by:

$$MR = \frac{8}{\pi^2} \sum_{\pi=0}^{\infty} \frac{1}{(2n+1)} exp\left[- \frac{(2n+1)^2 \pi^2 D_{eff} t}{4L^2} \right]$$

Where L is the half thickness of the product sample and D*eff* is the effective diffusivity. The drying time is expected to be long enough that the equation can be simplified as:

$$\ln MR = \ln \frac{8}{\pi^2} - \frac{\pi^2 D_{eff} t}{4L^2}$$

The drying time is proportional to the square of the thickness of the thin layer material and is inversely proportional to the effective diffusion coefficient of the material. After the appearance of cracks (during the rate of sinking), the drying process is regulated by the diffusion of water in the sludge.

Effective diffusion characterizes a complex mechanism involving water in two states: liquid and vapour, which depend on the temperature, pressure, and moisture content of the sludge(Nourhene Boudhrioua, 2004).The effective diffusivity coefficient (Deff) was calculated by plotting the slope of ln (MR) versus drying time and reported in Table 3.3. The results revealed that the effective diffusivity increases as the solar radiation energy increases.

Table 3.3 - The diffusion coefficient in the sludge drying process with respect to solar radiation (adapted from Ameri et al., 2020)

Solar radiation W/m^2	$-\frac{\pi^2 D_{eff}}{4L^2}$/h	D_{eff} m^2/s	R^2
300	−0.0304	2.14×10^{-11}	0.9371
400	−0.0621	4.37×10^{-11}	0.9467
500	−0.0699	4.92×10^{-11}	0.9459
600	−0.089	6.26×10^{-11}	0.9179
700	−0.1008	7.09×10^{-11}	0.9321

3.7.1 Water migration pathways in sludge.

Sludge is a porous medium, so during the drying process, changes occur in heat and mass transfer on the surface of the sludge in contact with hot air and migration of internal moisture and increase in temperature. The air-sludge interface exchange process that occurs is shown in Figure 3.4 (Ling et al., 2022).

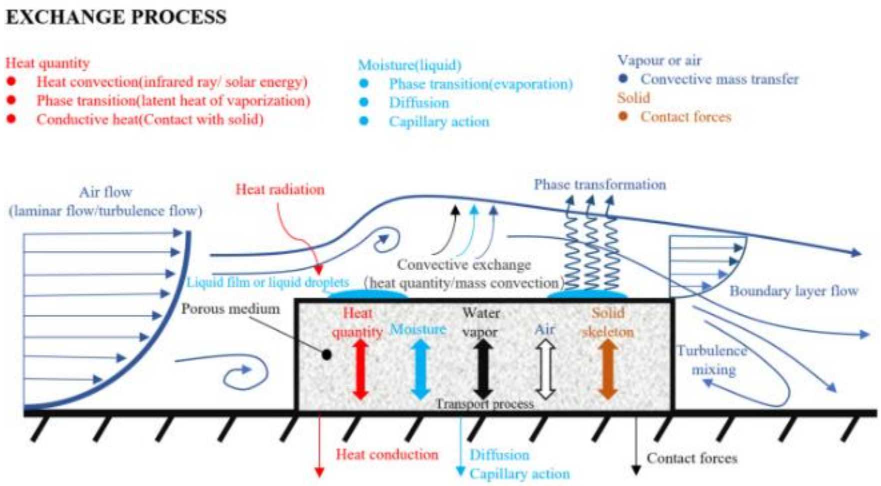

Figure 3.4 - Matter exchange processes and air-matter interface exchange (adapted from Defraeye, 2014)

In the convective heat transfer process, the sludge surface is an important place for mass and heat transfer. It is influenced by heat transfer (convection and thermal radiation) brought by the warm air and the surface moisture changes from the liquid to the gaseous phase. The surface of the sludge then begins to heat up. At the same time, heat conduction occurs inside the sludge, and the internal temperature of the sludge gradually increases from the outside to the inside. The phenomenon of air flow on the sludge surface causes the vapor pressure to decrease, and the moisture on the sludge surface evaporates easily. In this way, a part of the water in the sludge undergoes mass transfer under the driving force of the water gradient, and the water diffuses from the inside to the outside.

Due to the loss of water in the sludge, the quality of the sludge changes and undergoes internal mechanical deformation. In convective sludge drying, the heat

Exchange between the drying air and the sludge is convective, although heat conduction and radiation are involved(Ling et al., 2022). The specific transmission parameters are shown in

Table ***3.4***.

Table 3.4 - Transmission parameters (adapted from Ling et al., 2022)

Transported variable	Heat	Mass	Mass	Mass	Mass
		Liquid	Water vapor	Air	Solid
Transport mechanisms	• Diffusion • Advection	• Diffusion • Convection	• Diffusion • Convection	• Diffusion • Convection	• Mechanical deformation
Volumetric sources/sinks	• Phase change • Electromagnetic radiation/release energy	• Phase change • Chemical binding/release of water • Gravity	• Phase change	• None	• Gravity
Driving forces	• Temperature	• Capillary pressure • Gas/liquid pressure • Temperature	• Gas pressure • Concentration • Temperature	• Gas pressure • Concentration • Temperature	• Water content • Temperature

The factors that influence moisture migration are:

1. ***Temperature***: The heat brought by the hot air causes an increase in the temperature of the sludge surface and the vaporization of moisture on the sludge surface. The time required for sludge drying decreases significantly as the temperature of the drying air increases (Ali et al., 2016). When the sludge moisture content is 30%, the drying time at 70 °C is half that at 40 °C, and the average drying rate increases approximately 2.1 times (Ali et al., 2016). The increase in temperature increases the ability of the air to accept humidity and, at the same time, increases the temperature of the sludge, influencing the structure of the pores and the power of the sludge to release humidity. Therefore, for the same moisture content, the higher the temperature, the higher the drying rate.
2. ***Air Speed***: Increasing air speed allows more dry air to encounter the wet sludge so more air can carry more moisture. The higher air velocity thins the boundary layer thickness on the sludge surface and improves the heat and mass transfer coefficient of the sludge (Huang et al., 2016). The increased air velocity also accelerates the rate of diffusion of water vapor and maintains the pressure difference between the water vapor pressure at the sludge surface and the water vapor pressure in nearby air. Furthermore, the higher air velocity brings more heat to ensure stable heat transfer to the sludge for water evaporation. However, when the wind speed increases above the threshold, the weight of the influence on the sludge drying rate decreases. The speed of the air will also accelerate the additional energy consumption of the dryer and cause an increase in dust emissions (Zheng et al., 2021a).
3. ***Relative humidity***: Relative humidity represents the moisture absorption capacity of the air. Before air humidity and sludge moisture reach equilibrium, there is a difference in the humidity gradient, which is one of the driving forces for moisture transfer from inside to outside (Zheng et al., 2021a) .The higher the difference in moisture gradient, the greater the driving force. In general, the drying rate of sludge increases as relative humidity decreases (Ruiz & Wisniewski, 2008).

3.7.2 Particle size

At the same temperature, the drying time increases as the size of the particles increases. It was found that the total drying time of particles with a diameter of 10 mm is not much different from that of particles with a diameter of 6 m, while the total drying time of particles with a diameter of 18 mm increases significantly (Zhao et al., 2020). So, it can be noted that the smaller the particle size, the higher the drying speed, conversely the larger the particle size, the higher the resistance to heat and mass transfer. The sludge drying process is controlled by internal migration and drying rate and is determined by the rate of water diffusion (Zhao et al., 2020). So far, common factors studied for convective sludge drying include temperature, air velocity, relative humidity, and particle size (Figure 3.5). However, the factors influencing sludge dewatering are also related to the properties, cracking, and shrinkage capacity of the sludge (Ruiz & Wisniewski, 2008).

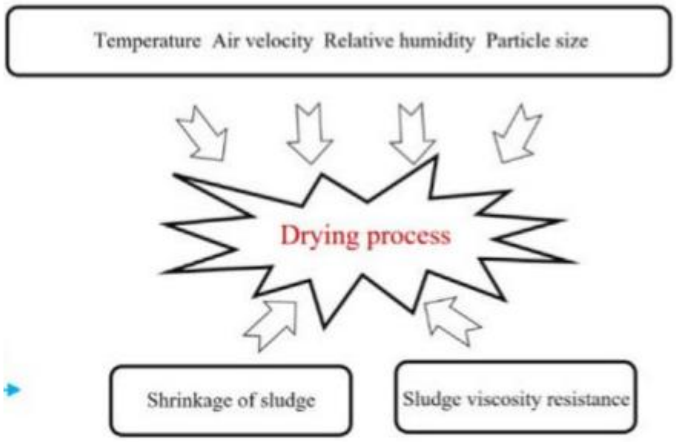

Figure 3.5 - Drying Process (adapted from Ling et al., 2022)

3.7.3 Sludge withdrawal

During the convective drying process, the removal of water from the sludge causes irregular forces within the sludge, resulting in shrinkage in size and shape. Volumetric shrinkage of sludge is a phenomenon in which the volume and size of sludge particles are reduced during the drying process. This shrinkage reduces the contact surface with the hot air, limiting the evaporation capacity of the water in the sludge (Font et al., 2011).

Bennamoun et al. (Ling et al., 2022) identified that the internal diffusion coefficient and the convective mass transfer coefficient without considering the effect of sludge volume shrinkage are twice as high when considering the shrinkage effect. Scalcon et al. (Ling et al., 2022) found that both surface shrinkage and volumetric shrinkage of sludge are linearly related to the dimensionless water content of the sludge. However, in most sludge studies, the shrinkage phenomenon is ignored. The withdrawal is expressed as follows (Bunyawanichakul et al., 2007).

$$Shrinkage = 1 - \frac{V_T}{V_0}$$

where V_0 and V_T are the sludge volumes before and during drying, respectively. The higher the temperature, the higher the sludge shrinkage rate. During the sludge withdrawal process, surface hardening and cracking are also produced. From 80 °C to 110 °C the sludge shrinkage rate increases; and from 110 °C to 140 °C the surface hardened, and water loss was inhibited, but sludge shrinkage was limited. Cracks on the surface of the sludge will increase the contact area between the sludge and hot air, while crusts that harden on the surface will hinder the transfer of moisture from inside the sludge to the outside. Cracked sludge has a higher peak drying rate than non-cracked sludge, which is attributed to the increased surface area caused by sludge cracking during drying (Cai et al., 2016). Increasing air velocity can accelerate the formation of sludge cracks, and the new cracks will increase the surface area of the sludge in contact with the air, which could lead to a faster drying rate. Through the camera and X-ray micro computerized tomographic scanner, the change in intensity of obvious phenomena such as shrinkage and cracks during the sludge dewatering process can be intuitively analysed and monitored.

3.7.4 Viscous resistance phenomenon

During the operation of convection drying systems, although sludge convection drying mainly uses hot air for direct contact with the sludge, it is inevitable that the sludge particles will directly contact the operating mechanical devices causing difficulties in transportation of the sludge and cause the dryer wall to stick. Meanwhile, sludge in the viscosity period has a significant tendency to agglomerate. These phenomena will change the hydrodynamics of dryers and reduce the efficiency of long-term operation of convective drying systems (Ling et al., 2022). The cohesive sludge tended to stick to the walls of the equipment, causing a local accumulation of wet materials, which changed the hydrodynamics of a dryer, especially those with active hydrodynamic regimes such as pneumatic dryers, fluidized bed dryers, and spray dryers. Mortier et al. (Mortier et al., 2011) suggested that viscosity causes a negative impact on fluidized bed drying. Gu et al., (Vaxelaire & Cézac, 2004) found that sludge viscosity and particle agglomeration capacity increase with sludge moisture content within a certain range.

This effect increases the interaction forces between the particles and the reactor wall as the sludge is dried in the fluidized bed, resulting in increased resistance to fluidization. These problems cannot be avoided in the application of other convective drying methods. Banooni et al., (Vaxelaire & Cézac, 2004) stated that cohesive forces and disintegration mechanisms in sludge agglomeration resulting from rapid drying were the main negative aspect. Few studies have been published on the sludge adhesion process, but the phenomenon of sludge adhesion certainly has a negative impact on drying processes. When the moisture content drops within a certain range, a very sticky sludge is formed, which will seriously reduce the drying efficiency during the sludge drying process.

Kudra (Vaxelaire & Cézac, 2004) used the “moisture content and temperature” curve reported in Figure 3.6 to describe the range of materials in the sticky region. The concept of “viscosity point temperature” is proposed to highlight the “viscosity region” of slurries by a given combination of temperature and moisture content. The continuous temperature of the viscosity points forms the "viscosity point curve", which forms the viscosity region. There are fluctuations in the viscosity region and even the non-viscous suspension starts to appear viscous when dried to a certain moisture content. Therefore, the curves of the upper and lower viscosity points are used to represent the range of the viscosity region. As shown in Figure 3.6, the material above the upper limit curve is in a continuous non-sticky state (liquid), the material below the lower limit curve is in a dispersed non-sticky state (dust particles), and the material between the upper and lower curves is in a viscous condition.

Sludge viscosity has a necessary relationship with moisture content, but the effect of sludge moisture content on its viscosity is nonlinear (Peeters et al., 2013). Li et al., (Vaxelaire & Cézac, 2004) found that sludges with a water content above 70 % are less viscous, while the viscosity of sludges becomes significantly higher at a water content of 45% -70 %, resulting in lower drying efficiency. When the moisture content is less than 45 %, the viscosity of the sludge begins to decrease. Since water acts as a plasticizer in sludge, after the water is reduced to a certain extent, the viscosity of the sludge also disappears (Adhikari et al., 2001). Sludge particles with a moisture content of less than 30 % are hardened and their moisture is mainly bound water. During the drying process, sludges with high initial moisture content are likely to cause sludge agglomeration and will not break down easily. In thin layer drying, although encrusted sludges with low water content are eventually dried, they still have a high internal water content.

Certainly, alkalinity can disrupt colloidal stability in sludge and reduce the water holding capacity and viscosity of sludge (Dong et al., 2011).

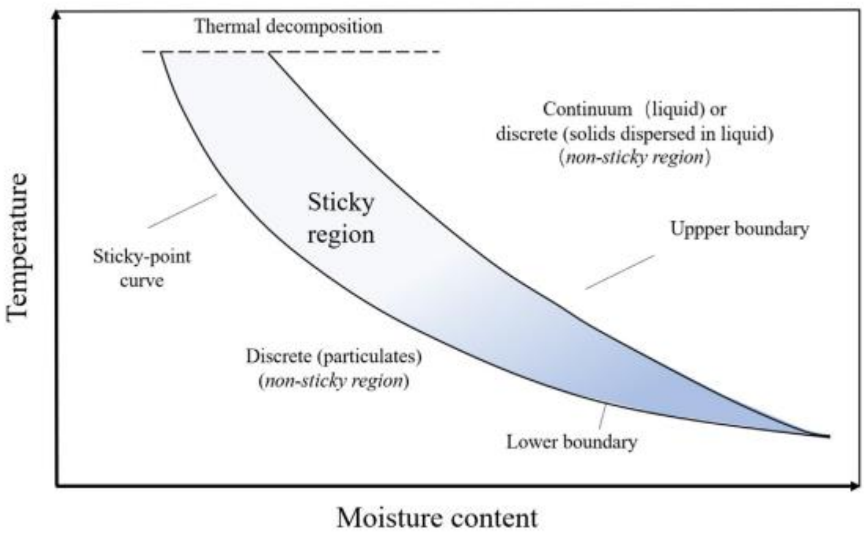

Figure 3.6 - Taking the “moisture content-temperature” curve as the viscous area of the material (adapted from Vaxelaire & Cézac, 2004)

3.8 The analysis of thermodynamic phenomena in the sludge dewatering process

"Drying" is defined as the operation by which the water content of a product is reduced by evaporation. Depending on how the process is conducted, a distinction is made between convection drying, when the operation is regulated by convective transport phenomena between air and product, and boiling drying, when the evaporation of the water occurs at its vapor pressure. Often, in the same process, the two phenomena occur simultaneously, but generally one of the two prevails. In physical terms, drying is a simultaneous and interdependent convective transport of matter and heat between air and product, conditioned by the liminal exchange coefficients at the interface between product and air. This convective transport determines, and is in turn conditioned by, a molecular transport of heat (conduction) and matter (diffusion) within the product.

3.9 The mechanisms of drying

The fundamental mechanisms of drying are schematized in Figure 3.7.

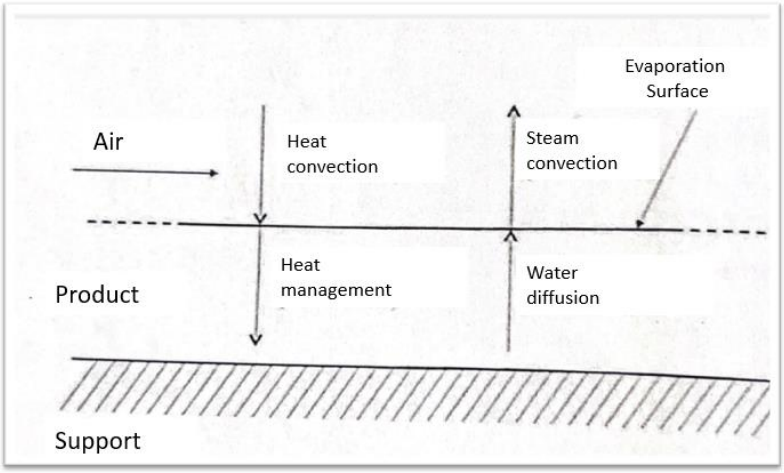

Figure 3.7 - Schematic representation of a drying phenomenon

The drying phenomenon is so complex that it does not allow exact analytical solutions. The approach to the study of drying requires some simplifications:

- the study must be broken down into phases which can be described either based on convective transport (constant progress phase) or based on the laws of diffusive transport (slow progress phase).
- constant air conditions are assumed, while in a real dryer these are different at every point and, considering the product, at every moment of the cycle.
- simplifications are applied to the various transport phenomena which are often far from reality: for convective transport of heat and matter, values of the liminal exchange coefficients are used assuming constant speeds

and directions of the air flow, without considering that they vary and have components tangential and normal to the product. Just as it is very difficult to accurately evaluate the exchange surface and consider the influence on it of the contraction and deformation phenomena resulting from dehydration, constant diffusivity coefficients are adopted for the molecular transport of heat and matter. of heat and water without considering the heterogeneities of the materials, their dependence on the variation in the humidity of the product and the phenomena of contraction and deformation on the actual thicknesses of the product.

Nor can we reasonably predict the effects of physical barriers such as cell membranes on water diffusion.

Since evaporation does not only occur on the surface of the product, but, starting from a certain moment, also inside it, diffusion affects both free water and steam, which can also condense and re-evaporate during its movement towards the surface. Capillarity transport mechanisms must not be overlooked. Finally, it should not be forgotten that internal diffusion involves water which acts as a solvent for various solutes, which are also involved in diffusion, with further complications due to the formation of gradients, precipitation due to in solubilization, etc.

3.9.1 Simplified approach

From the previous description, the impossibility of tackling the study of drying with a rigorous mathematical approach clearly emerges. On the other hand, a quantification of the phenomenon is necessary both for the sizing of the systems and for the optimization of the processes. Consider the case of a solid product, such as the infinite layer, in which the transport phenomena therefore occur mainly through the two largest surfaces (unidirectional transport). Consider that its geometry remains constant over time, which means that the unrealistic hypothesis is adopted that contraction and distortion phenomena do not occur as drying (shrinkage) proceeds. Assume that we operate with air having a dry bulb temperature θa and a wet bulb temperature θu and therefore having a constant humidity content *na* (kilograms of water/kilogram of dry air); let *ns* be the humidity of the liminal layer of air in contact with the surface of the product (kilograms of water/kilogram of dry air).

3.9.2 Constant trend phase

When the product is placed inside the dryer there is a short period of time during which the surface of the product heats up to the wet bulb temperature, after which the constant drying phase begins, during which the water begins to migrate from the inside of the product towards the surface, with a speed equal to the speed of evaporation of water from the surface of the product. This phase is prolonged until the value of *ns* remains higher than a critical value (*nscr)* which indicates that the speed of migration of the water inside the product towards the surface has reached a value such that, at the surface, a smaller quantity of water arrives than could evaporate. This is a very critical moment in the drying of many products. During the constant trend phase, the drying speed depends on the convective transport of heat and the transport of matter in the boundary layer at the interface between air and product.

The following relationships apply:

- for the heat: q= hc S (θa - θu) [J/s].
- for the substance: - mc= hm S (ns - na) [Kg/s].

Where:

- *q* represents the heat transport speed [J/s].
- *S* the surface area of the product [m^2].
- *hc* convective heat transport coefficient [J/m^2 s °C].
- *θa* - *θu* the dry bulb and wet bulb temperatures respectively [°C].
- *mc* drying speed, i.e. the variation of mass, as a function of time [Kg/s].
- *hm* mass transport coefficient [Kg/m^2s].
- *ns* - *na* respectively absolute humidity of the air and absolute humidity of the boundary layer of air at the air-product interface (kilogram of water/kilogram of dry air).

In this phase the surface of the product contains free water (*a_w=1*) and the heat supplied is entirely used to evaporate the water at the wet bulb temperature. There is therefore a balance between the heat supplied and the speed of material transport, understood as loss of humidity by the product. These phenomena are related by the following equation:

$$-m_c = \left[\frac{h_c S}{\Lambda\, u}\right](\theta_a - \theta_u)$$

where *Λ* u represents the latent heat of evaporation at wet bulb temperature. The convective heat transport coefficient *hc* is correlated with the mass flow rate of the air flow per unit surface area and therefore with the air speed, if divided by the density mass of the air:

$$[Kg/(m^2 s)] /(Kg/m^3) = (m/s)$$

The equations that correlate *hc* to the mass flow rate of the air are the following:

- when the air flow is parallel to the surface of the product *hc* =14.3 × $m^{0.8}$.
- when the air flow is perpendicular *hc* =24.2 ×$m^{0.37}$.
- where m represents the mass flow rate of air per unit area.

During this phase, in which, as has been said, evaporation occurs only from the surface of the solid, the drying time can be calculated starting from the following equation which can be written:

$$m_c = \frac{hc}{\rho \Lambda u x}(\theta_a - \theta_u)$$

where ρ represents the density of the solid (kg/m^3) and x represents the thickness of the product (layer) (m), considering that if the air hits the two upper and lower surfaces, x means the semi-thickness. Substituting and solving for time, we obtain:

$$t = \frac{\rho \Lambda u x(n_{si} - n_{scr})}{hc(\theta a - \theta u)}$$

where n_si indicates the initial absolute humidity (kilograms of water/kilogram of dry solids) and n_scr indicates the critical absolute humidity (kilograms of water/kilogram of dry solids). The critical humidity of the layer is not a constant and characteristic data of the product to be dried but depends on the trend of heat and material transport and on the thickness of the layer. It is the higher the thickness of the layer and the greater the $\Delta\theta$ between air and product. In other words, the faster the convective transport of heat and the transport of matter between the product and the air, the higher the critical humidity, and therefore the earlier the transition from the constant trend phase to the slow trend phase. Very often the constant progress phase is very short and strongly depends on the cellular structure present.

3.9.3 Slow-moving phase

At the end of the constant progress phase, the slow progress phase begins during which a humidity gradient forms within the product and the temperature gradually increases from that of the wet bulb to that of the dry bulb as the product dries. During this phase the surface of the product has an $a_w<1$ so there is no free water. Various expressions have been proposed to describe the progress of this phase. For small thicknesses compared to the surface and for long drying times, a simple expression that allows you to calculate the drying time between the beginning of the slow progress phase and the moment in which the product is in equilibrium with the humidity of the air used for drying, assuming some simplifications (air flow constant for example etc.) can be the following:

$$t = \frac{\rho x(n_{scr}-n_{se})}{hm(Ps-Pa)} ln \frac{n_{scr}-n_{se}}{n_s-n_{se}}$$

where n_{scr} represents the critical absolute humidity, n_s the equilibrium absolute humidity, n_s absolute humidity at time t, all in kilograms of water per kilogram of dry matter; h_m mass transport coefficient; Saturated vapor pressure at wet bulb temperature (torr); Pa partial pressure of vapor in air (torr); ρ density of the product (Kg/m^3) and x represents the thickness of the layer, or semi-thickness (m). If we consider that the steady-state phase is generally short, it is this last equation that describes the process. In practice, this equation derived from the theory of water vapor diffusion and from a series of simplified and reductive hypotheses, proves to be a good practical tool for the study of drying.

3.9.4 Different drying stages of sludge in convective heat transfer

As shown in Figure 3.8 the sludge drying process is generally divided into four phases: preheating phase, constant speed drying phase, first falling speed drying phase and second decreasing speed drying phase.

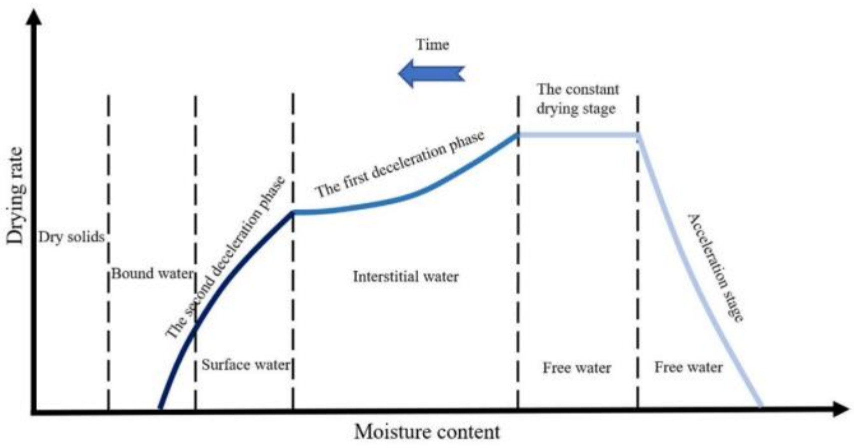

Figure 3.8 - Schematic diagram of sludge drying rate characteristics (adapted from Huang et al., 2016)

3.9.4.1 Preheating drying stage

This stage is mainly the process of preheating the wet sludge material, where a small amount of water is vaporized. The surface temperature of the thin layer rises rapidly due to the high driving force of heat transfer at the beginning of drying. Meanwhile, the drying rate also increases rapidly because the thin layer water with higher energy intensifies the irregular movement of water molecules and gas-liquid mass transfer (Huang et al., 2016) .

The initial temperature of the sludge is generally lower than the air temperature. The higher the initial temperature of the hot air, the shorter the preheating phase. At this stage, the diffusion resistance of water is lower than the evaporation resistance of surface water and free water is mainly removed.

3.9.4.2 Constant rate drying stage

When the sludge temperature reaches the wet bulb temperature, the drying rate reaches a certain value, and a constant rate drying phase occurs. In this phase, liquid water is present on the surface of the sludge particles and the heat transported by the hot air acts almost entirely on the surface of the sludge particles. This means that all the sensible heat supplied is converted into the latent heat necessary for the vaporization of the water and the surface temperature of the sludge is constant at the wet bulb temperature (Deng et al., 2015). As a result, both the surface temperature of the sludge and the evaporation rate of the water remain constant. In this phase mainly free water is removed.

3.9.4.3 First falling rate drying stage

In this phase, the diffusion rate of internal humidity gradually decreases compared to the rate of evaporation of humidity on the sludge surface, and mainly interstitial water is removed. Then, the drying rate begins to decrease until the drying moves to the second phase of decreasing rate. The dominant diffusion mechanism is due to the difference in moisture concentration and internal conditions (moisture content, temperature, and structure). The surface of the sludge gradually becomes dry, the temperature begins to rise exceeding the wet bulb temperature and the heat provided is partly used to vaporize the water and partly to heat the sludge.

3.9.4.4 Second falling rate drying stage

The temperature of the internal sludge drops slightly, approaching the dry temperature of the bulb of contained humidity. The average temperature is close to a fixed value and the mass transfer between the hot air and the sludge is close to equilibrium. In this phase the surface of the sludge is completely dried and the internal water spreads to the surface during evaporation. In this phase the sludge has a lower moisture content and high temperatures with weakening of heat transfer. Further removal of sludge moisture at this stage could destroy the sludge structure and lead to pore structure collapse. This stage mainly removes surface water and water-bound and the main dominant mechanism is vapor diffusion caused by the difference in moisture concentration and internal conditions.

3.9.5 Shrinkage and crack formation

The two phenomena that occur inside the sludge during the drying process are: shrinkage and crack formation. The shrinkage which begins immediately with the beginning of the process, consists in the reduction of the size of the product due to the loss of its water during the drying process, and continues at a constant rate until reaching a value of the V/V0 ratio between 0.4 and 0.2, where V is the measured volume and V0 the initial volume, depending on the origin of the sludge. Even the formation of cracks shows a constant increase up to values between 0.35 and 0.50 of the initial volume. However, this is greatly influenced by the operating conditions higher air speeds result in higher values of the V/V0 ratio.

Figure 3.9 - Crack formation

3.10 Sludge heat treatments

Digestion treatments (aerobic or anaerobic) and subsequent sludge dewatering allow to obtain a dry content not exceeding 30 - 40 % (by weight).

All this determines the need to dispose of large quantities of sludge (by weight and volume), often in landfills, due to the high-water content still present in it. The thermal treatment of sludge aims to drastically reduce the water content of the sludge and therefore the quantities in weight and volume to be disposed of. There are three technological options that can be used for this purpose:

- *High temperature drying*: the sludge is brought to a temperature of approximately 120 °C, at which the interstitial and capillary water are released, or up to 180 °C, at which the bound water is also released. In the first case, dry contents of 90 % can be obtained, while higher values can only be obtained in the second case (in fact the bound water is equal to approximately 10 % in wet weight); at these temperatures the composition of the dry substances does not change, so the organic substance content of the sludge remains unchanged: this can constitute an advantage, if an agronomic use of the sludge is foreseen. Thermal drying is a process capable of achieving dry matter contents above 90 %. From this process a stabilized and sanitized product with homogeneous grain size is obtained. The sludge brought to a temperature (approx. 180 °C) is freed from bound, interstitial, and capillary water. The drying of the sludge is achieved by contact with a hot carrier fluid through:
  - *Indirect contact*: between the heating fluid and the sludge there is a surface through which there is heat conduction.
  - *Direct contact:* the heating fluid is in direct contact with the sludge.
  - *Mixed contact:* the contact is partly direct and partly indirect.
- *Low temperature drying:* the sludge is deposited on a bed in a controlled atmosphere and mixed there.
- *Incineration:* in this case the sludge is brought to temperatures of around 600 - 900 °C, thus allowing not only the separation of the water content but also the combustion of dry organic substances. It is thus possible to treat even a sludge that has not been previously stabilized and obtain a residue having a dry substance weight content equal to approximately 20% of the initial value.

From a technical point of view, the main advantages that can be achieved with the thermal drying of sludge, in addition to the significant reduction in the quantities to be handled, are the following:

<u>*For disposal in landfill*</u> (Figure 3.10):better handling of the product (this characteristic makes dried sludge more welcome by landfill managers; sanitation of the product (the thermal process guarantees the destruction of pathogenic agents); possibility of use for the daily coverage of waste, instead of the inert material conventionally used.

Figure 3.10 - Landfill disposal

For reuse in agriculture (Figure 3.11): better handling of the product (in particular if the sludge is in granular and bagged form); product sanitation; possibility of storage in the months in which spreading is not permitted, thanks to the reduced volumes and the good stabilization graph (the almost total elimination of the water excludes the subsequent onset of putrefactive phenomena); amending power (since it is not a combustion process, drying keeps the organic substance content in the sludge unchanged).

Figure 3.11 - Reuse in agriculture

Incineration (Figure 3.12): better handling of the product and high calorific value, achieved thanks to the elimination of water. Although it presents undoubted advantages, it generally requires high energy consumption; in fact, with the normal dry contents of a sludge subjected to mechanical dehydration (30 - 40%) and with the typical values of the typical LCV for sludge (5000 Kcal/Kg SSV), one would obtain, in the hypothesis of humidity of 60% and a VS/TS ratio=0.4 a LCV value of approximately 800 Kcal/kg of sludge (in wet weight). In such conditions it is very difficult to obtain combustion without auxiliary fuel, especially considering the high temperatures imposed by the law for post-combustion (950°C).

Figure 3.12 - Incineration

3.11 Drying beds

Drying beds are generally used to dehydrate digested and thickened sludge from plants using the activated sludge treatment process without pre-thickening. They are therefore used for small and medium-sized communities (< 20,000 PE).

In a typical drying bed, the sludge is placed on layers of sand and gravel of various grain sizes and left to dry by gravity and evaporation from the surface exposed to the air. The drying beds are equipped with lateral drainage lines, using perforated plastic or clay pipes, are inclined by at least 1 % and spaced 2.4 - 6 m apart.

The area is generally divided into rectangular beds, with a ratio between the short side and the long side typically ranging from 1:3 to 1:6. Each individual bed is usually enclosed by a reinforced concrete wall cast in place or by prefabricated concrete slabs. The drainage layer commonly has an average thickness of 300 to 400 mm; the upper layer of sand, with a grain size between 0.3 and 0.75 mm, is typically around 5-10 cm thick. Deeper layers of sand generally delay the drainage process. The underlying layers consist of gravel and larger stones, with increasing grain size towards the bottom (Faragò et al., 2021).

The sludge is generally fed via an open channel or closed pipes. Furthermore, splash plates are positioned in front of the sludge outlets to spread the material over the bed and prevent sand erosion.

The sludge loading rate varies from 50 to 125 Kg/ (m^2 year) for open drying beds and from 60 to 200 Kg/ (m^2 year) for covered beds (Faragò et al., 2021) .

When the SS content in the sludge reaches values of approximately 30% (Nivala et al., 2017),, the sludge removal is carried out in the limited surface beds by manual shovelling while in the larger one’s small mechanical shovels can be used.

It should also be underlined that for closed drying beds SS values of up to 75% can be achieved.

Due to the unpleasant Odor, drying beds should be positioned at a sufficient distance from surrounding settlements and houses depending on their type and local situation. However, drying beds require large spaces on land, long dehydration times, have low flexibility, require already stabilized sludge, the design must take the climate into consideration and the removal of the dried sludge requires intense work. Therefore, the disadvantages related to this technique are the high requirement of large areas of land, the sensitivity of the process to climatic conditions, and the emission of unpleasant Odors.

Among the advantages are:

- Low cost of capital if land is available.
- Does not require specialized operators.
- Low energy consumption.
- Little or no consumption of chemical additives.
- Not very sensitive to sludge variability.
- Higher solids content than mechanical methods.

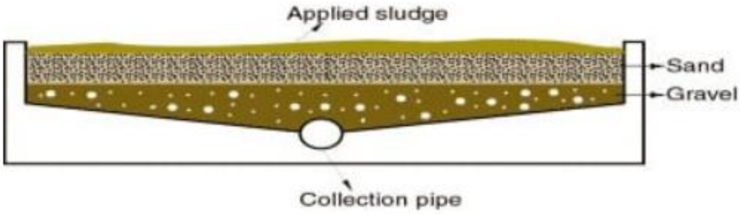

Figure 3.13 - Typical drying bed (adapted from Nivala et al., 2017)

4 Solar drying of sludge

4.1 Review of literature about Solar Greenhouse

The application of free solar energy can be an alternative solution to reduce the cost of the drying process. However, in contrast to drying with constant conditions, the drying kinetics obtained during solar drying exhibit some variations, as the operating conditions continuously change over time. It was found that as operating conditions vary, the sludge adapts its behaviour to the new conditions by varying the common direction of its drying kinetics with an instantaneous reaction and adaptation time.

Greenhouse drying beds represent a method of improving the dewatering and drying yields of liquid, thickened or dewatered sludge. Solar drying has become the best suitable solution for sludge dehydration in treatment plants with medium capacity and less than 100,000 population equivalents. This alternative to the classic thermal drying process is used to meet the needs of communities in compliance with regulations. Solar radiation represents the major source of energy for drying. Solar drying allows the dehydration of the sludge via solar radiation in special greenhouses, obtaining final SS contents of approximately 85 %(Suez, n.d.). This process consists of an economically and environmentally favourable solution.

EPA have classified biosolids into two distinct camps. The first are Class A biosolids, which are the highest quality. Any solids that do not quite meet these standards will be sorted into Class B biosolids. While this is a simplified version of the process, there are lots of different things that must be considered to ascertain overall quality. Class A biosolids are most typically produced by anaerobic digestion and extra treatments, like heating, pasteurization, composting.

Solar drying systems are usually not used for undigested primary sludge due to the production of unpleasant odors and the high final dry matters (DM) content, above 90 %, required to be included in class A- biosolids (defined as solids coming from wastewater treatments which, after stabilisation, can be used as an agricultural soil improver). Biosolids, to be disposed of without restrictions in agriculture, must comply with rigorous standards regarding metal content, odors and the attraction of possible disease vectors, with practically undetectable concentrations of pathogens.

This technology is therefore used more with stabilized sludge, which falls into class A of biosolids with lower SS values (SS of 75 %). The greenhouses used generally consist of a rectangular base, a translucent chamber, sensors to measure atmospheric conditions, air deflectors, circulation and ventilation fans, a mobile electromechanical device that agitates and moves the dried sludge, and a microprocessor that controls the environment. This system also allows the dehydration of liquid sludge but requires larger areas and often this factor reduces the advantage deriving from mechanical elimination and dehydration. Solar drying is best suited for tropical or arid environments; however, there are also installations in northern countries or in the mountains. The advantages include very high solids content, it does not produce odors, reduced operating and maintenance costs and a high level of automation.

The advantages of solar greenhouses are:

- Dehydration temperature up to 10 - 11°C higher than the external temperature (solar radiation and external air temperature process variables).
- Air speed control with appropriate sizing of the fans (forced convection VS natural convection).
- Protection from precipitation and external pollutants.
- Reduction of the quantity of sludge by 3 to 4 times.
- Use of renewable energy.
- Process with reduced carbon footprint.
- Inclusion of treatments for the reduction of odors and pathogenic substances (conveyed emission VS diffused emission).
- Sanitization of sludge.
- Introduction of an automatic mixer for the homogenization of the sludge layer.

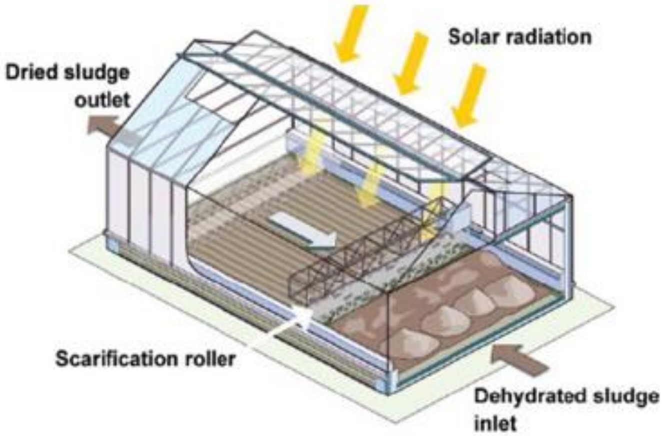

Figure 4.1 - Greenhouse (adapted from Suez, n.d.)

Greenhouse basically operates either in passive (natural convection) or active mode (forced convection) (Nayak & Tiwari, 2008).

Figure 4.2 shows the classification of greenhouse solar dryer based on literature review.

As noted by (Singh et al., 2018) there are various greenhouse configurations. In the passive mode of greenhouse dryer, ventilator or chimney is provided at the chimney for the natural circulation of air entering inside the dryer. While in case of the active dryer, exhaust fan is provided for moving humid air outside the dryer. Various modifications and research have been done to improve the greenhouse dryer's performance. Some of the modifications implemented on active and passive greenhouse solar dryers in literature are:

- PV (Photovoltaic) integrated greenhouse solar dryer.
- Used opaque northern wall to insulate it and prevent heat loss.
- Used thermal storage materials such as sand, rock-bed, black painted concrete floor and PVC sheet. So that greenhouse can be used during off sunshine period.
- Inclined and reflecting north wall to collect maximum radiations.

- Using greenhouse coupled with solar air heater to achieve faster drying.
- Provided additional area enhancing panels to increase drying area.

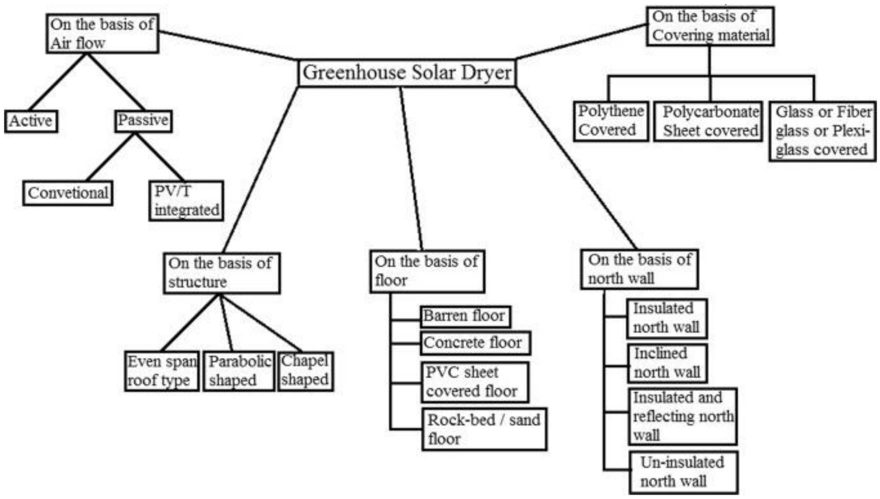

Figure 4.2 - Classification of greenhouse solar dryer (adapted from Singh et al., 2018)

All existing solar greenhouses have a very similar design. They consist of a greenhouse structure with a transparent roof, and the sludge is spread on a paved surface. The solar radiation directly reaches the layer of dry matter, passing through the transparent roof, and provides the heat necessary to evaporate the residual humidity.

According to (Gomes et al., 2023)greenhouse geometry is essential for the drying system. As reported in Figure 4.3 there are different greenhouse shapes. The “arch shape” and the “spherical shape” are the most used globally. The chapel greenhouse option should be preferred for better reception of solar radiation during winter and summer. An appropriate geometry and orientation should improve the radiation incident intensity to the greenhouse’s internal surfaces. An east-west orientation for greenhouse drying should be to use to maximize the use of solar radiation. The material used to cover the greenhouse should have high transmittance. For instance, polyethylene has a high transmittance; besides, it is relatively not expensive and easily installed. The greenhouse geometry is only one of the different important factors of drying systems.

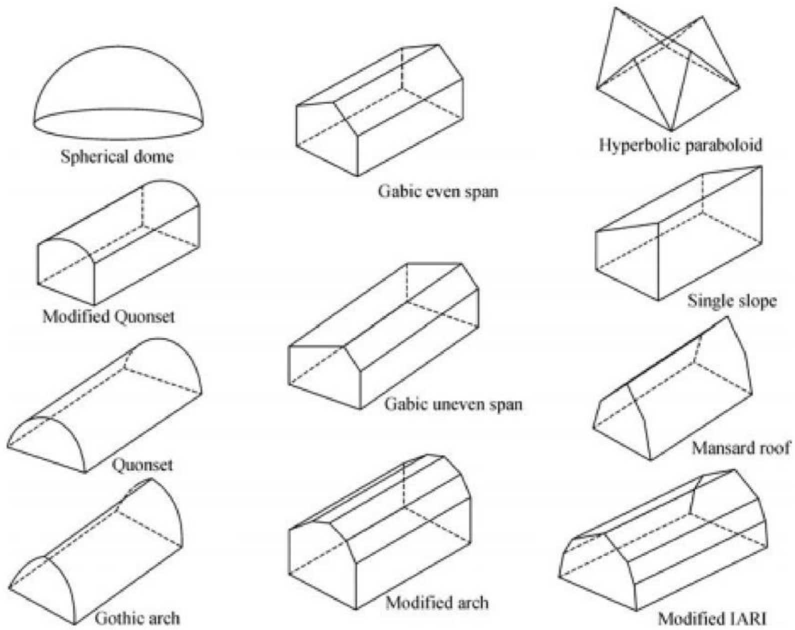

Figure 4.3- Different shapes of greenhouse (adapted from Gomes et al., 2023)

They analyzed the drying efficiency, specific energy consumption, and drying rate in three different conditions while drying white saffron. The conditions examined included mixed mode drying (Figure 4.4-a), indirect drying (ISD) (Figure 4.4-b), and open drying. In each experiment, a 20 kg sample of sliced saffron was subjected to solar drying. Thermal modelling of the drying processes was conducted, calculating thermal efficiency as the ratio of energy transmitted to the air to the energy absorbed by the collectors. The dryer efficiency was determined as the ratio of the energy required to evaporate water to the total energy available for drying. The ambient temperature varied between 20 and 25 °C, with relative humidity between 70 and 80 %. Inside the greenhouses, the average temperature was 47.6 °C for mixed mode drying and 36.1 °C for indirect drying. A constant airflow of 0.042 kg/s was maintained for both processes. The average drying rates were 0.1018 g.w/g.d.b-min for mixed mode, 0.0763 g.w/g.d.b-min for ISD, and 0.0354 g.w/g.d.b-min for open drying. The authors concluded (Gomes et al., 2023) that greenhouse drying in mixed mode can save 62 % of drying time compared to open drying, and the efficiency of drying in mixed mode was 17 % higher than that of

ISD. In Figure 4.4, two configurations of drying chambers are shown, where hot air generated by solar panels is introduced.

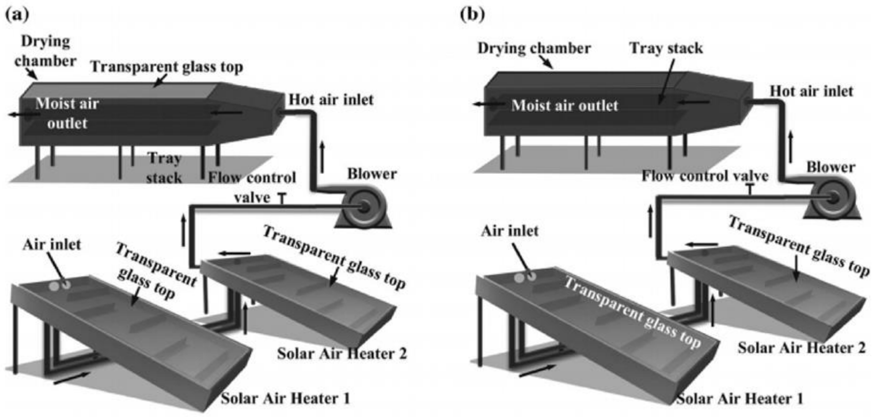

Figure 4.4 - Schematic view of mixed mode and ISD mode solar dryers (adapted from Gomes et al., 2023)

One of the first sewage sludge solar dryer in Poland was a pilot plant in Skarżysko-Kamienna. Their design includes a light steel structure settled on a plate of impervious concrete and covered with polycarbonate plates. Inside the facility a ventilation system and installation for sludge shuffling was installed. The ventilation system was designed to provide uniform air distribution over the surface of dried sludge through the number of nozzles (Badyda & Krawczyk, 2008). Designing the drying processes in which the surface of a dried body contacts with the drying gas blown from a nozzle is very difficult. This is because conditions of heat and mass transfer between the humid surface and blown gas vary depending on the distance from the nozzle axis. Additional difficulty is introduced by the heat flux resulting from solar radiation.
Another work that aims to contribute to the optimization of the solar sludge dryer is that conducted by (Ali et al., 2016) at the wastewater treatment plant of the city of Marrakesh through an experimental study in a forced convection solar dryer live. The drying kinetics were studied at three temperatures 50, 60 and 90 °C for an air flow rate set at 0.0083 m^3/s. The drying speed was determined empirically from the drying characteristic curve. Then the influence of the speed of the heated air, the air temperature, and the humidity content of the air on the drying kinetics of the sludge was studied.
The experimental apparatus used to study sludge drying is an indirect forced convection solar dryer, made up of shelves and with total or partial air recirculation. This dryer allows you to produce a flow of hot air with aerothermal temperature and air flow characteristics.

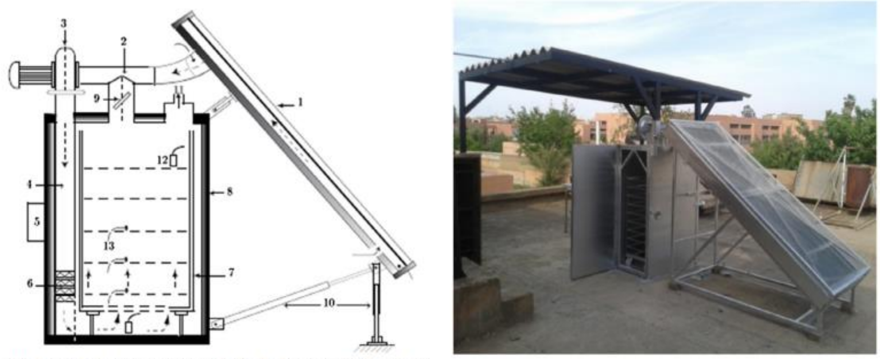

(1) solar collector, (2) ventilation duct, (3) fan, (4) suction line, (5) control box, (6) power supply, (7) floors, (8) drying cabinet, (9) air valve, (10) air inlet, (11) air outlet, (12) humidity probe, (13) thermocouple.

Figure 4.5 - Convective solar dryer installed in Marrakech (adapted from Ali et al., 2016)

The components of the dryer are (Figure 4.5):

- A solar collector.
- An aspirating aeraulic channel constituted of tunnel.
- A drying chamber consists of ten floors in trays.
- A centrifugal fan with a regulator which allows to vary the air flow rate.
- A thermo-regulator.
- Electrical resistances of power acting as auxiliary source.

In the study of (Ali et al., 2016), the most influential parameters of kinetics drying are temperature, the flow rate and relative humidity of drying air.
The principle of the experiment consisted of monitoring the variation of the moist mass product Mh(t) (product wet mass (kg) over time by performing rapid weighing outside the dryer. At the beginning of the experiment, the time interval between two successive measurements was 5 minutes. This interval gradually increased as the mass loss decreased, reaching a maximum of 40 minutes at the end. The drying experiment was terminated when three consecutive measurements of the sample mass displayed a difference of about 0.1 g. The experimental conditions were determined based on the values assigned to each of the aero-thermal variables. For each trial, the procedure was the same: the temperature was kept at the chosen values, while the flow rate was fixed at 0.083 m^3/s.
The operational parameters for the three drying experiments included drying time, initial and final moisture content, flow rate, and drying duration. The experiments were carried out at three different drying air temperatures: 50, 70, and 90 ± 0.3 °C. From it, Figure 4.6 and Figure 4.7 were particularly interesting, as they allowed observation of the evolution of moisture content and reduced moisture content of the sludge over time for all three experiments.

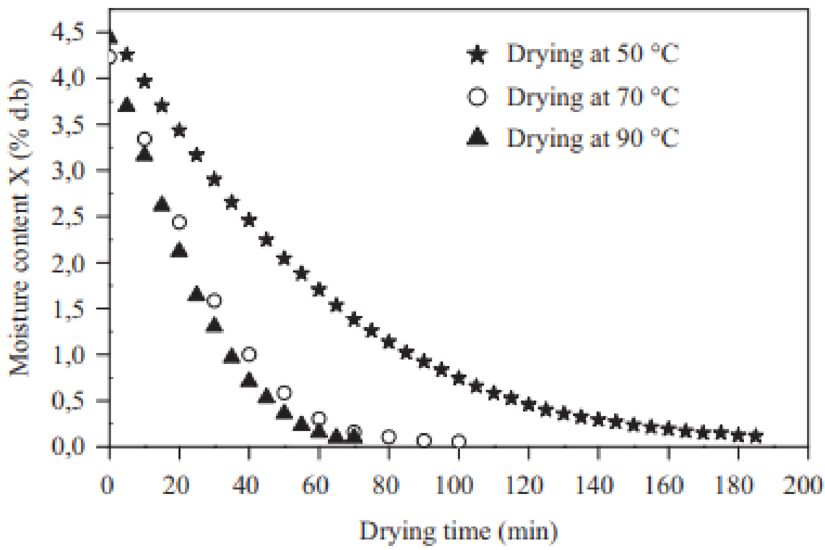

Figure 4.6 - Evolution of the moisture content of sludge versus the drying time for different conditions of drying air (adapted from Ali et al., 2016)

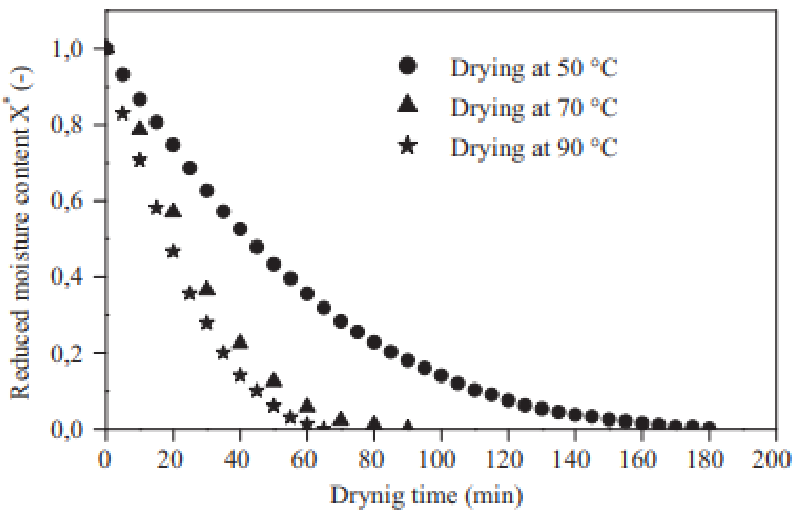

Figure 4.7 - Evolution of the reduced moisture content of the sludge versus the drying time for different conditions of drying air(adapted from Ali et al., 2016)

It was also noted the presence of two phases, I and II, in the drying curves of sewage sludge (

Figure ***4.8***). During the first phase, the heated air is used to evaporate the product water (generally represented by a constant velocity of drying). However, in the second phase the acquired energy was used to evaporate water from the product and to increase its temperature. This effect is represented by the decrease in the drying rate.

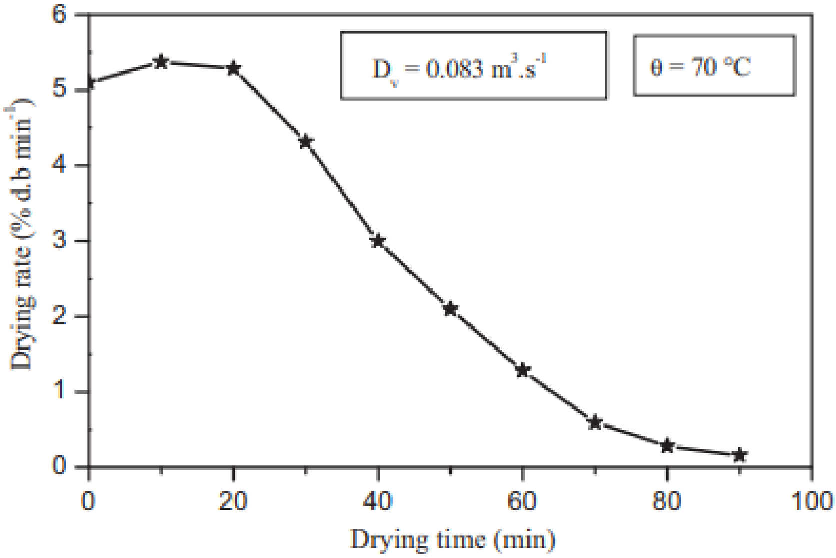

Figure 4.8 - Evolution of the drying rate (versus) the time for the temperature 70°C (adapted from Ali et al., 2016)

At the same air flow rate, it was noted that the drying rate continuously increased with the rise in temperature and moisture content (Figure 4.9).

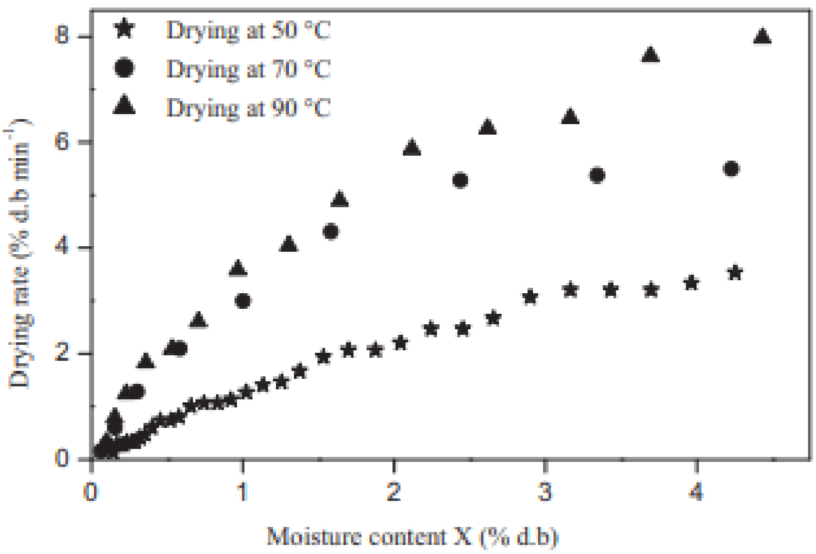

Figure 4.9 - Evolution of the drying rate versus the moisture content of the sludge for different conditions of drying air (adapted from Ali et al., 2016)

In the solar drying process of sludge, there are many factors that influence the drying rate. In (Bennamoun, 2012), the effect of air temperature and flow rate on the sludge drying rate was studied. In (An, 2017), the influence of solar radiation intensity on the drying characteristics of the sludge was examined. When the solar radiation intensity is higher, the final moisture content of the sludge is lower (Figure 4.10).

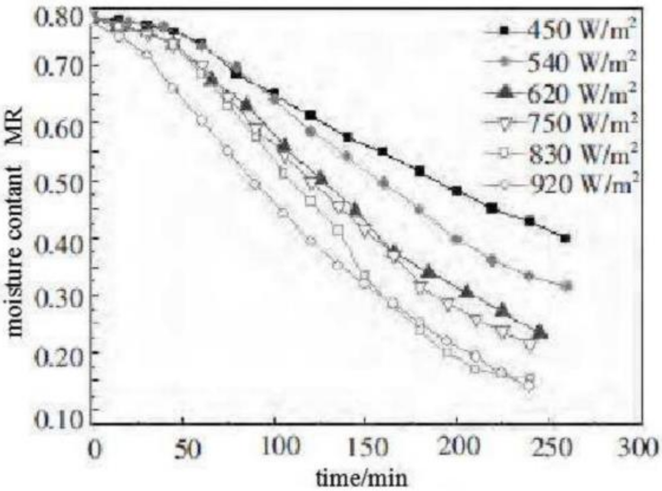

Figure 4.10 - Changes of water content of sludge under different solar radiation intensity in the exposed solar drying system (adapted from An, 2017)

The intensity of radiation is directly related to the sludge drying rate. In (Lei et al., 2009)the main changes in the sludge parameters in the solar greenhouse, without the use of auxiliary heating devices, were studied. The study observed that temperature and humidity in the solar greenhouse were the primary factors affecting the drying rate.

In a study by Zhang Yunyue reported in (An, 2017) research was conducted on sludge drying using solar greenhouses and ventilation cabins. During the summer trials, the sludge was spread on the floor with a thickness of 25 cm. A reduction in moisture from 90% to 34% was observed after 6 days. The study revealed that:

1. By using solar energy to dry the sludge, a savings of approximately 21 MJ in energy consumption can be achieved for each kilogram of sludge weight reduction.
2. The drying rate of sludge varies with different thicknesses.

In (Zheng et al., 2021b), a further laboratory-scale study (Figure 4.11) was conducted to evaluate the effects of air parameters (temperature, velocity, and relative humidity) on the drying characteristics of sewage sludge.

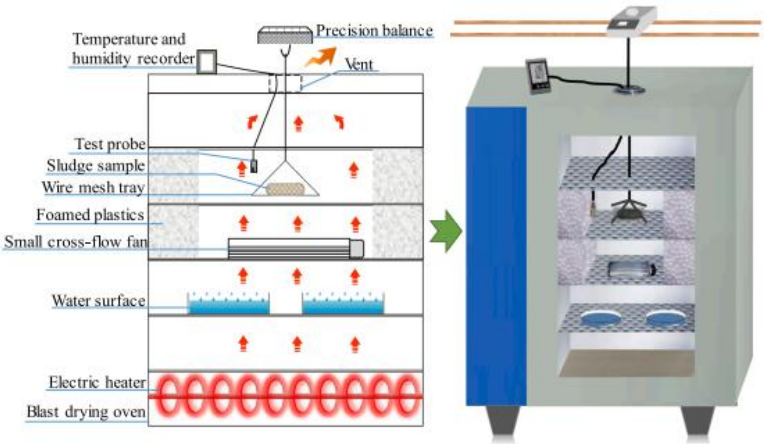

Figure 4.11 - Drying experiment table setup (adapted from Zheng et al., 2021b)

In Figure 4.12 shows the sludge drying process corresponding to different temperatures with a relative humidity of 20 % and an air velocity of 1.0 m/s. As shown in Figure 4.12 (a-b), the sludge moisture content decreases over time, and the drying time reduces with an increase in temperature.

For instance, the drying time at 70 °C is half that at 40 °C when the sludge moisture content is 30 %. When the drying temperature is 40 °C, the drying curve decreases more gently. As the drying temperature increases, the drying curve gradually becomes steep. These changes in the drying rate can be seen in Figure 4.12 (c). The drying rate reaches its maximum value after a short rapid rising stage, then decreases over time. Figure 4.12 (d) shows the drying rate curves of sludge at different temperatures. The results illustrate that temperature has a significant effect on the drying rate.

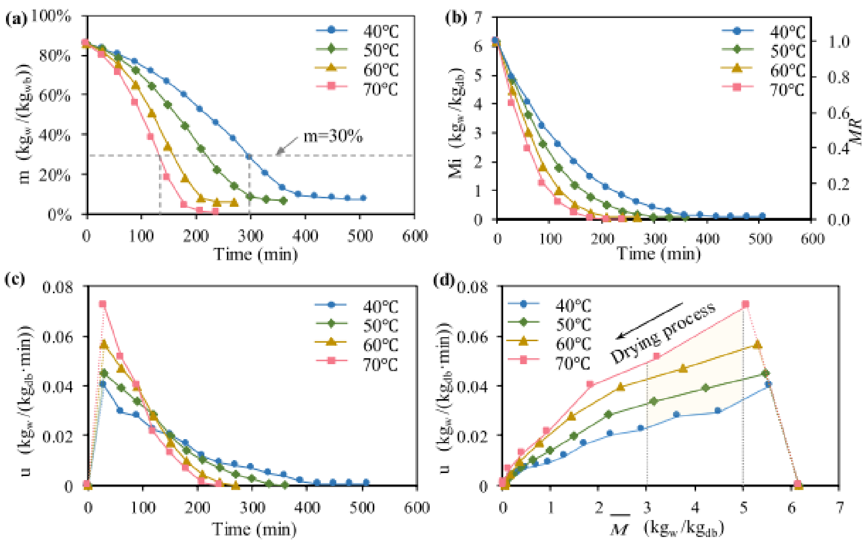

Figure 4.12 - Variation of the moisture content and drying rate for different temperatures, a relative humidity of 20%, air velocity of 1 m/s (a) Moisture content (wet basis) vs. time; (b) Moisture content (dry basis) vs. time and moisture content ratio vs. time; (c) Drying rate vs. time; (d) Drying rate vs. moisture content (dry basis). (adapted from Zheng et al., 2021b)

Figure 4.13 presents the influence of air velocity on the drying process. Figure 4.13 (a) represents the drying curves for different air velocities at 50 °C and 70 °C. At different temperatures, the increase in air velocity reduces the drying time of sludge. The required drying time corresponding to different air velocities are reported in Figure 4.13 (b). Figure 4.13 (c) depicts the drying rate curves for different air velocities at 50 °C and 70 °C. The results clearly show that air velocity can increase the drying rate. The increase in air velocity indicates that more air contacts the wet sludge, which can carry away more moisture. Moreover, a higher air velocity causes the thickness of the sludge surface boundary layer to be thinner, and the heat and mass transfer coefficients of the sludge are improved. Finally, the increase of the air velocity accelerates the cracking of sludge, and the new crack can lead to a faster drying rate. Figure 4.13 (d) shows as the air velocity increases from 1.0 m/s to 2.0 m/s, the reduction of drying time becomes smaller (the reduction rate from 1.0 m/s to 1.5 m/s is 27 – 45 %, and the reduction rate from 1.5 m/s to 2.0 m/s is 9–24%). We can reasonably speculate that when the air velocity increases beyond a threshold value, it has little effect on the sludge drying rate. In addition, air velocity increases the power consumption of fans and causes dust handling problems.

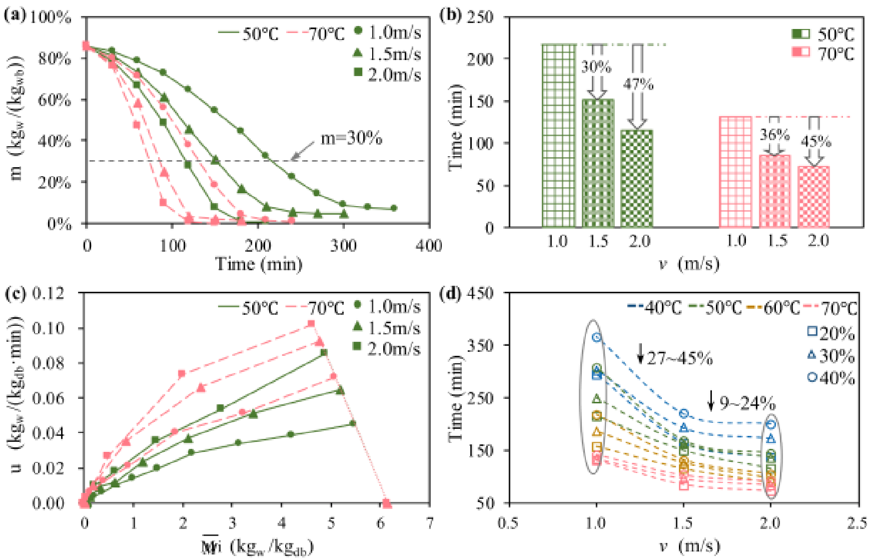

Figure 4.13 - Drying process for different air velocities, temperatures of 50°C and 70 °C, relative humidity 20% (a) Moisture content (wet basis) vs. time; (b) Drying time needed at different air velocities; (c) Drying rate vs. moisture content (dry basis)) and variation of drying time needed at different air velocities (d) (adapted from Zheng et al., 2021a)

Figure 4.14 clearly shows the drying difference caused by relative humidity under different temperature and air velocity conditions. The drying rate of sludge increased with the decrease of relative humidity. When the relative humidity is low, the humidity gradient between the sludge and the air is large, and water enters the air more easily. In Figure 4.14 (a-c) is shown that when air velocity increases, the effect of relative humidity on the drying rate is evident.

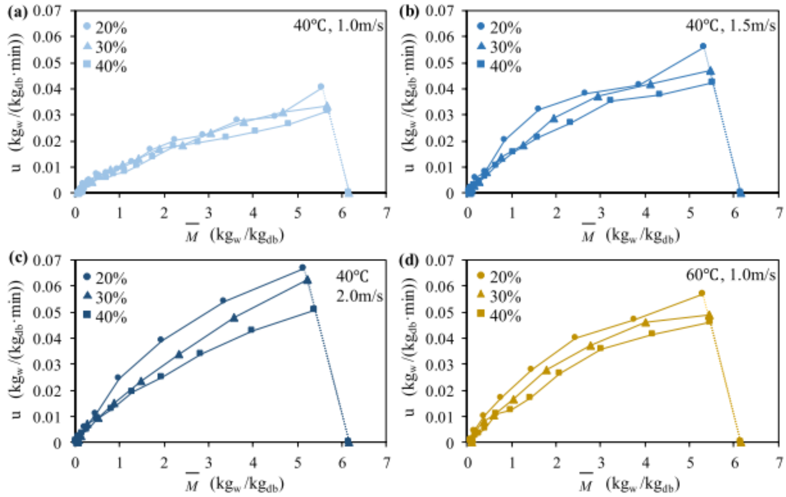

Figure 4.14 - Variation of drying rate for different relative humidity values (adapted from Zheng et al., 2021b)

As observed in (An, 2017), regardless of whether solar radiation acts directly on the material or not, solar drying systems can be categorized into two types: open solar dryers and covered solar dryers.
As shown in Figure 4.15, the sludge drying system is a covered type with a roof height of 2.5 meters. The enclosure was made of 10 mm transparent polycarbonate sheet with an 80% light transmission. The internal environment was controlled using a fan to manage humidity levels. The drainage layer consisted of a rock bed made of stones with a diameter of 48 mm and a thickness of 50 cm.

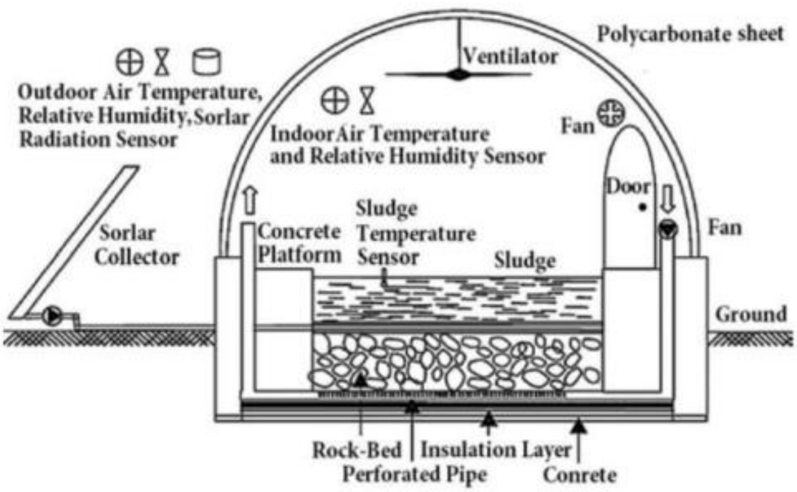

Figure 4.15 - Diagram of the Covered Solar Drying System (adapted from An, 2017)

In (Viega Group, 2021)has been described the largest solar-thermal sewage sludge drying plant in the world is the one in Bottrop, Germany. In this plant to be able to incinerate the 120,000 tons of sludge per year in the 2 furnaces of the adjacent heat-energy cogeneration plant at approximately 450 °C, the sludge must have a precise degree of drying. The optimal dry matter content is between 60-70 %. Previously, this result was achieved by adding 20,000 tons of hard coal during the incineration process; In the future, thanks to the solutions of the Emscher hybrid energy plant, the solar-thermal drying plant (STP, Figure 4.16) will aim to reduce this quantity as much as possible, minimizing combustion to contribute to protecting the environment and preserving precious resources at the same time.

Figure 4.16 - Sludge drying chamber in Bottrop WWTP (adapted from Viega Group, 2021)

To reach the milestone, the sewage sludge will be pre-dried in 32 chambers. Built as greenhouses, the drying chambers are located on approximately 61,000 m² of unsolidified soil, the former site of the sewage sludge basins. In the glassed chambers, the sludge is dried between 10-14 days under sunlight and moved regularly by an automated process another exemplary proof of environmental responsibility. In case of insufficient sunlight, the unit heaters arranged under the roofs of the rooms can be powered by the combined cycle plant itself or by a four-stage cascade cogeneration plant with a thermal output of 10 MW. One aspect in particular highlight the size of the plant in terms of capacity: every year, approximately 100,000 m³ of water evaporates from the sludge when the drying plant operates at full power. A sewage sludge drying plant on this scale is a huge step forward, especially when compared to similar plants built in the past, which reached a maximum of 10% of the treatment capacity of the current one.

The solar-thermal drying plant is part of the "Emscher hybrid energy plant", which allows saving up to 70,000 tons of CO_2 per year from electricity production thanks to 5 renewable energy sources:

- 1 wind turbine with a power of 3.1 MW.
- 4 new cogeneration plants, each with a power of approximately 1.2 MW.
- 1 photovoltaic system extending for approximately 500 m^2.
- 1 steam turbine with a power of at least 4 MW and obviously 1 solar-thermal sewage sludge drying system.

Another solar greenhouse is reported in (Enox SP, 2018). The technology developed at UCB Warsaw University of Technology assumes as a basis the use of sunlight energy in properly constructed halls allowing the greenhouse effect to take place. The halls are equipped with the following installations:

- Ventilation installation.
- Heating installation powered with heat from external sources (option).
- Automation and control system.
- Turner installation.

One of the key equipment of the technology is the control system, including the ventilation control system. The ventilation system control algorithm is responsible for switching on the exhaust fans to exchange the air inside the dryer. The control algorithm allows optimal air movement in a solar drying hall regardless of local atmospheric conditions. The key parameter is the potential for moisture collection of the drying air. Based on measurements of temperature and humidity of the air outside and inside the dryer, the drying potential of external and internal air is determined. The internal air potential (usually heated but with higher humidity) is compared with the outside air potential (usually cooler but drier). If the internal air potential is higher than the air should not be exchanged inside the dryer. Otherwise, the exhaust fans responsible for the air exchange in the dryer should be temporarily turned on. Control system is based on programmable controllers that manage the whole drying process.

Figure 4.17 - Solar Greenhouse (adapted from Enox SP, 2018)

4.2 Greenhouse gas emissions of sludge treatment

The rise in greenhouse gas (GHG) emissions in the atmosphere is widely recognized as the primary driver of global warming and climate change. Among the significant sources of these emissions are wastewater treatment plants (WWTPs), which release gases such as carbon dioxide (CO_2), methane (CH_4), and nitrous oxide (N_2O). Excessive greenhouse gases disrupt the Earth's energy balance, leading to extreme weather events. To achieve net-zero emissions by 2053, as outlined in the Paris Climate Agreement, water and wastewater utilities are at the forefront of efforts to reduce GHG emissions.

However, the carbon footprint associated with various treatment technologies and their contribution across different units within each WWTP configuration remains unclear. Carbon footprint analysis is a crucial tool for assessing the impact of WWTPs on climate change, focusing on CO_2, CH_4, and N_2O.

CO_2 emissions in WWTPs are primarily linked to energy consumption. High-energy units, such as those involved in biological treatment (aeration), pumping stations, and sludge management equipment, are the main sources of CO_2 emissions from electricity use. The global warming potential of GHGs like CH_4 and N_2O generated in treatment plants can be compared by converting them into carbon dioxide equivalents (CO_{2eq}). According to the literature, N_2O and CH_4 emissions from wastewater treatment and discharge accounted for 2.6 % and 3.6 % of total CO_2 emissions in industrialized countries in 2018, respectively.

CH_4 emissions originate from anaerobic ponds, biological treatment processes, and advanced treatment methods. In 2018 and 2019, the total CH_4 emissions from the plant were 8,548 and 45,061 tCO2eq, respectively, while N_2O emissions were 3,401 and 4,562 tCO2eq. As illustrated in Figure 4.18 the largest portion of indirect emissions in 2018 was from electricity consumption, totalling 1,800 tCO2eq (Karakas et al., 2024).

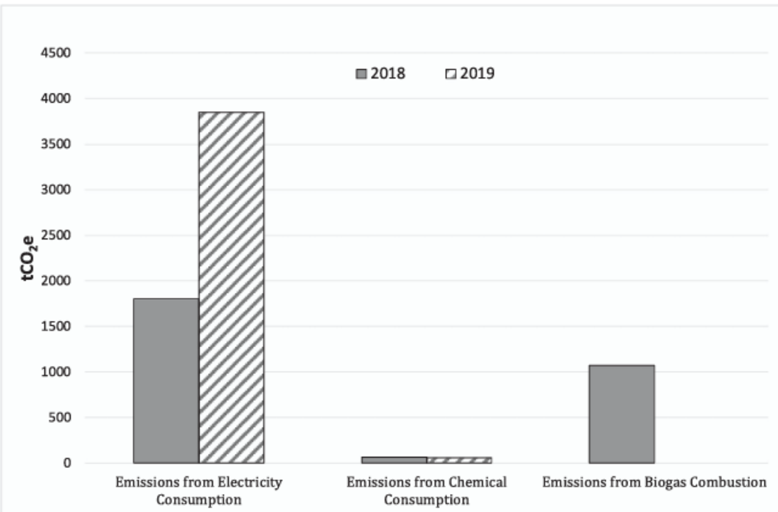

Figure 4.18 - Indirect greenhouse gas emissions of Advanced Biological WWTP for 2018 and 2019 (adapted from Karakas et al., 2024)

In the context of sustainable wastewater management, it is essential to implement measures to reduce greenhouse gas emissions, even though wastewater treatment plants are generally a minor source of such emissions compared to other municipal sectors. Understanding the production and emission pathways will help in developing early warning systems and operational strategies to mitigate greenhouse gas emissions, thus contributing to a reduced carbon footprint for wastewater treatment facilities. Additionally, since wastewater treatment plants are significant point sources of greenhouse gas emissions, they offer potential for more cost-effective solutions for emission reduction (Figure 4.19) (Kosse et al., 2016).

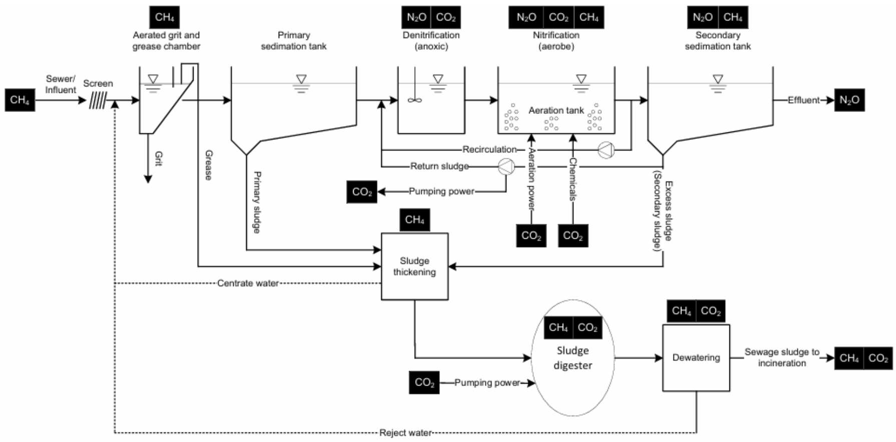

Figure 4.19 - Schematic overview about main greenhouse gas emissions (adapted from Kosse et al., 2016)

Sewage sludge can be treated through various methods, including composting, anaerobic digestion (AD), incineration (both mono- and co-incineration), hydrothermal treatment, or lime stabilization. In Europe, the main methods for sludge treatment are using it as a fertilizer for agricultural soils, composting, incineration, and landfilling. The treatment alternatives studied included: pile composting, anaerobic digestion, thermal drying followed by incineration, and incineration without prior thermal drying(Piippo et al., 2018).

CH_4 emissions from the storage and dewatering of digested sewage sludge account for between 2 % and 4.5 % of the total CH_4 production (Parravicini et al., 2016).

Mechanical dewatering, typically performed using centrifuges or filter presses, is often enhanced by adding coagulating or flocculating polymers. The consumption of flocculating polymers for both raw and digested sludge follows a normal distribution, with average values of 7.0 ± 4.2 kg/t Total Solids input and 10.6 ± 4.6 kg/t TS input, respectively. Similarly, electricity consumption also follows a normal distribution, with average values of 1.7 ± 0.2 kWh/t wet weight input for raw sludge and 7.3 ± 1.2 kWh/t wet weight input for digested sludge.

Thermal drying (TDR) is modeled as a belt dryer that uses heat to raise the drying temperature above 100 °C. Assuming that the carbon transfer coefficient to the exhaust air is equivalent to that of Volatile Solids, carbon is released as CO_2 into the atmosphere. Energy consumption for this process is estimated to be 2.2 ± 1.0

MJ per kg of wet weight, with heat accounting for 82 % and electricity for 18 % (Chang et al., 2023).

Moreover, energy consumption and chemical usage in wastewater treatment plants (WWTPs) have an indirect impact on their carbon footprints. A report indicates that managing sewage sludge outside of WWTPs could account for up to 40 % of additional greenhouse gas emissions beyond those from the standard wastewater treatment process. GHG emissions from WWTPs are divided into direct and indirect categories. Direct emissions occur within the plant and result from activities that release GHGs (e.g., CO_2, CH_4, and N_2O) into the atmosphere. Indirect emissions are related to activities within the plant but manifest outside of it. In this study, the main sources of indirect emissions were the consumption of electricity and chemicals, as well as the disposal of dewatered sludge (Shahid & Choi, 2023).

5 Plants bench scale

The experimental activity carried out has allowed for the development of an efficient and innovative system for the dewatering of wastewater sludge. This activity was divided into several phases:

1. Plants Bench Scale: to investigate the impact of optimal sludge thickness and specific airflow on sludge drying kinetics, a bench-scale plant was designed, constructed, and tested. Two distinct tests were carried out.
2. Greenhouse Prototypes: the results obtained from the Plants Bench Scale enabled the design of solar greenhouse prototypes. Throughout the entire experimental period, seven tests were conducted. The different configurations varied in: (a) the point of entry of the hot air, (b) the flow rate of the air introduced, (c) the thickness of the sludge introduced, and (d) the season in which the test was conducted. These configurations aimed to test the efficiency of these treatment systems under different operating conditions.
3. Scale-up Project: the design and construction of a full-scale solar greenhouse was essential for understanding and analysing the innovative sludge dewatering process in a plant with full-scale treatment capacity. During this period, two tests were conducted with different loading and unloading cycles of the sludge. This was done to understand the influence of the dehydrated sludge layers beneath the fresh ones on the dewatering process.

In subsection 5.1, the bench-scale experimental activity was described in order to evaluate the influence of some operational parameters on the sludge dehydration process.

5.1 Materials and methods

To study the effect of optimal sludge thickness and specific air flow on sludge drying kinetics, a bench-scale plant was designed, built, and tested. Specifically, two different tests were conducted.

The choice of operational parameters on which to base the bench-scale tests was made based on a previous study, specifically (Sorrenti et al., 2022). From this study, it was possible to understand that the parameters that most influenced the sludge dehydration process in the solar greenhouse were the thickness of the sludge layer and the airflow rate to be injected. Therefore, the methodology used took these operational aspects into account.

The experimental setup consists of five PVC cylinders with an 80 mm external diameter and varying heights, two air compressors, five flow meters, and a thermostatic refrigerator. Inside the cylinders, a drainage layer was arranged, consisting of three overlapping layers of coarse gravel, fine gravel, and finally sand, with a total thickness of 5 cm with a decreasing granulometry from bottom to top. At the contact surface between the last fine gravel layer and the sand, a tube for air insufflation was inserted.

Figure 5.1 - Cylinders in the preparation phase (in the photo they are upside down)

The cylinders were then placed inside a thermostatic refrigerator, which maintains an internal temperature of 40 °C. Above the drainage layer, a layer of surplus activated sludge, digested and thickened (Initial humidity 97.3 %) was deposited, which was taken from the wastewater treatment plant serving the city of Palermo with a variable thickness. Specifically, the thickness of the sludge used is reported in Table 5.1.

Table 5.1 - Sludge volume and thickness introduced into each cylinder

Cylinder	Sludge Volume [l]	Thickness [cm]
1	0.5	10
2	0.75	15
3	1	20
4	1.25	25
5	1.5	30

Additionally, to ensure thermal insulation, all the cylinders were placed inside other PVC cylinders, and the gap was filled with polyurethane foam. Figure 5.2 shows the installation of the bench-scale plant.

Figure 5.2 - Bench system installation

A total of 2 tests were conducted, each lasting 30 days. Specifically, only the air flow rate was varied using the 5 flow meters connected to each cylinder. The initial air flow rate was determined by considering an air flow rate of 10 Nm^3/h, resulting in an air flow rate of 0.04 m^3/m^2x h relative to the cylindrical surface area. The second test was conducted with an air flow rate equal to 50 % of the flow rate of test 1. The air flow rate of 10 Nm^3/h was used, based on the percentages of sludge reduction achieved during the previous test (Sorrenti et al., 2022).

Table 5.2 - Air flow rate used

Test	Q [m^3/m^2xh]
1	0.04
2	0.02

To assess the water content in the drainage layer in terms of percentage moisture, the Field Water Capacity (FWC) was calculated before starting the two tests (Table 5.3). Field Water Capacity is given by the difference between the volume of water added to the cylinder and the volume of water exiting, relative to the volume of the drain. The percentage of water volume exiting the drainage layer will be less than the volume of water input, as a portion of the water volume will be retained by the drainage layer itself. Below is the equation used to calculate the field capacity value.

$$FWC = \frac{V_{in} - V_{out}}{V_{drain}} \ [\%]$$

- V_{in} is the initial water volume [l];
- V_{out} is the final water volume [l];

- V_{drain} is the drain volume [l].

Table 5.3 - Field water Capacity

N°	V in [l]	V out [l]	Drain [cm]	V drain [l]	FWC [%]
Cylinder1	0.25	0.175	5	0.21	0.36%
Cylinder2	0.25	0.18	5	0.21	0.33%
Cylinder3	0.25	0.17	5	0.21	0.38%
Cylinder4	0.25	0.18	5	0.21	0.33%
Cylinder5	0.25	0.18	5	0.21	0.33%

5.1.1 Results Test 1

The first test started on 28/10/2022 and lasted for 30 days. At the beginning of the test, the empty cylinders were weighed using a digital scale to obtain the tare, and the full cylinders (sludge + drainage layer) were also weighed. At the end of the test, the full cylinder was weighed, and with the tare of the cylinder, it was possible to determine the final weight of the sludge in each cylinder. The percentage of weight reduction was then calculated for each cylinder (Table 5.4).

Table 5.4 - Initial Weight, Final Weight, and Weight Reduction of the sludge _Test 1

Cylinder	Initial Sludge Weight [kg]	Final Sludge Weight [kg]	Weight Reduction [%]
C1	0.500	0.292	41.6
C2	0.750	0.37	50.7
C3	1.000	0.306	69.4
C4	1.250	0.073	94.2
C5	1.500	0.043	97.1

As shown in Figure 5.3, the percentage of weight reduction of the sludge is higher for cylinder C5 (97.1 %), followed by cylinder C4 (94.2 %). The lowest reduction is observed in cylinder C1 (41.6 %). The trend of the weight reduction percentages increases with the thickness of sludge placed inside the cylinder. In fact, the percentage of weight reduction is greater for the cylinders that contained a higher thickness of sludge (cylinders C4 and C5).

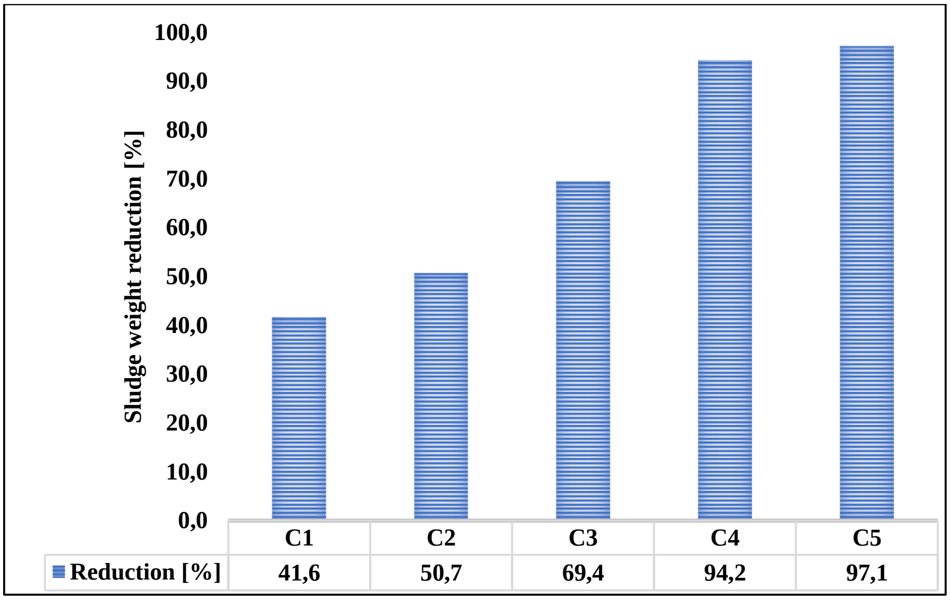

Figure 5.3 - Sludge weight reduction _Test 1

5.1.2 Results Test 2

The second test began on February 8, 2023, and concluded on March 9, 2023, lasting 30 days. Table 2 presents the measured data and results at the end of the test regarding the final weight of the sludge in each cylinder and the corresponding percentage of weight reduction.

Table 5.5 - Initial and final weight and weight reduction of the sludge_ Test 2

Cylinder	Initial Sludge Weight [kg]	Final Sludge Weight [kg]	Weight Reduction [%]
C1	0.500	0.359	28
C2	0.750	0.387	48
C3	1.000	0.491	51
C4	1.250	0.423	66
C5	1.500	0.353	76

As shown in Figure 5.4, the percentage of weight reduction of the sludge is highest for cylinder C5 (76 %), followed by cylinder C4 (66 %). The lowest reduction is observed in cylinder C1 (28 %). This test also demonstrated an increasing trend in weight reduction percentages with the thickness of sludge placed inside the cylinders.

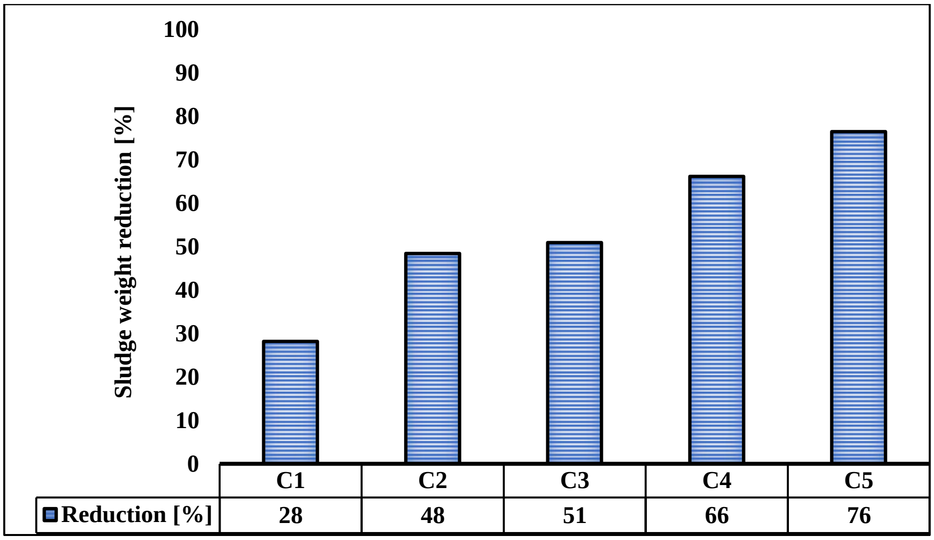

Figure 5.4 - Sludge weight reduction_ Test 2

5.1.3 Comparison

Figure 5.5 shows comparison graphs between the two tests conducted with different airflow rates. The comparison between the two tests reveals a significant difference in the final weight values of the sludge and their respective percentages of weight reduction. The highest weight reduction percentages were observed in Test 1, which was conducted with a higher airflow rate introduced into the system. From this observation, it was possible to conclude that, in addition to the thickness of sludge placed inside the system, another key parameter for the design of these systems is the airflow rate introduced. Therefore, as the thickness of the sludge increases, there is a greater percentage of sludge reduction. While with lower flow rates there is still an increase in sludge reduction with increasing thickness, the percentages remain lower compared to higher airflow rates. These results confirm previous experience (Sorrenti et al., 2022). Airflow rates around 10 Nm^3/h allow for a high weight reduction of up to 99 %.

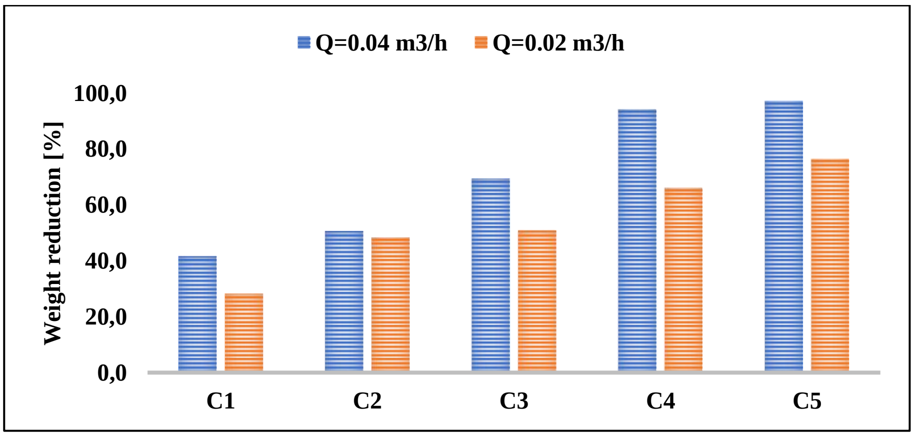

Figure 5.5 - Comparison of sludge weight reduction percentages for the two tests

6 An innovative methodology for drying sludge: greenhouse prototypes

6.1 Introduction

The objective of the experimental analysis conducted was to evaluate the sludge drying process using solar greenhouses, which specifically involves the introduction of hot air obtained from solar energy. Different configurations of solar greenhouses were created based on the point of hot air introduction to assess the effectiveness of the sludge drying treatment. The study of the sludge dehydration process in solar greenhouse prototypes involved the design and construction of several units:

- hot air production system;
- solar greenhouse structure construction;
- insulation system;
- ventilation system;
- drainage system;
- air distribution system.

6.2 Hot air production system

For the first experimental trial, a SolarAir panel was used. The SolarAir panel utilizes the sun to produce heat, and consequently, its performance is directly influenced by the amount of sunlight reaching the collector. Therefore, a careful study of the placement is essential for a satisfactory result. Unlike other solar collectors, these panels produce hot air rather than hot water. They can heat the air sufficiently to ventilate and dehumidify indoor spaces. These panels consist of a heat absorber and a cover glass, held together by a frame. Inside the absorber, the finned structure allows fresh or lukewarm air from the outside environment to pass through, which is then heated and dehumidified before being directed into the spaces to be heated. Unlike conventional solar systems, air panels do not require storage tanks or heat exchangers, as the heated air is used directly. The hot air is circulated using one or more fans; for this reason, some models are equipped with a small photovoltaic panel to power the fan in the absence of a connection to the electrical grid.
In Figure 6.1, the diagram of a typical SolarAir panel is shown.

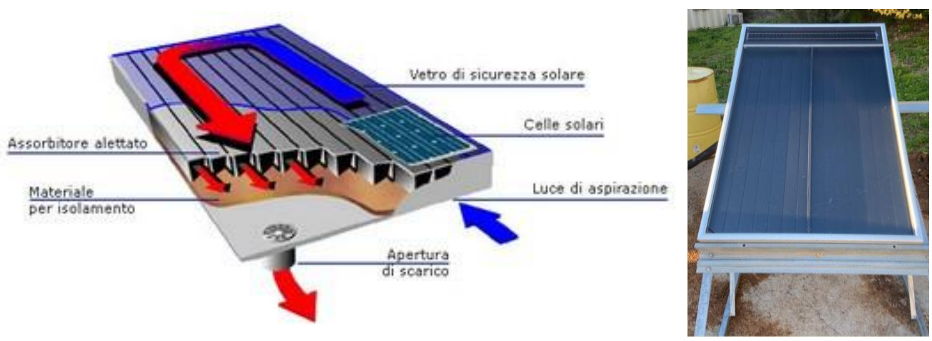

Figure 6.1 - SolarAir panel (adapted from doc.SolarAir)

Since the panel uses solar energy to produce hot air for the environment, its performance will be influenced by solar radiation. For this reason, each SolarAir panel is "custom-made", meaning that evaluations need to be conducted regarding the specific application, panel placement, ducting specifics, orientation, and inclination. In the pilot plant, the flat version of the SolarAir panel (SolarAir) model "Twin Solar 1.3" was used (Figure 6.1), with its technical characteristics listed in Figure 6.2.

Performance	
Gross collector area	1,3 m²
Thermal peak performance	0,9 kWp
Maximum air performance (free blowing)	90 m³/h
Recommended room size	10-20 / 15-30 m²
Maximum tube length	5 m

Figure 6.2 - Characteristics of the panel Twin Solar 1.3 (adapted from doc.SolarAir)

For the placement of the panel, 30° angled brackets oriented to the south were used. To avoid shadowing on the panel's collecting surface caused by buildings and equipment, the panel was positioned above scaffolding (Figure 6.3).

Figure 6.3 - Panel Solar Placement

On the back of the panel, there are two rectangular openings: one for intake and the other for the outlet of the produced hot air. A PVC pipe was connected to the outlet opening and linked to a blower, which in turn delivered the hot air into the greenhouses. To supply the hot air produced by the solar panel, a side-channel blower, model SCB-MSMF from Bigiesse (Figure 6.4/a), was used. It has a motor power of 0.2 kW and an airflow rate of 40 m^3/h.

Figure 6.4 - (a) Blowe, (b) Flow meters

Finally, the blower operation was timed to activate at 9:00 AM and deactivate at 5:00 PM for all days of the experiment. To measure the air flow rate, two flow meters were used, installed at the entrance of the hot air inlet (Figure 6.4/b).
The great versatility and modularity of the panel SolarAir allow for different positioning approaches, each with its own advantages and disadvantages.
These differences are largely due to the various inclinations: a vertically positioned panel, for example, performs progressively better in the winter season, whereas a roof-sloped panel is very effective in the mid-seasons but less efficient in the middle of winter.
The flat SolarAir panel can be installed on any flat surface with the aid of suitable brackets, making it easier to install.
Specifically, 2 modules were installed, facing south with an inclination of 40°.Below, in Figure 6.5, the performance curve of each individual panel is shown based on the conversion factor with temperature difference. On the vertical axis, the efficiency of the panel η_o is reported, and on the horizontal axis, the conversion factor with temperature difference is shown.

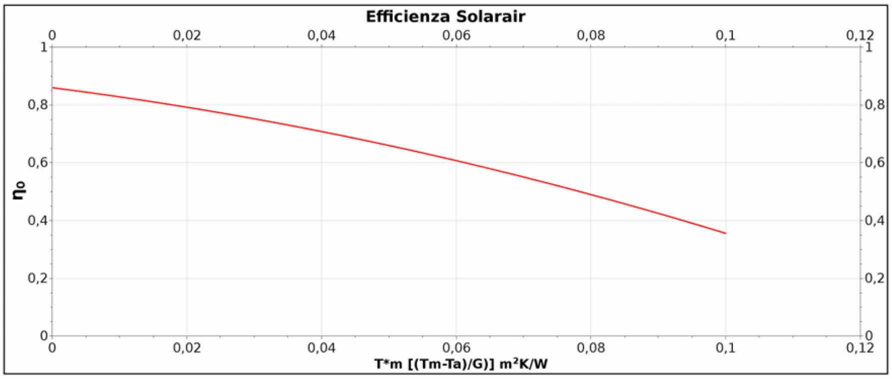

Figure 6.5 - Panel performance

For this calculation, the following formula was used (Solarkup s.r.l., 2015):

$$\eta = \eta_0 - a_1 \frac{T_m - T_a}{G} - a_2 \left(\frac{T_m - T_a}{G} \right)^2$$

Considering the following values from tests:

- η_0 is the efficiency equal to 0.846;
- a_1 is a coefficient equal to 2.023;
- a_2 is a coefficient equal to 0.0192;
- G is the radiation value equal to 800 W/m^2;
- T_m represents the temperature of the panel's material;
- T_a indicates the ambient temperature.

It is worth noting that in the case of air collectors, the efficiency of the collector is approximately equal to the actual efficiency of the entire system, as all the heat is released directly into the environment along with the working fluid (the air) without further losses due to thermal exchanges.

It should be noted that for air collectors, the collector's performance is approximately equal to the actual performance of the entire system, as all the heat is directly released into the environment along with the transfer fluid (the air) without further losses due to heat exchanges. As mentioned earlier, this mode has the following advantages:

- does not require electrical connections;
- does not consume electricity;
- does not require a control unit.

In the second experimental part, however, another solar panel of larger dimensions was used Figure 6.6.

Figure 6.6 - Photovoltaic power supply for engine

In the Figure 6.7 the operating characteristics of the motor are listed.

ENGINE TYPE A

Voltage [V]	24
Flow Rate [m^3/h]	360
Noise level [dB]	6.2
Duration at 40° C [h]	80000

Figure 6.7 - Engine characteristics (Solarkup s.r.l., 2015)

The great advantage of this solution is that the manifold is already fully assembled, the motor is integrated into the manifold and does not require any connection for operation. In this type of manifold, there is a "bridged" contact where a switch or thermostat can still be inserted if needed. The panel is 7 cm thick; only the motor requires more space as it protrudes from it (Figure 6.8).

Figure 6.8 - Panel detail

6.3 Solar greenhouse construction

6.3.1 Structure

The experimental setup involved the construction of several solar greenhouses that operated under different conditions; in particular, they varied based on the method of air supply and the different flow rates. For the construction of the prototypes, PVC boxes were used.

Figure 6.9 - PVC boxes

In the case of the greenhouses, a covering was constructed with a stainless-steel frame and transparent 16 mm polycarbonate honeycomb panels.
Polycarbonate honeycomb is a thermoplastic polymer derived from carbonic acid, used in various types of roofing for both private and industrial buildings. The term “honeycomb” refers to the presence of cells, or air pockets, enclosed between the two layers of polycarbonate. Honeycomb polycarbonate sheets are ideal for applications requiring high thermal insulation, excellent light transmission, and good mechanical resistance.
These are rigid sheets produced through extrusion, resistant to weather and chemical agents; additionally, there is UV protection on both sides to protect the polycarbonate panel from solar rays, yellowing, and aging. Lastly, this material is characterized by its light weight, ease of installation, cost-effectiveness, and versatility. In Figure 6.10 the honeycomb polycarbonate covering made for the solar greenhouse prototypes is shown.

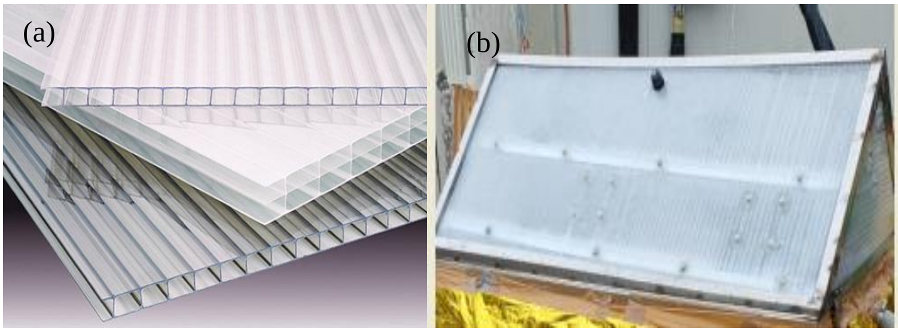

Figure 6.10 – (a) Polycarbonate panel; (b) covering structure

The PVC boxes used for the prototypes have a length of 0.97 m, a width of 0.64 m, and a height of 0.54 m, with a total volume of 0.34 m³. The wall thickness is 25 mm. In Figure 6.11, the top view and longitudinal section of the box are shown.

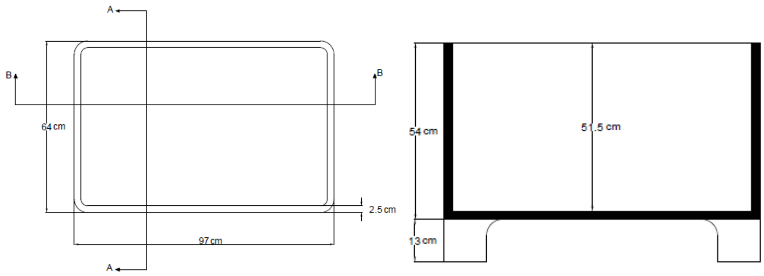

Figure 6.11 - Top view and longitudinal section of the PVC box

6.3.2 Insulation system

Additionally, for better thermal insulation, the boxes were externally covered with polyurethane foam (Figure 6.12) and an insulating blanket. Once solidified, polyurethane foam creates a breathable and filtering material that seals and forms an effective thermal and acoustic barrier. The most important characteristics of polyurethane foam are resistance to aging, high resistance to many chemicals (e.g., oils, fats, solvents, fuels), excellent adhesion to common construction materials, can be cut and painted, resistance to temperatures from -40 °C to +100 °C, high soundproofing capability, high thermal conductivity coefficient, and it is not hazardous to health.

Figure 6.12 - Polyurethane foam coating and insulating blanket

On the other hand, polyurethane foam is not resistant to UV rays. For this reason, insulating blankets were used, featuring a golden layer that allows solar rays to pass through easily and a silver layer that tends to reflect them. This characteristic allows the blankets to be used both for dispersing and retaining heat. Additionally, the insulating blankets provide windproof and waterproof protection.

6.3.3 Ventilation system

To ensure adequate air turbulence within the greenhouses, 5 electric mini fans were used. These fans measure 80 mm × 80 mm × 25 mm, operate at a voltage of 12 V with a current of 0.41 A, and were positioned on the honeycomb polycarbonate coverings (Figure 6.13).

Figure 6.13 - Electric mini fans

The hot air, in contact with the cooler internal surfaces, leads to the formation of condensate. Therefore, it was necessary to implement a system to capture and remove it. This system was created using 4 inclined stainless-steel channels, positioned within the covering to funnel the condensate into a designated drain. This setup allowed for the measurement of the amount of condensate produced daily (Figure 6.14).

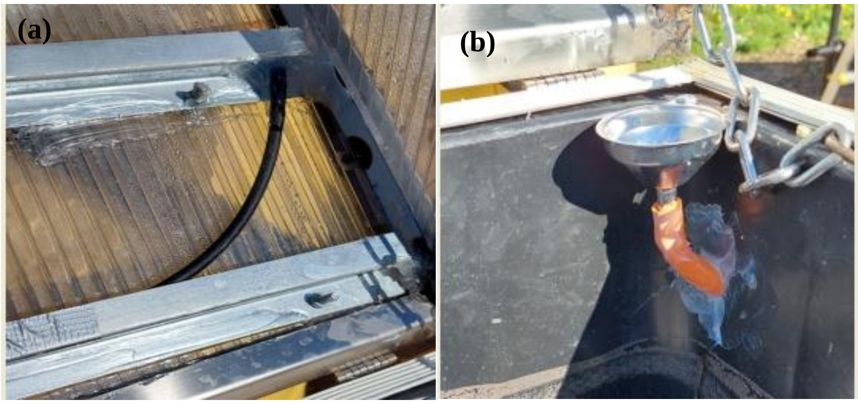

Figure 6.14 - (a) Condensate drainage – (b) Channels and piping for conveyance

6.3.4 Drainage system

For all the greenhouse prototypes, the base was shaped using a concrete conglomerate to ensure a 1% slope, which facilitates the drainage of water into a longitudinal drainpipe positioned centrally.
This was connected to a ball valve to allow the correct state of the bed during the starting phase in which it is loaded with sludge.
In fact, the valve, if closed, has the purpose of avoiding the immediate drainage of the sludge water that would quickly filter into the drainage layer and that would not allow an exact evaluation of the drained volume in the initial phase. Therefore,

the filtering and draining layer, before loading with the sludge, is made unsaturated by adding water up to the sand-atmosphere interface, so that the bed is loaded with the sludge up to the preset thickness. Only in this way can that thickness be fixed, otherwise, by immediately starting the drainage of the free water, reaching the level corresponding to a preset volume of sludge to be dried would never be achievable.
Inside the prototypes, starting from the base, a drainage material with different granulometries was placed, with decreasing diameters from bottom to top, for a total thickness of 15 cm. Specifically, a lower layer of 5 cm of gravel was formed, over which by a second layer of 5 cm of smaller gravel, and a top layer of 5 cm of sand were superimposed.
Before installing the filter sand layer, it was characterized by determining the granulometric curve. This is shown in Figure 6.15. The curve is plotted as points on a cartesian plane, where the ordinate represents the weight percentages of soil particles with the same diameter, and the abscissa shows the corresponding diameters on a logarithmic scale.

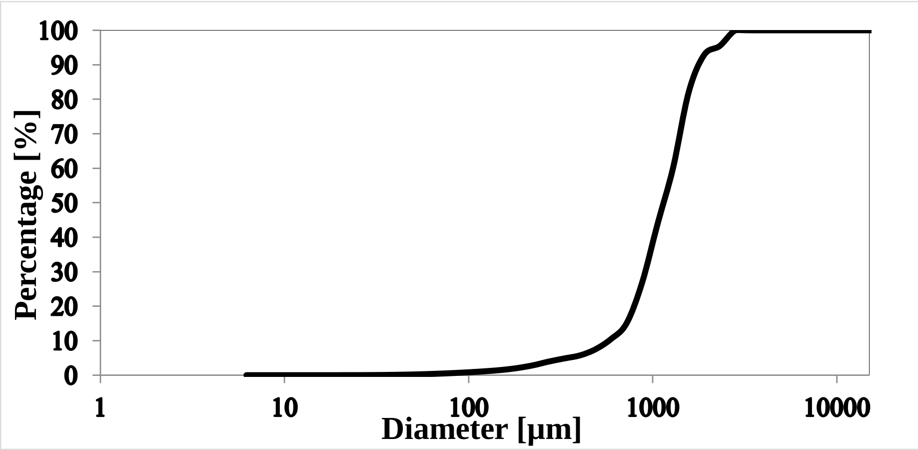

Figure 6.15 - Cumulative granulometric curve

Table 6.1 shows the characteristic diameters used to determine the coefficient of uniformity:

Table 6.1 - Characteristic diameters

de_{10}	**de_{50}**	**de_{60}**	**de_{90}**
[μm]	**[μm]**	**[μm]**	**[μm]**
576.61	1147.7	1290.12	1813.38

with:
- **de_{10}**: effective diameter.
- **de_{50}**: median diameter.
- **de_{60}**: reference diameter.

The coefficient of uniformity (U) was found to be 2.24, and it was determined using the following formula:

$$U = \frac{de_{60}}{de_{10}}$$

For uniformity coefficient values less than 4, the soil is considered uniform, whereas for values greater than 6, the soil is considered poorly uniform. Therefore, in this case, the soil can be considered uniform.

6.3.5 Air distribution system

At the contact surface between the gravel and the sand in one greenhouse, a perforated copper coil with a diameter of 16 mm was installed (Figure 6.16).The holes in the coil allowed for the introduction of hot air into the system, promoting the heating of the drainage layer and consequently the heating of the sludge. The innovation of this pilot system lies precisely in supplying hot air directly beneath the sludge layer.

Figure 6.16 - Copper coil

To prevent the sludge from blocking the holes, a cover was created using L-shaped steel profiles placed over the coil in a pitched roof design. Finally, a varying amount of sludge was introduced for the different tests.

6.4 The proposed operating scenarios

To evaluate the drying process using solar greenhouse prototypes, seven tests were conducted, each lasting approximately 30 days. The tests varied in terms of configurations adopted, airflow rate, and the initial thickness of sludge placed inside the solar greenhouse prototypes. The experimental tests were conducted in different periods of the year (seasons) to assess the influence of climate on the solar drying process of sludge.

The adopted configurations were different in terms of hot air injection mode in the solar greenhouse, they were the following:

- hot air injection above the sludge layer;
- hot air injection below the sludge layer;
- mixed air injection (both above and below the sludge layer).

Furthermore, in some tests, a solar greenhouse configuration without air injection and a natural, open-air drying bed were also compared with the previous ones.

The tests were conducted using airflow rates ranging from a maximum of 24 m^3/m^2x h to a minimum value of 2 m^3/m^2x h. In addition, different thicknesses of digested and thickened sludge were placed inside the solar greenhouses in the various tests. The yield and operating parameters of each test are detailed in Table 6.2 below.

In Test 1, two solar greenhouses and one drying bed were used, with a sludge thickness of 18 cm. In solar greenhouse A, the air injection occurred from above the sludge layer with an airflow rate of 24 m^3/m^2 x h. In solar greenhouse B, the air supply came from below, with a variable airflow rate between 8 and 24 m^3/m^2 x h; additionally, in this prototype, the air injection started on the 10th day of the experiment. Finally, the third prototype functioned as a traditional drying bed.

It is specified that Test 1 was a preliminary trial to test the functionality of the prototypes and evaluate some operational parameters. For this reason, the results of this test were not subject to comparison with the other tests.

The solar greenhouse A and solar greenhouse B maintained the same air intake configuration throughout all the tests. Specifically, in greenhouse A, the air intake was always from the top; in solar greenhouse B, however, the air intake was always from the bottom. For greenhouse C, the operating configuration varied across the tests. In tests 2, 3, and 5, greenhouse C operated as a conventional solar greenhouse, without air intake; to distinguish it from the other tests, this configuration was labeled as C*. In tests 4, 6, and 7, hot air was introduced into greenhouse C from both the bottom and the top.

In Test 2, three solar greenhouses were used, with a sludge thickness of 25 cm. In solar greenhouses A and B, the air injection occurred from above and below the sludge layer, respectively, with an airflow rate of 16 m^3/m^2 x h.

Test 3 was conducted using the same configuration as Test 2, but with a sludge thickness of 27 cm and an airflow rate of 23 m^3/m^2 x h injected into solar greenhouses A and B.

In Test 4, three solar greenhouses were used, with a sludge thickness of 25 cm. In solar greenhouses A and B, the air injection occurred from above and below the sludge layer, respectively, with an airflow rate of 3 m^3/m^2 x h. For solar greenhouse C, the air injection occurred in a mixed mode; specifically, the airflow rate was 1.5 m^3/m^2 x h from above and 1.5 m^3/m^2 x h from below.

In Test 5, three solar greenhouses were used, with a sludge thickness of 28 cm. In solar greenhouses A and B, air injection occurred from above and below the sludge layer, respectively, with an airflow rate of 6 m^3/m^2 x h.

In Tests 6 and 7, three solar greenhouses were used, with a sludge thickness of 25 cm. In solar greenhouses A and B, air injection occurred from above and below the sludge layer, respectively, with an airflow rate of 2 m^3/m^2 x h for Test 6 and 4 m^3/m^2 x h for Test 7. For solar greenhouse C, the air injection occurred in a mixed mode for both tests. Specifically, for Test 6, the airflow rate was 1 m^3/m^2 x h, and for Test 7, it was 2 m^3/m^2 x h.

Table 6.2 - Configurations test *(Greenhouse C* represents a configuration of traditional solar greenhouse)*

Test n.	Configurations			
1	**Prototypes**	**Greenhouse A**	**Greenhouse B**	**Drying Bed C**
	Insufflation modality	Above Sludge	Under Sludge (Starting from the 10th day)	-
	Air Flow Rate (m^3/m^2xh)	24	8-24	-
	Sludge thickness (cm)	18	18	18
2	**Prototypes**	**Greenhouse A**	**Greenhouse B**	**Greenhouse C***
	Insufflation modality	Above Sludge	Under Sludge	-
	Air Flow Rate (m^3/m^2xh)	16	16	-
	Sludge thickness (cm)	25	25	25
3	**Prototypes**	**Greenhouse A**	**Greenhouse B**	**Greenhouse C***
	Insufflation modality	Above Sludge	Under Sludge	-
	Air Flow Rate (m^3/m^2xh)	23	23	-
	Sludge thickness (cm)	27	27	27
4	**Prototypes**	**Greenhouse A**	**Greenhouse B**	**Greenhouse C**
	Insufflation modality	Above Sludge	Under Sludge	Above/Under Sludge
	Air Flow Rate (m^3/m^2xh)	3	3	1.5 (above sludge) 1.5 (under sludge)
	Sludge thickness (cm)	25	25	25
5	**Prototypes**	**Greenhouse A**	**Greenhouse B**	**Greenhouse C***
	Insufflation modality	Above Sludge	Under Sludge	-
	Air Flow Rate (m^3/m^2xh)	6	6	-
	Sludge thickness (cm)	28	28	28
6	**Prototypes**	**Greenhouse A**	**Greenhouse B**	**Greenhouse C**
	Insufflation modality	Above Sludge	Under Sludge	Above/Under Sludge
	Air Flow Rate (m^3/m^2xh)	2	2	1 (above sludge) 1 (under sludge)
	Sludge thickness (cm)	25	25	25
7	**Prototypes**	**Greenhouse A**	**Greenhouse B**	**Greenhouse C**
	Insufflation modality	Above Sludge	Under Sludge	Above/Under Sludge
	Air Flow Rate (m^3/m^2xh)	4	4	2 (above sludge) 2 (under sludge)
	Sludge thickness (cm)	25	25	25

6.5 Methods for carrying out experimental tests in the laboratory and field measurements

In the following paragraph, the experimental tests conducted to calculate a series of parameters necessary to evaluate the progress of the sludge dewatering process are described. Based on the measurements taken at the plant, the field water capacity (FWC), total suspended solids (TSS), volatile suspended solids (VSS), and moisture content were determined. In order to evaluate the dehydration process, in addition to laboratory measurements, it was necessary to perform some field measurements.

6.5.1 Field Capacity of drain layer

To assess the water content in the drain layer in terms of percentage moisture, the field capacity was calculated. Table 6.3 shows typical field capacity values for a range of drain layers.

Table 6.3 - Characteristic values of field capacity

Layers	Field Capacity (%)
Sandy	10 - 15
Medium dough	25 - 40
Clay	45 - 50

Field capacity is given by the difference between the volume of water added to the greenhouse and the volume of water exiting, relative to the volume of the drain. Below is the equation used to calculate the field capacity value.

$$FWC = \frac{V_{in} - V_{out}}{V_{dreno}} \ [\%]$$

6.5.2 Total Suspended Solids

Total suspended solids (TSS) refer to the residue that remains in a container after evaporating a sample and drying it in an oven at a temperature of 105°C (Figure 6.17) for 24 hours. The following equation is used to calculate TSS:

$$SST = \frac{(P_{105°C} - P_0)}{V} \ [g/l]$$

where:

- $P_{105°C}$: weight of the capsule after drying in the 105°C oven [g].
- P_0: weight of the tare (empty capsule) [g].
- V: volume of the sample [l].

Figure 6.17 - 105°C Oven for sludge drying

To evaluate the total solids content of the sludge at the start of the tests, a sample of sludge was taken from each prototype, then dried in an oven and weighed. The weighing was performed using the Sartorius analytical balance (Figure 6.18).

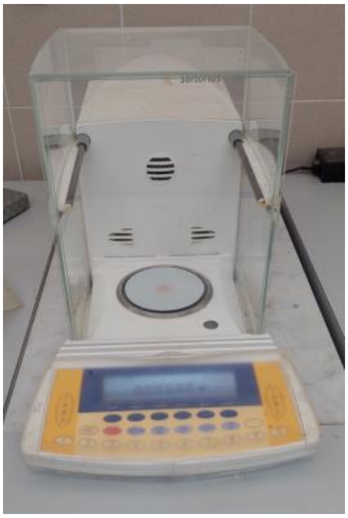

Figure 6.18 - Sartorius balance

6.5.3 Volatile Suspended Solids in the sludge

The procedure consists of placing the samples in a container of known weight. After weighing it, the samples are dried at 105 °C until a constant weight is achieved, determining the dry residue. Subsequently, the container with the sample is placed in a muffle furnace (Figure 6.19) at a temperature of 550 °C for one and a half hours. After weighing, the fixed residue is determined.

Figure 6.19 - Muffle furnace

The difference of weight between the fixed residue and the total solids represents the volatile suspended solids. Specifically, the following equation was used to determine the volatile suspended solids:

$$VS = \frac{(P_{105°C} - P_{550°C})}{(P_{105°C} - P_0)} \; [\%]$$

With:

- $P_{105°C}$: weight of the sample after drying in an oven at 105 °C [g].
- $P_{550°C}$: weight of the sample after incineration in a muffle furnace at 550 °C [g].
- P_0: weight of the empty container [g].

6.5.4 Humidity

At the beginning of each test, to calculate the initial moisture content, four sludge samples, each having a volume of 25 ml were collected and weighed. Subsequently, the samples were dried in an oven at 105 °C for 24 hours and then weighed again. Using the obtained data, the initial moisture content was calculated as the average of the four samples, according to the following relationship:

$$U = \frac{P_{01} - P_{105°C}}{P_{01} - P_0} \; [\%]$$

With:

- P_{01}: weight of the sludge sample and the container [g].
- $P_{105°C}$: weight of the sample after drying at 105 °C [g].
- P_0: weight of the empty container [g].

6.5.5 Field measurements for process evaluation

The drying process initiated in the experimental installations was monitored through measurements of temperature, air velocity, the amount of drained water, and sludge thickness. A digital scale was used to measure the drained water, which is essential for determining the drainage curve. Temperature measurements included the external temperature (ambient temperature), the air temperature at the solar panel outlet, the temperature at the inlet of the solar greenhouse prototypes, and the temperature inside the greenhouses.

Weather and climate parameters during the first test were monitored and recorded by consulting the website of the Sicilian Agrometeorological Information Service (SIAS), specifically referencing the Palermo station at Uditore (UTM coordinates: 4221667N; 353448E). For the internal temperatures of the solar greenhouses and the air velocity within them, also during the first test, a hot-wire anemometer was used (Figure 6.20). This device consists of a display unit and a hot-wire probe, allowing for quick and precise measurement. Thanks to the combination of a telescopic rod and a slim measuring head, the hot-wire anemometer can be used in confined spaces or where the measuring point is difficult to reach.

Figure 6.20 - Anemometer

For all the other tests, weather and climate parameters were monitored by installing a weather station (Cabled Vantage Pro Sensor Suite Weather Station - SKU 6322C, 6322CM) on the panel, while the other temperatures were recorded using automated sensors that could be managed remotely (Figure 6.21). The Vantage Pro2 Sensor Suite Weather Station (SKU 6322C, 6322CM) is a comprehensive weather monitoring system designed for accurate measurement of a variety of environmental parameters. This weather station typically includes the following key components:

- anemometer: measures wind speed and wind direction.
- rain gauge: measures rainfall amount and intensity.
- temperature and humidity sensors: measures outdoor temperature and relative humidity.

The temperature and humidity measurements at the air outlet from the solar panel, at the air inlet into the greenhouses and inside the greenhouses themselves were performed using numerous meters equipped with Elitech data loggers, model GSP-6 (Figure 6.22).

Figure 6.21 - Weather station

Figure 6.22 - Sensors

Finally, the sludge thickness was measured using a graduated rod until cracks formation was observed in the sludge (Figure 6.23).

Figure 6.23 - Graduated rod

6.6 Results

In this subsection, the results obtained during the experimental tests with the solar greenhouse prototypes are presented. For clarity, each individual test is reported separately, describing its characteristics and the different results obtained.

6.6.1 Test 1

The first test began on 14/02/2022 and ended on 15/03/2022, with a total duration of 30 days. The configuration adopted for this test involved the use of three solar greenhouse prototypes: Greenhouse A with hot air introduced above the layer of sludge, Greenhouse B with hot air introduced below the layer of sludge, and a traditional drying bed. The air flow rate injected into Greenhouse A and Greenhouse B was 24 m^3/m^2x h.

The sludge introduced into the greenhouses was a mixed sludge (primary and secondary biological sludge) and thickened but not digested, as evidenced by the high SSV values (see paragraph 6.6.1.2). The initial thickness of the sludge placed inside the three prototypes was 18 cm with an overall initial weight of 115 kg. The sludge inserted into the greenhouses is thickened but not digested.

6.6.1.1 Field Water Capacity (FWC)

To assess the water content in the drain layers in terms of percentage humidity, the field capacity was calculated. Specifically, for Greenhouse A, a field capacity (FWC) value of 14 % was obtained, for Greenhouse B, 15%, and for the traditional drying bed, 6 %. The summary data for the calculation of the field capacity are provided in Table 6.4 below.

Table 6.4 - Field water capacity

	V_{in}	V_{out}	Drain thickness	V_{drain}	FWC
	[l]	[l]	[cm]	[l]	[%]
Greenhouse A	40	28	15	88	14 %
Greenhouse B	53	40	15	88	15 %
Drying Bed C	50	45	15	88	6 %

The FWC values were considered to take into account the residual humidity that remained in the drainage layer and, therefore, the volume that did not have to be counted in the water balance of the system. Since the draining layer used in the 7 tests was the same, this determination was made only for this test; of course, the FWCs for the other tests are the same as those reported in the Table 6.4.

6.6.1.2 Measurement of volatile suspended solids

The high content of volatile solids observed in all three cases significantly affects the dewaterability characteristics of the sludge, particularly worsening as this parameter increases. Additionally, these very high values indicate that the sludge was not digested (stabilizated). At the beginning of the experiment, the VS/TS ratio values were 84.84 %, 83.62 %, and 84.93 % for Greenhouse A, Greenhouse B, and the drying bed C, respectively. At the end of the experimentation, the VS/TS ratio were found to be 73 %, 73 %, and 77 % for Greenhouse A, Greenhouse B, and the drying bed, respectively.

6.6.1.3 Measurements humidity

At the beginning of the experimental test, sludge samples were taken from each prototype to determine their initial moisture content. The initial moisture content for the sludge introduced into Greenhouse A was found to be 96.73 %, for Greenhouse B was 96.71 %, and for the drying bed C was 96.66 %. As can be observed, very high moisture values were obtained in all three prototypes. These results indicate that the sludge was well thickened. Starting from the initial moisture value measured on the first day of the experiment (14/02/2022), a sample of sludge was taken daily from each prototype and subjected to drying in an oven at 105 °C to assess the daily variation in moisture and, consequently, the evolution of the process, as shown in Table 6.5. Certainly, the sampling from the surface does not represent the actual overall drying of the sludge, but it was not considered appropriate to proceed differently so as not to artificially create preferential escape routes for the blown air, proceeding with sampling of a thickness equal to that of the sludge bed.

Table 6.5 - Humidity_ test 1

	Days of Experimentation	Greenhouse A [%]	Greenhouse B [%]	Drying Bed C [%]
Period 1	1	96.73%	96.71%	96.66%
	2	95.36%	95.83%	96.63%
	3	91.32%	95.35%	95.72%
	4	88.54%	93.92%	95.16%
	5	87.62%	93.25%	95.44%
	8	87.60%	89.04%	92.89%
	9	87.32%	88.23%	90.50%
Period 2	10	84.54%	87.36%	92.35%
	11	79.71%	86.43%	95.53%
	12	79.68%	80.95%	87.65%
	15	77.98%	79.38%	86.09%
	16	74.19%	76.67%	86.29%
	17	72.99%	75.10%	89.61%
	18	72.67%	74.84%	88.87%
	19	71.48%	73.22%	87.54%
	22	70.34%	72.03%	86.31%
Period 3	23	68.32%	72.01%	85.29%
	30	66.26%	43.94%	80.71%

As shown in Table 6.5, the initial moisture content of the sludge was nearly the same across all systems but decreased over the 30-day experimental period. The experiment is divided into three distinct periods of 9, 13, and 8 days, during which the operating conditions of Greenhouse B varied.
Specifically, in the first period, Greenhouse B operated as a traditional greenhouse. During the second period, bottom aeration was activated with a flow rate of 8 m^3/m^2 x h, and in the third period, this flow rate was increased to 24 m^3/m^2 x h to study the effects of this flow rate on moisture reduction performance. Below, Figure 6.24 illustrates the moisture trends of the sludge in the three prototypes.

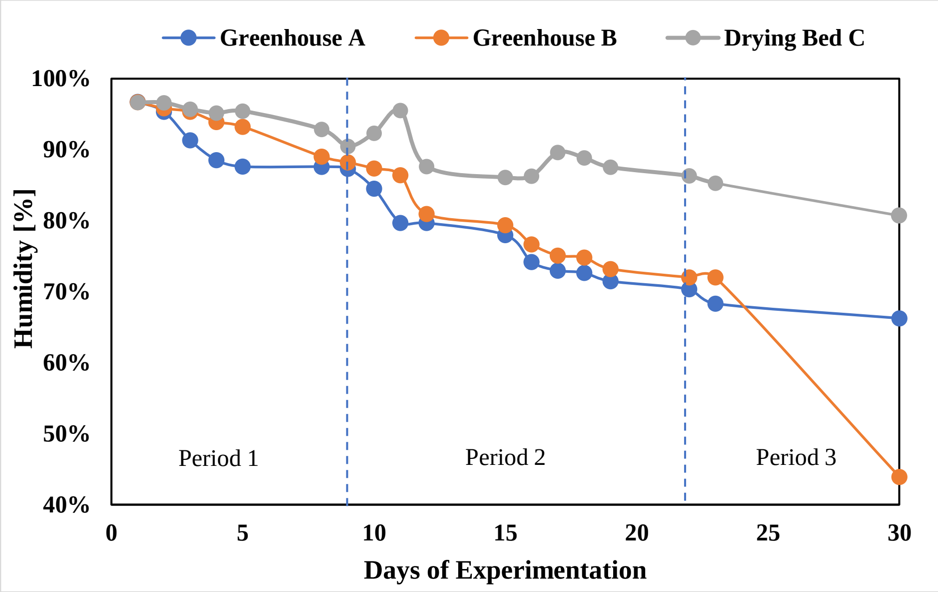

Figure 6.24 - Humidity trend_ test 1

During the first period, it can be observed that the best results were achieved in Greenhouse B (indicated by the orange line). These results were expected due to the introduction of hot air below the sludge layer. The performance of Greenhouse A (shown in blue), although slightly higher in moisture content, followed a similar trend to Greenhouse B, achieving a lower final moisture value. In contrast, the traditional drying bed (Greenhouse C) demonstrated a much lower reduction capacity compared to both greenhouse prototypes. This can be attributed to the lack of a cover, which prevented heat accumulation above the sludge layer, as well as adverse weather conditions on several days during the observation period.
This is easily observed in the second period with reference to the 11th and 17th day in which the moisture values increased compared to the decreasing trend of the previous day's owing to the rain.
During this second period, the increased airflow introduced from below did not significantly improve the process, as the moisture content of the sludge in Greenhouse B remained about 2 percentage points higher than the correspondent value in Greenhouse A. However, when the flow rate was increased threefold in the third period, a drastic reduction in moisture was observed, dropping from approximately 72 % to about 44 %. Surely, this drastic reduction in moisture in Greenhouse B was due to a higher airflow introduced below the sludge layer, thus promoting the water loss from the sludge, which did not occur with the airflow introduced from above.
Regarding the traditional drying bed, a much more limited reduction in moisture was observed (indicated by the grey line). Below, Figure 6.25 illustrates the appearance of the sludge during the filling of the three prototypes on the first day of experimentation.

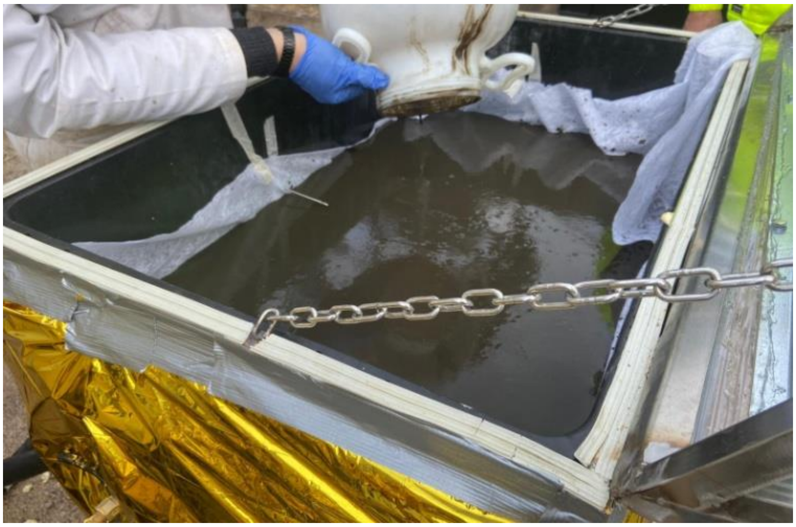

Figure 6.25 - State of the sludge on the first day of testing

As seen in Figure 6.25 the sludge was in a fluid state with a moisture content of 97 % at the beginning. By the end of the experimental phase, the results obtained from the three prototypes were different and are presented below.

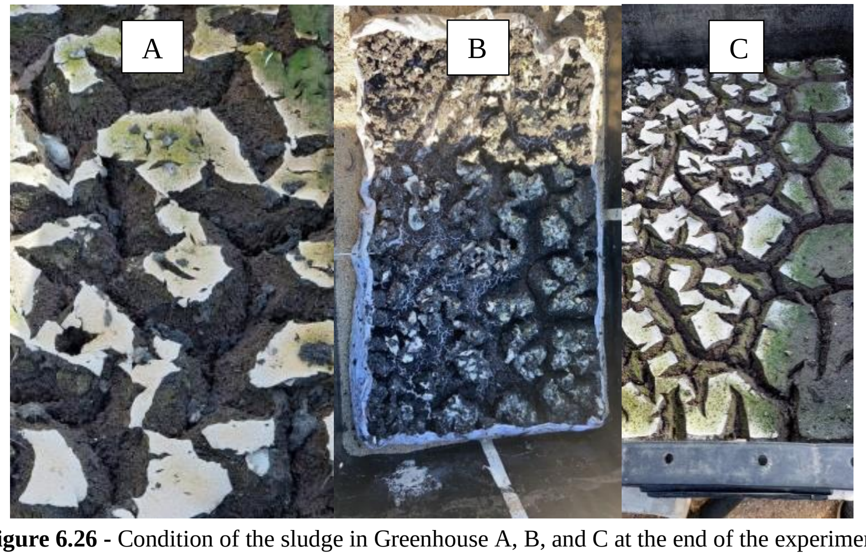

Figure 6.26 - Condition of the sludge in Greenhouse A, B, and C at the end of the experiment

6.6.1.4 Sludge Layer Thickness

During the 30-day experiment, starting from February 14, 2022, one of the parameters monitored daily was the evaluation of the sludge layer thickness. On the first day (when the prototypes were filled), a thickness of 18 cm was measured for each prototype. One week into the experiment, the sludge thickness was 8.8 cm in Greenhouse A, 9 cm in Greenhouse B, and 11.4 cm in the traditional drying bed. As the process progressed, a significant reduction in the sludge layer thickness was observed in all three prototypes. Specifically, Greenhouse A exhibited the greatest reduction in sludge thickness, owing to the hot air being injected above the sludge layer. Data from Greenhouse B show a smaller reduction in sludge thickness compared to Greenhouse A, but greater than in the traditional drying bed. This is attributed to the cover, which creates a greenhouse effect, retaining more heat than the traditional drying bed. It should be noted that until the ninth day of the experiment, no air was blown from below in Greenhouse B.

The introduction of bottom-up airflow on the 9th day can be justified as a subsequent step to improve the evaporation rate of moisture from the sludge. After an initial phase of surface drying, the bottom-up airflow helps remove the internal moisture of the sludge, accelerating deep drying. The airflow rate was further increased in order to study the variation in the dehydration process.

Starting from the 7th day after filling, cracks and fissures began to appear in the sludge layer (Figure 6.27).This phenomenon was more pronounced in Greenhouse A, while it was less evident in Greenhouse B and the traditional drying bed.

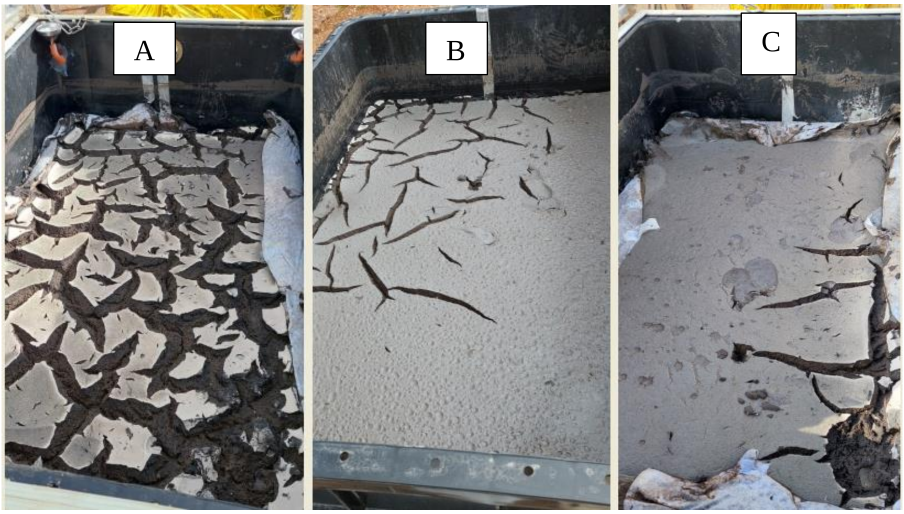

Figure 6.27 - Condition of the sludge on the 7th day of the experiment: (a) Greenhouse A; (b) Greenhouse B; (c) Bed C

Starting from the tenth day of the experiment, the operational conditions of Greenhouse B were altered. Specifically, an airflow rate of 8 m^3/m^2xh was introduced from the coil for a total of 13 days of observation. For the final 8 days of the experiment, the airflow rate was increased to 24 m^3/m^2 x h. The increase in airflow in Greenhouse B led to the widespread formation of cracks and fissures, which made it impossible to measure the thickness of the sludge layer. At the end of the experiment, the final weight of the sludge in Greenhouse A was 20.466 kg, while the final weight in Greenhouse B was 7.88 kg, and Drying bed was 12 kg compared to the initial weight of 115 kg.

6.6.1.5 Trend of external climatic variables

Temperature is one of the key parameters that significantly influences the sludge drying process. Higher temperatures lead to faster drying kinetics and promote more effective reduction of pathogens. Depending on the operating temperature,

substrate characteristics, and operational conditions, the duration of the drying process can vary. The external temperature, internal temperature, temperature of the absorbing surface, and blown air temperature were monitored daily. The external temperature affects the production of hot air by the SolarAir panel.
Figure 6.28 shows the recorded data for external temperature (T_{out}), temperature on the absorbing surface of the SolarAir panel (T_{surf_capt}), and solar cell temperature ($T_{solar\ cell}$).

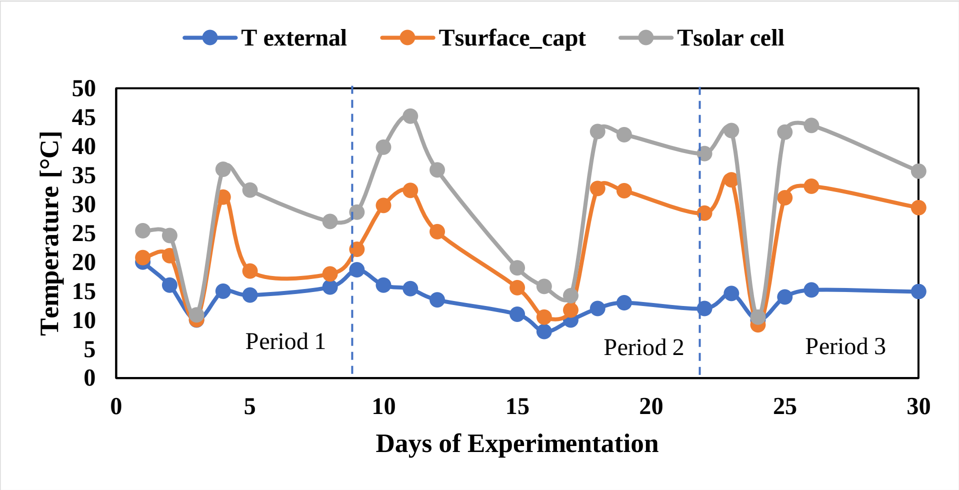

Figure 6.28 - Temperature test_1

The surface of the sludge also heats up proportionally to the solar radiation, which leads to an increase in the drying rate of the sludge. The trend of solar radiation is a crucial parameter for the efficiency of the process; the higher the radiation, the greater the capacity of the SolarAir panel to supply hot and dry air to the greenhouses. The maximum solar radiation values are reached during the daylight hours, with peaks occurring particularly between 12:00 PM and 2:00 PM.
Another variable that was monitored is daily precipitation, as it interferes with the sludge drying process, particularly in the traditional drying bed, which lacks a cover. By evaluating this variable, it was possible to identify the days when the drying process was partially slowed down (Figure 6.29).

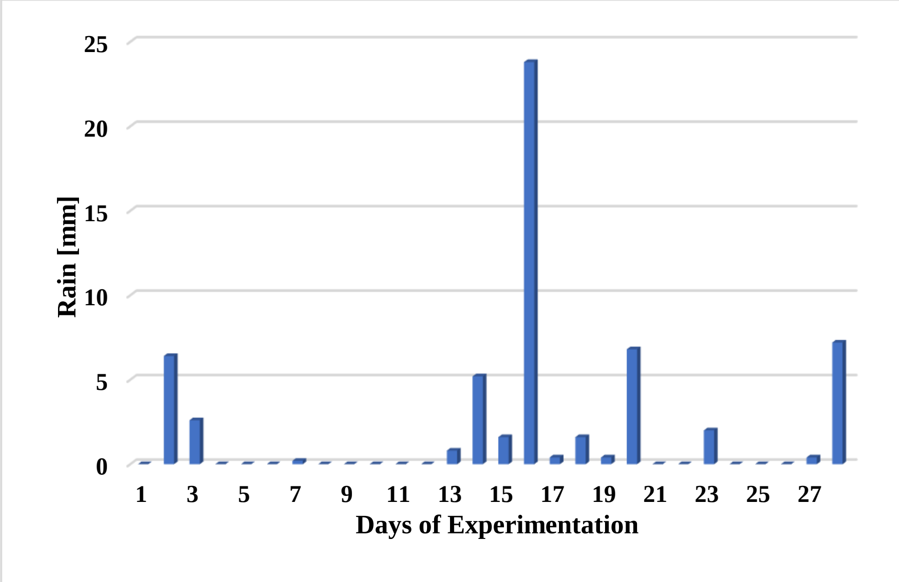

Figure 6.29 - Precipitation trend_ test 1

6.6.1.6 Internal Climatic Variables Trend

As previously mentioned, it was necessary to monitor the trends of the climatic variables within the solar greenhouse prototypes to assess how they influence the sludge drying process. Specifically, attention was given to the temperature inside the solar greenhouses and the humidity percentage recorded inside Greenhouse A. The trends of these variables, recorded during the experimental period, are shown in Figure 6.30.

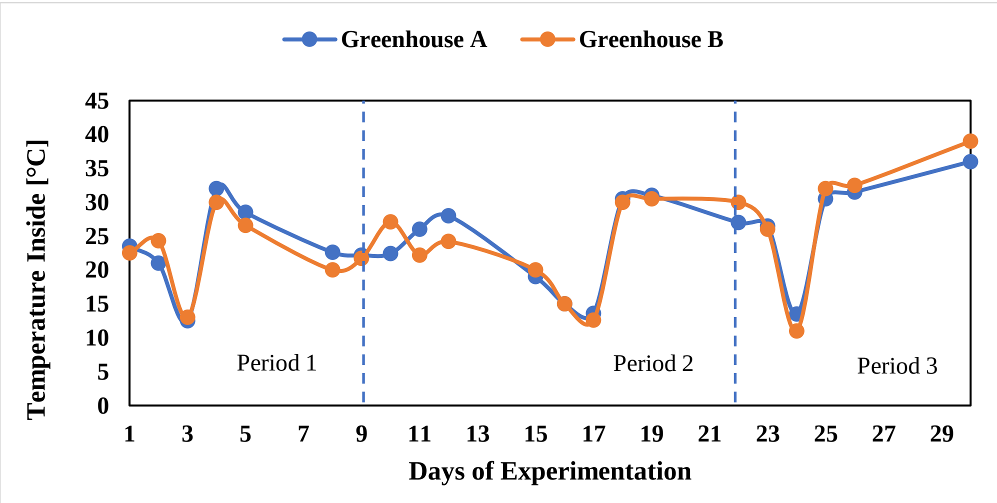

Figure 6.30 - Temperature trend inside Greenhouse A and Greenhouse B

6.6.1.7 Drainage Curve

To determine the drying rate, the sludge drying kinetics model was used. This model is based on constructing the characteristic drainage curve, for which the following data are required: time between measurements (t), corresponding volume (Vol), cumulative volume (V_{cum}), residual volume (V_{res}), and cumulative time (t_{cum}).

The initial residual volume was calculated as the product of the initial volume of sludge introduced into the prototypes and the percentage moisture content. The drying volume was determined as the ratio of the volume expressed in liters to the time elapsed between two measurements.

The behaviour of the sludge during the drying process can be divided into four distinct periods:

1) *First Phase:* removal of free water. This phase shows a relatively constant drying rate.
2) *Second Phase:* decrease in drying rate as interstitial water is removed.
3) *Third Phase:* further decrease in drying rate as surface water is removed.
4) *Final Phase:* a brief interval where bound water is removed, and the moisture content reaches equilibrium.

In terms of drying rate, the first phase is characterized by a nearly constant rate, while subsequent phases show decreasing rates due to the removal of free, interstitial, and surface water requiring more time.

Figure 6.31, Figure 6.32 and Figure 6.33 show the trends of the three drainage curves, which exhibited very similar patterns. At the end of the test the volume of water lost for each prototype was measured (Table 6.6).

Table 6.6 - Drained water test_1

Greenhouse A	Greenhouse B	Drying Bed C
68.3 l	62.8 l	84.7 l

The drainage curve of the sludge for greenhouse A showed the typical profile of the sludge drainage process. Specifically, the beginning of the curve was characterized by a constant water loss rate corresponding to the removal of free water. In this phase, the drying rate decreased from 3.177 l/min to 3.102 l/min. After this phase, the removal of interstitial and surface water followed. Specifically, during the interstitial water loss phase, the drying rate decreased drastically from 3.102 l/min to 0.21 l/min; during the surface water loss phase, the drying rate dropped from 0.21 l/min to 0.0264 l/min. The final part of the curve showed a further decrease in the drying rate down to a value of 2.2×10^{-4} l/min (Figure 6.31).

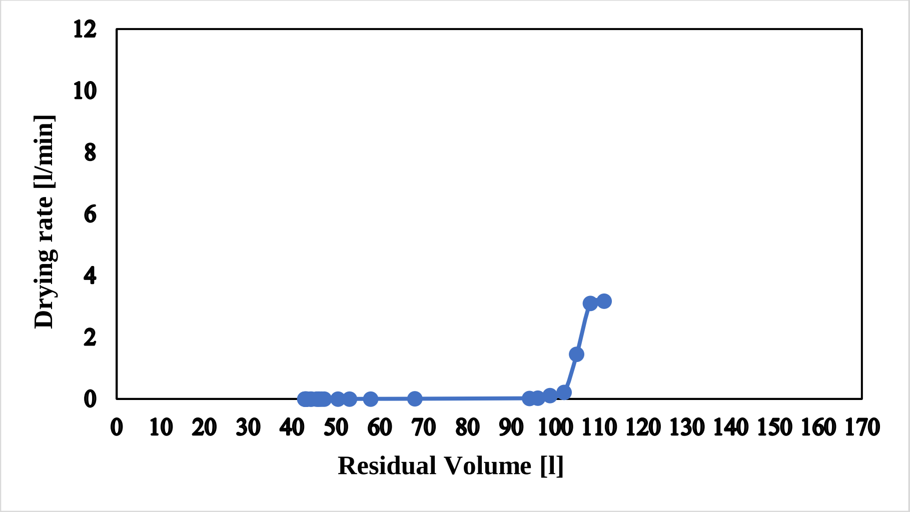

Figure 6.31 - Drainage curve of the sludge in Greenhouse A_ test 1

In Figure 6.32 the drainage curve of the sludge for greenhouse B was reported. During the free water loss phase, the curve exhibited a constant trend, decreasing from a value of 3.187 l/min to 3.176 l/min. Subsequently, during the interstitial water removal phase, the drainage rate underwent a drastic decrease, dropping from 3.176 l/min to 0.240 l/min. Additionally, during the surface water loss phase, the drainage rate further decreased to a value of 0.042 l/min. The final part of the curve, corresponding to the deep-water phase, showed a further decrease in the drainage rate to a value below 0.042 l/min.

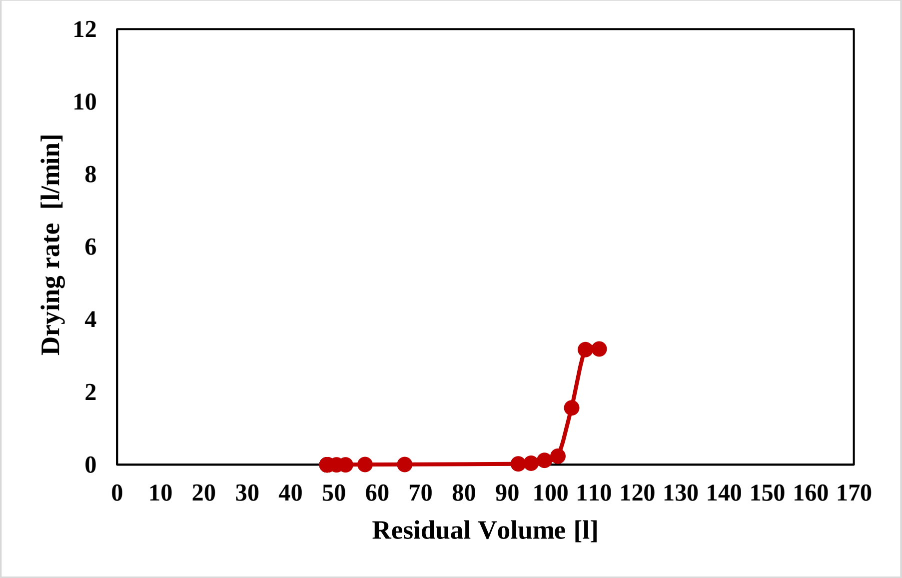

Figure 6.32 - Drainage curve of the sludge in Greenhouse B_ test 1

In Figure 6.33 the drainage curve of the sludge for drying bed C was reported. During the free water loss phase, the curve exhibited a constant trend, decreasing from a value of 3.152 l/min to 3.142 l/min. Subsequently, during the interstitial water removal phase, the drainage rate underwent a drastic decrease, dropping from 3.142 l/min to 0.236 l/min. Additionally, during the surface water loss phase, the drainage rate further decreased to a value of 0.031 l/min. The final part of the curve, corresponding to the deep-water phase, showed a further decrease in the drainage rate to a value of 5.1 $\times 10^{-4}$ l/min.

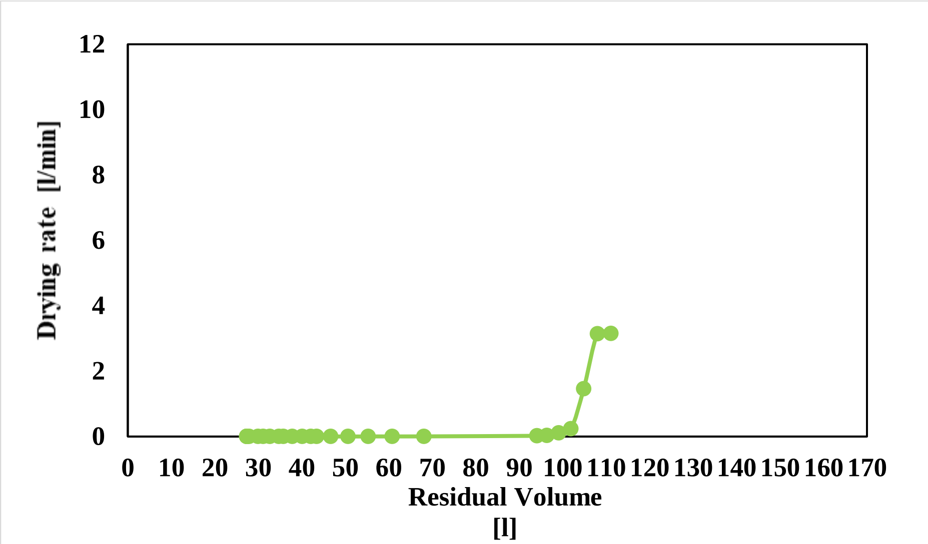

Figure 6.33 - Drainage curve of the sludge in drying bed_test 1

For this test, Greenhouse B showed the best performance in terms of sludge weight reduction (93.04 %).

Table 6.7 - % Reduction test_1

Test 1			
% Reduction	**Greenhouse A**	**Greenhouse B**	**Drying Bed C**
Weight	82.60	93.04	89.56

Regarding the reduction of volatile solids, the fraction of organic solids depends on the type of sludge, the drying conditions, and the efficiency of the drying process. In particular, the initial values of VS/TS ratio were around 84.5 %. The high volatile solids content observed in the three cases has a significant impact on the dewaterability characteristics of the sludge, particularly worsening as this parameter increases. Additionally, very high values indicate a low level of sludge stabilization. At the end of the experiment, the VS/TS ratio was found to be 73 %, 73 %, and 77 %, respectively, for Greenhouse A, Greenhouse B, and the drying bed.

6.6.2 Test 2

The second test began on 08/03/2023 and ended on 06/04/2023, with a total duration of 30 days. The configuration adopted for this test involved the use of three solar greenhouse prototypes: Greenhouse A with hot air introduced above the layer of sludge, Greenhouse B with hot air introduced below the layer of sludge, and Greenhouse C* covered but without hot air introduction. The airflow rate injected into Greenhouse A and Greenhouse B was 16 m^3/m^2xh. The initial thickness of the sludge placed inside the three greenhouses was 25 cm with an initial weight of 155 kg. The sludge inserted into the greenhouses is thickened but not digested.

6.6.2.1 Measurements Humidity

In Table 6.8 and Figure 6.34 the moisture values for the three solar greenhouses during the experimental period were reported, along with their trends over time. Starting from an initial sludge moisture content of 98 %, which was the same for all three greenhouses, a decrease in moisture was observed, reaching 6 % for greenhouse A, 7 % for greenhouse B, and 44 % for greenhouse C*.

Table 6.8 - Humidity_ test 2

Days of Experimentation	Greenhouse A	Greenhouse B	Greenhouse C*
1	98%	98%	98%
2	96%	89%	89%
3	76%	70%	79%
6	72%	67%	75%
7	68%	66%	70%
13	67%	64%	69%
20	42%	47%	66%
22	26%	45%	60%
24	10%	39%	49%
30	6%	7%	44%

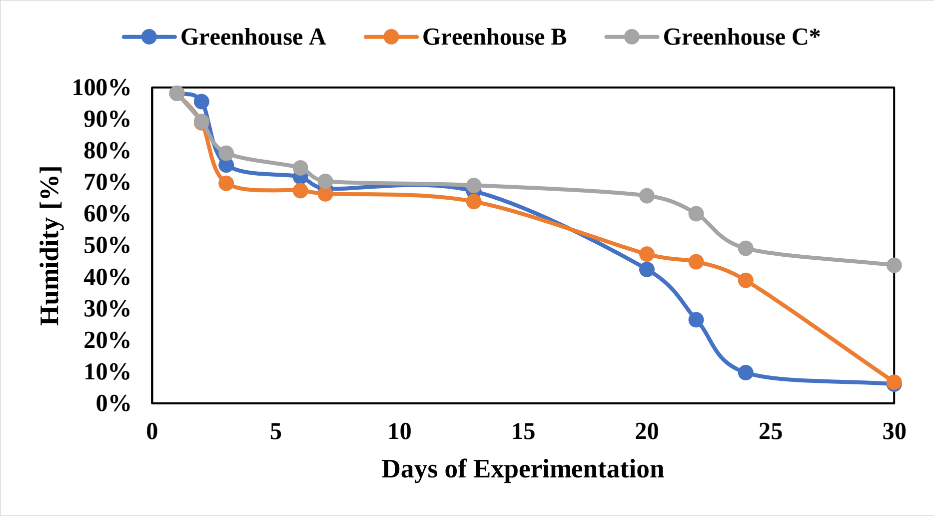

Figure 6.34 - Humidity Trend_ Test 2

6.6.2.2 Temperature

Figure 6.35 shows the temperature trends monitored during the experimental period. Obviously, due to the air insufflation inside greenhouses A and B, the internal temperature is higher than the external temperature.

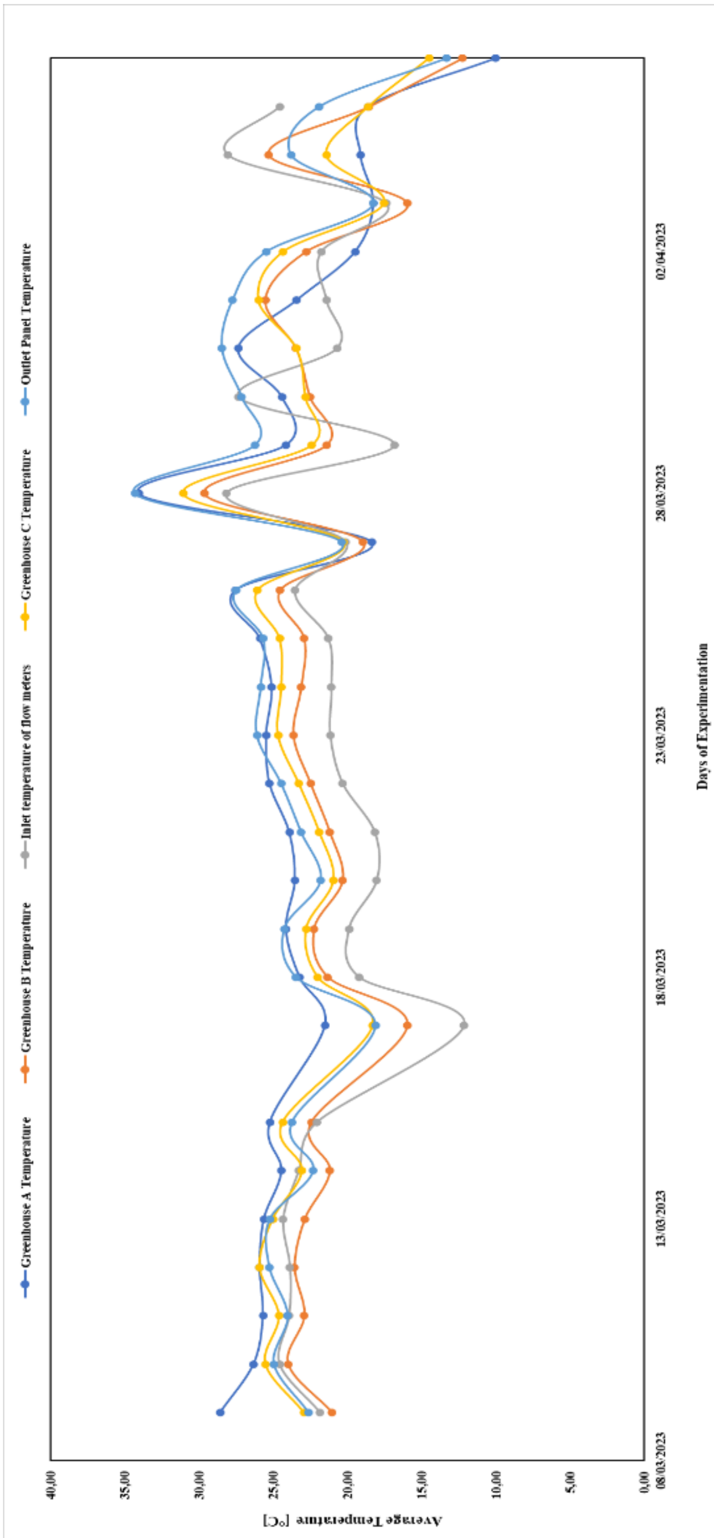

Figure 6.35 - Temperature Trend - test 2

6.6.2.3 Drainage Curve

In Figure 6.36, Figure 6.37 and Figure 6.38 the drainage curves for the three solar greenhouses were reported. During the free water loss phase, the drying rate remained constant for all three greenhouses, with values of 5 l/min, 6.5 l/min, and 5 l/min for greenhouses A, B, and C*, respectively. Subsequently, during the interstitial water removal phase, the drying rate drastically decreased to 0.6 l/min for all three greenhouses. During the surface water loss phase, the drying rate further decreased to 0.02 l/min, 0.1 l/min, and 0.04 l/min. The final part of the curve, corresponding to the deep-water phase, showed a further decrease in the drying rate to a value close to zero for all three solar greenhouses. Table 6.9 shows the overall volume of water lost for the three solar greenhouses.

Table 6.9 - Drained water_ test 2

Greenhouse A	Greenhouse B	Greenhouse C*
76.7l	65.3 l	63.7 l

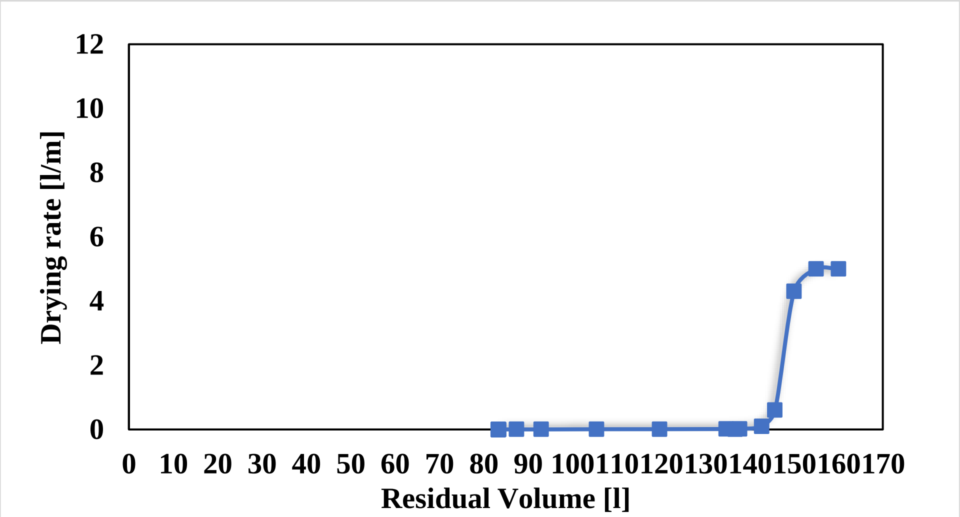

Figure 6.36 - Greenhouse drainage curve A_ test 2

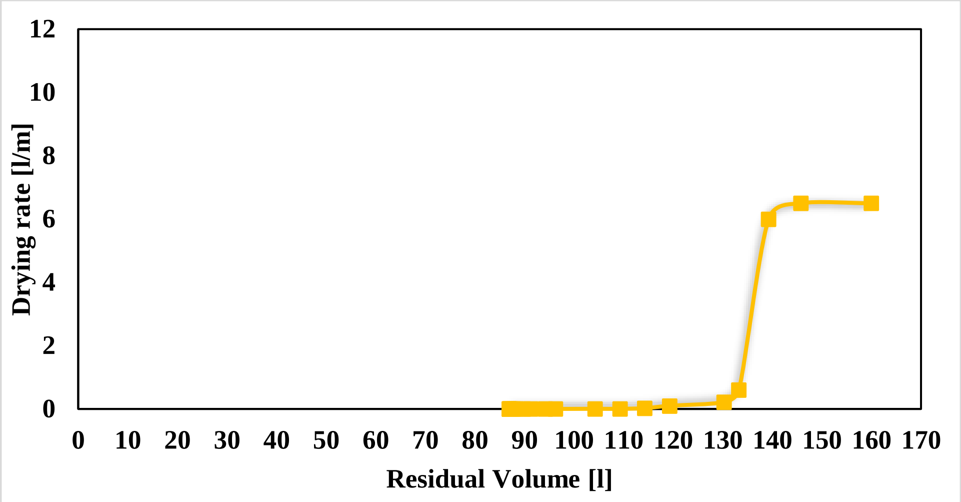

Figure 6.37 - Greenhouse drainage curve B_ test 2

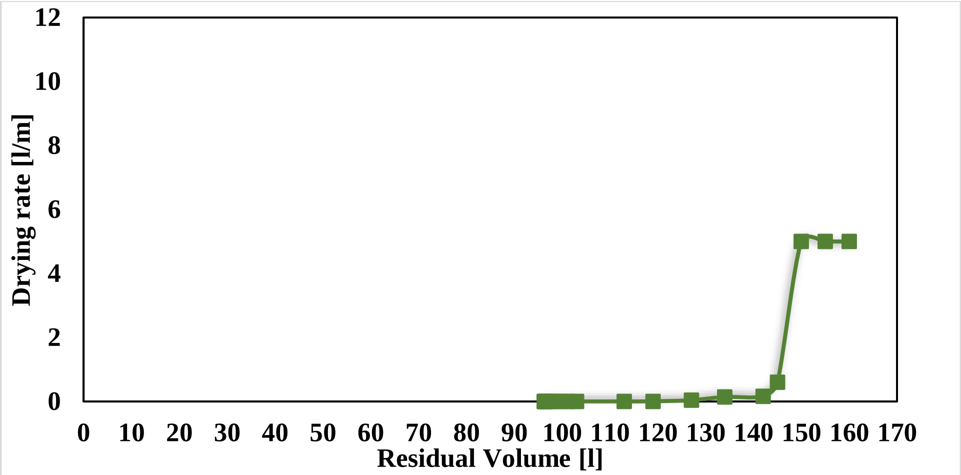

Figure 6.38 - Greenhouse drainage curve C*_ test 2

6.6.2.4 Weight Sludge reduction

Figure 6.39 shows the physical conditions of the sludge at the end of the second experimental period.

Figure 6.39 - Condition of the sludge in Greenhouse A, B, and C* at the end of test_2

At the end of the test, the final weight of the sludge was 4 kg in greenhouse A, 3.9 kg in greenhouse B, and 19 kg in greenhouse C* (Figure 6.40).

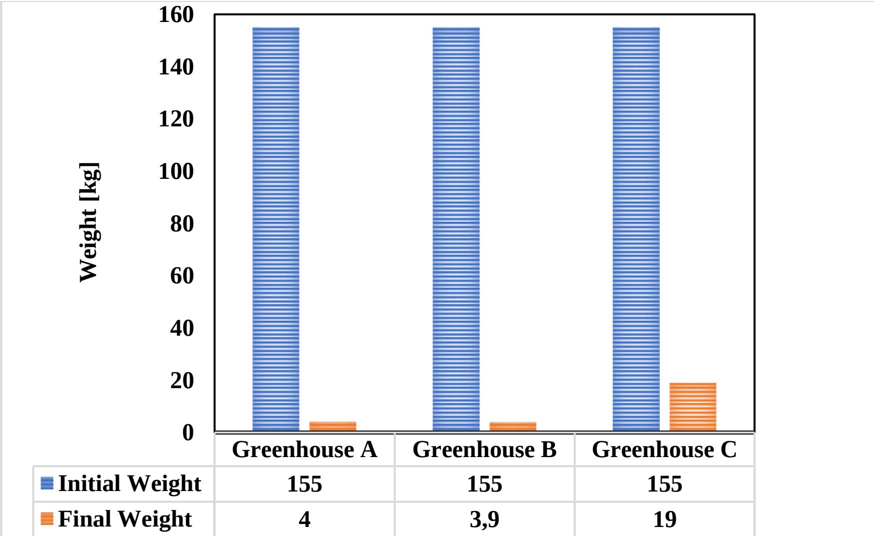

Figure 6.40 - Weight_ Test 2

Table 6.10 shows the percentage reduction in sludge weight for the three solar greenhouses. The greenhouse B has been resulted the best greenhouse in terms of weight sludge reduction.

Table 6.10 - % Reduction test_2

Test 2			
% Reduction	**Greenhouse A**	**Greenhouse B**	**Greenhouse C***
Weight	97.41	97.48	87.74

At the end of the second test the VS/TS ratio was found to be 41.6 % for Greenhouse A, 41.34 % for Greenhouse B, and 47.8 % for Greenhouse C*. The average initial value of VS/TS ratio at the start of the test was 73.41 %. It was observed that the final sludge in Greenhouse A and Greenhouse B is stabilized. In

Greenhouse C*, the ratio is slightly higher, indicating a sludge that is more or less stabilized.

6.6.3 Test 3

The third test began on 19/04/2023 and ended on 18/05/2023, with a total duration of 30 days. The configuration adopted for this test involved the use of three solar greenhouse prototypes: Greenhouse A with hot air introduced above the layer of sludge, Greenhouse B with hot air introduced below the layer of sludge, and Greenhouse C* without hot air introduction. The airflow rate injected into Greenhouse A and Greenhouse B was 23 m^3/m^2xh. The initial thickness of the sludge placed inside the three greenhouses was 27 cm with an initial weight of 167 kg. The sludge inserted into the greenhouses is thickened but not digested.

6.6.3.1 Measurements Humidity

Table 6.11 and Figure 6.41 show the moisture values for the three solar greenhouses during the experimental period and their trends over time. Starting from an initial sludge moisture content of 97 %, which was the same for all three greenhouses, a decrease in moisture was observed, reaching 6% for greenhouse A, 4.92 % for greenhouse B, and 34.30 % for greenhouse C*.

Table 6.11 - Humidity_ test 3

Days of Experimentation	Greenhouse A	Greenhouse B	Greenhouse C*
1	97%	97%	97%
6	77%	96.55%	96.55%
8	62%	66.76%	76.74%
10	56%	58.71%	73.28%
14	37%	54.06%	63.55%
16	10%	38.74%	51.13%
23	8%	13.00%	48.73%
30	6%	4.92%	34.30%

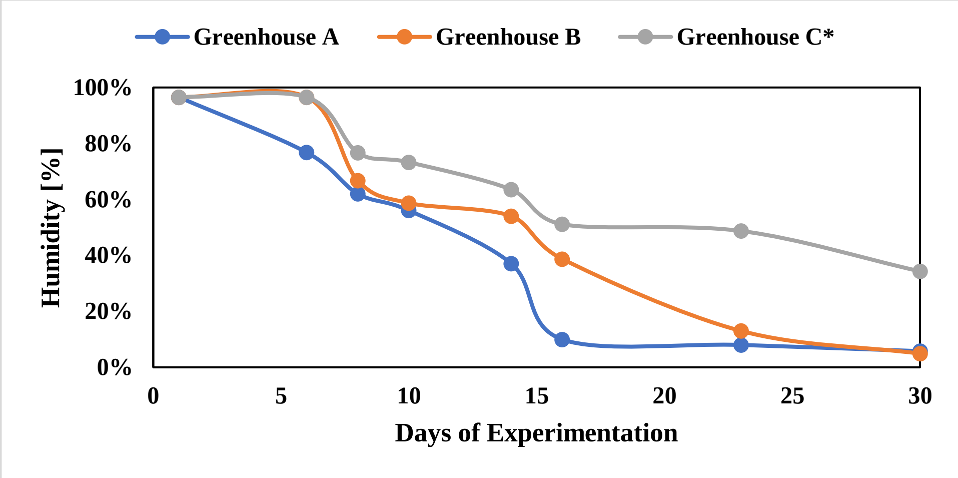

Figure 6.41 - Humidity Trend_ Test 3

6.6.3.2 Temperature

Figure 6.42 shows the temperature trends monitored during the experimental period. It is important to note that the temperatures monitored for this test were: the air temperature at the outlet of the solar panel, the temperature at the inlet of the flow meters installed upstream of the solar greenhouses, and the temperatures inside the solar greenhouses. The temperature trends inside the three solar greenhouses are almost identical, while the trend with the most significant fluctuations is represented by the air temperature at the panel outlet. Indeed, this trend shows a sharp drop from 05/05/2023 to 10/05/2023, likely due to a decrease in the intensity of the incident solar radiation.

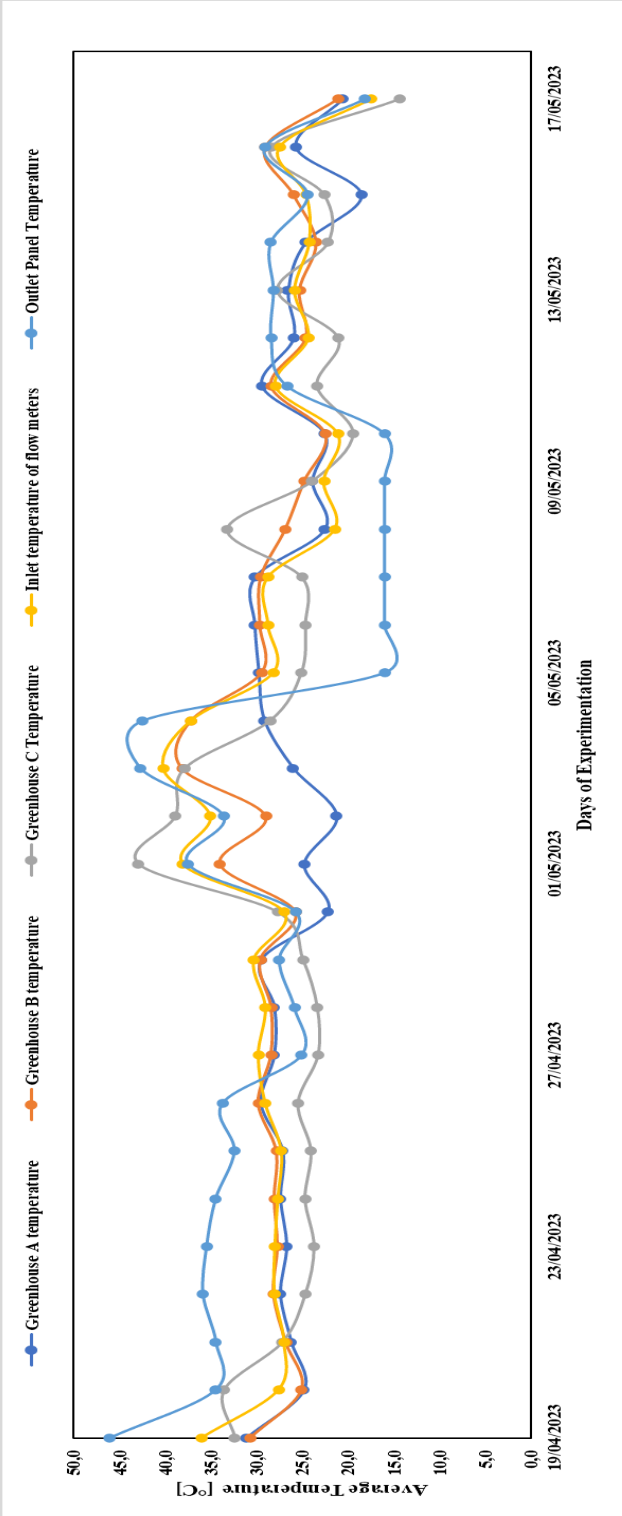

Figure 6.42 - Temperature Trend_ test 3

6.6.3.3 Drainage Curve

Table 6.12 shows the total amount of water lost from the solar greenhouses during the experimental period. It was observed that greenhouse B had the highest volume of water lost during the test (72.62 liters).

Table 6.12 - Drained water_ test 3

Greenhouse A	Greenhouse B	Greenhouse C*
43.32 l	72.62 l	71.8 l

Figure 6.43, Figure 6.44, and Figure 6.45 show the drying speed trends for the three solar greenhouses. Specifically, for greenhouse A (Figure 6.43), during the free water loss phase, the drying speed remained constant at 8 l/min, then decreased to 0.6 l/min during the interstitial water loss phase. This decrease continued until reaching a value of 0.05 l/min (superficial water loss phase), and finally, during the deep-water loss phase, the drying speed was nearly zero. For greenhouse B (Figure 6.44), the drying speed trend was slightly different. During the free water loss phase, the speed decreased from 9.7 l/min to 9 l/min. This decreasing trend continued until it reached a speed of 1.6 l/min (interstitial water loss phase) and then 0.25 l/min during the superficial water loss phase. Finally, for greenhouse C* (Figure 6.45), an initial constant drying speed of 5 l/min was observed during the free water loss phase. In this case as well, the speed then decreased: first dropping to 0.25 l/min (interstitial water loss phase) and then to 0.04 l/min (superficial water loss phase).

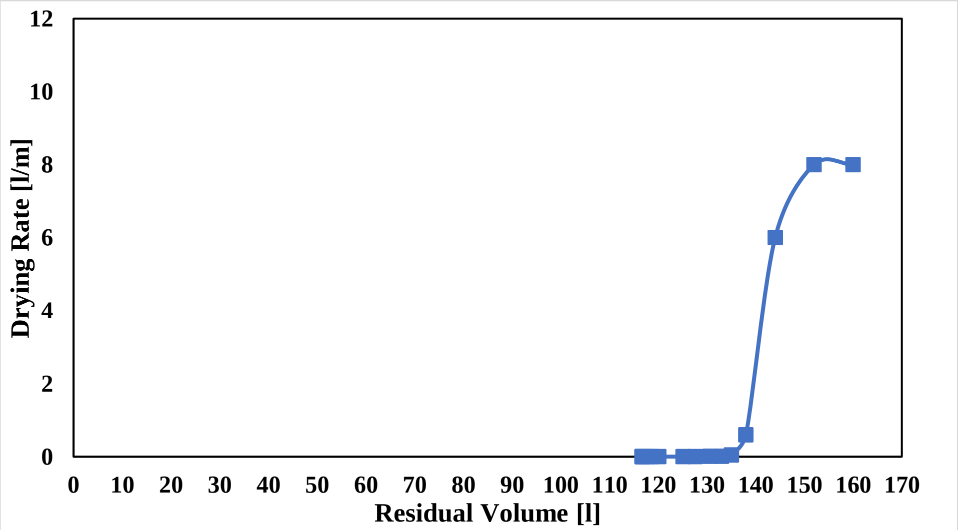

Figure 6.43 - Greenhouse drainage curve A_ test 3

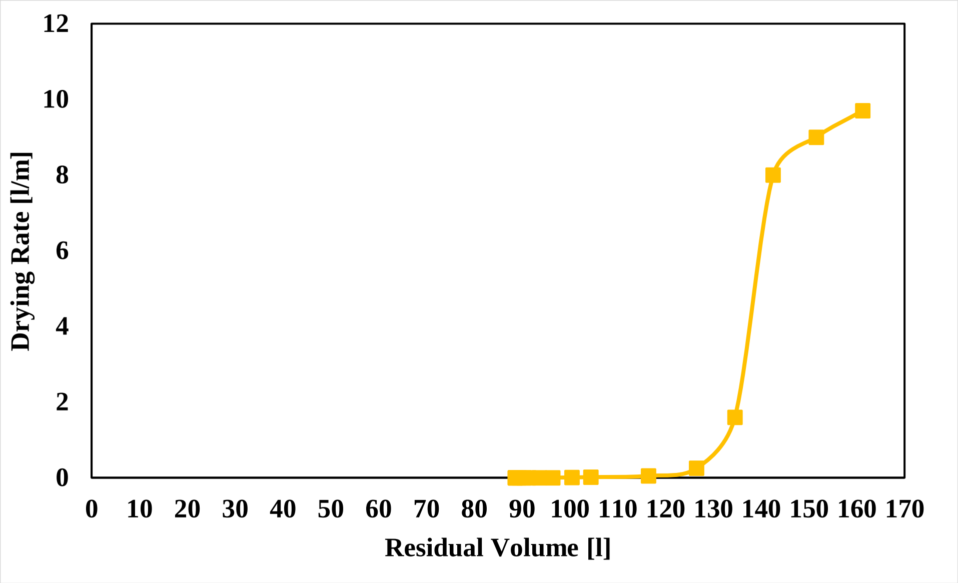

Figure 6.44 - Greenhouse drainage curve B_ test 3

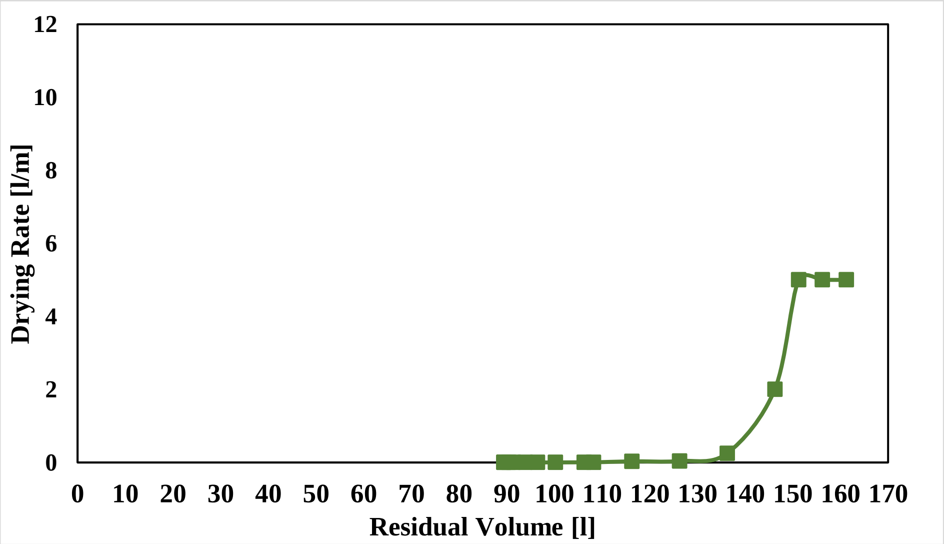

Figure 6.45 - Greenhouse drainage curve C*_ test 3

6.6.3.4 Weight Sludge reduction

At the end of the test, the surfaces of the sludge bed inside the greenhouses were observed (Figure 6.46), which made it possible to determine the final weight of the sludge remaining at the end of the test (Figure 6.47). The final weight of the sludge inside greenhouses A and B was 8 kg, while in greenhouse C* it was 10 kg.

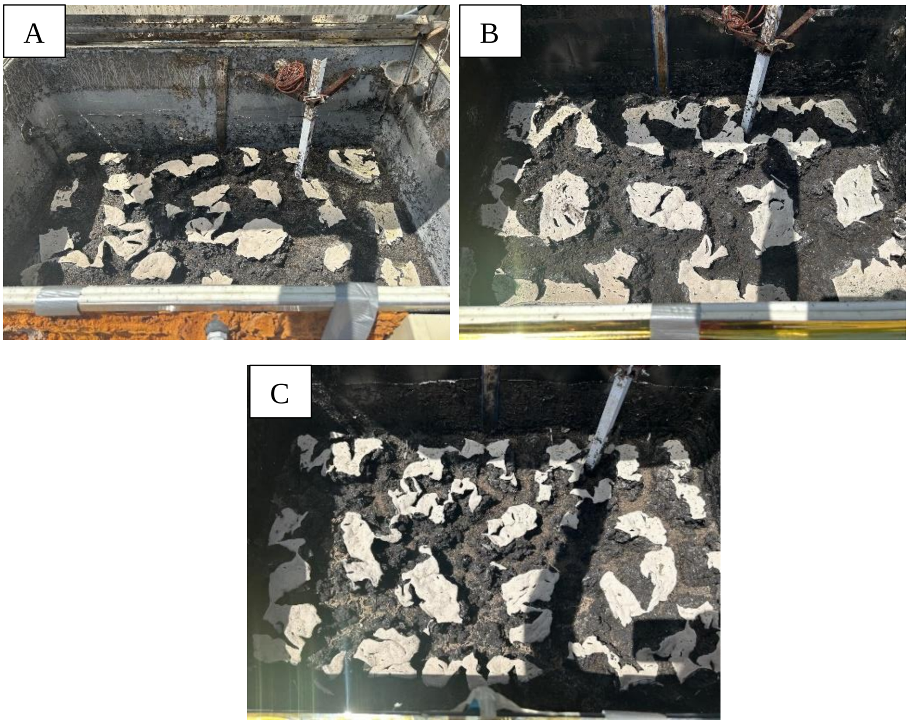

Figure 6.46 - Condition of the sludge in Greenhouse A, B, and C* at the end of test_3

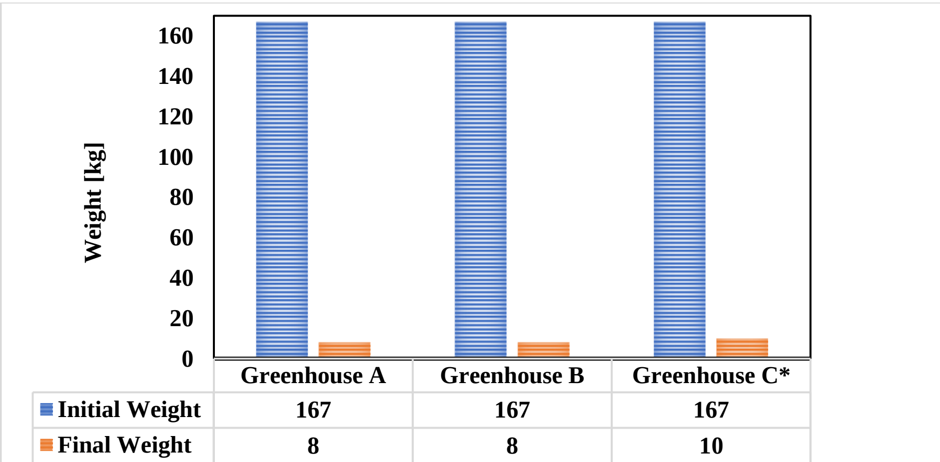

Figure 6.47 - Weight_ test 3

As can be seen in Table 6.13, greenhouse A and greenhouse B showed the highest percentage reductions in sludge weight, both at 95.21 %.

Table 6.13 - % Reduction test_3

Test 3			
% Reduction	**Greenhouse A**	**Greenhouse B**	**Greenhouse C***
Weight	95.21	95.21	94.01

The initial volatile content in the sludge was 86 %. At the end of the test, the volatile content was observed to be 67.3 %, 65.2 %, and 74 %, respectively, for Greenhouse A, Greenhouse B, and Greenhouse C*.

6.6.4 Test 4

The fourth test began on 21/06/2023 and ended on 15/07/2023, with a total duration of 25 days. The configuration adopted for this test involved the use of three solar greenhouse prototypes: Greenhouse A with hot air introduced above the layer of sludge, Greenhouse B with hot air introduced below the layer of sludge, and Greenhouse C with hot air introduced both above and below the layer of sludge. The airflow rate injected into all three greenhouses was 3 m^3/m^2x h. The initial thickness of the sludge placed inside the three greenhouses was 24 cm with an initial weight of 149 kg. The sludge inserted into the greenhouses is thickened but not digested

6.6.4.1 Measurements Humidity

Table 6.14 and Figure 6.48 show the moisture values for the three solar greenhouses during the experimental period and their trends over time. Starting from an initial sludge moisture content of 96.07 %, which was the same for all three greenhouses, a decrease in moisture was observed, reaching 5.78 % for greenhouse A, 4.22 % for greenhouse B, and 4.12 % for greenhouse C.

Table 6.14 - Humidity_ test 4

Days of Experimentation	Greenhouse A	Greenhouse B	Greenhouse C
1	96.07%	96.08%	97.00%
2	91.78%	91.88%	90.63%
3	88,75%	88.63%	80.52%
7	76.01%	77.44%	75.80%
8	68.47%	65.22%	64.73%
10	55.08%	57.21%	50.86%
13	47.87%	38.55%	38.45%
16	15.53%	26.95%	22.35%
17	10.33%	11.70%	7.86%
25	5.78%	4.22%	4.12%

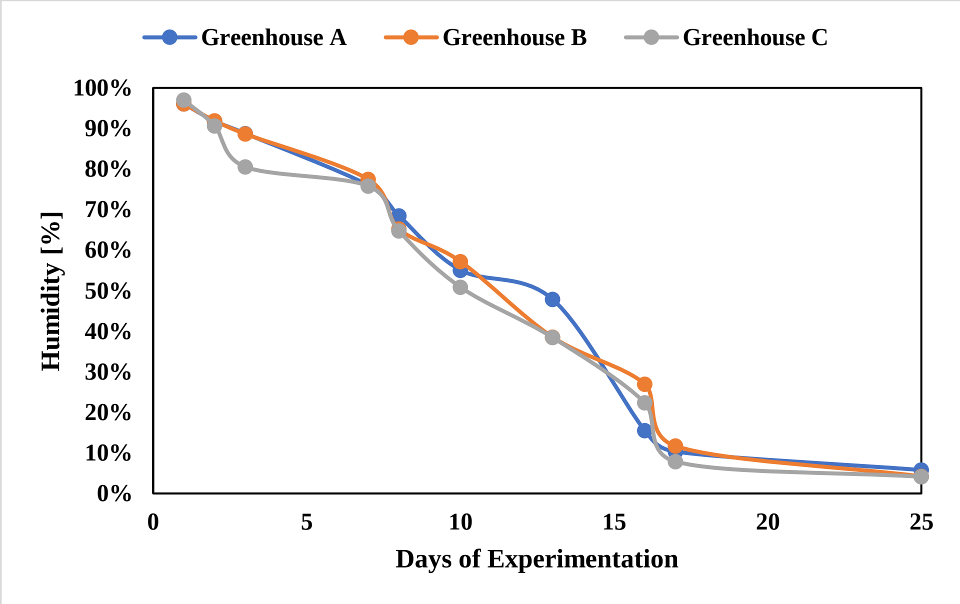

Figure 6.48 - Humidity Trend_ test 4

6.6.4.2 Temperature

Figure 6.53 shows the temperature trends recorded for this test. A lower fluctuation in temperatures is observed, particularly noting a minimum point on 28/06/2023.

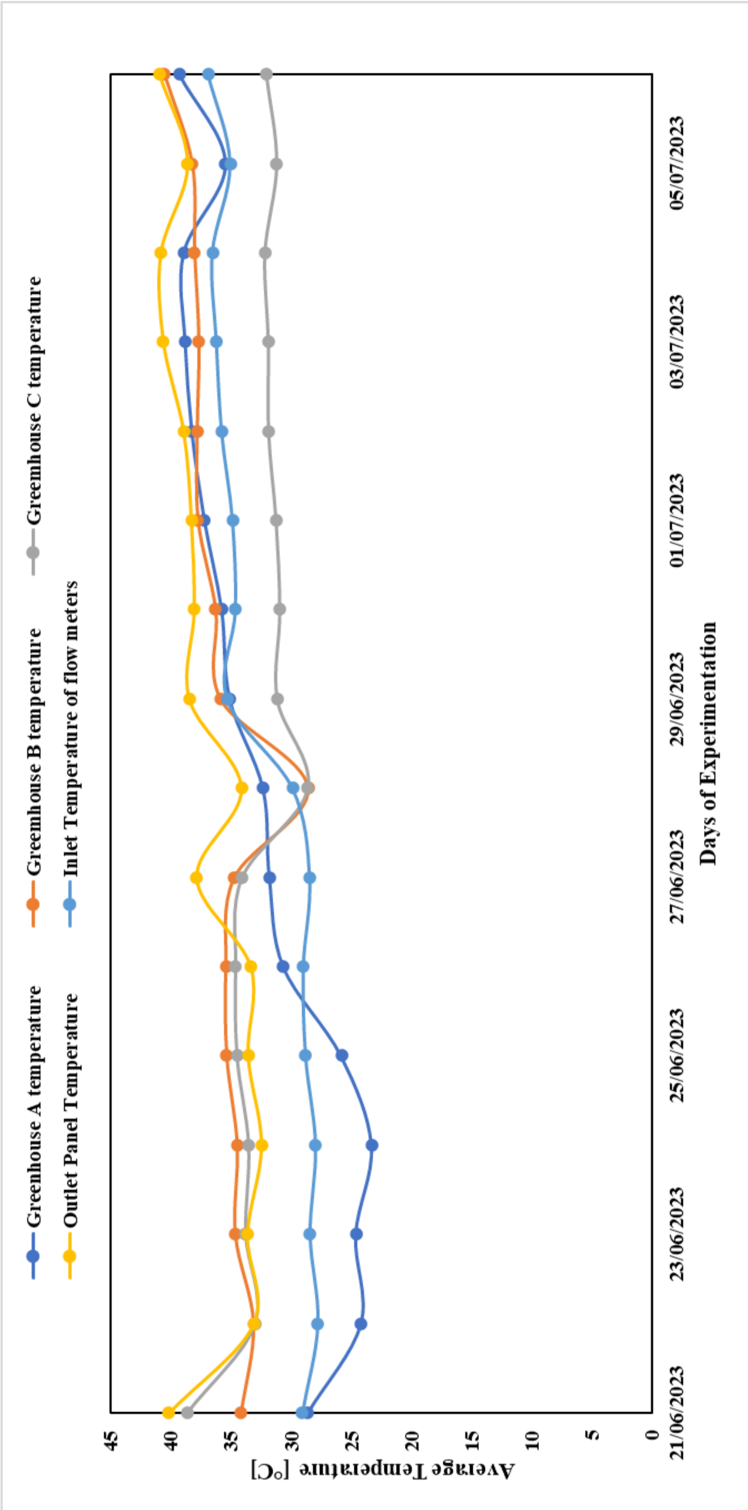

Figure 6.49 -Temperature Trend- test 4

6.6.4.3 Drainage Curve

Table 6.15 shows the total amount of water lost from the three solar greenhouses. It is observed that the highest amount of water lost during this test period was in greenhouse C, with 73 liters. This is followed by greenhouse A, and finally greenhouse B, with 56 liters.

Table 6.15 - Drained water_ test 4

Greenhouse A	Greenhouse B	Greenhouse C
57.5 l	56 l	73 l

The drainage curves of the solar greenhouses are shown in Figure 6.50, Figure 6.51 and Figure 6.52, 101, and 102. For all three curves, the free water loss phase was characterized by a constant drainage speed of 10 l/min. The subsequent interstitial water loss phase was marked by a significant decrease in drainage speed, reaching 1.2 l/min for greenhouse A, 0.5 l/min for greenhouse B, and 1 l/min for greenhouse C. During the superficial water loss phase, the drainage speeds for all three greenhouses reached a value of 0.125 l/min.

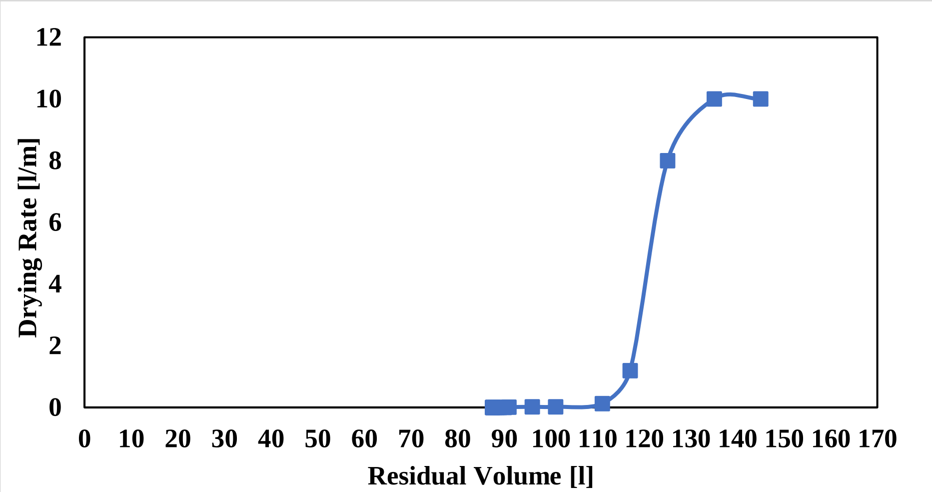

Figure 6.50 - Greenhouse Drainage curve A_ test 4

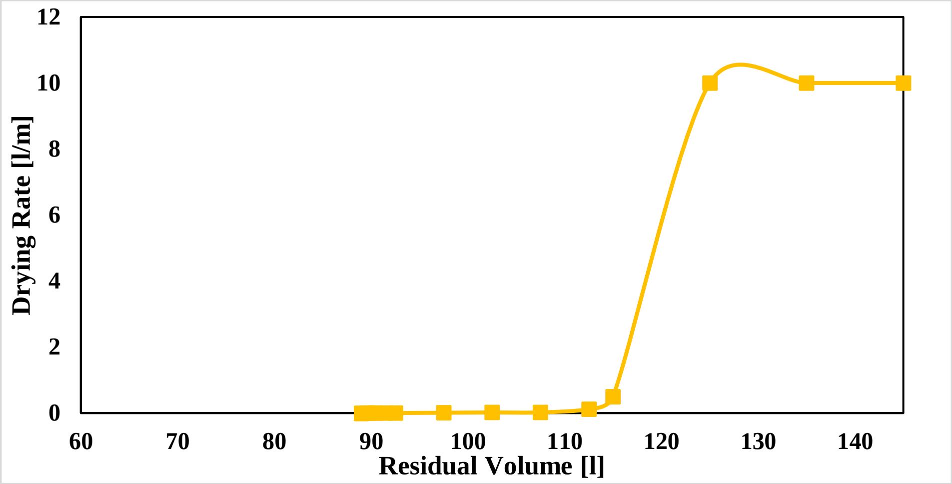

Figure 6.51 - Greenhouse Drainage curve B_ test 4

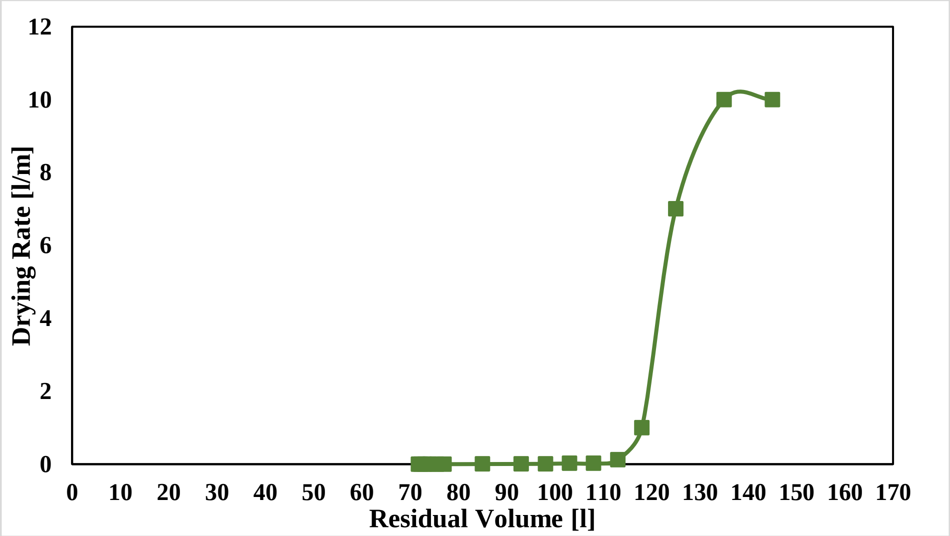

Figure 6.52 - Greenhouse Drainage curve C_ test 4

6.6.4.4 Weight Sludge reduction

At the end of the test (Figure 6.53), the final sludge weights inside the three greenhouses were recorded (Figure 6.54). Greenhouse C showed better performance, reaching a final sludge weight of 3.74 kg with a weight reduction percentage of 97.49 % (Table 6.16).

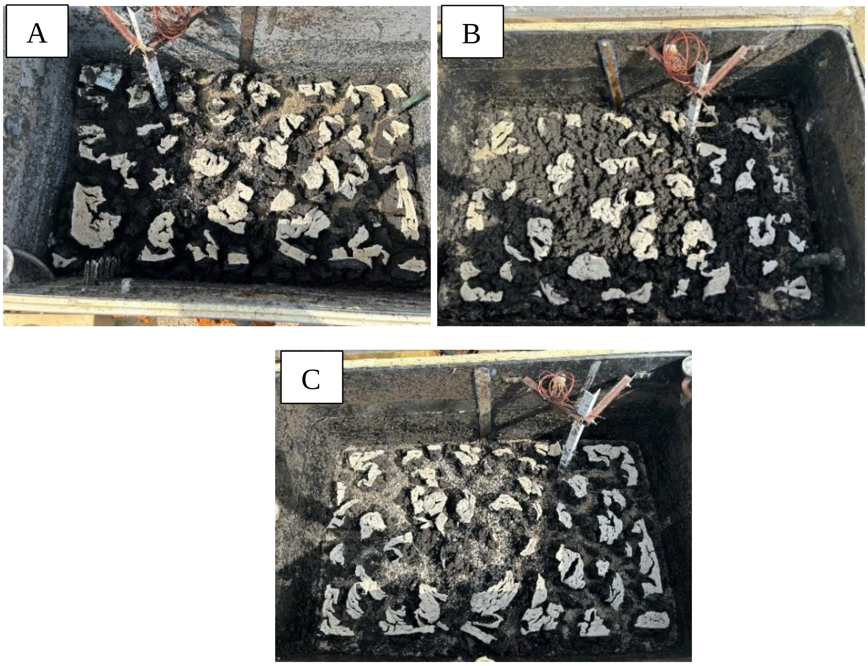

Figure 6.53 - Condition of the sludge in Greenhouse A, B, and C at the end of test_4

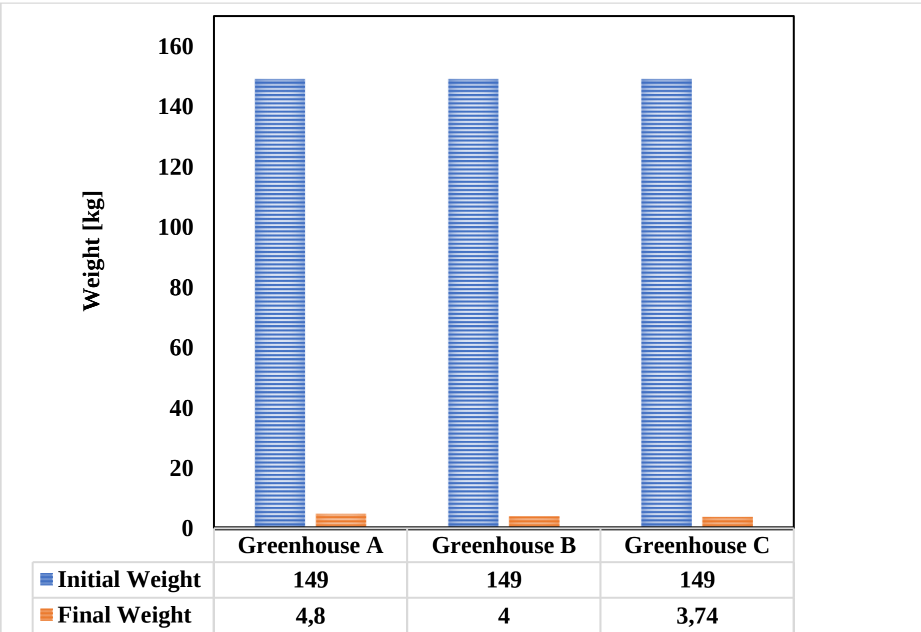

Figure 6.54 - Weight_Test 4

Table 6.16 - % Reduction test_4

Test 4			
% Reduction	**Greenhouse A**	**Greenhouse B**	**Greenhouse C**
Weight	96.78	97.31	97.49

The initial volatile content in the sludge was 86 %. At the end of the test, the volatile content was observed to be 52 %, 50 %, and 62 %, respectively, for Greenhouse A, Greenhouse B, and Greenhouse C.

6.6.5 Test 5

The fifth test began on 22/08/2023 and ended on 15/09/2023, with a total duration of 25 days. The configuration adopted for this test involved the use of three solar greenhouse prototypes: Greenhouse A with hot air introduced above the layer of sludge, Greenhouse B with hot air introduced below the layer of sludge, and Greenhouse C* without hot air introduction. The airflow rate injected into Greenhouse A and Greenhouse B was 6 m^3/m^2xh. The initial thickness of the sludge placed inside the three greenhouses was 28 cm with an initial weight of 174 kg. The sludge inserted into the greenhouses is thickened but not digested.

6.6.5.1 Measurements Humidity

Table 6.17 and Figure 6.55 show the moisture values for the three solar greenhouses during the experimental period and their trends over time. Starting from an initial sludge moisture content of 97 %, which was the same for all three greenhouses, a decrease in moisture was observed, reaching 6.19 % for greenhouse A, 4.06 % for greenhouse B, and 6 % for greenhouse C*.

Table 6.17 - Humidity_ test 5

Days of Experimentation	Greenhouse A	Greenhouse B	Greenhouse C*
1	96.76%	96.76%	97%
2	84.94%	82.49%	90%
3	70.37%	74.20%	71%
7	60.77%	52.51%	54%
8	54.35%	45.93%	51%
10	43.29%	41.67%	43%
13	32.24%	31.89%	38%
16	21.14%	20.31%	23%
17	16.93%	11.24%	20%
25	6.19%	4.06%	6%

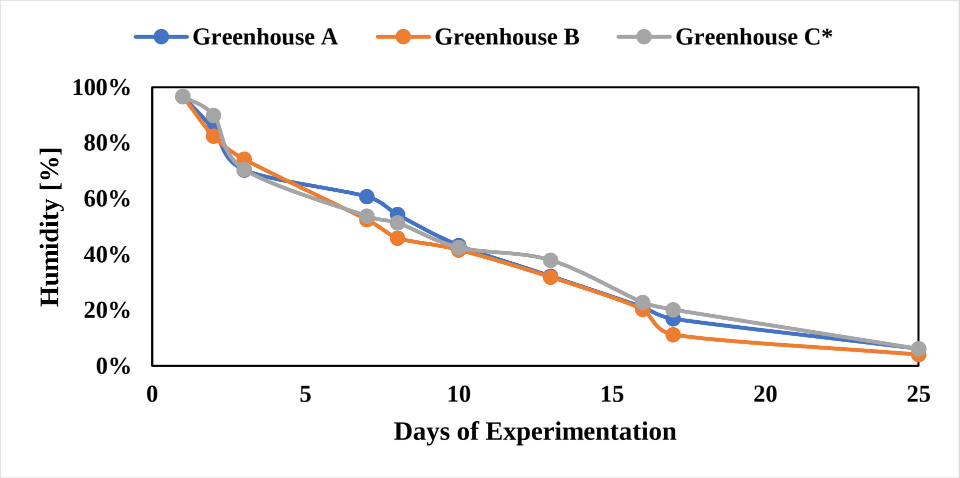

Figure 6.55 - Humidity Trend_Test 5

6.6.5.2 Temperature

The temperature trends for the following test can be observed in Figure 6.56. Specifically, the air temperature at the panel outlet shows high values, representing the greatest contribution to the heating of the solar greenhouses. The internal temperatures of the greenhouses exhibit a nearly identical trend, although greenhouse A shows higher values.

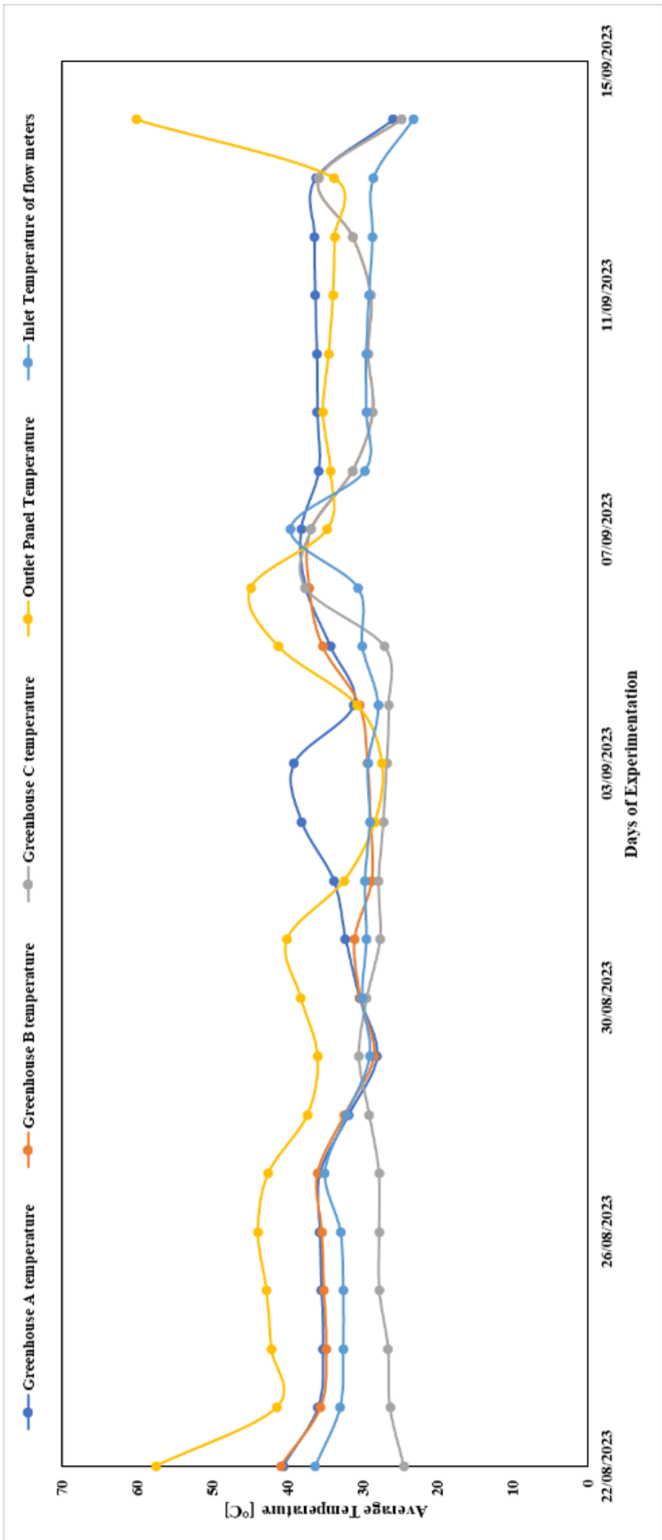

Figure 6.56- Temperature trend_ test 5

6.6.5.3 Drainage Curve

The total amount of water drained from the three greenhouses was 51.20 liters for greenhouse A, 52.50 liters for greenhouse B, and 53.24 liters for greenhouse C* (Table 6.18).

Table 6.18 - Drained water_ test 5

Greenhouse A	Greenhouse B	Greenhouse C*
51.20 l	52.50 l	53.24 l

During the test, the drying speed values for the three greenhouses were analyzed, revealing different profiles. During the free water loss phase, the drying speed decreased from 10 to 9 l/min for greenhouse A, from 8 to 4 l/min for greenhouse B, and remained constant at 10 l/min for greenhouse C*. Following this phase, the drying speed experienced a rapid decline, reaching values of 1.6 l/min, 0.42 l/min, and 2.5 l/min for greenhouses A, B, and C*, respectively (interstitial water loss phase). During the superficial water loss phase, a further decrease in drying speed was observed, dropping to 0.15 l/min for greenhouse A, 0.008 l/min for greenhouse B, and 0.22 l/min for greenhouse C*. In the final phase (deep water loss), the drying speed approached zero for all three greenhouses.

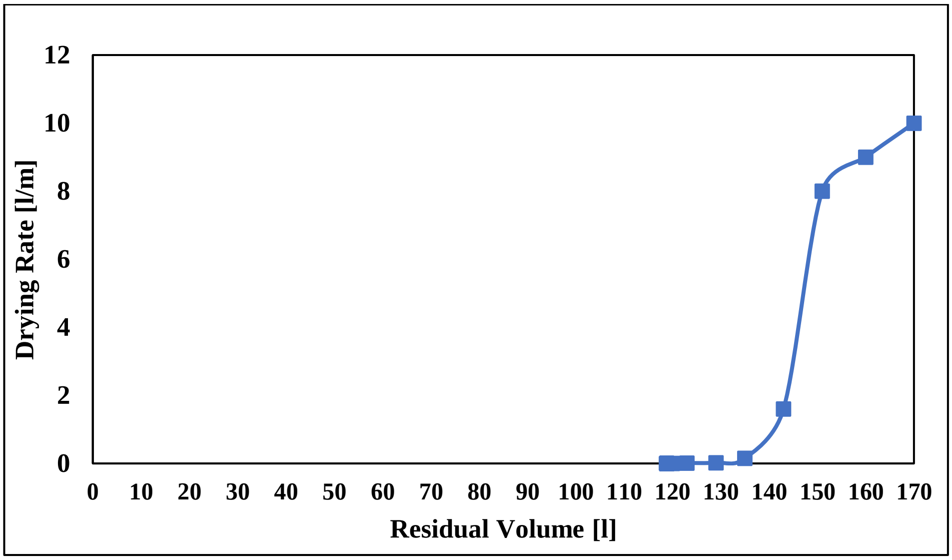

Figure 6.57 - Greenhouse Drainage curve A_ test 5

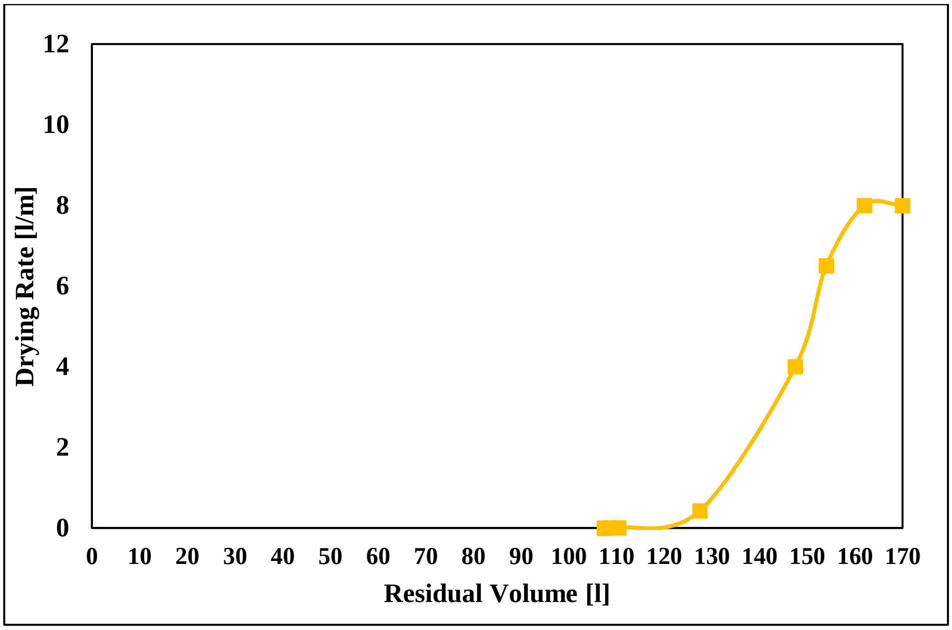

Figure 6.58 - Greenhouse Drainage curve B_ test 5

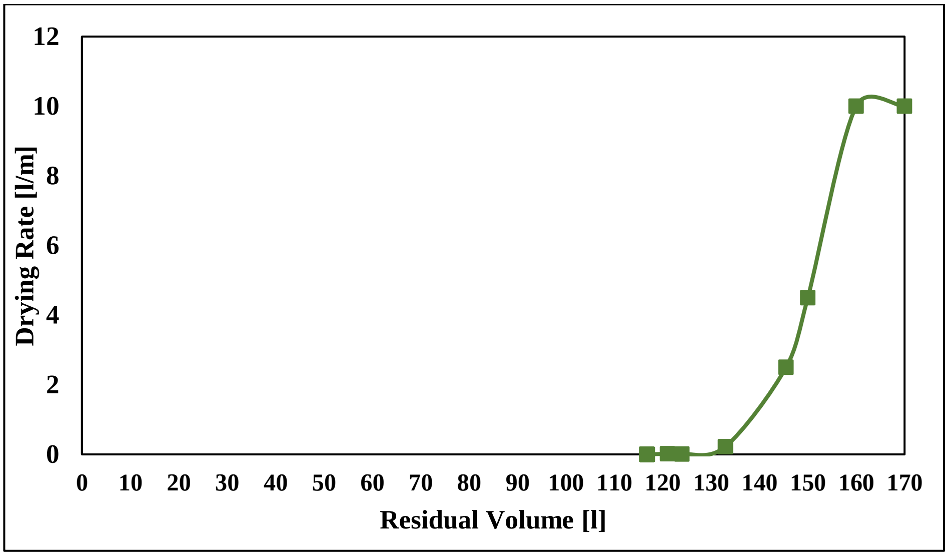

Figure 6.59 - Greenhouse Drainage curve C* _ test 5

6.6.5.4 Weight Sludge reduction

After the experimental period, the final sludge weights inside the three greenhouses were recorded (Figure 6.60). As shown in Figure 6.61, Figure 6.61, the final sludge weights were 3.6 kg, 2.8 kg, and 6.2 kg for greenhouses A, B, and C*, respectively. The best weight reduction percentage was achieved by greenhouse B, with a value of 93.39 % (Table 6.19).

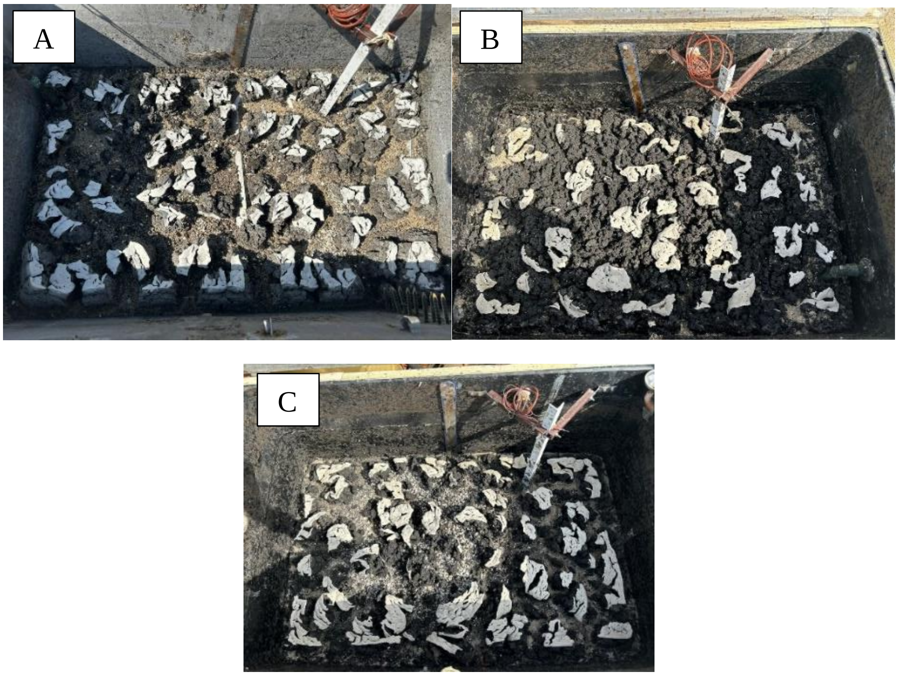

Figure 6.60 - Condition of the sludge in Greenhouse A, B, and C* at the end of test_5

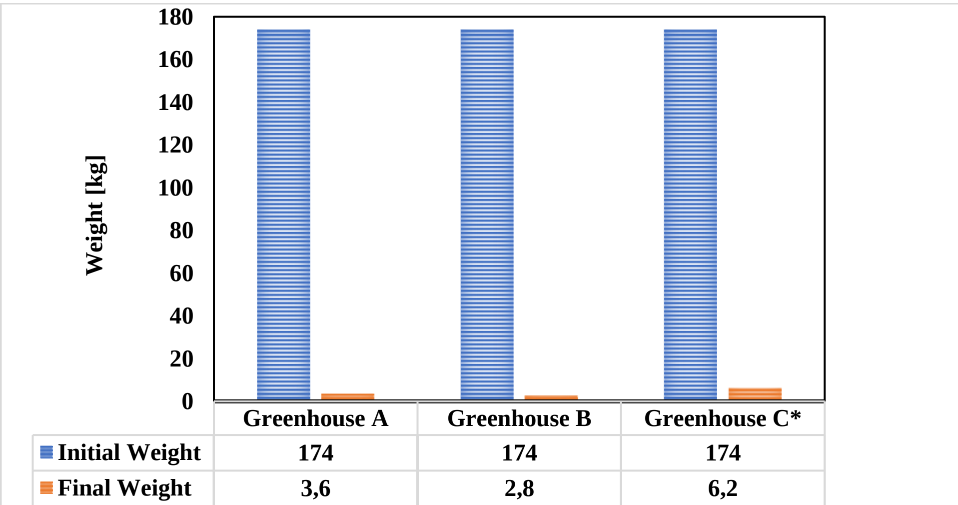

Figure 6.61 - Weight_Test 5

Table 6.19 - % Reduction test_5

Test 5			
% Reduction	**Greenhouse A**	**Greenhouse B**	**Greenhouse C***
Weight	97.93	98.39	96.44

The initial volatile content in the sludge was 86%. At the end of the test, the volatile content was observed to be 57 %, 50 %, and 69 %, respectively, for Greenhouse A, Greenhouse B, and Greenhouse C*.

6.6.6 Test 6

The sixth test began on 22/01/2024 and ended on 21/02/2024, with a total duration of 30 days. The configuration adopted for this test involved the use of three solar greenhouse prototypes: Greenhouse A with hot air introduced above the layer of sludge, Greenhouse B with hot air introduced below the layer of sludge, and Greenhouse C with hot air introduced both above and below the layer of sludge. The airflow rate injected into all three greenhouses was 2 m^3/m^2xh. The initial thickness of the sludge placed inside the three greenhouses was 25 cm with an initial weight of 155 kg. The sludge inserted into the greenhouses is thickened but not digested.

6.6.6.1 Measurements Humidity

Table 6.20 and Figure 6.62 show the moisture values for the three solar greenhouses during the experimental period and their trends over time. Starting from an initial sludge moisture content of 96.67 %, 95.18 % and 94.69 % for three greenhouses, a decrease in moisture was observed, reaching 21.76 % for greenhouse A, 19.63 % for greenhouse B, and 20.52 % for greenhouse C.

Table 6.20 - Humidity_ test 6

Days of Experimentation	Greenhouse A	Greenhouse B	Greenhouse C
1	96.67%	95.18%	94.69%
3	81.92%	77.40%	76.48%
7	78.64%	74.23%	73.57%
9	75.94%	72.26%	71.87%
10	68.00%	66.52%	65.44%
14	60.37%	65.68%	62.04%
16	57.93%	50.08%	52.72%
18	52.74%	45.44%	48.82%
22	43.46%	38.12%	38.09%
24	34.32%	30.60%	31.35%
28	29.77%	26.91%	27.58%
30	21.76%	19.63%	20.52%

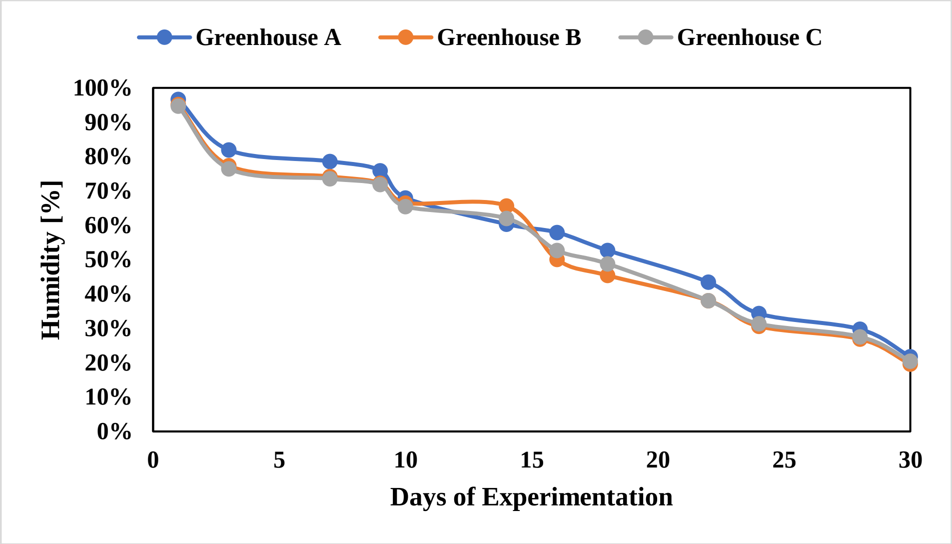

Figure 6.62 - Humidity Trend_ test 6

6.6.6.2 Temperature

Figure 6.63 shows the temperature trends during the test. In particular, it can be stated that the temperature trend is almost consistent over time. Additionally, a maximum temperature point is observed on 10/02/2024 and a minimum temperature point on 08/02/2024. The highest internal temperature is recorded in solar greenhouse A.

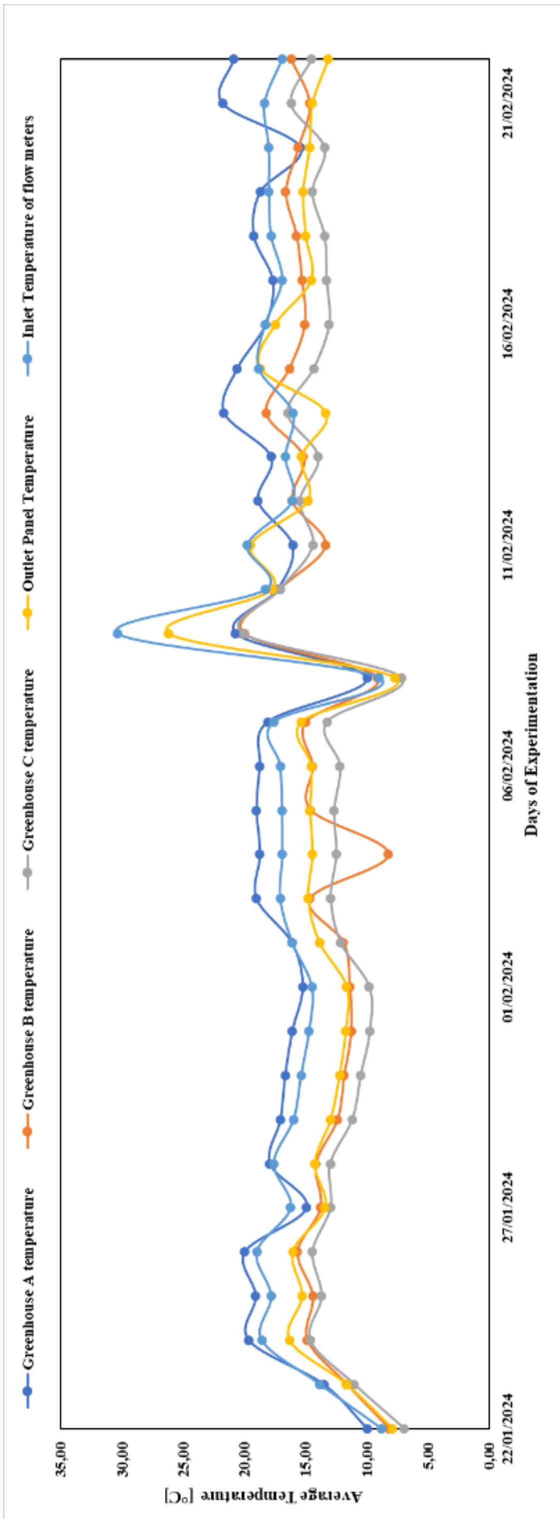

Figure 6.63- Temperature trend_ test 6

6.6.6.3 Drainage Curve

Table 6.21 shows the total amounts of water lost during the experimental period. Specifically, greenhouse C has the highest volume with 67.3 liters, followed by greenhouse B with 65.5 liters, and finally greenhouse A with a water loss volume of 64.2 liters.

Table 6.21 - Drained water_ test 6

Greenhouse A	Greenhouse B	Greenhouse C
64.2 l	65.5 l	67.3 l

Greenhouses A and B showed similar drying speed trends (Figure 6.64 and Figure 6.65). During the free water loss phase, the drying speed remained constant at 5.4 l/min for greenhouse A and 5 l/min for greenhouse B. During the interstitial water loss phase, the drying speed decreased for both greenhouses to 0.45 l/min. This phase was followed by a further reduction in drying speed to 0.006 l/min for greenhouse A and nearly zero for greenhouse B. In contrast, greenhouse C exhibited a slightly different trend (Figure 6.66). During the free water loss phase, the speed decreased from 6.6 l/min to 5.16 l/min. This was followed by a decrease to 0.45 l/min (interstitial water phase) and then a further drop to nearly zero (superficial and deep-water loss).

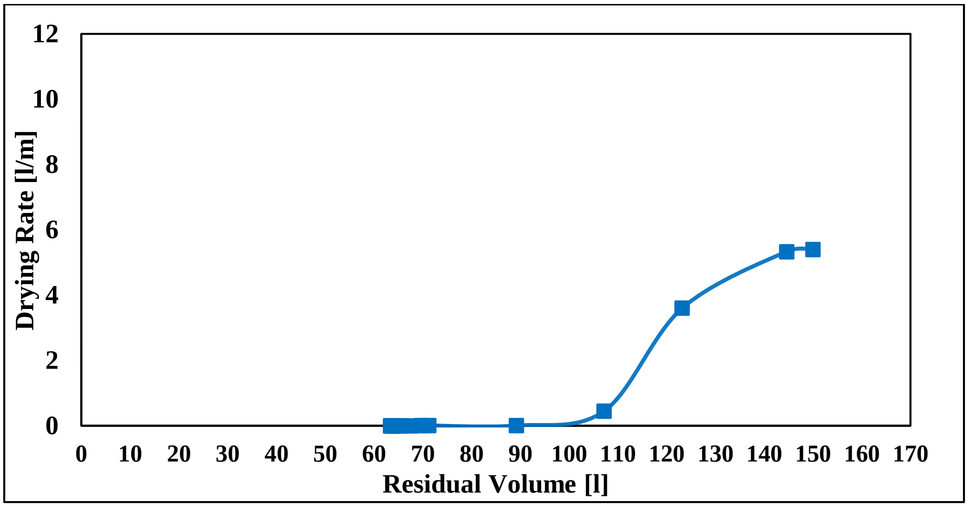

Figure 6.64 - Greenhouse Drainage curve A_ test 6

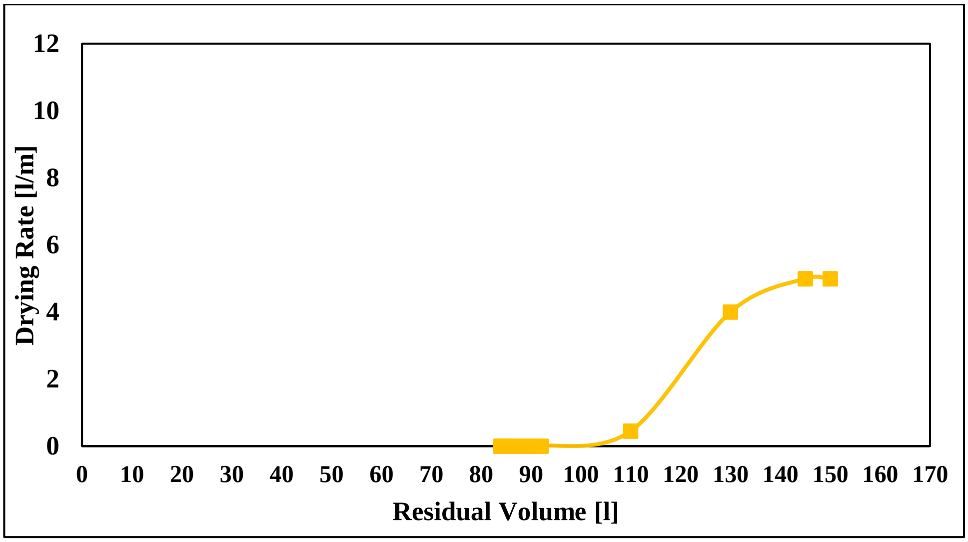

Figure 6.65 - Greenhouse Drainage curve B_ test 6

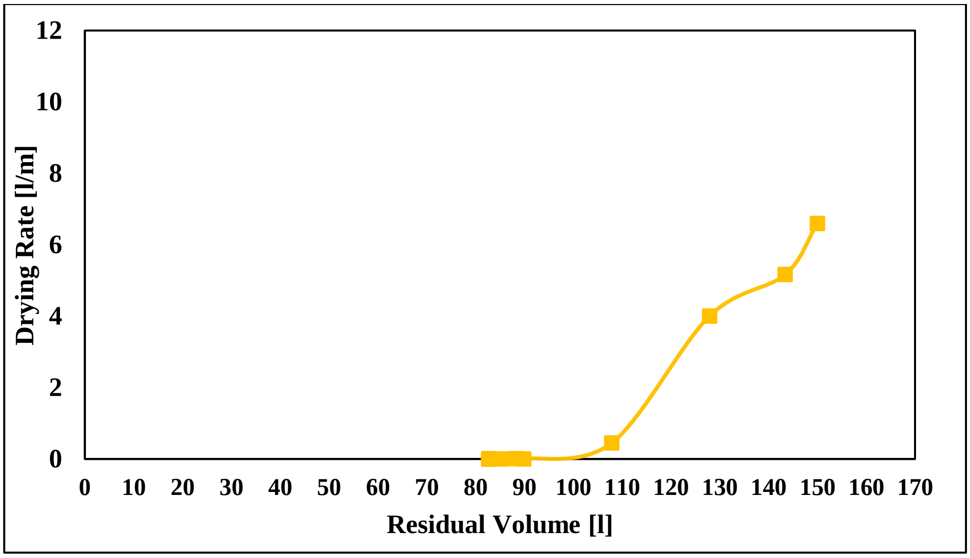

Figure 6.66 - Greenhouse Drainage curve C_ test 6

6.6.6.4 Weight Sludge reduction

The effect of solar drying on the surface of the sludge inside the greenhouse is observable in Figure 6.67. The dehydration effect is clearly visible due to the presence of cracks on the surface of the sludge bed. At the end of the test, the weights of the sludge inside greenhouses A, B, and C were measured, respectively, as 16.3 kg, 14.6 kg, and 16.8 kg (Figure 6.68). The best performance in terms of weight reduction was achieved by greenhouse B, with a value of 90.58 % (Table 6.22).

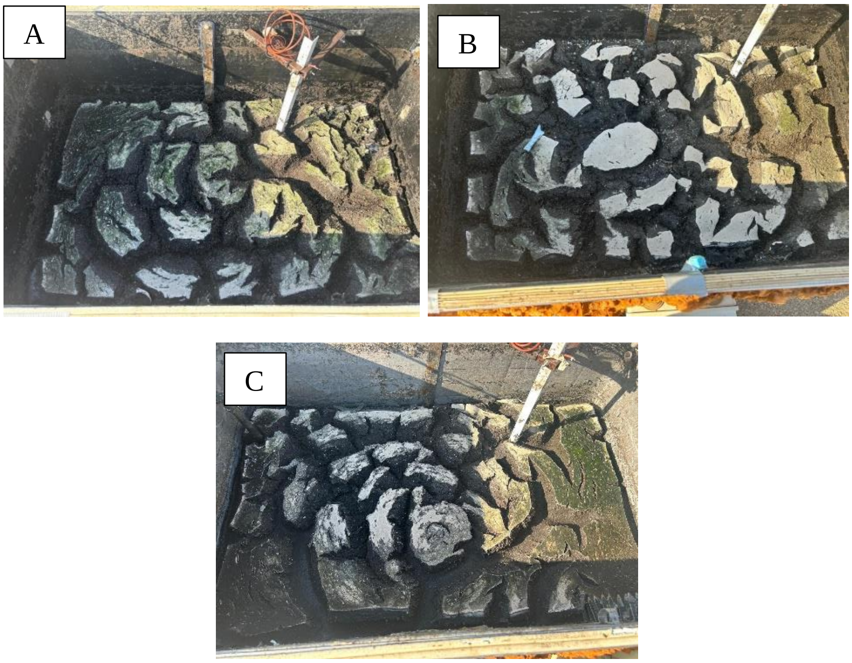

Figure 6.67 - Condition of the sludge in Greenhouse A, B, and C at the end of test_6

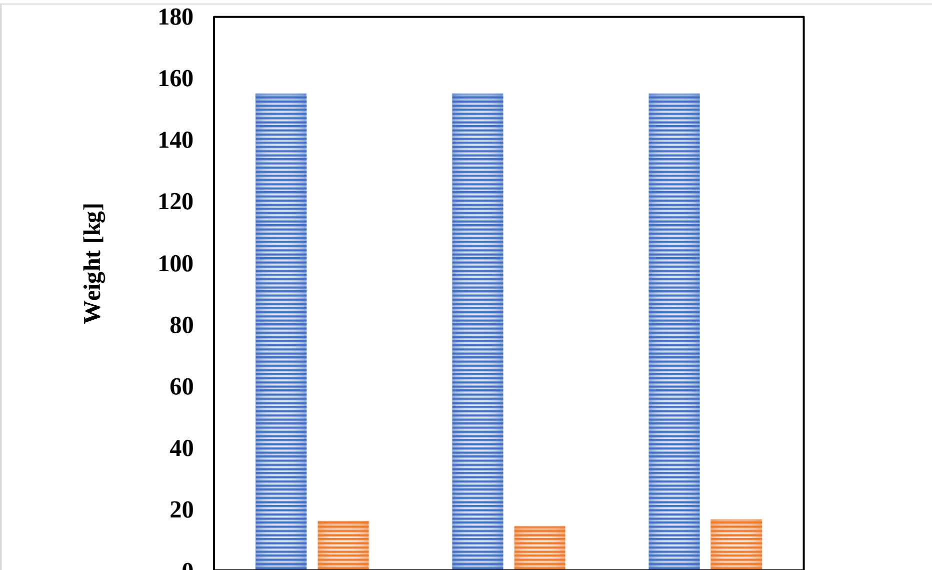

	Greenhouse A	Greenhouse B	Greenhouse C
Initial Weight	155	155	155
Final Weight	16,3	14,6	16,8

Figure 6.68 - Weight_Test 6

Table 6.22 - % Reduction test_6

Test 6			
% Reduction	**Greenhouse A**	**Greenhouse B**	**Greenhouse C**
Weight	89.48	90.58	89.16

The initial volatile content in the sludge was 86 %. At the end of the test, the volatile content was observed to be 61 %, 53 %, and 65 %, respectively, for Greenhouse A, Greenhouse B, and Greenhouse C.

6.6.7 Test 7

The seventh test began on 29/05/2024 and ended on 27/06/2024, with a total duration of 30 days. The configuration adopted for this test involved the use of three solar greenhouse prototypes: Greenhouse A with hot air introduced above the layer of sludge, Greenhouse B with hot air introduced below the layer of sludge, and Greenhouse C with hot air introduced both above and below the layer of sludge. The airflow rate injected into all three greenhouses was 4 m^3/m^2xh. The initial thickness of the sludge placed inside the three greenhouses was 25 cm with an initial weight of 162 kg. The sludge inserted into the greenhouses is thickened but not digested.

6.6.7.1 Measurements Humidity

Table 6.23 and Figure 6.69 show the moisture values for the three solar greenhouses during the experimental period and their trends over time. Starting from an initial sludge moisture content of 97 % for three greenhouses, a decrease in moisture was observed, reaching 5.13 % for greenhouse A, 4.60 % for greenhouse B, and 5.22 % for greenhouse C.

Table 6.23 - Humidity_ test 7

Days of Experimentation	Greenhouse A	Greenhouse B	Greenhouse C
1	97%	97%	97%
3	85.00%	84.00%	87%
7	81.01%	76.87%	78.54%
9	77.00%	64.30%	77.20%
10	74.23%	52.31%	73.00%
14	64.52%	44.29%	63.25%
16	54.20%	37.46%	54.15%
18	45.00%	26.34%	39.45%
22	38.00%	18.77%	37.90%
24	24.00%	14.50%	28.00%
28	11.63%	7.97%	13.64%
30	5.13%	4.60%	5.22%

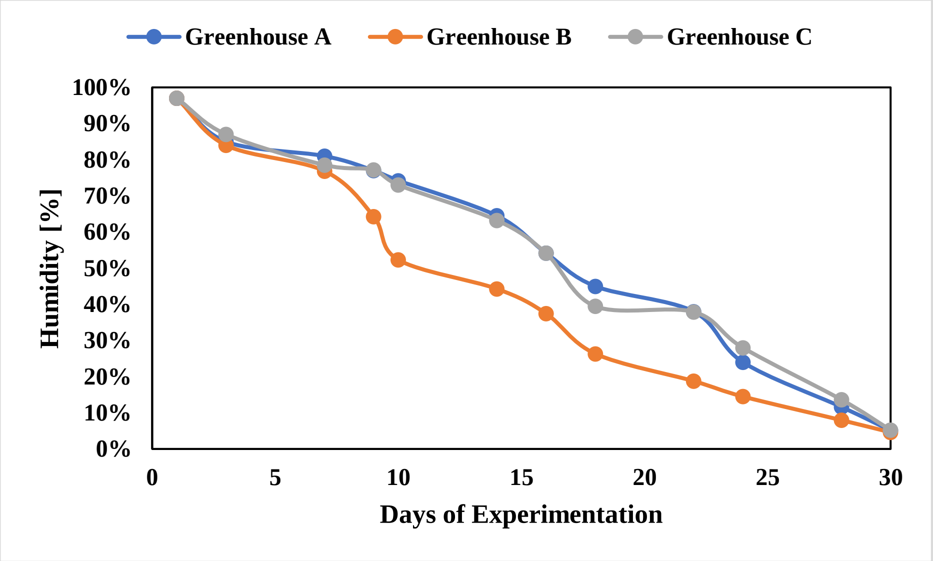

Figure 6.69 - Humidity Trend_ test 7

6.6.7.2 Drainage Curve

Table 6.24 shows the total volumes of water lost for the three solar greenhouses. Specifically, greenhouse B had the highest volume of water lost, amounting to 55 liters.

Table 6.24 - Drained water_ test 7

Greenhouse A	Greenhouse B	Greenhouse C
46 l	55 l	46 l

Figure 6.70, Figure 6.71 and Figure 6.72, show the drainage curves for the three greenhouses. These curves exhibited similar trends. Specifically, during the free water loss phase, a rapid decrease in drying speed was observed, dropping from 10 l/min to 2.6 l/min for greenhouse A, 3.33 l/min for greenhouse B, and 2.6 l/min for greenhouse C. Subsequently, during the interstitial water loss phase, the speed decreased to 0.175 l/min for greenhouse A, 0.125 l/min for greenhouse B, and 1 l/min for greenhouse C. Finally, during the superficial water loss phase, greenhouse A and greenhouse B experienced a further decrease in speed to values approaching zero, whereas greenhouse C had a drainage speed of 0.125 l/min.

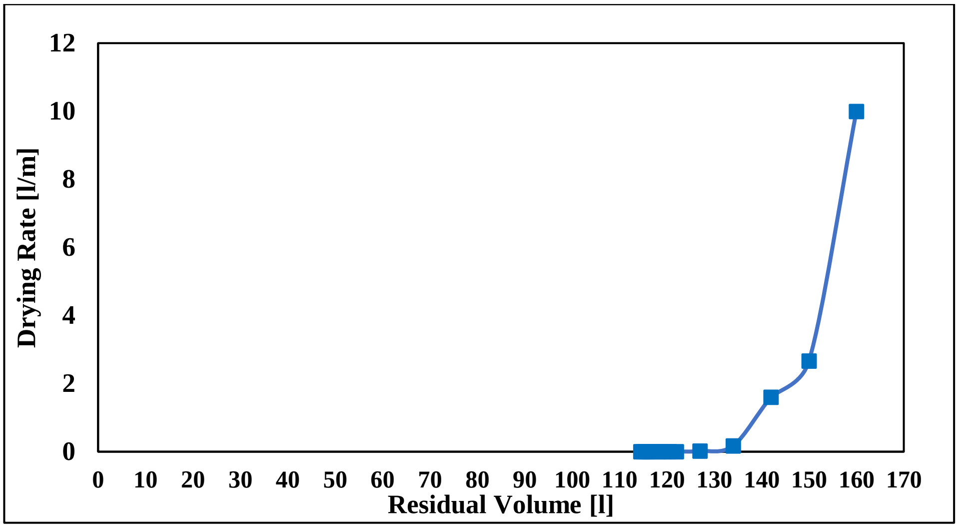

Figure 6.70 - Greenhouse Drainage curve A _ test 7

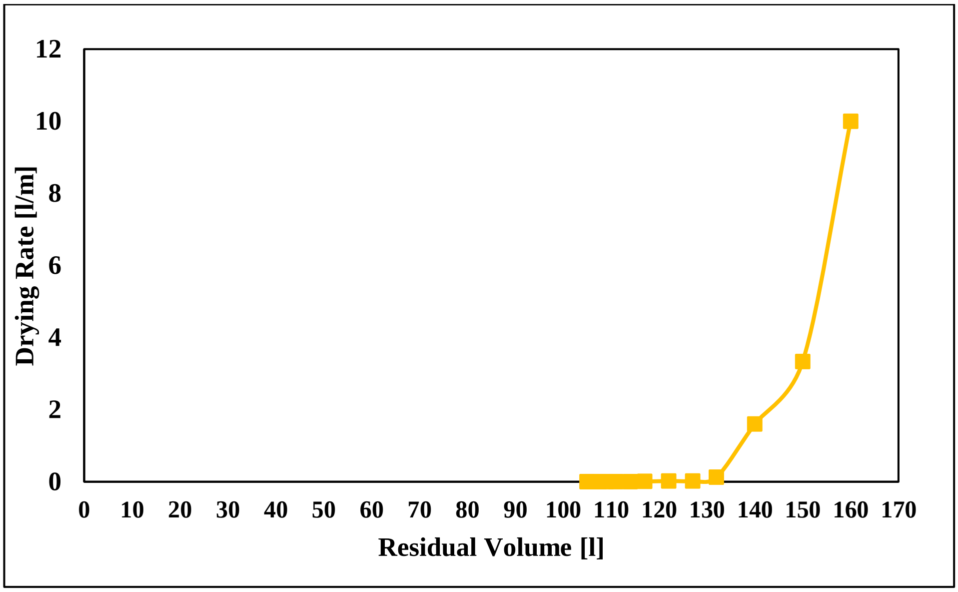

Figure 6.71 - Greenhouse Drainage curve B_ test 7

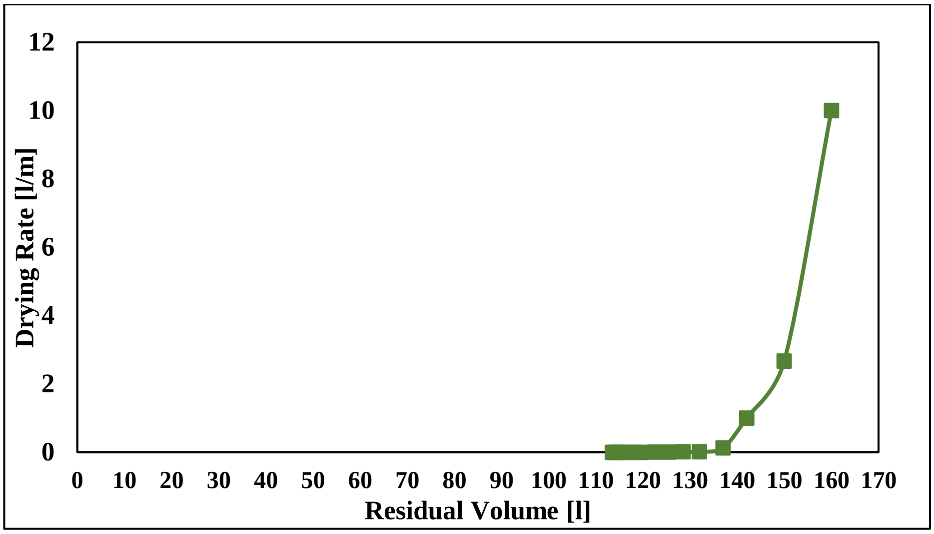

Figure 6.72 - Greenhouse Drainage curve C _ test 7

6.6.7.3 Weight Sludge reduction

The final conditions of the sludge are shown in Figure 6.73. The final sludge weight was 2.6 kg for greenhouse A, 2.5 kg for greenhouse B, and 3.1 kg for greenhouse C (Figure 6.74). The highest weight reduction percentage was 98.46 % for greenhouse B, followed by 98.39 % for greenhouse A (Table 6.25).

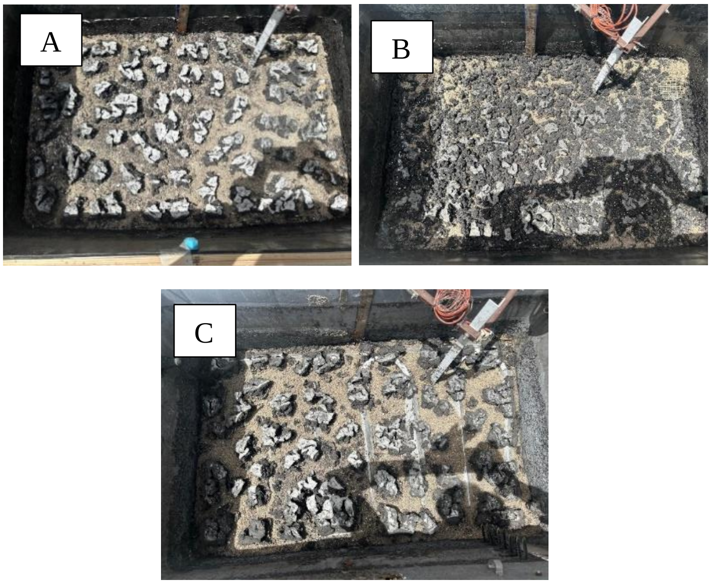

Figure 6.73 - Condition of the sludge in Greenhouse A, B, and C at the end of test_7

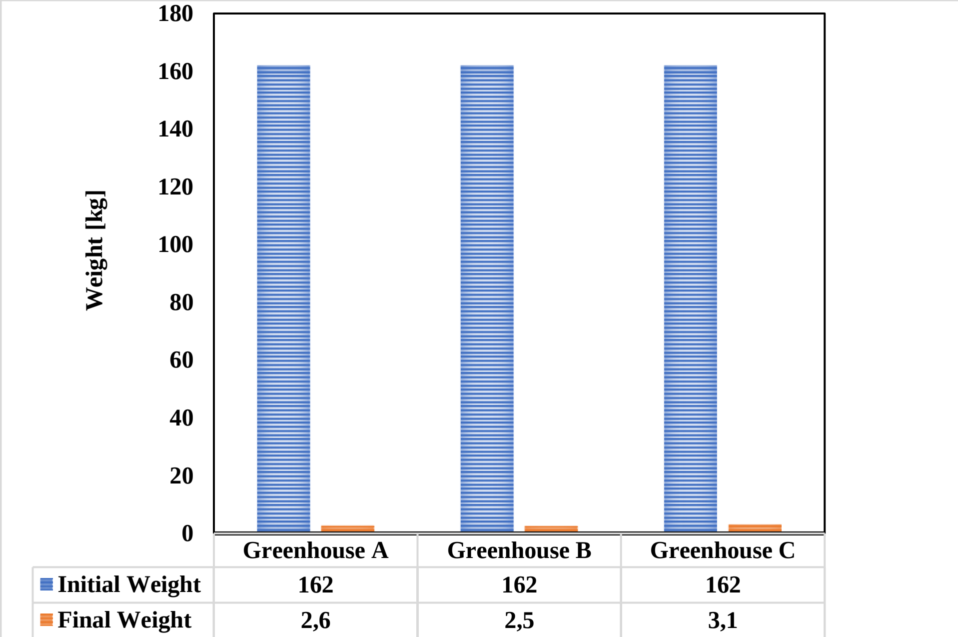

Figure 6.74 - Weight_ Test 7

Table 6.25 - % Reduction test_7

Test 7			
% Reduction	**Greenhouse A**	**Greenhouse B**	**Greenhouse C**
Weight	98.39	98.46	98.09

The initial volatile content in the sludge was 86 %. At the end of the test, the volatile content was observed to be 63 %, 44 %, and 64 %, respectively, for Greenhouse A, Greenhouse B, and Greenhouse C.

7 Analysis and discussion of experimental results from solar greenhouse prototypes

In the following chapter, the drainage curve trends for each individual test conducted on solar greenhouse prototypes A, B, and C (Figure 7.8,Figure 7.9 and Figure 7.10) are discussed. Furthermore, the trends of humidity during the individual tests (Figure 7.17, Figure 7.18 and Figure 7.19) are presented, and finally, comparison graphs of the sludge weight reduction efficiency as a function of specific air flow rate for the different tests (Figure 7.21, Figure 7.22 and Figure 7.24) are shown.

In the graphs shown in Figure 7.8, Figure 7.9 and Figure 7.10, the x-axis represents the residual water volume within the sludge, that is, the amount of water that still needs to evaporate or be drained. Monitoring the residual volume is essential to understand how effective the dehydration process is and to determine when the optimal moisture level for final disposal has been reached. The y-axis, on the other hand, indicates the rate at which the water evaporates or is drained from the sludge. In the context of a solar greenhouse, this rate depends on various factors such as sunlight intensity, ventilation, internal temperature, and the type of sludge being treated.

A high drying rate is desirable to reduce the overall dehydration time and optimize the operational capacity of the solar greenhouse. Specifically, the different drainage curves obtained in the individual tests (Test 1 to Test 7) and for each respective solar greenhouse prototype (Greenhouse A, B, and C) are presented. These curves differ due to variations in the initial moisture content and differences in operational conditions. They provide valuable information about the behaviour of the sludge under specific conditions, helping to predict drying times and optimize the process. The analysis of the drainage curves allows for studying the process in order to:

- Optimize ventilation and temperature of the greenhouse: Solar greenhouses can be optimized to achieve a higher drying rate by using appropriate ventilation systems and maintaining high internal temperatures.
- Manage the sludge layer thickness: For sludges that show slower drainage curves, the thickness of the sludge layer distributed within the greenhouse could be reduced, increasing the evaporation surface area and shortening drying times.

Next, the trends of sludge humidity over the course of the experimental days will be discussed. For each greenhouse, the changes in the sludge humidity values observed during each of the seven tests conducted are presented (Figure 7.17, Figure 7.18 and Figure 7.19).

Finally, three graphs were created (one for each greenhouse prototype), showing the weight reduction values of the sludge observed for each individual test. For each test, the specific air flow rate introduced into the system and the percentage weight reduction of the sludge were reported. These graphs are crucial for understanding the variation in performance of the solar greenhouse prototypes based on the air flow rate introduced into the system.

7.1 Discussion of drainage curve

The following figures show the drainage kinetics for the different tests conducted. It can be observed that the curves for the seven tests start at different points, which is due to varying initial amounts of sludge and moisture introduced into the greenhouses. Specifically, the initial residual volume is calculated as the product of the sludge volume and the initial moisture percentage.
It is specified that the drainage curves from Test 1 were discussed, but the results obtained were not subject to comparison in sections 7.1.8, 7.1.9 and 7.1.10. This is because, as previously discussed, Test 1 was a preliminary trial to better understand the operation of the solar greenhouse prototypes.

7.1.1 Comparison of results from the prototypes in Test 1

In the Figure 7.1, the drainage curves for Test 1 are shown. It can be observed that starting from an initial residual volume of 110 l, the final residual volumes were 42.93 l, 48.39 l, and 27.35 l for greenhouse A, greenhouse B, and drying bed C, respectively. As noted in the previous chapter and in particular in Figure 6.24 and Table 6.5, the residual humidity content was found to be 66 %, 44 %, and 81 % for greenhouse A, greenhouse B, and drying bed C, respectively. In terms of humidity reduction, greenhouse B exhibited the best performance.

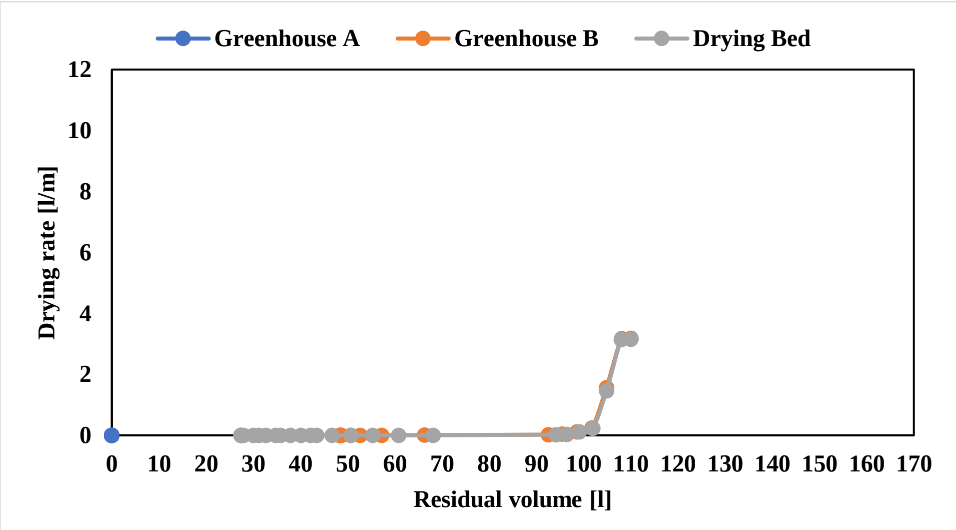

Figure 7.1 - Drainage curves test 1

7.1.2 Comparison of results from the prototypes in Test 2

In the Figure 7.2, the drainage curves for Test 2 are shown. It can be observed that starting from an initial residual volume of 160 l, the final residual volumes were 83.28 l, 86.94 l, and 96.29 l for greenhouse A, greenhouse B, and greenhouse C, respectively. As noted in the previous chapter and in particular in Figure 6.34 and Table 6.8, the residual humidity content was found to be 6 %, 7 %, and 44 % for greenhouse A, greenhouse B, and greenhouse C, respectively. In terms of humidity reduction, greenhouse A exhibited the best performance.

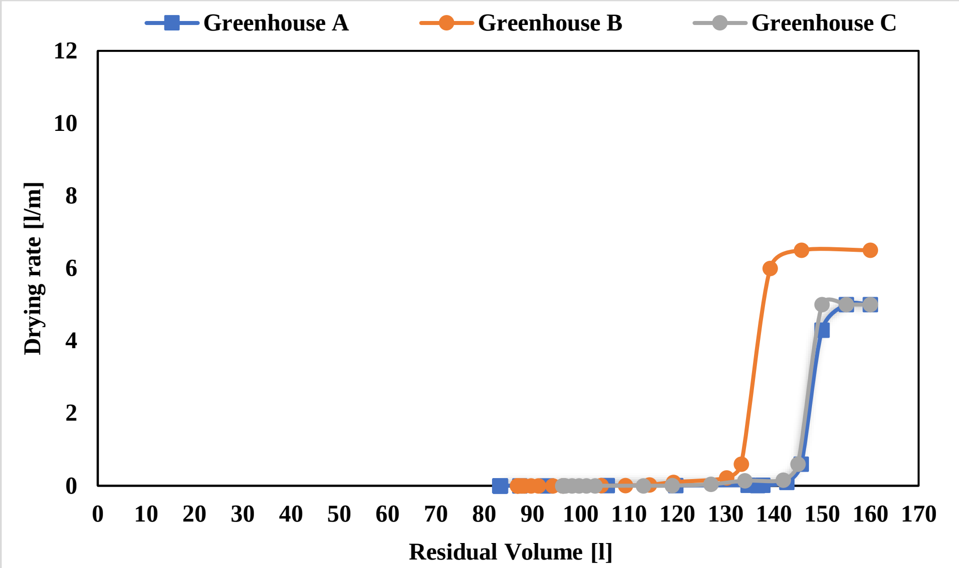

Figure 7.2 – Drainage curves test 2

7.1.3 Comparison of results from the prototypes in Test 3

In the Figure 7.3, the drainage curves for Test 3 are shown. It can be observed that starting from an initial residual volume of 160 l, the final residual volumes were 117 l, 88 l, and 89 l for greenhouse A, greenhouse B, and greenhouse C, respectively. As noted in the previous chapter and in particular in Figure 6.41 and Table 6.11, the residual humidity content was found to be 6 %, 4.92 %, and 34 % for greenhouse A, greenhouse B, and greenhouse C, respectively. In terms of humidity reduction, greenhouse B exhibited the best performance.

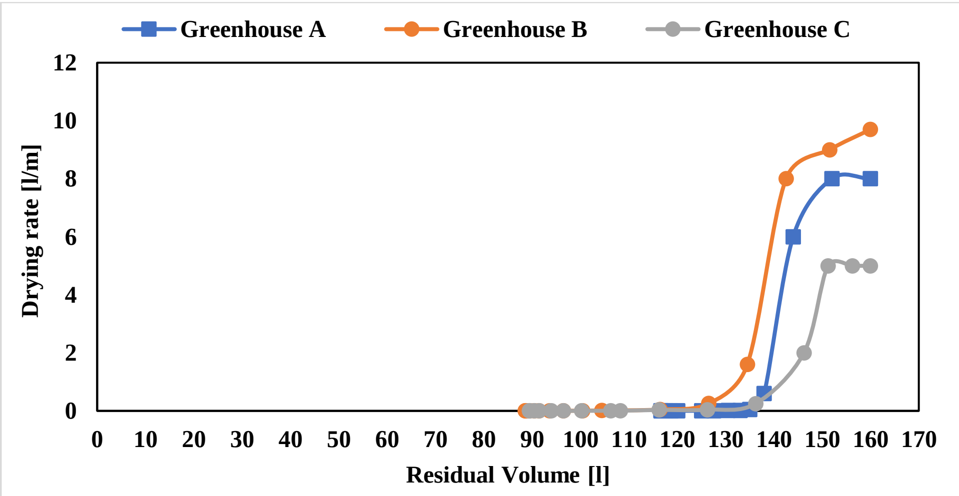

Figure 7.3 – Drainage curves test 3

7.1.4 Comparison of results from the prototypes in Test 4

In the Figure 7.4 the drainage curves for Test 4 are shown. It can be observed that starting from an initial residual volume of 145 l, the final residual volumes were 85.5 l, 89 l, and 71.7 l for greenhouse A, greenhouse B, and greenhouse C, respectively. As noted in the previous chapter and in particular in Figure 6.48 and Table 6.14, the residual humidity content was found to be 5.78 %, 4.22 %, and 4.12 % for greenhouse A, greenhouse B, and greenhouse C, respectively. In terms of humidity reduction, greenhouse B and C exhibited the bests performances.

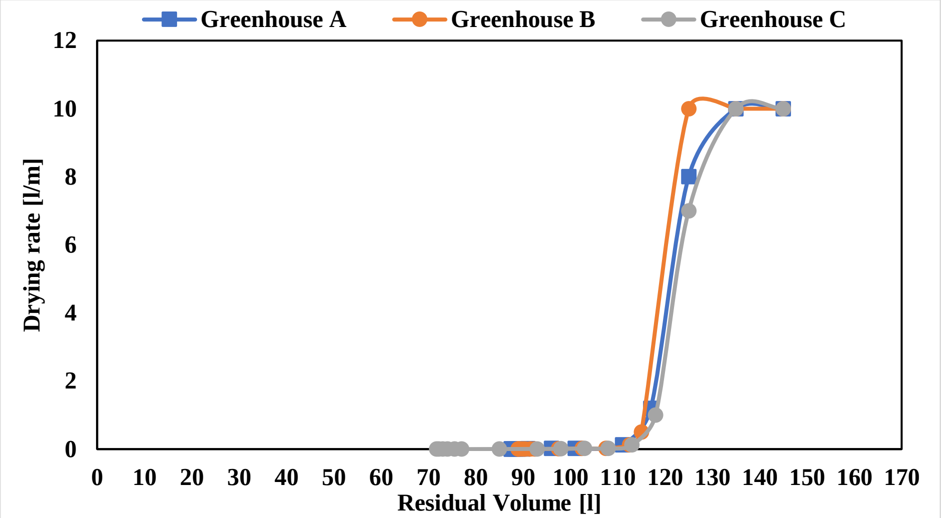

Figure 7.4 – Drainage curves test 4

7.1.5 Comparison of results from the prototypes in Test 5

In Figure 7.5 , the drainage curves for Test 5 are presented. Starting with an initial residual volume of 170 l, the final residual volumes were 119 l, 107.5 l, and 116.7 l for greenhouses A, B, and C, respectively. As detailed in the previous chapter, particularly in Figure 6.55 and Table 6.17, the residual moisture content was measured at 6.19 %, 4.06 %, and 6 % for greenhouses A, B, and C, respectively. In terms of moisture reduction, greenhouses B demonstrated the best performance.

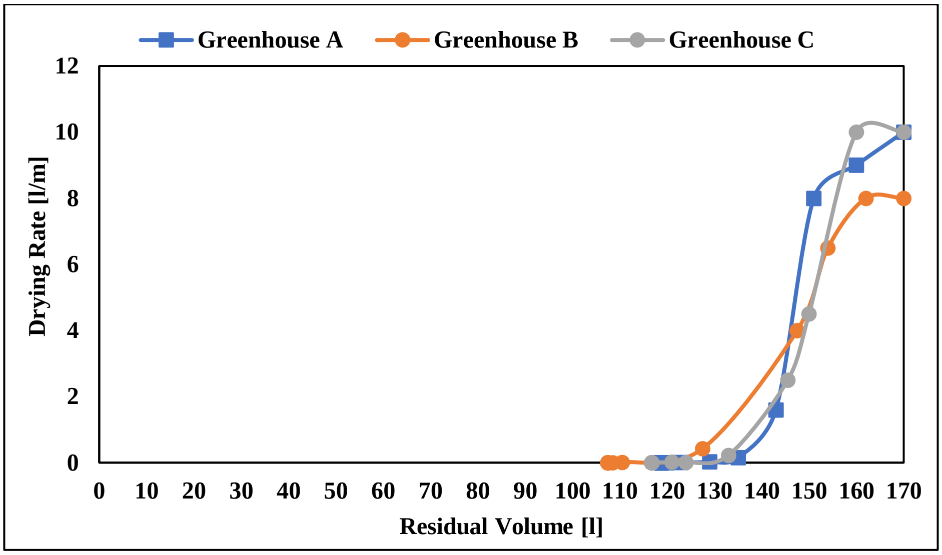

Figure 7.5 – Drainage curves test 5

7.1.6 Comparison of results from the prototypes in Test 6

In Figure 7.6, the drainage curves for Test 6 are presented. Starting with an initial residual volume of 150 l, the final residual volumes were 63.4 l, 84 l, and 82.7 l for greenhouses A, B, and C, respectively. As detailed in the previous chapter, particularly in Figure 6.62 and Table 6.20, the residual moisture content was measured at 21.76 %, 19.63 %, and 20.52 % for greenhouses A, B, and C, respectively. In terms of moisture reduction, greenhouses B demonstrated the best performance.

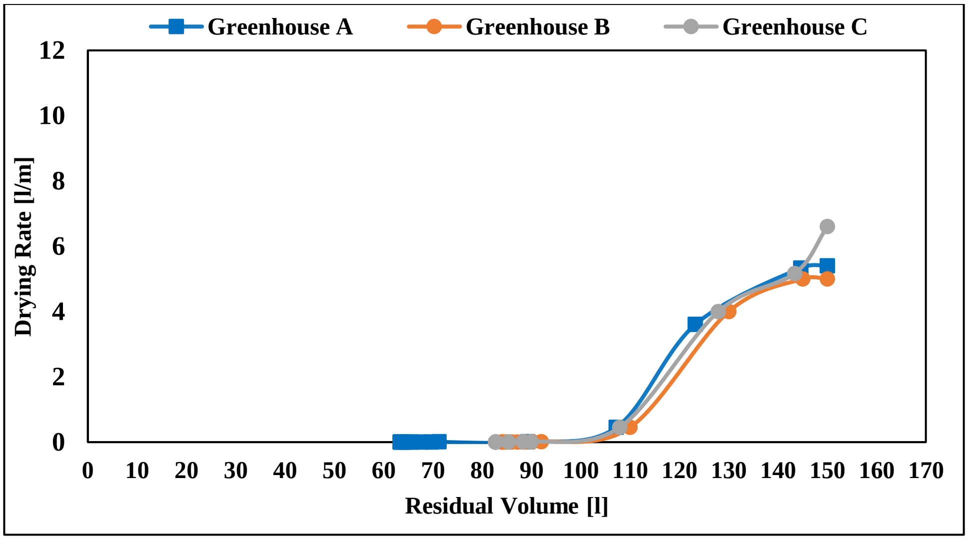

Figure 7.6 – Drainage curves test 6

7.1.7 Comparison of results from the prototypes in Test 7

In Figure 7.7, the drainage curves for Test 6 are presented. Starting with an initial residual volume of 160 L, the final residual volumes were 114.5 l, 105 l, and 113.5 l for greenhouses A, B, and C, respectively. As detailed in the previous chapter, particularly in Figure 6.69 and Table 6.23 the residual moisture content was measured at 5.13 %, 4.60 %, and 5.22 % for greenhouses A, B, and C, respectively. In terms of moisture reduction, greenhouses B demonstrated the best performance.

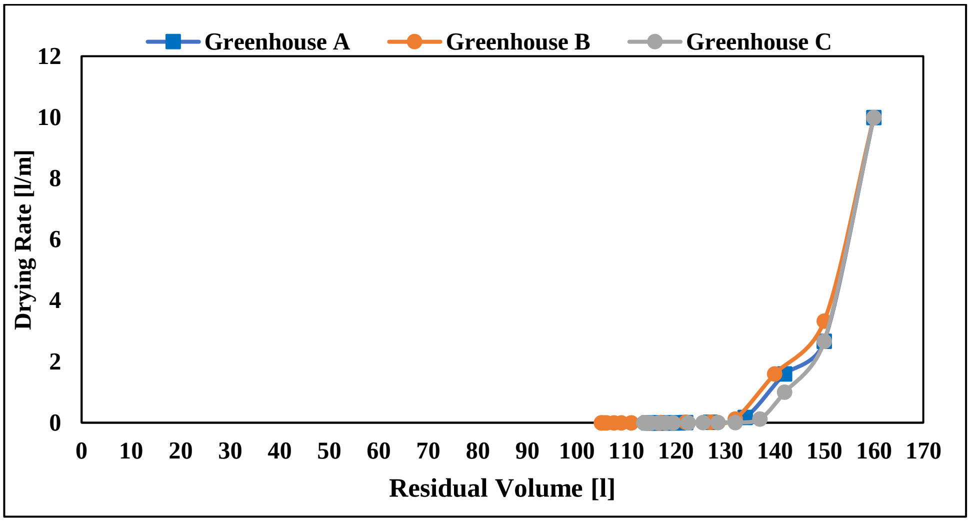

Figure 7.7 – Drainage curves test 7

7.1.8 Greenhouse A

The curve for Test 2 shows a sharp increase in the drying rate around 150 liters of residual volume, with a rapid but limited peak (about 5-6 l/min). This curve indicates that the sludge in Test 2 releases water suddenly only after reaching a certain saturation level. It may be sludge that releases water quickly once a specific moisture threshold is reached.

The curve for Test 3 shows one of the steepest increases, reaching a residual volume of about 116 liters. This behavior is typical of highly draining sludges, with a structure that allows water to evaporate rapidly once the drying process begins. Test 4 follows a trend similar to Test 3, with a maximum drying rate of about 11 l/min. The point where the drying rates start to decrease begins around 110 liters. This curve indicates extremely efficient drainage, suggesting a greenhouse configuration that favors evaporation.

The curve for Test 5 shows a slower trend compared to the others, with a maximum drying rate of about 10 l/min. The drying rate begins to decrease around 130 liters of residual volume. The trend of this curve could represent sludges with very fine particles or high organic content, which tend to retain moisture longer, slowing the evaporation process.

Finally, the curve for Test 7 shows one of the slowest drying rate decreases, with a peak reached around 10 l/min at 160 liters of residual volume. Test 7 represents greenhouse conditions less favourable to evaporation.

It can be concluded that Tests 3 and 4 show trends with high and rapid peaks, suggesting that the dehydration process occurs optimally. The corresponding sludge in the greenhouse can be dried in shorter times.

Tests 6, and 2 show curves with moderate peaks, representing a controlled sludge drainage rate. Likely, the operational conditions allow for stable dehydration without excessive water release in a short time. Finally, Tests 5 and 7 have the lowest peaks and a gradual, delayed water release. In these two tests, the sludge is probably more difficult to dehydrate and may require interventions to improve the process (Figure 7.8).

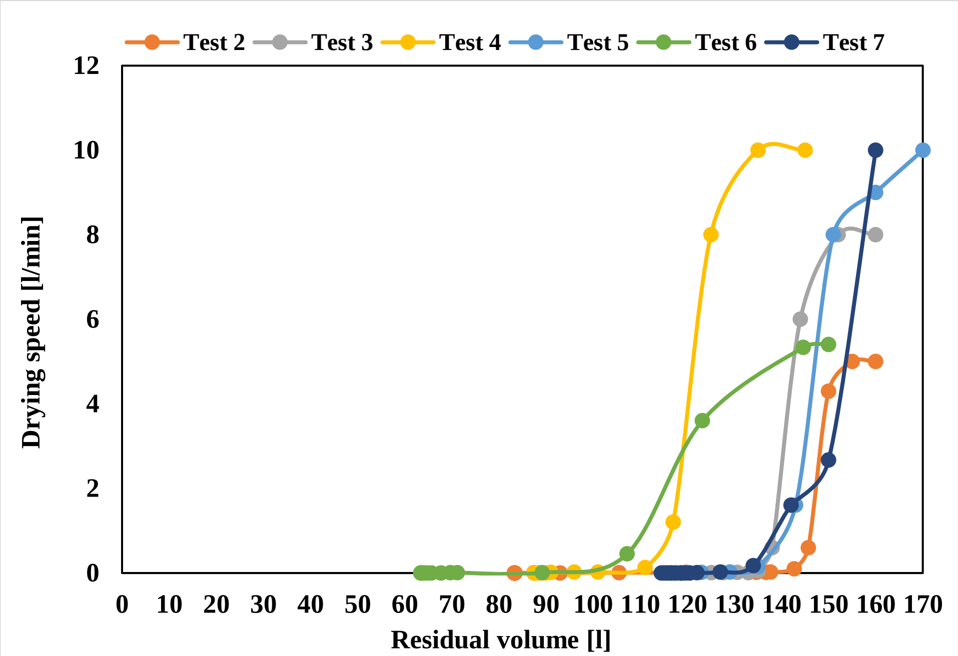

Figure 7.8 - Drainage Curve Greenhouse A

7.1.9 Greenhouse B

For Test 2, the curve presents a maximum drying rate around 160 liters, with a value of about 7 l/min.

The curve for Test 3 shows a clear increase in drying rate starting from about 142 liters, with a rate of about 8 l/min. This curve reflects an effective drainage of the sludge, likely due to more favourable ventilation or temperature conditions.

Test 4 shows the curve with the highest peak, reaching nearly 10 l/min. The acceleration starts around 125 liters, with rapid and sharp drainage. This curve represents an excellent sludge drainage process, suggesting an optimal dehydration process. The curve for Test 5 shows a more moderate loss of surface water, with a drying rate of about 4 l/min at a residual volume of 130 liters. The release of water from the sludge occurs more slowly, similar to what was observed in Greenhouse

A. Greenhouse B does not seem to significantly improve the drainage process compared to Greenhouse A.
In Test 6, the drainage curve shows a regular trend with an acceleration in water loss between 110 and 130 liters. Test 6 represents a moderate drainage behavior. In Greenhouse B, the process seems to slightly improve compared to Greenhouse A, possibly due to more uniform ventilation.
Finally, the curve for Test 7 shows a significant drying rate, dropping from 10 l/min to 1.6 l/min in the residual volume range of 160-140 liters. In Greenhouse B, the same behavior observed in Greenhouse A is shown, indicating that specific interventions may be necessary to improve dehydration (Figure 7.9).

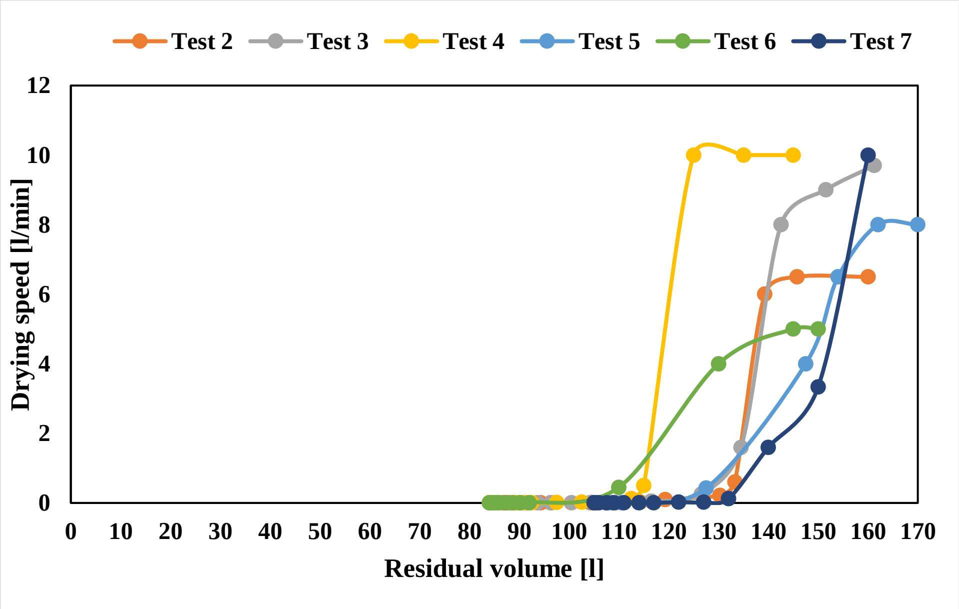

Figure 7.9 - Drainage Curve Greenhouse B

7.1.10 Greenhouse C

In Test 2, the initial residual volume decreases rapidly starting from 150 liters, with a drying rate of 5 l/min. Test 3 shows a trend almost identical to the drainage curve of Test 2.
For the curve of Test 4, a decrease in residual volume begins at 110 liters, with a drying rate of 10 l/min. The curve is very steep, indicating a rapid drainage once a certain drying rate is reached, which quickly brings the residual volume to 113 liters. In Test 5, the drainage rate begins to increase around 160 liters, with an initial drying rate of 10 l/min.
For Test 6, a much slower water loss trend is observed compared to the other tests, as seen in the moderate slope of the curve. Finally, for Test 7, the curve shows a high slope, dropping from 10 l/min to 1 l/min over a residual volume range between 160 and 142 liters. In summary, in Greenhouse C, the drainage curves indicate variability between tests. Specifically, the trends of Test 4 and Test 5 are similar, with drying rates of the same order of magnitude. The same was observed for

Test 2 and Test 3, but with lower drying rates compared to Tests 4 and 5. This variability could be linked to changes in the greenhouse's environmental conditions, which affect the drying and drainage behavior (Figure 7.10).

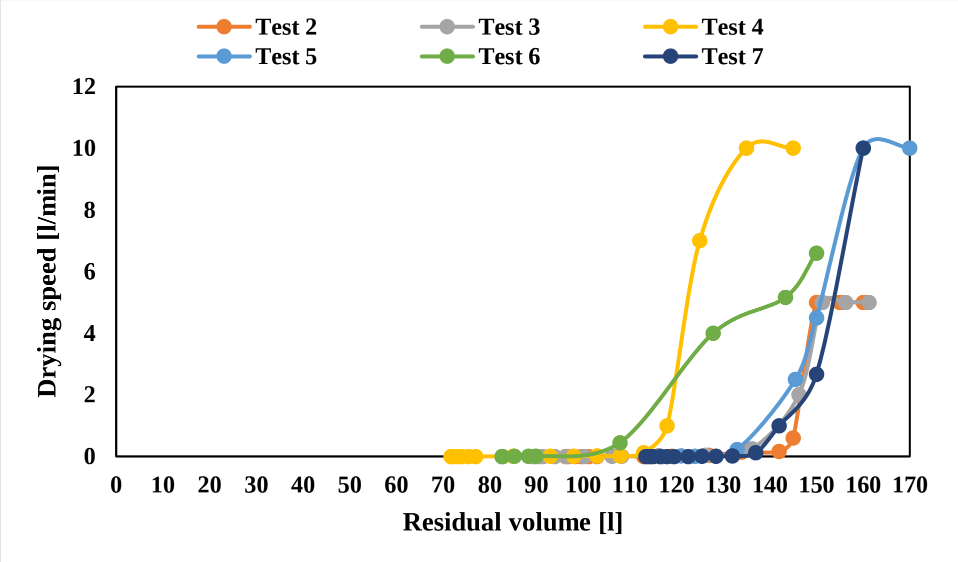

Figure 7.10 - Drainage Curve Greenhouse C

7.2 Discussion of water balance inside solar greenhouse

The water balance within each solar greenhouse prototype was necessary to determine the percentage of the water volume that is drained (V_D), retained by the drain (FWC), remains in the dehydrated sludge (V_R), and evaporates during the process (V_E). The initial water volume (V_i) was calculated as the product of the mass of sludge introduced into the greenhouse and its moisture content. For each test, the field capacity is the same, specifically the drain for greenhouse A will retain 12 liters, for greenhouse B 13 liters, and for greenhouse C 5 liters. The volume of water drained was measured during the test. The volume of water in the dehydrated sludge was determined as the product of the final weight of the sludge and its residual moisture content. The volume of evaporated water was calculated as follows:

$$V_E = V_i - V_D - FWC - V_R$$

7.2.1 Comparison of results from the prototypes in Test 2

During the test, the average temperature inside each greenhouse was recorded. Specifically, for greenhouse A, an average temperature of 23.9 °C was observed, while for greenhouses B and C*, the temperatures were 22.2 °C and 23.2 °C, respectively. Figure 7.11 the obtained values are summarized. It can be observed that for greenhouse A the greatest water loss is constituted by the drained one (50.46%), while in the other two (B and C*) the loss by evaporated water prevails (48.31% and 53.93%) respectively.

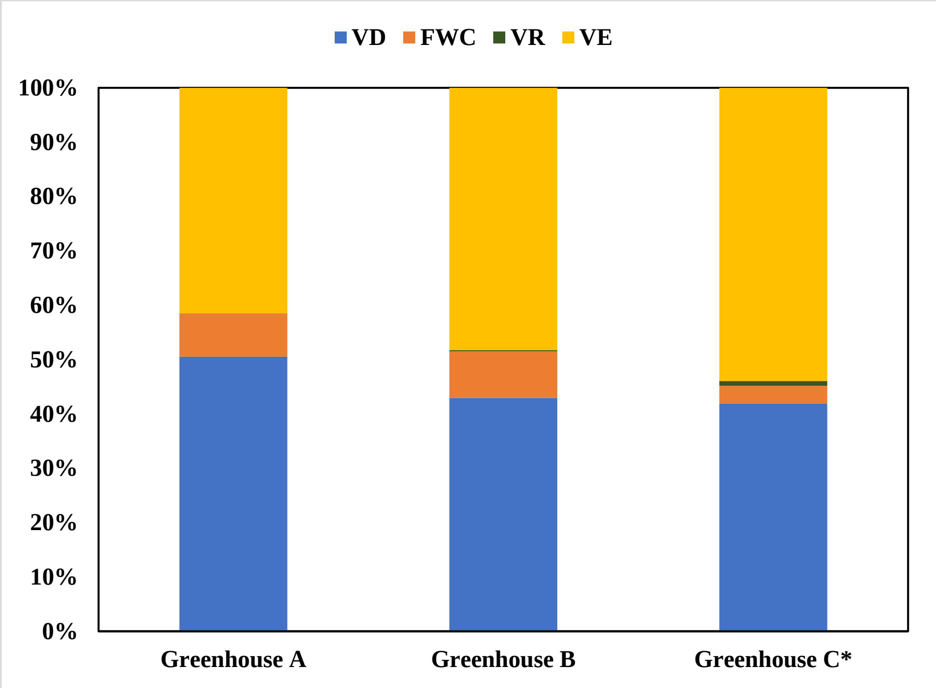

Figure 7.11 – Water Balance test 2

7.2.2 Comparison of results from the prototypes in Test 3

During the test, the average temperature inside each greenhouse was recorded. Specifically, for greenhouse A, an average temperature of 26.3 °C was observed, while for greenhouses B and C*, the temperatures were 28.2°C and 27.2°C, respectively. It can be observed that for greenhouse A the greatest water loss is constituted by the evaporated one (65.55 %), while in the other two (B and C*) the loss by evaporated water prevails (46.90 % and 50.49 %) respectively (Figure 7.12) It can be observed that for greenhouse A the greatest water loss is constituted by the evaporated one (65.55 %), while in the other two (B and C*) the loss by evaporated water prevails (46.90 % and 50.49 %) respectively.

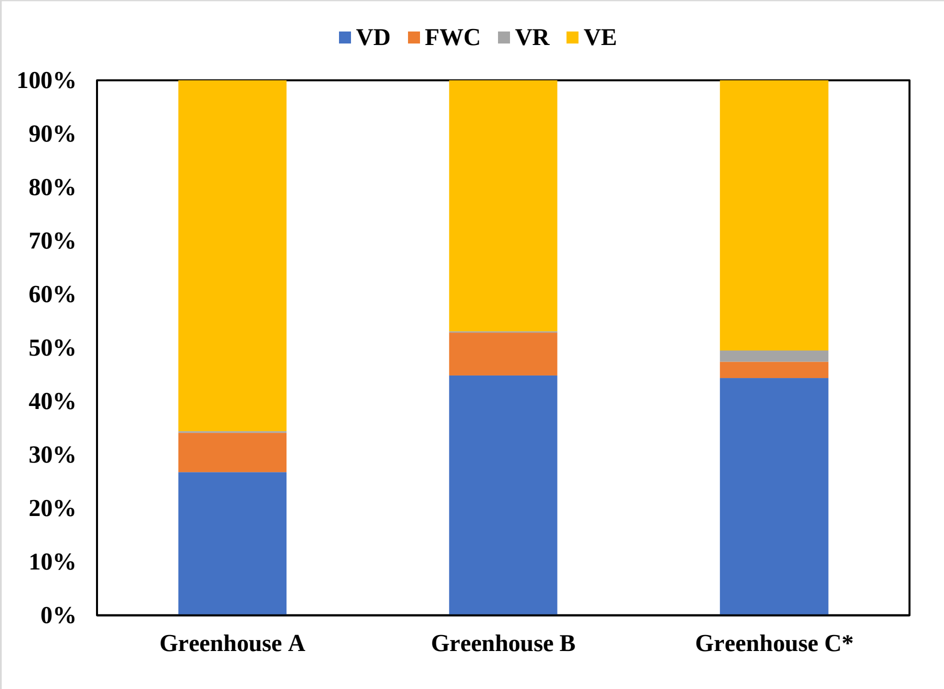

Figure 7.12 - Water Balance test 3

7.2.3 Comparison of results from the prototypes in Test 4

During the test, the average temperature inside each greenhouse was recorded. Specifically, for greenhouse A, an average temperature of 33.9 °C was observed, while for greenhouses B and C, the temperatures were 35.46 °C and 32.2 °C, respectively. It can be observed that for greenhouse A the greatest water loss is constituted by the evaporated one (51.22 %), while in the greenhouse B the greatest water loss is constituted by evaporated loss (51.36 %) and in the greenhouse C by drained water loss (51.24 %). Figure 7.13 the obtained values are summarized. It can be observed that for greenhouse A the greatest water loss is constituted by the evaporated one (51.22 %), while in the greenhouse B the greatest water loss is constituted by evaporated loss (51.36 %) and in the greenhouse C by drained water loss (51.24 %).

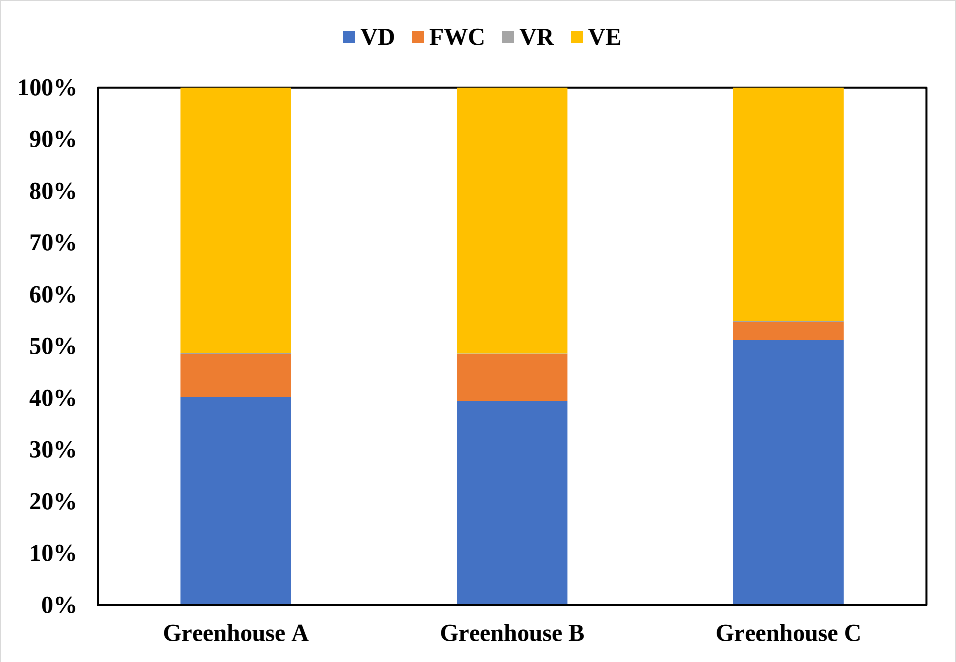

Figure 7.13 - Water Balance test 4

7.2.4 Comparison of results from the prototypes in Test 5

During the test, the average temperature inside each greenhouse was recorded. Specifically, for greenhouse A, an average temperature of 35.2 °C was observed, while for greenhouses B and C*, the temperatures were 33.5 °C and 33.4 °C, respectively. Figure 7.14 the obtained values are summarized. It can be observed that for greenhouse A the greatest water loss is constituted by the evaporated one (62.42 %), while in the other two (B and C*) the loss by evaporated water prevails (55.20 % and 65.27 %) respectively. This result is likely due to the high temperatures inside the greenhouses, which allowed most of the water initially present in the sludge to evaporate.

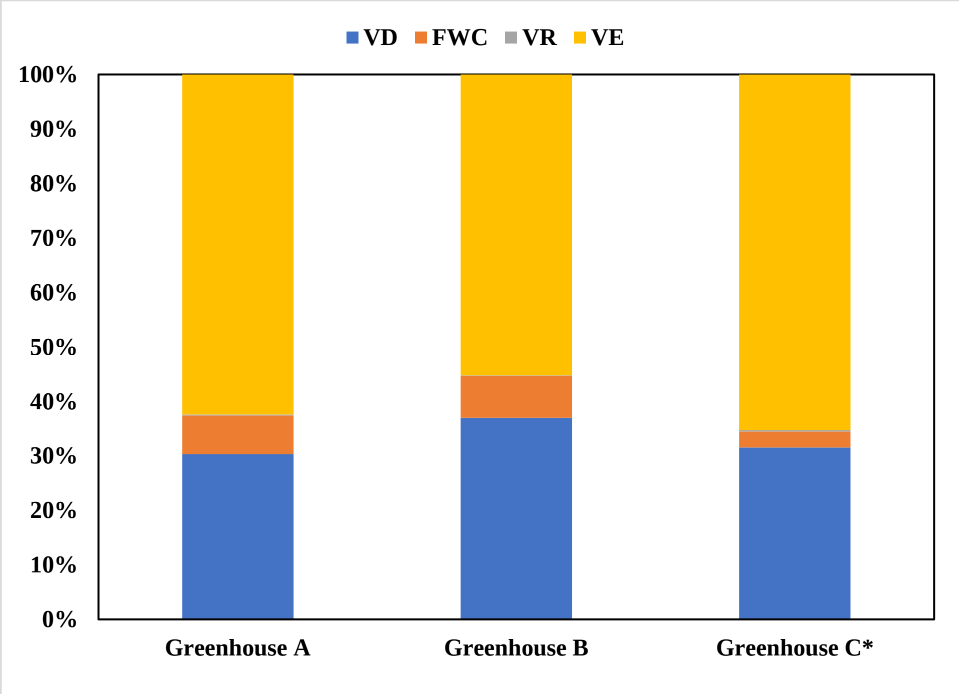

Figure 7.14 - Water Balance test 5

7.2.5 Comparison of results from the prototypes in Test 6

During the test, the average temperature inside each greenhouse was recorded. Specifically, for greenhouse A, an average temperature of 18°C was observed, while for greenhouses B and C, the temperatures were 14.48 °C and 13 °C, respectively. It can be observed that for greenhouse A the greatest water loss is constituted by the evaporated one (46.93 %), while in the other two (B and C) the loss by evaporated water prevails (45.94 % and 49.68 %) respectively. Figure 7.15 the obtained values are summarized. It can be observed that for greenhouse A the greatest water loss is constituted by the evaporated one (46.93 %), while in the other two (B and C) the loss by evaporated water prevails (45.94 % and 49.68 %) respectively.

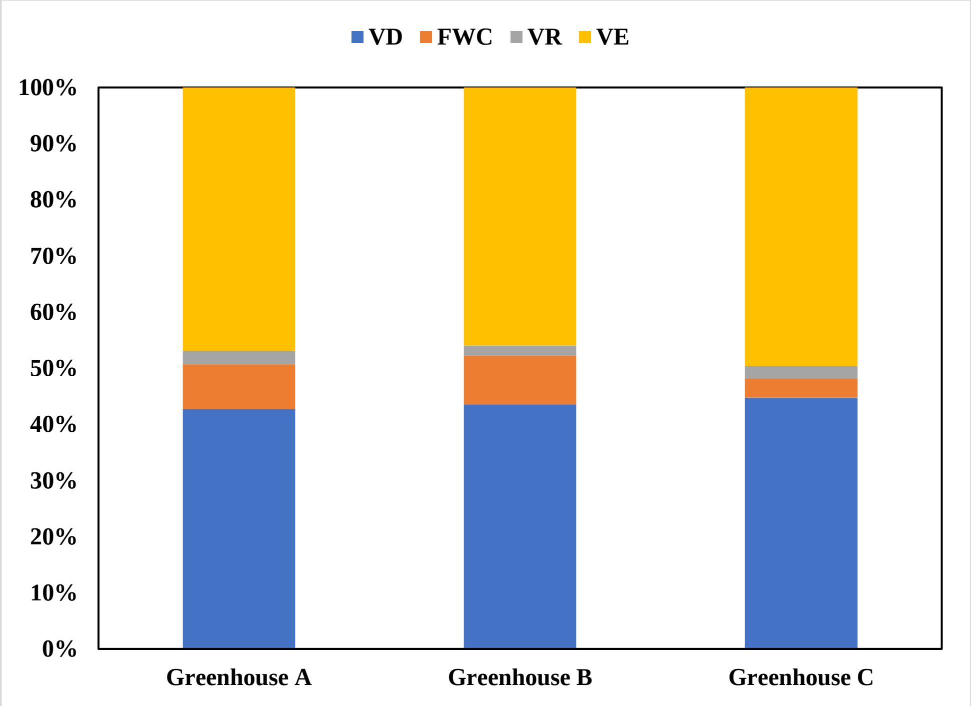

Figure 7.15 - Water Balance test 6

7.2.6 Comparison of results from the prototypes in Test 7

During the test, the average temperature inside each greenhouse was recorded. Specifically, for greenhouse A, an average temperature of 27.9 °C was observed, while for greenhouses B and C, the temperatures were 29.3 °C and 29.7 °C, respectively. Figure 7.16 the obtained values are summarized. It can be observed that for greenhouse A the greatest water loss is constituted by the evaporated one (65.14 %), while in the other two (B and C) the loss by evaporated water prevails (56.65 % and 67.12 %) respectively. This result is likely due to the high temperatures inside the greenhouses, which allowed most of the water initially present in the sludge to evaporate.

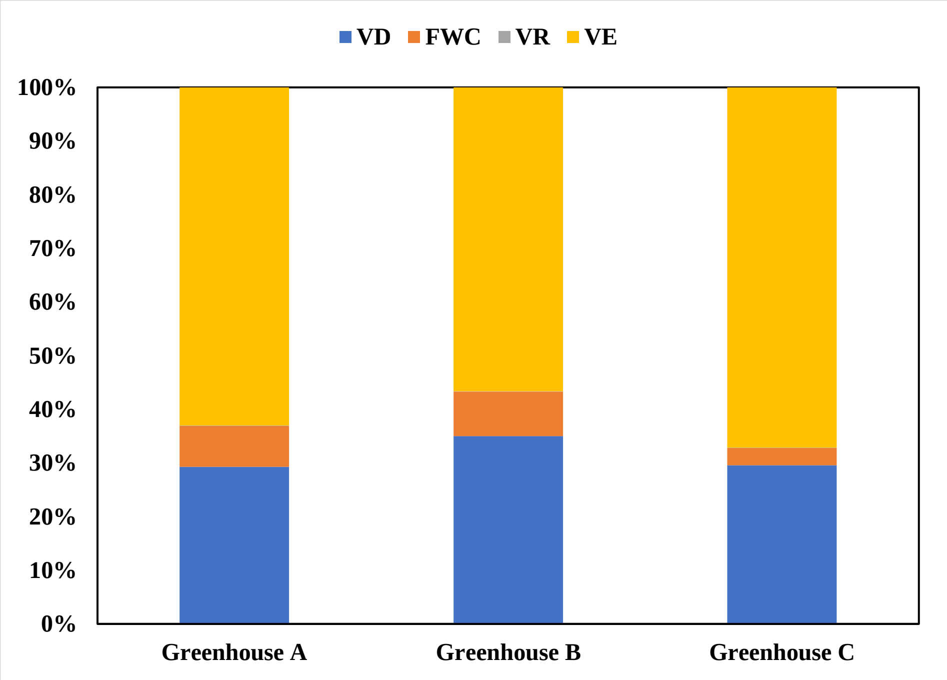

Figure 7.16 - Water Balance test 7

7.3 Discussion of humidity curve

All tests had a duration of 30 days, except for Test 4 and Test 5, which lasted 25 days. This difference is due to the fact that by the 25th day of testing, a steady-state value of residual moisture had been reached, so the tests were terminated. It is specified that the results obtained Test 1 were not subject to comparison in the next sections. This is because, as previously discussed, Test 1 was a preliminary trial to better understand the operation of the solar greenhouse prototypes.

7.3.1 Comparison of results from the tests conducted in Greenhouse A

Figure 7.17 shows the trend of humidity during the experiment for each of the tests conducted on the solar greenhouse prototype A. All tests have residual humidity values lower than 25 %. Among these, Test 6 has the highest final humidity value (21.76 %), while all the other tests have a residual humidity value of around 5 – 6 %. The same graph shows three curves representing the humidity trends of the sludge during the tests conducted in the solar greenhouse C* (traditional solar greenhouse). These curves were included in the graph to allow a comparison between the humidity trends of the sludge during the tests conducted in the prototype solar greenhouse A with top air injection and those obtained from the tests conducted in conventional solar greenhouses. The three curves show different behavior, probably due to the varying operating conditions. In particular, the average internal temperature inside the solar greenhouse C* during test 2 was 23.18°C, 27.19°C for test 3, and finally, for test 5, it was 33.4°C.

By comparing the humidity trend of the sludge during test 2 conducted in solar greenhouse A and C*, it can be observed that in both cases, the final humidity of the sludge is the same, at 7 %. Starting from the 20th day of the experiment, the humidity values of the sludge in greenhouse A are lower than those in C*. Test 2 was conducted during the March-April period, so under these conditions, greenhouse A with top air injection allows for faster achievement of low humidity values.
Regarding test 3, it was observed that at the end of the test, the final humidity in greenhouse C* was 34 %, a value higher than that obtained in greenhouse A (6 %). The humidity trends in the two greenhouses are initially similar, but they diverge on the 6th day. From the 14th day onwards, a sharp decrease in sludge humidity is observed in greenhouse A.
Finally, during test 5, the humidity trends in both greenhouses are similar, with an equal final humidity value of 6 %. Therefore, from a general perspective, greenhouse C* could be considered the better option due to its lower energy consumption compared to greenhouse A, due to the lack of forced ventilation.

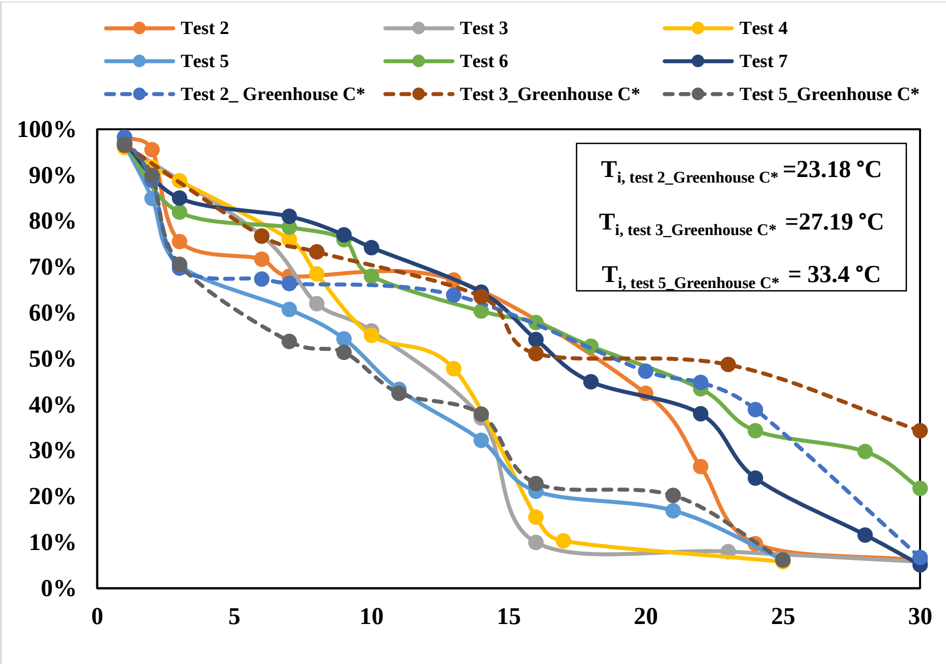

Figure 7.17 - Humidity Curve Greenhouse A

7.3.2 Comparison of results from the tests conducted in Greenhouse B

Figure 7.18 shows the trend of humidity during the experiment for each of the tests conducted on the solar greenhouse prototype. All the tests have final humidity values below 20 %. The Test 6 shows the highest residual humidity value (19.63 %), which is lower than the value observed for solar greenhouse A (21.76 %). All the

other tests show values around 4 - 5 %, which are also lower than those observed in greenhouse A.
By comparing the humidity trend of the sludge during test 2 conducted in solar greenhouse B and C*, it can be observed that in both cases, the final humidity of the sludge is the same, at 7%.
Regarding test 3, it was observed that at the end of the test, the final humidity in greenhouse C* was 34.3%, a value higher than that obtained in greenhouse B (4.9%). The humidity trends in the two greenhouses are similar and diverge starting from day 16, with greenhouse B reaching the residual humidity value of the sludge more quickly.
Finally, during test 5, the humidity trends in the two greenhouses are slightly different, with a final sludge humidity value of 6% in C* and 4.06% in greenhouse B.
Therefore, from a general perspective, greenhouse C* shows good performance during the August-September period, favored by the internal temperature of the greenhouse. However, it is important to note that bottom air injection (greenhouse B) allows for higher performance.

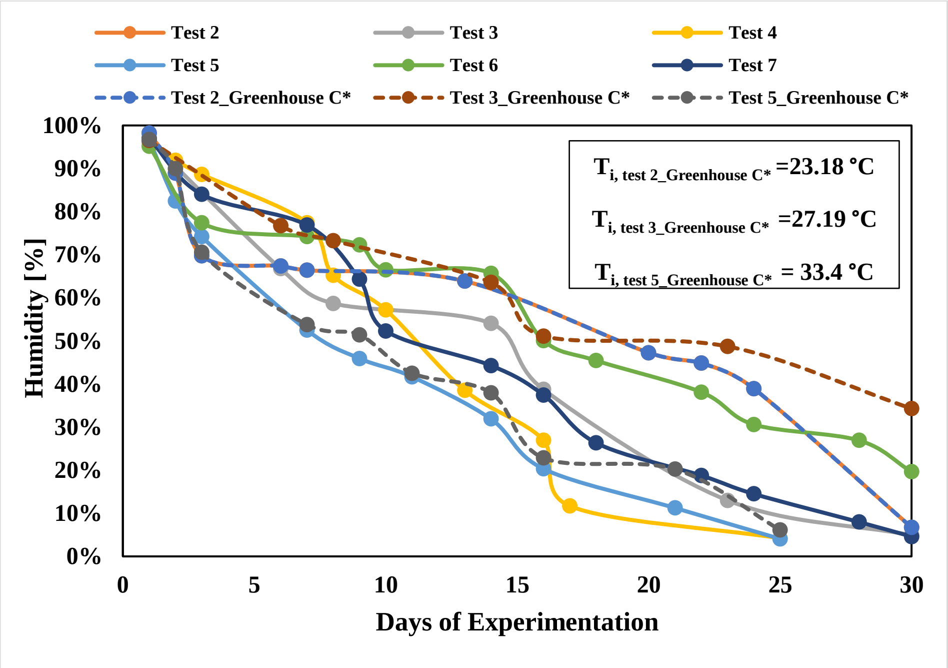

Figure 7.18 - Humidity Curve Greenhouse B

7.3.3 Comparison of results from the tests conducted in Greenhouse C

Figure 7.19 shows the trend of humidity during the experiment for each of the tests conducted on the solar greenhouse prototype C.
All the tests have residual humidity values below 35 %. Among these, Test 3 shows the highest residual humidity value (34.3 %), followed by Test 6 (20.52 %), which

is lower than the value observed for solar greenhouse A (21.76 %) but higher than that observed for greenhouse B (19.63%). All the other tests have final humidity values of about 5 %. The final humidity of the sludge achieved during tests 4 and 5 is the same. On day 16 of the experimental period, the humidity trends of the sludge diverge; in particular, the solar greenhouse prototype in test 4 reaches the final humidity value of the sludge more quickly. However, it is important to note that from a management perspective, on day 16, the ventilation system could be turned off, as the sludge humidity reached is almost identical to the final value.
By comparing the results obtained in test 2 and test 6, it can be observed that the final humidity in the prototype with top and bottom air injection has a higher final humidity value compared to the traditional solar greenhouse prototype (20.52% versus 7%).
Meanwhile, by comparing the results of test 2 with those of test 7, it can be seen that the humidity trends of the sludge are similar until day 18. After that, the sludge humidity in test 7 reaches the final value of 5% more quickly, while the value of 7% is reached with the greenhouse in test 2.

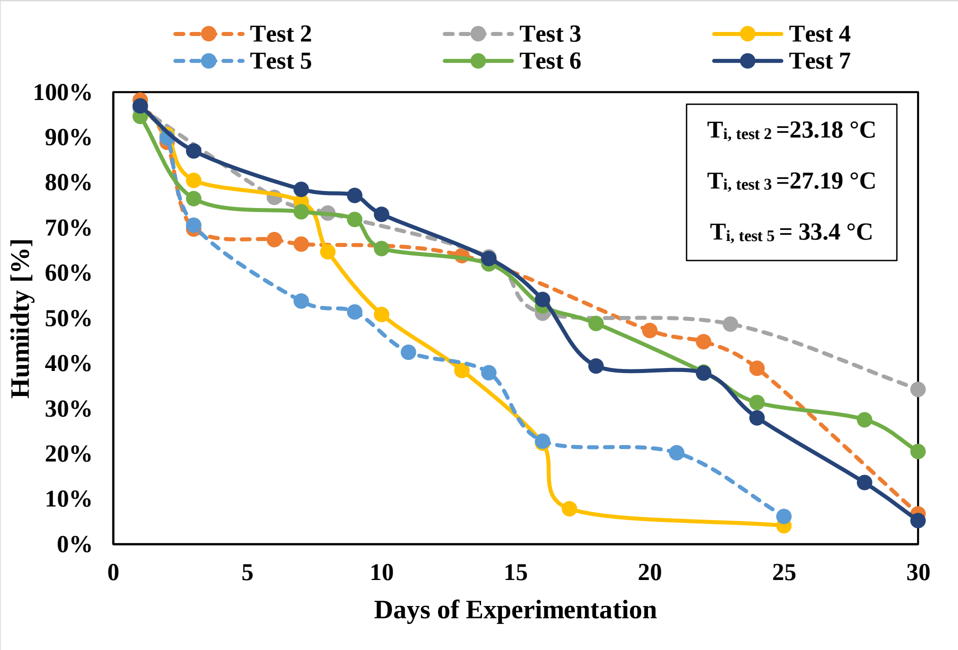

Figure 7.19 – Humidity Curve Greenhouse C

The comparison of residual humidity values for each test and solar greenhouse prototype (Figure 7.20) leads to the following conclusions:

- Test 6 exhibits the highest residual humidity values;
- Tests 2, 4, 5, and 7 show the lowest residual humidity values, all below 10 %;
- Test 3, with the exception of the residual humidity value of about 35% for Greenhouse C, also presents final moisture values below 10 %;

- In all tests (except for Test 2), the lowest residual humidity values were observed for Greenhouse B.

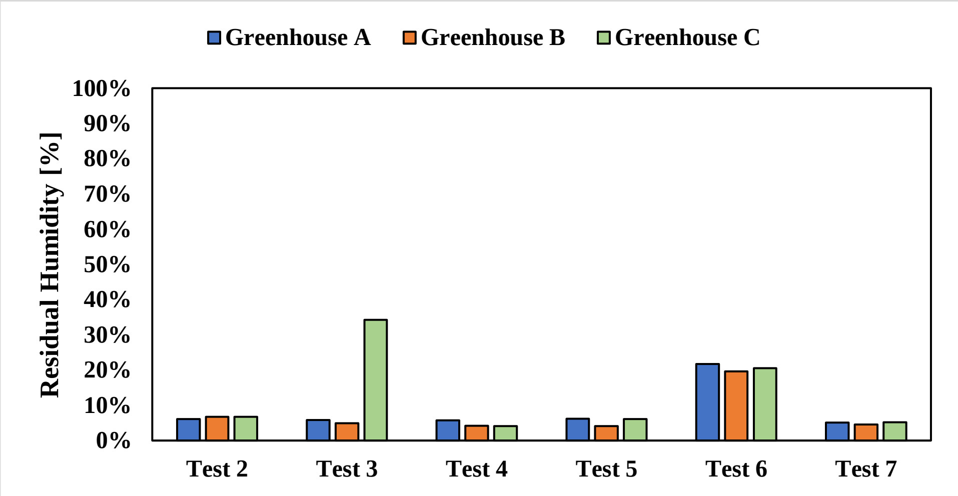

Figure 7.20 - Comparison of the residual moisture obtained in the different tests

The results obtained have demonstrated that through the implemented solar greenhouse prototypes, it is possible to achieve a residual humidity content of the sludge close to 5 %. In general, the residual humidity values observed in conventional thermal dryers and conventional solar greenhouses reported in,(Zheng et al., 2021b) were higher. In (Boguniewicz-Zablocka et al., 2020), a purely solar-driven greenhouse facility for sewage sludge drying achieved a residual humidity content lower than 10 %. Moreover, (Kurt et al., 2015) reported a residual sludge humidity content of 70 % of the residual dry matter.

7.4 Discussion of drying performance

This section discusses the trend of the reduction in sludge weight as a function of the specific air flow rate introduced into the system. It is specified that the results obtained Test 1 were not subject to comparison in the next sections. This is because, as previously discussed, Test 1 was a preliminary trial to better understand the operation of the solar greenhouse prototypes.

7.4.1 Comparison of results from the tests conducted in Greenhouse A

For solar greenhouse A, an increasing trend in the weight reduction of the sludge was observed as the specific air flow rate introduced into the system increased, reaching a value of 4 m^3/m^2xh. Beyond this point, the performance remained nearly constant up to a value of 16 m^3/m^2xh, after which it decreased until the weight reduction of 95 % reached at 23 m^3/m^2xh. The greatest weight reduction of the sludge was observed in Test 7 (98.4 %) and Test 5 (97.9 %), followed by Test 2 (97.4 %) and Test 4 (96.7 %). The respective values of the specific air flow rate introduced into the system were 4 and 6 m³/m²xh for Tests 7 and 5, and 16 and 3 m³/m²xh for Tests 2 and 4 (Figure 7.21).

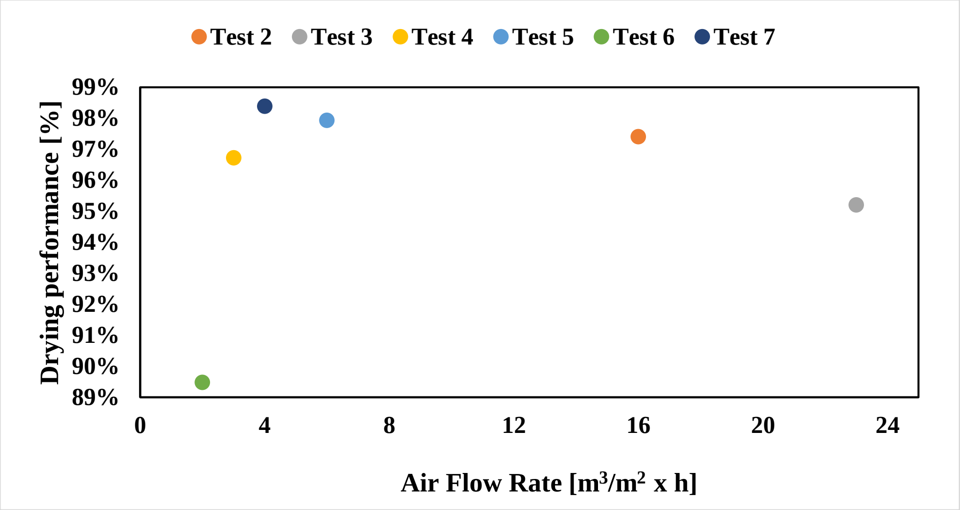

Figure 7.21 - Drying performance Greenhouse A

7.4.2 Comparison of results from the tests conducted in Greenhouse B

For solar greenhouse B, as with greenhouse A, an increasing trend in the weight reduction of the sludge was observed as the specific air flow rate introduced into the system increased, up to a value of 4 m³/m²xh. Beyond this point, the performance remained nearly constant up to a value of 16 m³/m²xh, after which it decreased until the weight reduction of 95.21 % reached at 23 m³/m²xh. The greatest weight reduction of the sludge was observed in Test 7 (98.46 %) and Test 5 (98.39 %), followed by Test 2 (97.48 %) and Test 4 (97.31 %). The respective values of the specific air flow rate introduced into the system were 4 and 6 m³/m²xh for Tests 7 and 5, and 16 and 3 m³/m²xh for Tests 2 and 4 (Figure 7.22).

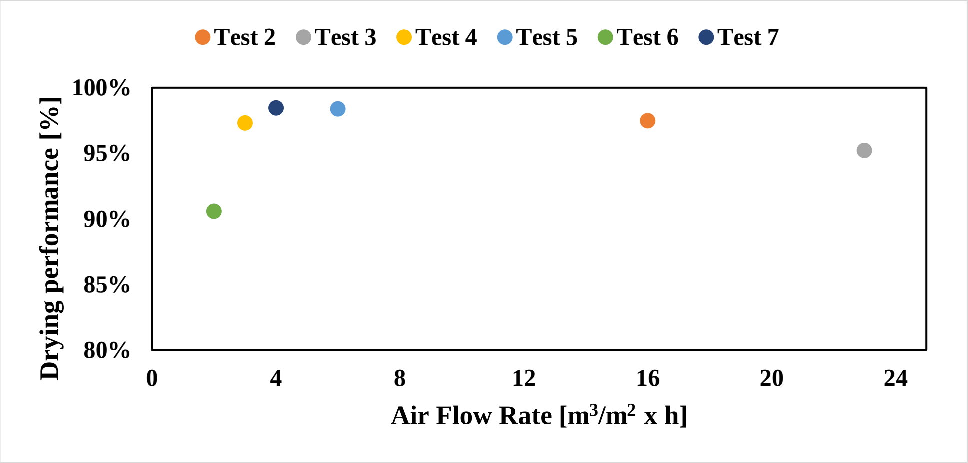

Figure 7.22 - Drying performance Greenhouse B

The weight reduction of the sludge for Greenhouse A and Greenhouse B as a function of the specific air flow rate introduced into the system is similar for all tests, except for Tests 4 and 6. In Test 4, performed with a specific air flow rate of 3 m^3/m^2xh, a sludge weight reduction of 96.7 % and 97.3 % was observed for Greenhouse A and Greenhouse B, respectively. In contrast, for Test 6, performed with a specific air flow rate of 2 m^3/m^2xh, a lower sludge weight reduction of 89.5 % and 90.58 % was observed for Greenhouse A and Greenhouse B, respectively (Figure 7.23).

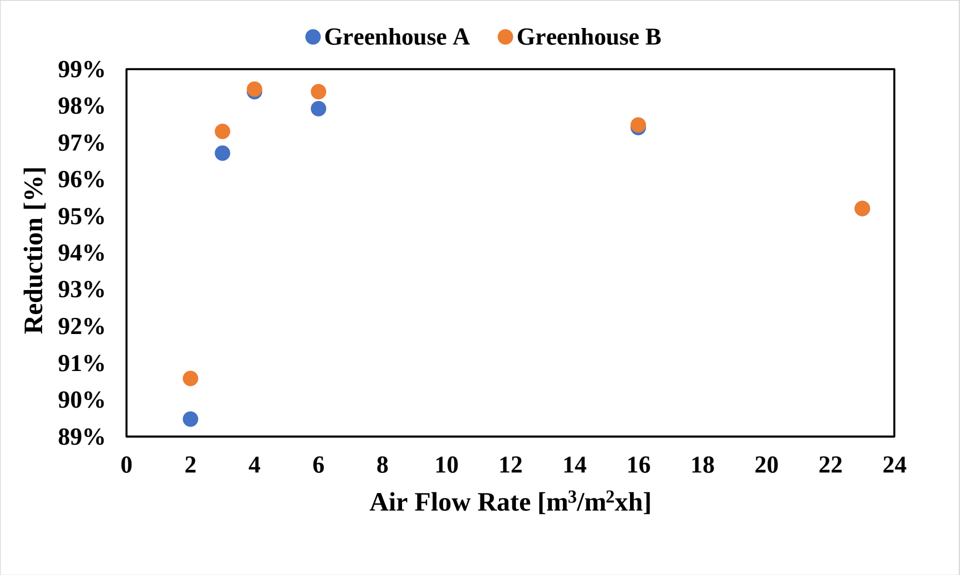

Figure 7.23 – Comparison of weight sludge reduction in function of air flow rate for tests in greenhouse A and greenhouse B

7.4.3 Comparison of results from the tests conducted in Greenhouse C

Tests 2, 3, and 5 were conducted without the introduction of air into the greenhouse; for these tests, the greenhouse was used as a traditional solar greenhouse with only a cover.

For solar greenhouse C, an increasing trend in the weight reduction of the sludge was observed as the specific air flow rate introduced into the system increased, up to a value of 4 m^3/m^2xh. The greatest weight reduction of the sludge was observed in Test 7 (98.09 %) and Test 4 (97.49 %), with the respective specific air flow rates introduced into the system being 4 and 3 m^3/m^2xh (Figure 7.24).

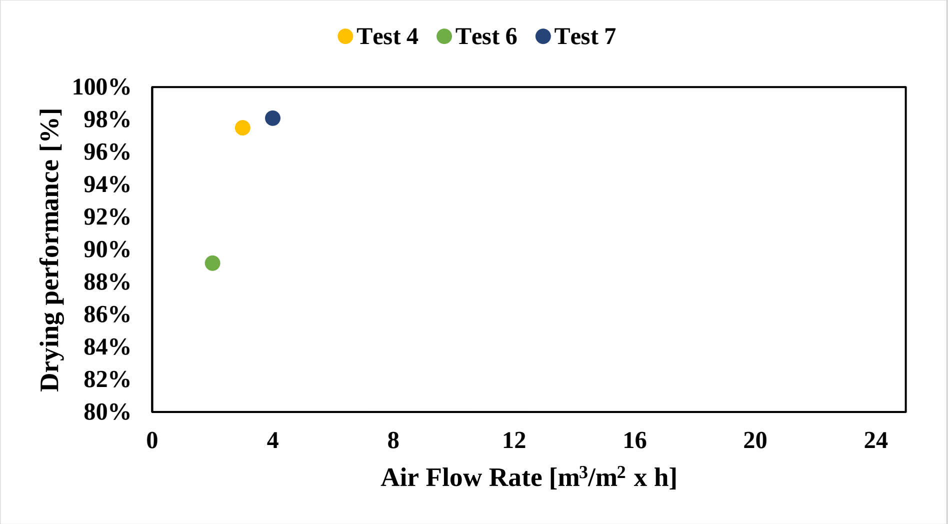

Figure 7.24 - Drying performance Greenhouse C

The results suggest a significant influence of the air flow rate introduced into the system on the dehydration process.
All the graphs show that it is not necessary to go beyond a certain value of specific air flow, as the system's performance does not change. In particular, it can be stated that an optimal specific air flow rate could be considered in the range of 4-5 $m^3/m^2 \cdot h$.
The air flow over the sludge surface causes a reduction in vapor pressure, which facilitates the evaporation of moisture from the sludge (Ling et al., 2022). A higher air flow rate corresponds to a higher air speed, which improves the evaporation process by enabling more dry air to come into contact with the wet sludge, thus carrying away more moisture. Increasing the air speed also reduces the boundary layer thickness on the sludge surface, enhancing heat and mass transfer efficiency. These findings suggest that the airflow rate supplied from beneath the sludge layer plays a crucial role in improving both the drying performance and the drying kinetics of the sludge. As reported by (cite your article) the results from this study indicate that the proposed systems configurations leads to faster drying kinetics compared to conventional solar greenhouses.
The results suggest that increasing air flow enhances the drying rate, especially when the sludge layer is thin. Recent research confirms that providing air in such conditions leads to a notable increase in drying efficiency (He et al., 2018).

7.5 Discussion of the variation in the degree of sludge stabilization

The Figure 7.25 shows the initial and final values of the volatile content of the sludge, expressed as VS/TS, for each test. Greenhouse B achieves a lower VS/TS ratio compared to the other greenhouses. Specifically, Test 2 and Test 7 allow for the best stabilization, reaching a value close to 0.4 VS/TS.

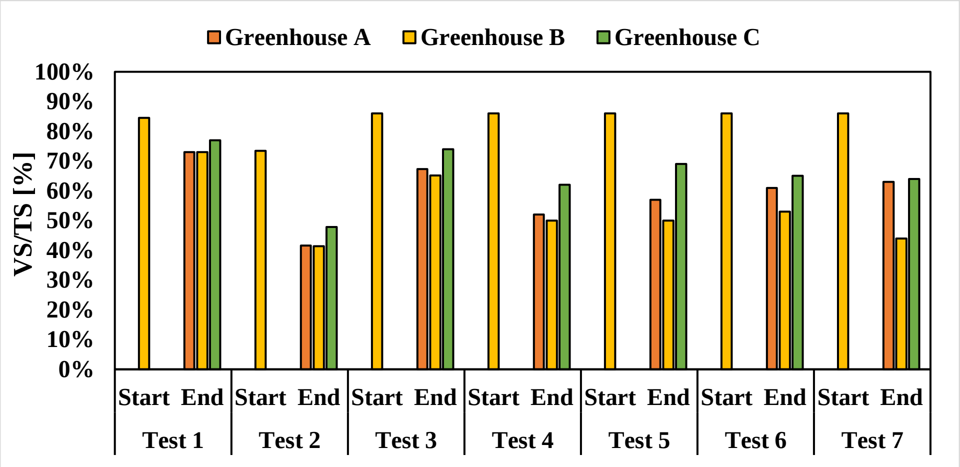

Figure 7.25 - Initial and final values of the SSV/SST ratio in the different tests

This suggests that the air supply played a key role in the stabilization of the sludge as a secondary effect. As reported by (Sorrenti et al., 2022) this finding is particularly significant because it indicates that both dewatering, and stabilization of the sludge occurred simultaneously in the modified solar greenhouse. The combined effect of aeration, solar radiation, and humidity reduction likely contributed to both the stabilization and sanitization of the sludge alongside its drying process. Previous studies have reported that the lowest VS/TS ratio achieved in a solar greenhouse was around 55 – 60 %. In the study, the reduction in volatile solids content by up to 40 % ensured the production of fully stabilized sludge. As a result, the stabilization phase typically carried out in aerobic digesters could potentially be reduced or eliminated in small-scale wastewater treatment plants (WWTPs), leading to significant savings in both footprint and energy usage.

8 Scale-up project

8.1 Introduction

The experimental campaigns and preliminary research conducted have allowed for an improvement in knowledge on some critical points in defining certain parameters, including the airflow rate to be supplied and the thickness of the sludge layer to be inserted within the solar greenhouses.
In particular, in the solar greenhouse prototypes, it was observed that the process efficiency varied depending on the type of air input (above/below the sludge layer), the airflow rate, the sludge thickness, and the testing season. In general, the best performance was observed in prototypes where air was introduced below the sludge layer. The optimal airflow rate for weight reduction ranged between 3-6 m^3/m^2xh, with a sludge thickness between 25 and 28 cm. The aim is to find a correlation between the optimal operating parameters of the solar greenhouse prototypes and the full-scale plant.
In the case of the full-scale plant, the use of a thinner sludge layer and a higher airflow rate might reflect the need for a greater airflow to ensure adequate dehydration over a larger surface area with increased ventilation capacity.
However, the increase in airflow might not be directly comparable with the prototypes, as the higher airflow could require a different adaptation time depending on the type of full-scale plant and its operational conditions (e.g., dimensions, shading, natural ventilation, etc.).
This possible correlation could arise from the need to adjust the airflow rate and sludge thickness based on the size and specific characteristics of the plant. The full-scale plant may require a higher airflow rate to achieve the same dehydration efficiency, but an increase in airflow could also affect other aspects of the process, such as the management of relative humidity and temperature inside the greenhouse.
The final phase of this work was the scale-up of the project, with the construction of the full-scale solar greenhouse, measuring 3 x 10 meters, at the wastewater treatment plant in Caltanissetta, powered by a solar panel. The start-up of the experimental plant was included in the PhD. Figure 8.1 shows the constructed solar greenhouse.

Figure 8.1 - Greenhouse Scale-up

The drain bed of the greenhouse consists of 5 cm of drainage material of various types: gravel, small pebbles, and crushed stone.
Between the layer of small pebbles and the gravel, a perforated coil, realized with zinc steel perforated pipes, was inserted, allowing for the injection of hot air. This was produced by 3 panels in parallel with a total size of 6 x 1 meter. The Figure 8.2 shows the coil used and string of panels.

Figure 8.2 - Constructive details: a) perforated coil; b) solar panels

The construction of the greenhouse was entirely carried out by Caltaqua. The greenhouse was built within a drying bed. The cover is made of a polycarbonate frame with metal rods. The air is produced by the solar panels installed outside and is blown into the greenhouse through the blower, using a perforated steel coil placed between the drainage layer and the sludge layer. The blower was timed using a timer to prevent it from operating at night, so it had an automatic operation system that adjusted to the seasons of the trials. The sludge was loaded into the greenhouse via containers during each trial; it was thickened but undigested sludge. For water drainage, a discharge pit was created (30 x 30 x 30 cm), which was monitored by measuring the water level.

8.2 Tests conducted

Two different types of tests were conducted: one with a single load of sludge followed by final disposal, and the other with three different loads of sludge. In the latter test, the dried final sludge was not removed, but the greenhouse was refilled two more times to study the effect of the dry sludge at the bottom of the greenhouse and to simulate real operating conditions in a wastewater treatment plant. Before activating the aerated drying greenhouse, preliminary tests were performed. Specifically, the greenhouse was first filled with clean water until the drainage layer was completely saturated, and then up to an inundation level of 30 cm above the visible surface of the sand. The volume of water introduced was measured.
Thus:

- The geometry of the drainage and condensation water collection compartment was precisely measured, constructing the volume/level curve (which will be essential later for measuring these flows).
- The bottom drainage gate valve was closed.
- The volume of water lifted to reach the level of the visible sand surface was determined and labelled as V1.

- The bed filling continued, and the volume of water lifted to reach the level +30 cm above the visible sand surface was determined and labelled as V2.
- Once the bed filling was completed, still with the bottom valve closed, the blower was activated, and the proper bubbling of the air in water was checked.
- After this verification, the bottom valve was opened, and the bed was drained. The total drained volume, V3, was determined.
- The field water capacity (FWC) was calculated as the difference between V2 and V3, resulting 11 %.

Table 8.1 - Field Water Capacity

Field capacity (FWC)		
V in	18246	l
V out	17746	l
V drain	4500	l
	FWC	**11%**

8.2.1 Monitoring of management parameters

All operational parameters of the solar greenhouses, including data related to the hot air injection pumps, were managed by a informatic platform developed by Caltaqua SPA (Figure 8.3). The schematic of the plant is shown in the figure. The monitored operational parameters were:

- External temperature.
- Airflow rate.
- Panel inlet temperature.
- Panel temperature.
- Solar greenhouse inlet temperature.
- Air temperature inside the solar greenhouse.
- Drained water.
- Surface temperature of the sludge.
- Sludge humidity at different depth of the thickness.

For the characterization of the sludge, the moisture content was periodically determined according to standardized procedures. Additionally, the percentage of volatile solids was determined only at the beginning and at the end of the test to verify the degree of sludge stabilization.

The diagram in the Figure 8.3 shows the layout of the system with all the sensors positioned and the operational parameters that could be monitored. In this way, the parameters were monitored in real time, and it was also possible to control the turning on and off of the blower by setting a timer to prevent it from operating during the nighttime hours.

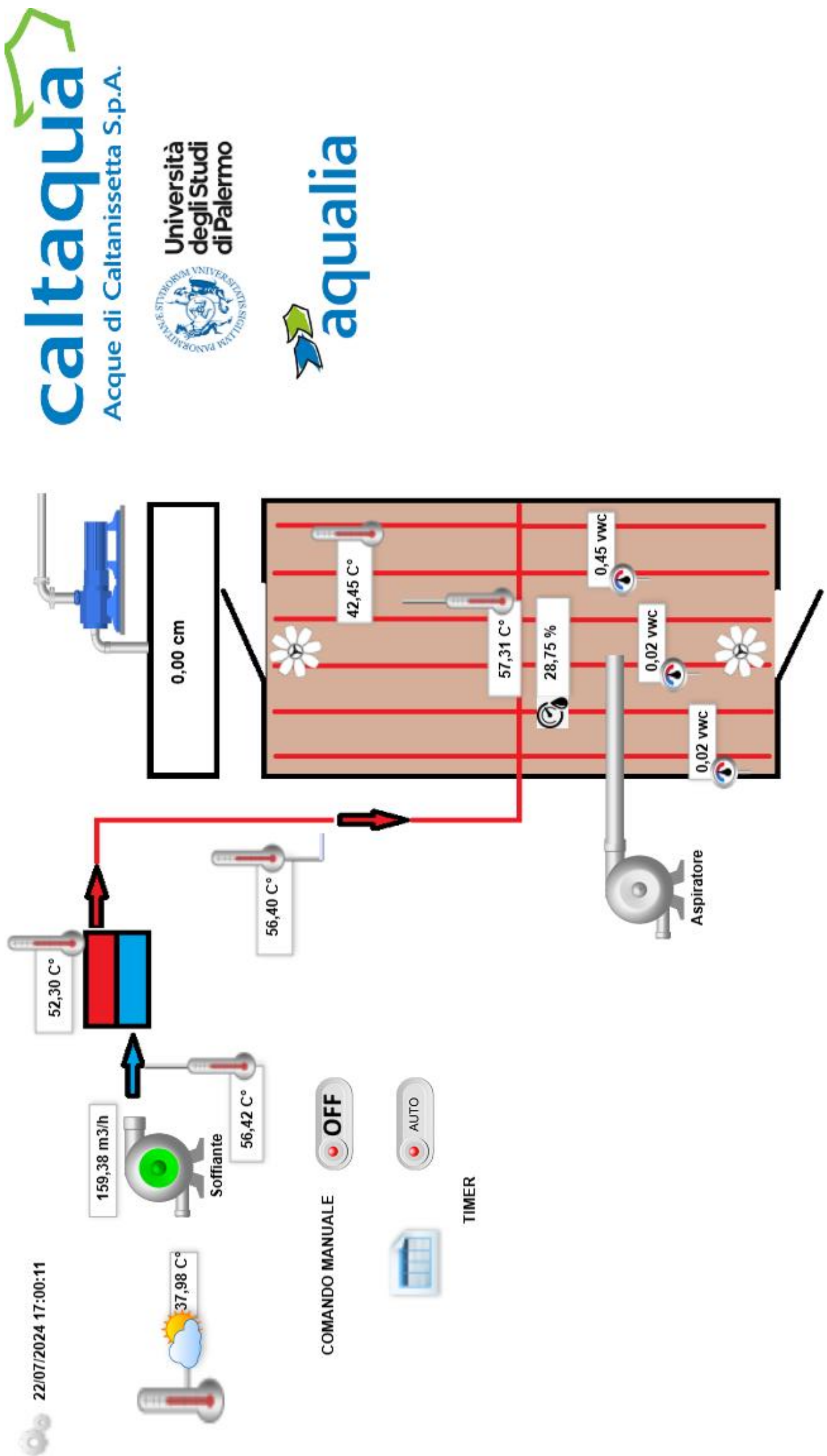

Figure 8.3 - Synoptic

8.2.2 Test 1

The first test was conducted from 22/03/2023 to 20/05/2023, for a total of 60 days. The greenhouse was filled with 15 cm of thickened, undigested sludge taken directly from the plant.

The characterization of the sludge allowed for determining the trend of sludge moisture within the greenhouse during the experimental period. During this period, as can be observed in the Table 8.2 and Figure 8.4 the moisture trend was decreasing, proceeding from an initial moisture value of 97 % to a value of 3.5 %.

Table 8.2 - Humidity test 1

Days of experimentation	Humidity [%]
0	97
9	89,44
16	75,36
21	50
30	22,52
37	7,14
43	5,00
60	3,5

It is important to note that during the test, the airflow rate was variable. Specifically, until the fourth day of the experiment, the average value was 243.58 m^3/h, in other words, 8 m^3/m^2x h and then it increased to an average value of 401.90 m^3/h until the end of the test. The increase in the injected airflow rate allowed for a greater reduction in sludge moisture. It is specified that the increase in airflow rate was determined by the installation of an additional blower to double the injected airflow rate. The Figure 8.4 shows the trend of moisture throughout the entire experimental period. In particular, the first section highlighted in purple represents the period with a single blower, while the second section in yellow represents the period of operation with two blowers.

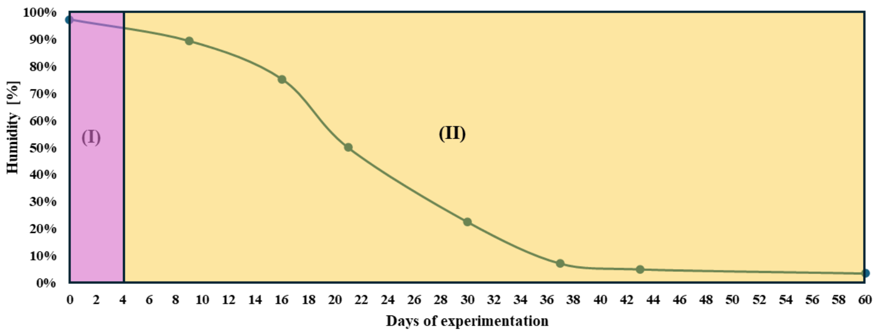

Figure 8.4 - Trend of humidity with airflow rate

During the test, an 80 % reduction in sludge weight was observed, decreasing from an initial value of 10.000 kg to a value of 2.000 kg. The VSS/TSS ratio changed from 78 % to 72 %, indicating a slight variation in the degree of sludge stabilization (Figure 8.5). This slight variation was likely due to the low stabilization of the sludge coming out of the anaerobic digester.

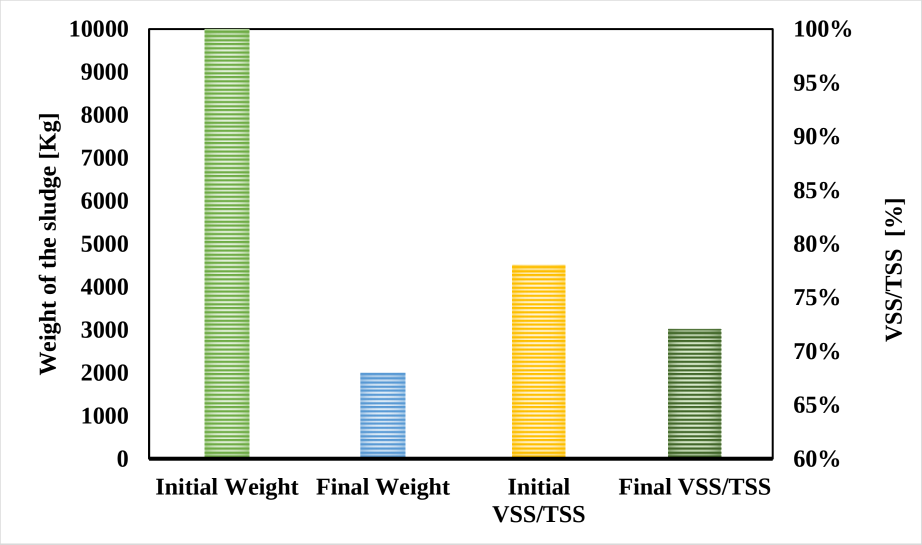

Figure 8.5 - Initial and final valued of VSS/TSS and weight of the sludge

Three sensors were placed at different depths within the sludge layer to investigate the distribution of water content. These were allocated at the following distance above the sludge-draining bed interface:

- Sensor V3 was positioned 8 cm from the bottom.
- Sensor V2 was positioned 4 cm from the bottom.
- Sensor V1 was positioned 1.5 cm from the bottom.

The figure shows the trend of sludge moisture recorded by the three sensors during the test. It can be observed that the moisture values measured by sensors V2 and V1 followed a similar trend: initially increasing as water drained into the immediately lower sludge layer and then decreasing sharply to zero when the sludge layer thickness was reduced to the point of eliminating contact between the sludge and the sensor. This was not the case for sensor V3, which, not receiving water from the upper sludge layers, showed a gradual decrease in moisture over time and then rapidly dropped to zero when the sensor was no longer in contact with the sludge.

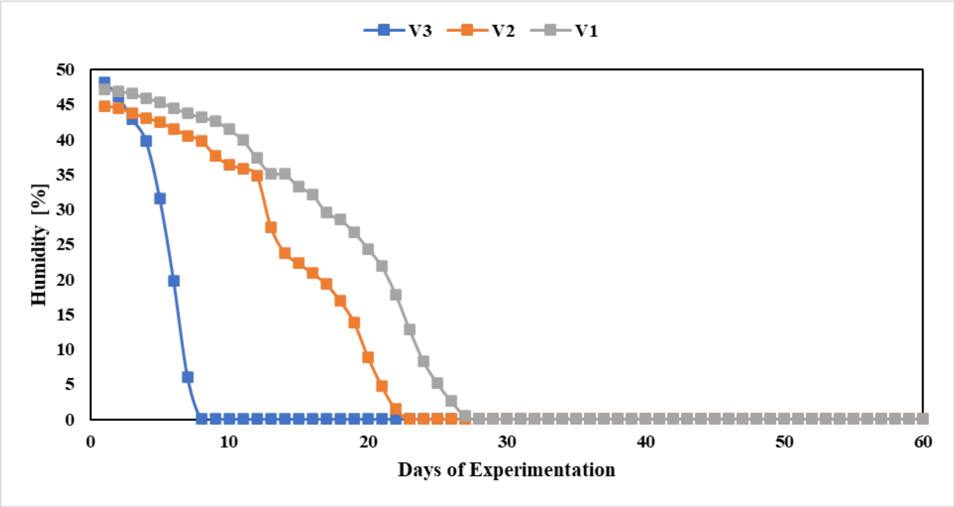

Figure 8.6 – Trends of sludge humidity at different levels within the sludge

Using the meteorological data from the Caltanissetta weather station provided by SIAS-Servizio Infomativo Agrometereologico Siciliano it was possible to obtain data on precipitation, as well as trends in temperature and relative humidity. As shown in Figure 8.7, during the first experimental period, daily precipitation levels were generally low, with some days showing no precipitation at all, while on other days the rainfall was more or less abundant. The day with the highest recorded precipitation occurred on the 55th day.

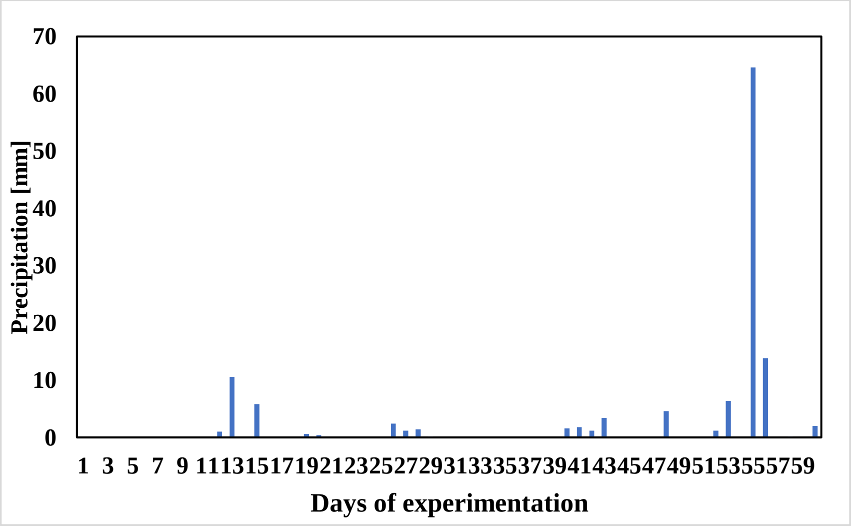

Figure 8.7 – Precipitation during first period of experimentation

Through SIAS, it was also possible to obtain data on the daily average air temperature and relative humidity. In Figure 8.8, the corresponding trends are shown. Specifically, the average air temperature was 13.65 °C, with a minimum value of 8.11 °C and a maximum value of 19.14 °C. Meanwhile, the average relative humidity of the air was 71.41 %, with a minimum value of 48.08 % and a maximum value of 99.42 %.

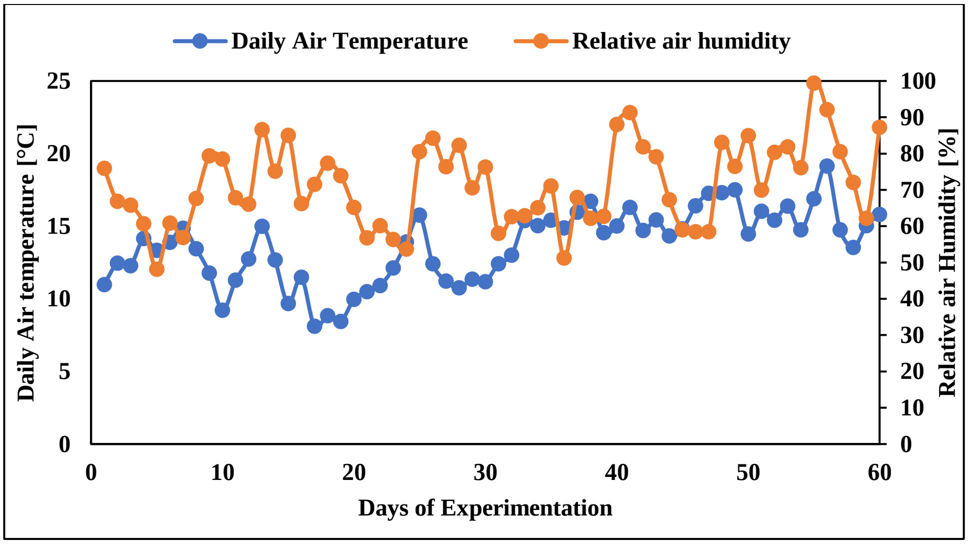

Figure 8.8 – Daily air temperature and relative aur humidity trends during first period of experimentation

Thanks to the data management software, it was possible to report the temperature trends recorded at various points in the system during the test. It can be observed that the ambient temperature inside the greenhouse is higher than the external air temperature, due to the thermal conditions promoted using a solar greenhouse.
During the first period, the average external temperature was 13.15 °C, while the temperature inside the greenhouse was 21.84 °C. In the second period, the average external temperature was around 12.45 °C, with an internal temperature of 24.99 °C, which was higher than in the first period. The panels, on the other hand, maintained nearly the same temperature throughout the 60-day experimental period, with an average value of 24.03 °C. Therefore, the temperature increases between the exterior and interior during the first period was about 10°C, while in the second period it was 13 °C. It is important to note that these are average values. The data provided by the SIAS meteorological station were compared with the data recorded by the sensors located within the treatment plant. From this comparison, it was observed that the temperature trends were nearly identical, with small differences likely due to the different locations of the data recording points.

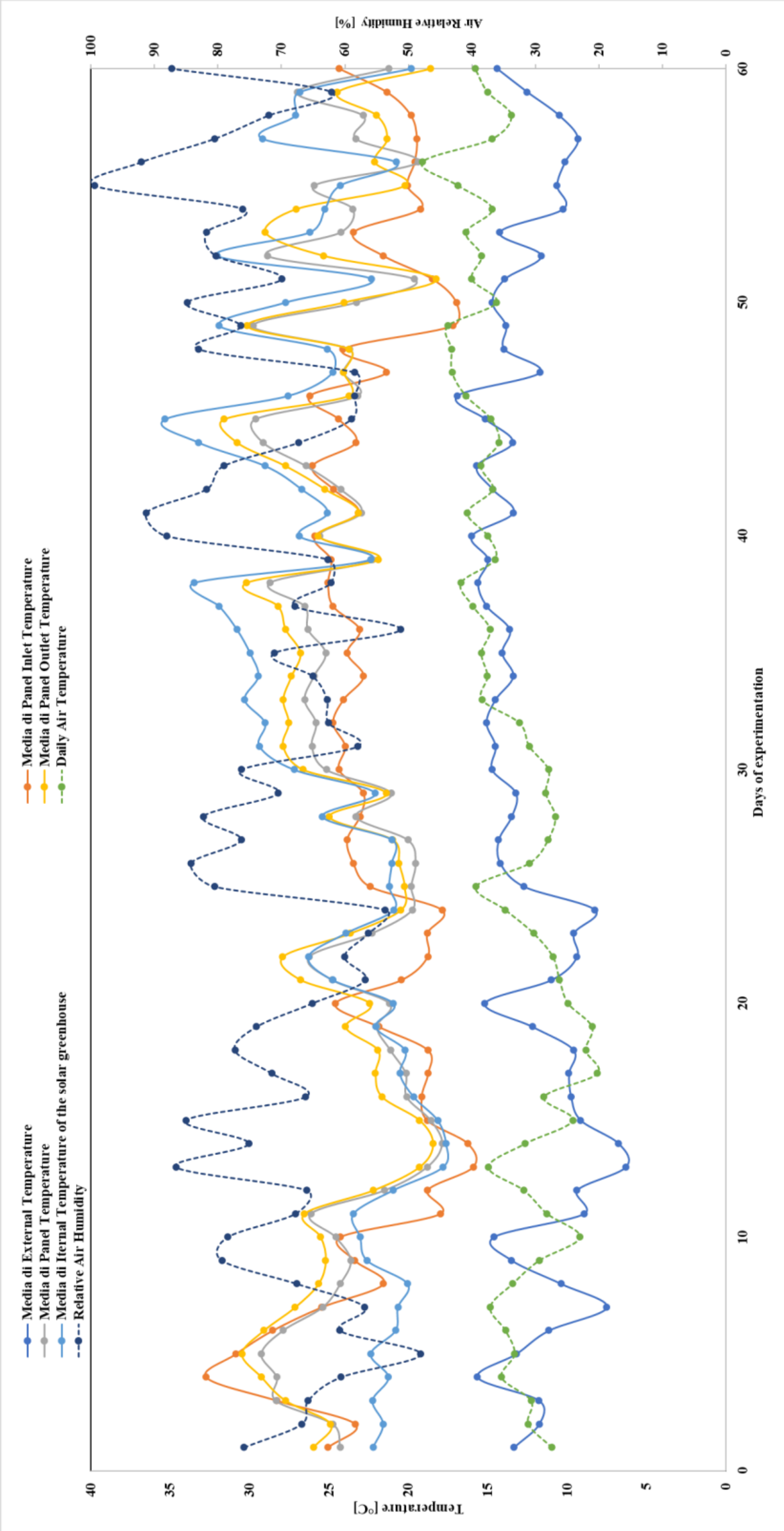

Figure 8.9 - Trends of the average temperature measured in different points

The figure shows the initial and final conditions in terms of the morphological appearance of the sludge surface inside the solar greenhouse. It is observed that at the beginning of the test, the sludge has a watery appearance due to its high-water content. By the end of the test, however, the sludge is characterized by high porosity because of the dehydration effect.

Figure 8.10 - Images of the sludge at the beginning and end of the test: a) at the beginning and b) at the end of the test

8.2.3 Test 2

The second test was conducted differently from the previous one. Specifically, it involved 3 distinct phases of loading the solar greenhouse and only 1 phase of unloading, which took place at the end of the experimental period.
The experiment began on 04/07/2023 and ended on 21/11/2023. The objective of this trial was to study the effects of periodic sludge loading in the solar greenhouse without emptying it. Thus, the aim was to examine the effect of dried sludge beneath the layer of fresh (thickened and digested) sludge introduced into the solar greenhouse in terms of weight and moisture reduction.
At the end of the experimental period, the percentage weight reduction of the sludge from the start to the end of the test was evaluated, considering the initial weight as the sum of the weights of the three individual loads and the final weight as the weight of the dried sludge removed from the greenhouse. Also in this case, the three sensors positioned at different depths in the sludge layer provided the humidity values.

8.2.3.1 Load 1°

The beginning of this trial (1st Load) took place on 04/07/2023 and ended on 27/07/2023 (24 days of experimentation).
The duration of this phase of the experiment was shorter compared to that of Load 2° and 3°. This was primarily due to management issues that arose during the execution of the test. As a result, the final sludge moisture was likely not optimal.

The solar greenhouse was loaded with 10 m³ of fresh (thickened, undigested sludge taken directly from the plant) sludge, totalling approximately 10.000 kg, with an initial moisture content of 97 %. Therefore, the total weight of the sludge is 10.000 kg, of which 300 kg is dry matter, and 9.700 kg is the weight of water. The weight of the sludge, excluding the water content, is therefore 300 kg. The operating conditions of the drainage bed were the same as those described in the first test (5.3.2 Test 1). Air insufflation occurred continuously with an average flow rate of about 8 m³/m²xh (250 m³/h).
Using the meteorological data from the Caltanissetta weather station provided by SIAS-Servizio Infomativo Agrometereologico Siciliano it was possible to obtain data on precipitation, as well as trends in temperature and relative humidity, during the second experimental period, and in particular in the load 1° the daily precipitation levels were zero.
Through SIAS, it was also possible to obtain data on the daily average air temperature and relative humidity. In Figure 8.11, the corresponding trends are shown. Specifically, the average air temperature was 29.87 °C, with a minimum value of 25.68 °C and a maximum value of 35.13 °C. Meanwhile, the average relative humidity of the air was 32.50 %, with a minimum value of 15.66 % and a maximum value of 50.66 %.

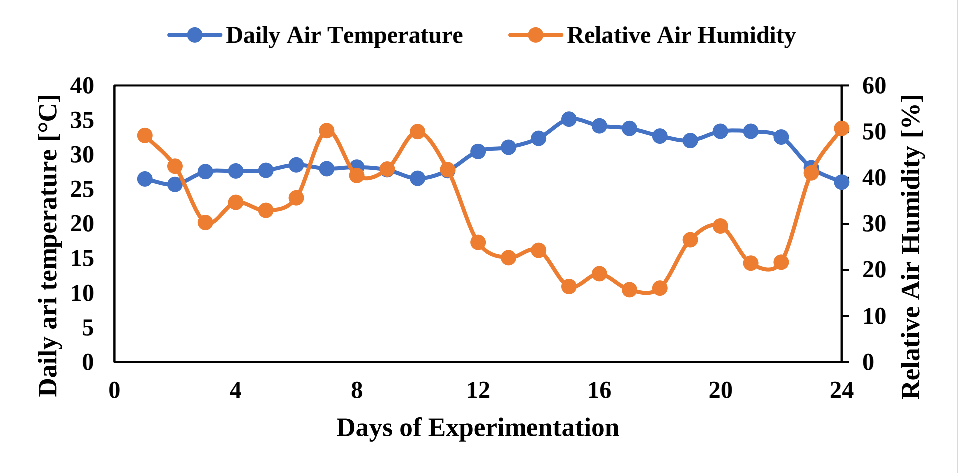

Figure 8.11 - Daily air temperature and relative aur humidity trends during second period of experimentation_ 1°load

The environmental conditions inside and outside the solar greenhouse, as well as the temperature at the inlet, outlet, and on the panel itself, were monitored through the previously described platform. The average external temperature was 27.23°C, with a maximum value of 30 °C. The maximum panel temperature recorded was 43 °C, with an average value of 40.47 °C. Inside the solar greenhouse, the average temperature was consistently 34 °C. In Figure 8.12, the temperature trends during the test are shown. A sinusoidal pattern can be observed for the internal temperature parameter of the solar greenhouse, due to the thermal variation between day and night. The effect of the solar panel on the air temperature can be observed by comparing the temperature trends at the panel's inlet and outlet. In fact, the thermodynamic action of the solar panel results in an increase in the inlet air temperature. This allows the inside of the solar greenhouse to maintain a higher temperature compared to the outside, which can have potential benefits for the thermal drying process. The data provided by the SIAS meteorological station were compared with the data recorded by the sensors located within the treatment plant. From this comparison, it was observed that the temperature trends were nearly identical, with small differences likely due to the different locations of the data recording points.

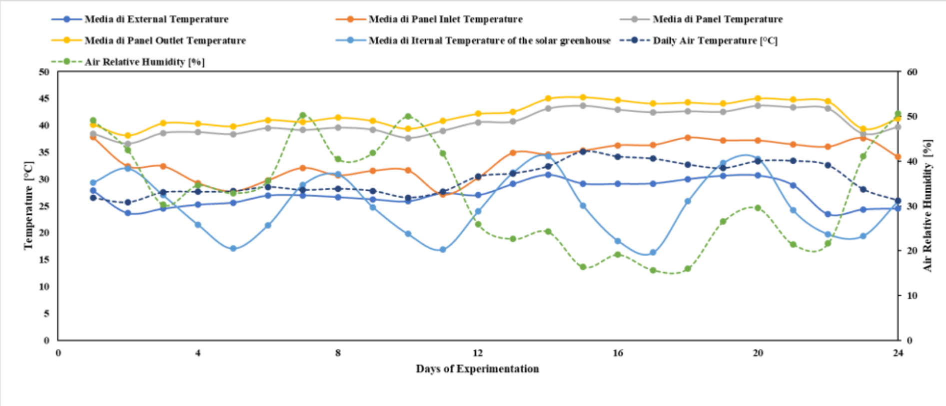

Figure 8.12 - Trends of the average temperature measured in different points, 1° sludge load

During the test, a moisture reduction of 70.3 % was observed, decreasing from 97.1 % to 28.8 % (Table 8.3).

Table 8.3- Humidity test, 1° sludge load

Days of experimentation	Humidity [%]
1	97.1
10	87.8
17	51.1
24	28.8

As observed in Figure 8.13, on the 10th day of the experiment, the moisture content of the sludge decreased from 97.1% (day 1) to 87.8%. As the test progressed, the most significant reduction in moisture was observed, dropping from 87.8% to 28.8% (day 24, end of the experiment).

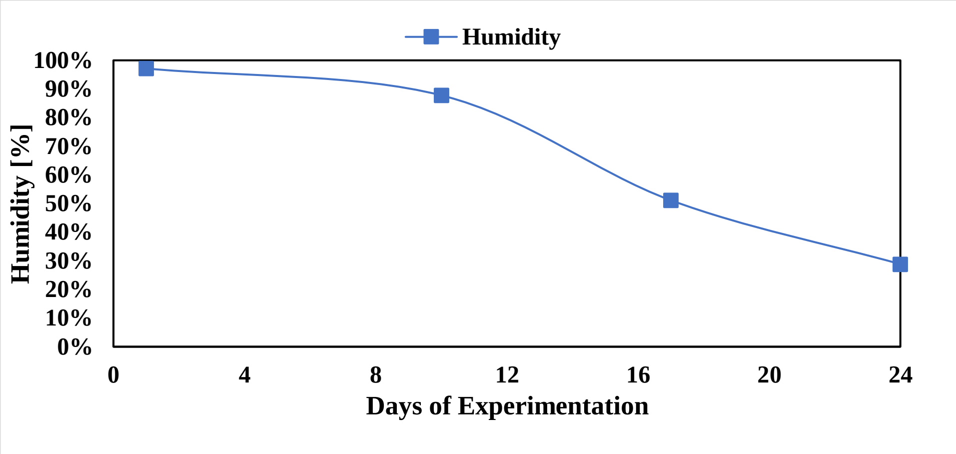

Figure 8.13 - Trend of humidity 1°sludge load

In Figure 8.14 the water content trends (Volumetric Water Content) of the sludge during the test, monitored through sensors V1, V2, and V3, are reported. In other words, the amount of water present within the sludge, expressed as a percentage. The V3 sensor, which is the most superficial one, is no longer in contact with the sludge layer starting from 07/16/2023, due to the volume reduction of the sludge caused by water loss. The V2 sensor is not in contact with the sludge layer starting from 07/19/2023. The water content value of the sludge recorded by this sensor shows a slight increase starting from 07/07/2023 due to water drainage from the upper layer, then gradually decreases until it reaches zero. On the other hand, the moisture trend recorded by the V1 sensor appeared different compared to that recorded by the V2 and V3 sensors; this is certainly due to the drainage of water from the upper layers.

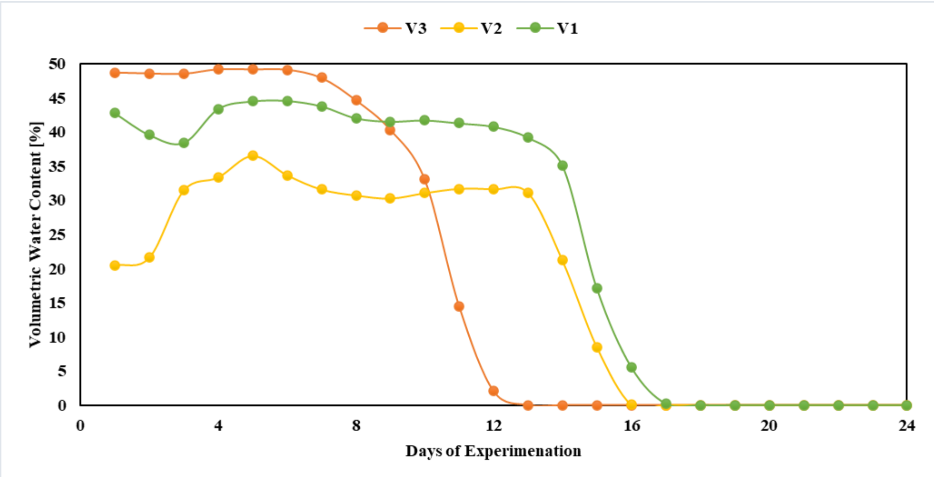

Figure 8.14 - Trends of sludge humidity at different levels within the sludge, 1° sludge load

8.2.3.2 Load 2

The beginning of the next trial (2nd Load) took place on 30/08/2023 and ended on 17/10/2023 (47 days of experimentation). The second filling of the greenhouse took place after about 30 days due to operational issues with the operator. Additionally, this trial was supposed to last the same amount of time as the first load, but due to the same operational issues, the duration was different and lasted 47 days. The solar greenhouse was loaded with 10 m^3 of fresh (thickened and digested) sludge, totalling approximately 10.000 kg. With a sludge moisture content of 95 % and an initial weight of 10.000 kg, the weight of the dry matter is 500 kg, with the weight of the water being 9.500 kg. The load was placed on top of the dried sludge from the 1st load (Figure 8.15). Air insufflation occurred continuously with an average flow rate of about 8 m^3/m^2xh (250 m^3/h).

Figure 8.15 - 2° sludge load over the dried sludge of first load

Using the meteorological data from the Caltanissetta weather station provided by SIAS-Servizio Infomativo Agrometereologico Siciliano it was possible to obtain data on precipitation, as well as trends in temperature and relative humidity, during the second experimental period, and in particular in the load 2° the daily precipitation levels were zero. Through SIAS, it was also possible to obtain data on the daily average air temperature and relative humidity. In Figure 8.16, the corresponding trends are shown. Specifically, the average air temperature was 21.26 °C, with a minimum value of 18.85 °C and a maximum value of 24.35 °C. Meanwhile, the average relative humidity of the air was 57.27 %, with a minimum value of 28.16 % and a maximum value of 82.04 %.

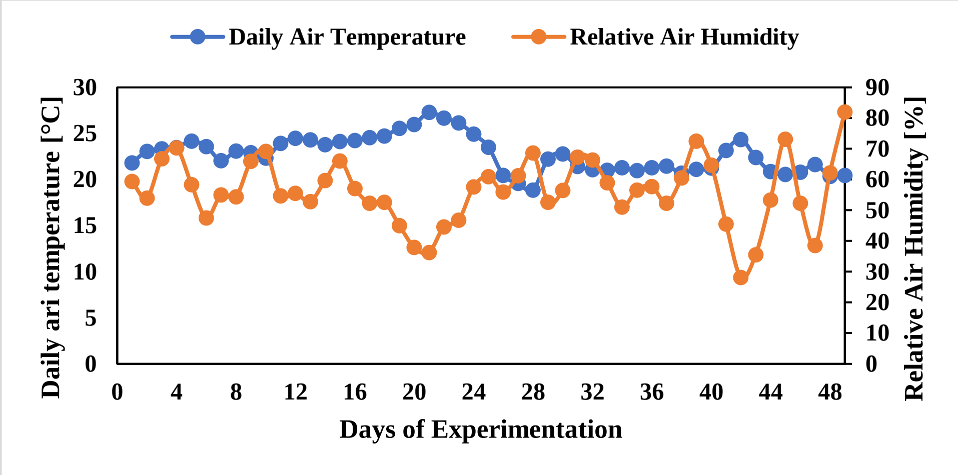

Figure 8.16 - Daily air temperature and relative aur humidity trends during second period of experimentation_ 2°load

In, Figure 8.17 the average temperature trends at different measurement points are shown. The temperature trend inside the greenhouse exhibits less daily fluctuation compared to the previous load. This may be due to the different seasonal period of the trial. An average external temperature of 21.39°C and an average panel temperature of 34.70°C were observed. Inside the greenhouse, the average temperature throughout the entire trial was 30.78°C. As for the maximum temperatures, the highest external temperature reached was 25°C, while the internal temperature of the greenhouse was about 36°C, resulting in an increase of approximately 10°C. The data provided by the SIAS meteorological station were compared with the data recorded by the sensors located within the treatment plant. From this comparison, it was observed that the temperature trends were nearly identical, with small differences likely due to the different locations of the data recording points.

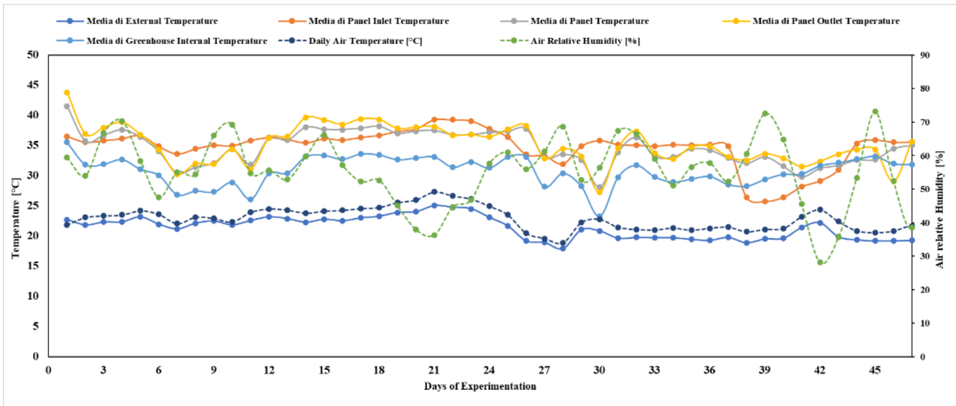

Figure 8.17 - Trends of the average temperature measured in different points 2° sludge load

During the test, a moisture reduction of 92.3% was observed, decreasing from 95 % to 7 % (Table 8.4).

Table 8.4 - Humidity test 2° sludge load

Days of Experimentation	Humidity [%]
0	95
12	84
22	65
26	40
35	35
43	14
47	7

As observed in Figure 8.18, until the 22nd day, the decrease in sludge moisture appears gradual (65 %), followed by a sharp decline on the 26th day (40 %), and then a return to a more moderate decrease until the end of the test.

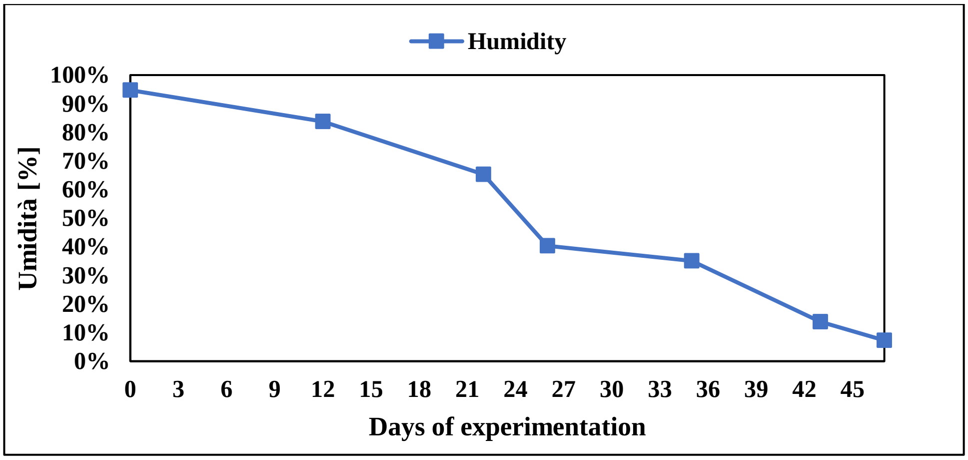

Figure 8.18 - Trend of humidity 2° sludge load

In Figure 8.19, the water content trends (Volumetric Water Content) of the sludge during the test, monitored through sensors V1, V2, and V3, are reported. In other words, the amount of water present within the sludge, expressed as a percentage. The V3 sensor, which is the most superficial, is no longer in contact with the sludge layer starting from 09/27/2023, due to the volume reduction of the sludge caused by water loss. The V2 sensor is no longer in contact with the sludge layer starting from 09/28/2023, while the V1 sensor is no longer in contact with the sludge layer starting from 10/02/2023.

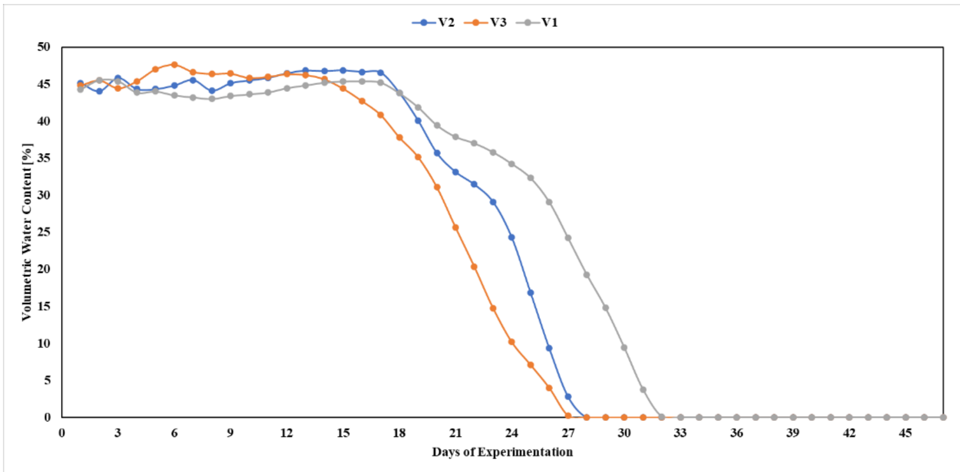

Figure 8.19 - Trends of sludge humidity at different levels within the sludge 2° sludge load

8.2.3.3 Load 3

The beginning of the final trial (3rd Load) took place on 17/10/2023 and ended on 21/11/2023 (36 days of experimentation). The solar greenhouse was loaded with 10 m³ of fresh (thickened and digested) sludge, totalling approximately 10.000 kg. Exactly, with an initial weight of 10.000 kg and a moisture content of 93 %, this means that 93 % of the total weight is water, and the remaining 7 % is dry matter. Therefore, you have approximately 700 kg of dry matter and 9.300 kg of water. The load was placed on top of the dried sludge from the 1st and 2nd loads. In this case as well, the duration of the trial was not the same due to operational issues with the operator. It started on the same day as the end of the second load.
Using the meteorological data from the Caltanissetta weather station provided by SIAS-Servizio Infomativo Agrometereologico Siciliano it was possible to obtain data on precipitation, as well as trends in temperature and relative humidity. As shown in Figure 8.20, during the second experimental period, daily precipitation levels were generally low, with some days showing no precipitation at all, while on other days the rainfall was more or less abundant. The day with the highest recorded precipitation occurred on the 18th day.

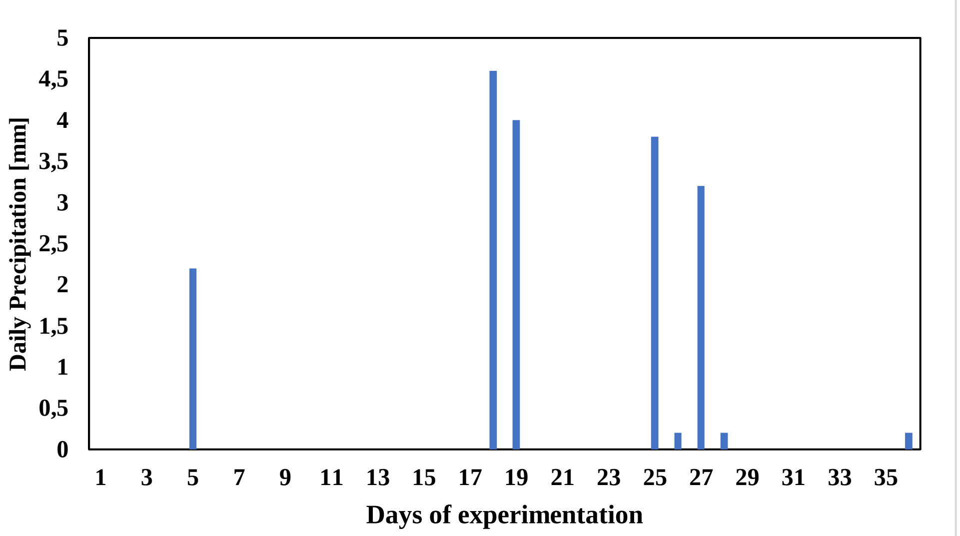

Figure 8.20 – Daily precipitation during the 3° load on the second experimentation period

Through SIAS, it was also possible to obtain data on the daily average air temperature and relative humidity. In Figure 8.21, the corresponding trends are shown. Specifically, the average air temperature was 16.35°C, with a minimum value of 12.58 °C and a maximum value of 21.72 °C. Meanwhile, the average relative humidity of the air was 75.54 %, with a minimum value of 53.37 % and a maximum value of 94.29 %.

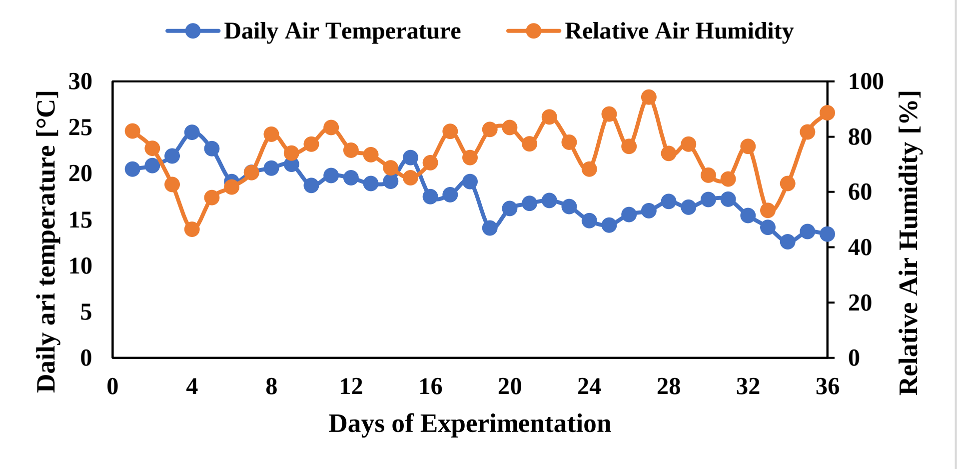

Figure 8.21 - Daily air temperature and relative aur humidity trends during second period of experimentation_ 3°load

In Figure 8.22 the average temperature trends at different measurement points during the test are reported. The environmental conditions of the autumn period are also reflected in the average temperature values. As the external temperature is lower compared to previous tests, the temperatures of the air entering and exiting the panel, and consequently inside the greenhouse, are also lower. The average temperatures observed were an external temperature of 16°C, a solar panel temperature of 25.8°C, and an internal temperature of the solar greenhouse of 23.53°C. Regarding the maximum temperatures, the external temperature reached 21°C, compared to 36°C for the panel and 28°C inside the solar greenhouse. The data provided by the SIAS meteorological station were compared with the data recorded by the sensors located within the treatment plant. From this comparison, it was observed that the temperature trends were nearly identical, with small differences likely due to the different locations of the data recording points.

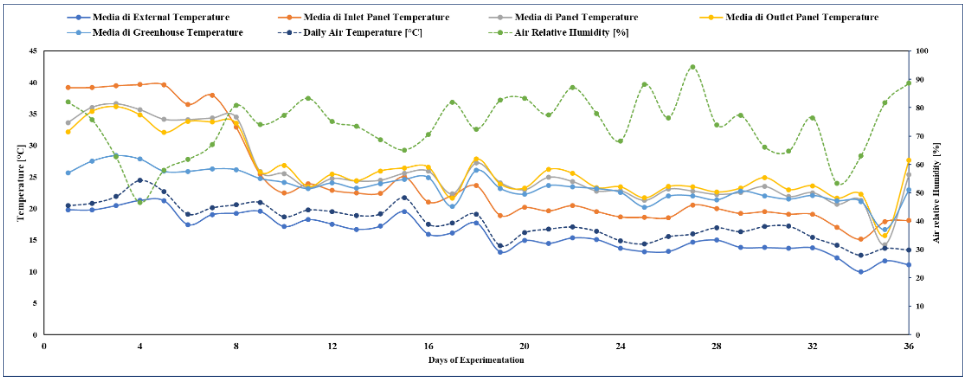

Figure 8.22 - Trends of the average temperature measured in different points 3° sludge load

In this case, air insufflation was carried out differently compared to the previous tests. Specifically, the average insufflation rate until 10/24/2023 was 6 m^3/m^2xh (190 m^3/h). From 10/25/2023 onward, with an average insufflation rate of 2 m^3/m^2xh (70 m^3/h), the aeration system was set to a timed operation, with automatic shutdown starting at 5:00 PM each day until 9:00 AM the following morning. This was done to prevent excessive moisture buildup inside the greenhouse. During the test, a moisture reduction of 39.7% was observed, decreasing from 93.5 % to 56.4 % (Table 8.5).

Table 8.5 - Humidity test, 3° sludge load

Days of experimentation	Humidity [%]
1	93.5
10	88.5
20	82.3
24	78.5
35	56.4

The results of this trial were found to be poor. One possible explanation is that a very low SSV (Suspended Solids Volatile) value was measured in the sludge, due to the high presence of inert materials. This could be a plausible explanation.

Indeed, the presence of inert materials in the sludge can slow down the drying process. Inert materials, such as sand, gravel, or other non-organic particles, do not contribute to the evaporation of water. On the contrary, they can increase the density of the sludge, hindering a faster evaporation of the water contained within it. Moreover, these materials do not absorb water, so they do not assist in the dewatering process of the sludge. As a result, a high presence of inerts reduces the efficiency of drying, making the moisture removal process more difficult and prolonged.
In Figure 8.23 the water content trends (Volumetric Water Content) of the sludge during the final test, monitored through sensors V1, V2, and V3, are reported. In other words, the amount of water present within the sludge, expressed as a percentage. In this case, the final moisture values recorded by the sensors were greater than zero. This could be due to less-than-optimal water drainage conditions from the sludge. Specifically, below the layer of fresh sludge, in addition to the drainage bed, there were the dried sludges from the two previous loads. This may have affected the drainage capacity of the free water from the sludge through the bed. Additionally, the final moisture values detected by the sensors could also be related to the overall final moisture content of the sludge, which is around 56 %.

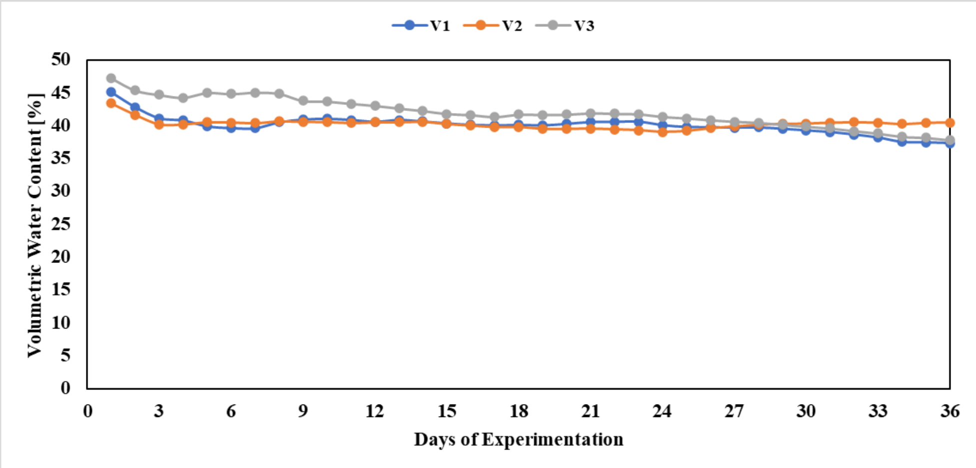

Figure 8.23 - Trends of sludge humidity at different levels within the sludge, 3° sludge load

At the end of this experimental period, samples of dried sludge were taken from the bed of the solar greenhouse (Figure 8.25 and Figure 8.26). The final weight of the dried sludge and the VSS/TSS ratio were determined. In Figure 8.24 the initial and final values of the sludge weight and its stabilization degree (VSS/TSS) are compared. A 90% weight reduction of the sludge was observed, with an initial weight of 30.000 kg (the sum of the sludge loads from the three tests) and a final weight of 3.000 kg (measured from the total dried sludge present in the greenhouse bed). Additionally, only an 8% reduction in the degree of stabilization was observed, decreasing from an initial VSS/TSS value of 36 % to a final value of 33 %. Discussions with the plant operators revealed that the low initial VSS/TSS value was due to a low volatile solid content in the sludge, resulting from a high inert content. This explains the small reduction in the degree of stabilization of the dried sludge.

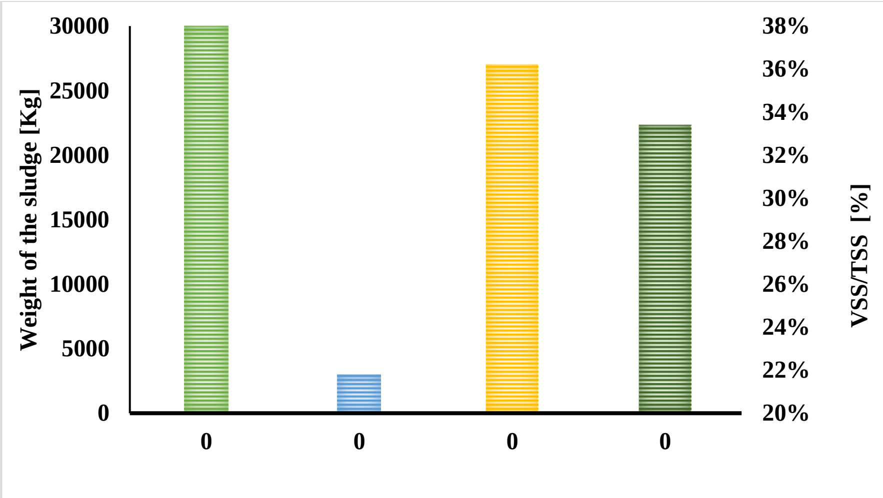

Figure 8.24 - Initial and final valued of VSS/TSS and weight of the sludge

Figure 8.25 - Dried sludge at the end of the experimentation period

Figure 8.26- Detail of the dried sludge at the end of the experimentation period

9 Economic evaluation

9.1 Introduction

The reproducibility of the solar drying treatment of sludge depends not only on the performance analysis of the treatment, for obvious reasons, but also on the assessment of the economic feasibility of the plant in question.
The economic feasibility of the plant was analysed using the economic indicator called "Net Present Value (NPV)", calculated over N=20 years and with reference to (Sorrenti et al., 2022).
The NPV is an index that is calculated based on all expected revenues and costs over the course of a given project. The index is defined as the sum of the present values of inflows (benefits) and outflows (costs) over a period. This tool allows one to determine whether a project can generate a net profit (positive NPV > 0), indicating that the investment may add value to the company, or a loss (NPV < 0), indicating that the investment could detract value from the company (Gaspars-Wieloch, 2019).
The determination of NPV involves several steps, including the calculation of the initial capital investment and the evaluation of net cash inflows and outflows during a single period.

9.2 Initial investment capital

The initial investment capital (I_0) is an investment that must be made to launch a new project and cover the initial operating expenses. In the following evaluation, the initial investment capital has been calculated as the sum of three investment costs:

- the costs for the construction of the solar greenhouse drying process (I_1).
- the costs for the installation of solar energy generation structures (solar panels and photovoltaic systems) (I_2).
- the costs for the purchase of all necessary equipment for the proper functioning of the solar greenhouse (sensors, blowers, etc.) (I_3).

$$I_0 = I_1 + I_2 + I_3$$

To compare the costs with each other, they have been normalized to the surface area of the solar greenhouse.
The construction costs of the solar greenhouse drying process were set at 300 EUR/m² with reference to Zimmer et al. (2022) (Zimmer et al., 2022). The power supply for the blower motor, which provides ventilation for the greenhouse, is 0.2 kW. The activation of this motor was powered by energy produced by a photovoltaic panel. The generation of the hot air to be injected into the greenhouse was achieved through the solar panel.
The specific cost related to photovoltaic and solar panels was set, following a review of commercial catalogues, at 3000 EUR/kW and 800 EUR/m², respectively. Finally, the costs for the purchase of all necessary equipment for the proper functioning of the solar greenhouse were set at 10 % of the sum of the other two cost items (Table 9.1).

Table 9.1 - Specific implementation costs

Cost of Solar Greenhouse	Cost of Photovoltaic Panel	Cost of Solar Panel
€/m^2	€/kW	€/m^2
300	3000	800

The calculation related to the investment required for the implementation of the previously discussed solar drying treatment of sludge was first referred to the unit surface area of the solar greenhouse prototype and subsequently to a full-scale greenhouse with a treatment capacity of 1000 kg/day of sludge. It has been hypothesized that traditional dehydration technologies typically achieve a residual sludge moisture content of 75 %. As observed in the previous chapters, the solar greenhouse prototypes studied were able to reach an average residual sludge moisture content of 5 %. The disposal of sludge with a 75 % moisture content is associated with a cost that depends on the weight of the sludge to be disposed of. Obviously, sludge with a moisture content of 5 % has a lower weight compared to sludge with a moisture content of 75 % and therefore will incur a lower disposal cost. The further reduction in moisture achievable through the solar greenhouse was considered as an “avoided cost”: since the lower the weight of sludge to be disposed of in the landfill, the lower the cost associated with landfill sludge disposal.

9.2.1 Investment required for the construction of a solar greenhouse prototype

The investment was determined with reference to one of the various configurations of solar greenhouses used during the experimental trials. Specifically, the configuration from trial 4 was chosen. During this trial, starting from 149 kg of sludge (with an initial moisture content of 96 %), a final moisture content of 5 % was achieved in 25 days. The treatment capacity (C) of the prototype was calculated as follows:

$$C = \frac{W_i}{d * S}$$

where W_i is the initial weight of the sludge introduced into the greenhouse, d is the duration of the trial, and S is the surface area of the greenhouse.
Assuming that the ratio between the surface area of the solar greenhouse and that of the solar panel is constant, the specific surface requirement for the air-to-thermal panel (T) relative to the unit surface area of the solar greenhouse is 2.1 m^2 panel/m^2 greenhouse. In contrast, the energy requirement of the photovoltaic panel (F) was estimated based on the installed power of the air blower and was found to be 0.323 kW/m^2. These parameters are summarized in Table 9.2.

Table 9.2 - Summary table

W_i	d	Ui	Uf	S	C	Sp	T	P_engine	F
kg	gg	-	-	m^2	kg/m^2xd	m^2	m^2panel/m^2greenhouse	kW	kW/m^2
149	25	0.96	0.05	0.62	9.61	1.3	2.1	0.2	0.323

From this, it was possible to determine the costs I_1, I_2, and I_3:

$$I_1 = cost_{Greenhouse} * S$$

$$I_2 = cost_{photovoltaic} + cost_{solar\ panel} \quad F * cost_{photovoltaic} + T * cost_{solar\ panel}$$

$$I_3 = 0.10 * (I_1 + I_2)$$

These costs represent the initial investment capital for the construction of the solar greenhouse prototype (Table 9.3).

Table 9.3 - Capital cost for the construction of a solar greenhouse prototype

I_1	$I_{2\ photovoltaic}$	$I_{2\ solar}$	I_3	I_0
€	€	€	€	€
186.00	967.74	1677.42	283.12	3114.28

9.2.2 Investment required for the construction of a full-scale solar greenhouse

The determination of the investment costs necessary for the construction of the solar greenhouse prototype was required to calculate the investment costs for the construction of a full-scale solar greenhouse with a sludge treatment capacity of 1000 kg/day. Given that the prototype solar greenhouse has a treatment capacity of 5.96 kg/day, a multiplicative factor of 168 is needed to scale up to a plant with a capacity of 1000 kg/day. Thus, the initial investment capital amounts to € 522529.77.

9.3 Determination of the Net Present Value (NPV)

The Net Present Value (NPV) was calculated using the following formula:

$$NPV = -I_0 + \sum_{t=1}^{20} \frac{C_t}{(1+i)^t}$$

Where I_0 is the initial investment capital, C_t is the net cash inflow-outflows during a single period t, "i" is the discount rate (5 %), and t is the time of the cash flow.
The annual cash flow was determined as the difference between the sludge disposal cost resulting from the dewatering process with 75 % residual moisture (which would occur if a traditional dewatering process were used) and the solar drying

process with 5 % residual moisture. The cost of sludge disposal in a landfill was set at € 300 per ton (Collivignarelli et al., 2019).
The Actual Cash Flow (ACF) refers to the actual cash flow generated by a project over a specific period of time, considering the interest rate of the investment.

$$ACF = \frac{C_t}{(1+i)^t}$$

Thus, starting from 1000 kg of sludge with 96 % moisture, a moisture reduction from 96 % to 5 % results in a final sludge weight of 42.11 kg to be disposed of after treatment in the solar greenhouse with a cost of 4611.045 €/year. If the solar greenhouse had not been present, the annual disposal cost of sludge with a 75% moisture content (typical mechanical dewatering treatment) would have been 109500 € /year.
The annual cash flow was calculated to be 104888.955 €/year. Therefore, it was possible to determine the NPV over a time of 20 years.
Based on the economic analysis, it was determined that the net present value (NPV) after 20 years is significantly positive, confirming the investment's viability. Additionally, the estimated payback period starts from to 6 years (Figure 9.1, Table 9.4). It is worth emphasizing that the proposed sludge drying solution is environmentally sustainable, as it utilizes clean and free energy. From an environmental perspective, several benefits can be identified. First, the energy required for sludge drying is lower than that of traditional drying systems and has zero environmental impact, as it is generated using solar technologies. Furthermore, the reduced sludge volume can decrease the number of transport trips to disposal sites and the need for additional landfill space for sewage sludge. Future research is needed to estimate the system’s carbon footprint to fully assess the environmental advantages of sludge drying using solar greenhouses.

Table 9.4- Determination of NPV

Years	ICC	ACF	NPV	Interest rate
0	-522529.76	0	-522529.760	0.05
1		99894.242	-422635.525	
2		95137.374	-327498.151	
3		90607.023	-236891.128	
4		86292.402	-150598.725	
5		82183.240	-68415.484	
6		78269.753	9854.268	
7		74542.622	84396.890	
8		70992.973	155389.863	
9		67612.355	223002.219	
10		64392.719	287394.939	
11		61326.399	348721.338	
12		58406.094	407127.433	
13		55624.852	462752.286	
14		52976.049	515728.335	
15		50453.380	566181.716	
16		48050.838	614232.555	
17		45762.703	659995.259	
18		43583.527	703578.786	
19		41508.121	745086.907	
20		39531.544	784618.451	

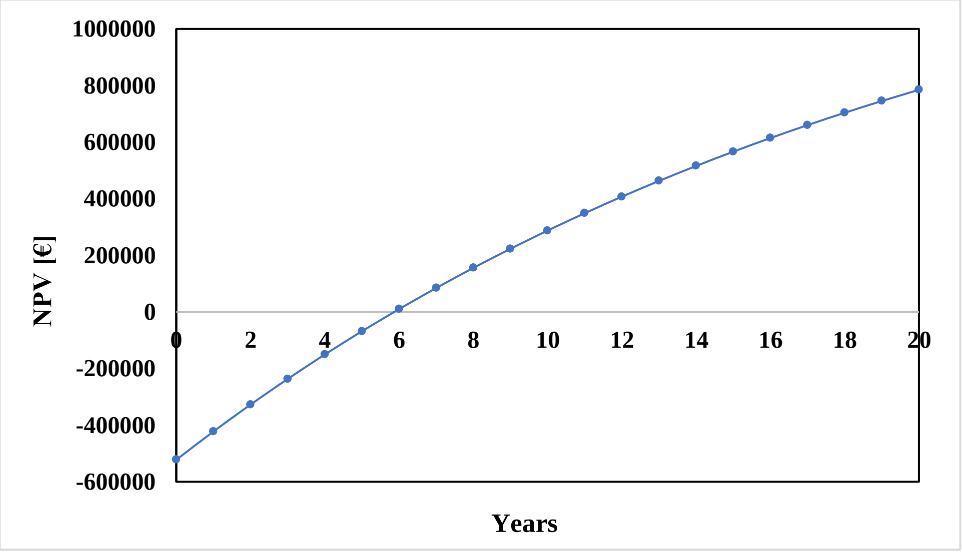

Figure 9.1 - Time trend of the NPV

10 Carbon Footprint

10.1 GHG determination for sludge dewatering processes

GHG emissions were determined for three sludge dewatering technologies. Two of these are traditional sludge treatment technologies used in wastewater treatment plants, specifically traditional mechanical dewatering technologies and drying beds. The third technology is represented by the solar greenhouses discussed in this study.

The determination of the Global Warming Potential (GWP), which represents the total effect of greenhouse gases, depends on the equivalence parameter between different substances, specifically the residence time, which is the average time that greenhouse gas molecules remain in the atmosphere before being removed. The residence time of carbon dioxide and nitrogen dioxide is over a century, whereas methane has a residence time of about a decade; therefore, the former will have a significantly greater and longer-lasting effect on global warming.

The determination of CO_2, CH_4, and N_2O emissions into the atmosphere takes into account the conversion factors.

Emission conversion factors are values used to convert data related to specific activities (such as fuel consumption, energy production, or other industrial activities) into emissions of specific greenhouse gases, such as CO_2, CH_4, and N_2O. These factors express the amount of a particular greenhouse gas emitted per unit of activity or product.

Conversion factors are calculated for three different time horizons of 20, 100, and 500 years: the longer the time horizon, the smaller the impact of some substances, as it is assumed that over time these substances will react with other atmospheric components, leading to their degradation and reduced effect. For the calculation of GHG emissions, the following formula was applied:

$$GHG\ [ton/anno] = CO_2 \times \mathrm{GWP_{CO2}} + \mathrm{CH_4} \times \mathrm{GWP_{CH4}} + \mathrm{N_2O} \times \mathrm{GWP_{N_2O}}$$

The CO_2 equivalent conversion factors for GWP are presented in Table 10.1 , while the greenhouse gas emissions will be determined separately. In the case at hand, only the time horizon of T=20 years was considered.

Table 10.1- Conversion factors to CO_2 equivalent

T [Years]	GWP $_{CH4}$	GWP $_{N2O}$	GWP $_{CO2}$
20	87	273	1
100	40	273	1
500	7.60	130	1

The methodological approach used was inspired by (Pan et al., 2023). It is important to specify that some considerations were made based on the cited study to adapt the approach to the objectives of the research and to understand the range of values for the parameters necessary to calculate the greenhouse gas emissions from sludge treatment processes, as reported in the literature cited by the study.

10.1.1 Carbon Footprint of mechanical dewatering

The mechanical dewatering process can indirectly contribute to GHG emissions, such as:

- carbon dioxide (CO_2): produced from the energy used to power the dewatering machinery, especially if the energy comes from fossil fuel sources;
- methane (CH_4): can be released from sludge that contains organic matter undergoing anaerobic decomposition, particularly if the sludge has been previously stored or treated in oxygen-deprived conditions.

To calculate the GHG associated with using a generical mechanical dewatering machine for sludge, two main sources of emissions must be considered:

- direct emissions associated with the release of gases such as methane (CH_4) or carbon dioxide (CO_2) directly from the sludge during the process.
- indirect emissions related to the energy consumption of the machine, i.e., the amount of electricity used, which in turn is linked to the energy mix and the emissions associated with the production of that energy.

The total greenhouse gas emissions (ET) for a dewatering machine were calculated using the following formula:

$$ET = (E \times F) + P_{CH4}$$

Where:

- E is the energy consumption of the generical dewatering machine, expressed in kWh per ton of sludge treated.
- F is the emission factor for electricity, indicating CO_{2eq} (carbon dioxide equivalent) emissions per kWh consumed. This varies by country and the energy mix used (coal, natural gas, renewables, etc.). In Italy, the average emission factor is approximately 0.33 kg CO_2/kWh.
- P_{CH_4} is the methane (CH_4) produced directly from the sludge during dewatering (this depends on the characteristics of the sludge, such as organic content).

The energy consumption of a dewatering machine ranges between 30 - 50 kWh/ton of sludge treated. In this case, it was set at 40 kWh/ton of sludge. The energy emissions are given by the product of energy consumption and the emission factor.

Energy Emissions = 40 kWh x 0.33 kg CO_2/kWh = 13.2 kg CO_2eq/tons of sludge

These emissions were calculated based on the annual quantity of sludge to be treated, assuming the dewatering machine has a treatment capacity of 20000 kg/day (digested and thickened sludge with 95 % moisture content).

Direct emissions from the sludge are more difficult to estimate and depend on the organic content of the sludge and treatment conditions. Generally, during the dewatering process, sludge may emit small amounts of methane or other gases. However, these emissions are often negligible compared to energy consumption, especially if the sludge has already been stabilized. For simplicity, it is assumed that direct emissions from the sludge are negligible.

The total greenhouse gas emissions for a dewatering machine are therefore equal to the sum of energy emissions and direct emissions. Given that the latter are negligible, total emissions are equal to 13.2 kg CO_2eq / ton of sludge treated (Table 10.2). In Table 10.3 GHG emissions for mechanical dewatering have been reported.

Table 10.2 - Emission CO_2 for mechanical dewatering

Energy consumption	kWh/ton sludge	40
Emission factor	kg CO_2/kWh	0.33
Direct emissions	kg CO_2eq/ton sludge	0
Energy emissions	kg CO_2eq/ ton sludge	13.2
Total emissions	kg CO_2eq/ ton sludge	13.2
Total annual sludge	ton/year	7300
Annual CO_2 emissions	kg CO_2eq/year	96360
T	years	20
GWP_{CO2}	-	1
CO_{2eq}	ton/year	96.4

Table 10.3 - GHG Mechanical Dewatering

CO_{2eq}		ton/year	96.4
N_2O_{eq}		ton/ year	0
$CH_{4\,eq}$		ton/ year	0
CH_4	GWP	–	87
N_2O	GWP	–	273
CO_2	GWP	–	1
GHG		ton/ year	**96.4**

10.1.2 Carbon Footprint of drying beds

Drying beds are a technology used for the natural dewatering of sludge, which relies on the evaporation of water through the action of sunlight and air. In this case, greenhouse gas emissions will primarily be associated with direct emissions from the sludge and any additional energy consumption (such as pumps for air or water movement, if present).

Unlike other technologies such as filter presses, drying beds generally have low energy consumption, so most emissions will come from gases released by the sludge itself. For the purpose of calculating emissions, the following factors need to be considered:

- quantity of greenhouse gases emitted by the sludge: the production of methane (CH_4) and nitrous oxide (N_2O) depends on the type of sludge, its organic composition, and drying conditions (temperature, ventilation, exposure time);

- emission factor for methane and nitrous oxide per ton of dried sludge;
- direct methane (CH_4) emissions: sludges containing organic matter that dehydrate under anaerobic conditions can produce methane. It has been assumed that a drying bed produces methane emissions at a rate of 0.04 kg CH_4/ ton of sludge;
- direct nitrous oxide (N_2O) emissions: N_2O is another greenhouse gas that can be emitted by sludge, especially when the drying process involves the decomposition of nitrogenous compounds under anaerobic and aerobic conditions. It is assumed that 0.005 kg of N_2O is released per ton of dry sludge;
- indirect emissions: suppose the drying bed uses 5 kWh / ton of sludge for auxiliary operations (pumps, fans). With an emission factor for electricity of 0.33 kg CO_2eq/kWh:

Energy Emissions = 5 kWh x 0.33 kg CO_2eq/kWh = 1.65 kg CO_2eq/ tons of sludge

Indirect emissions related to energy consumption are much lower compared to other technologies such as dewatering machine.
In Table 10.5 and Table 10.5 the calculated emissions and the GHG value are reported.

Table 10.4 - Emission for drying beds

CH_4 emission	Kg CH_4/ton sludge	0.1
Total annual sludge	ton/year	7300
CH_{4eq}	**ton/year**	**0.730**
N_2O emission	Kg N_2O /ton sludge	0.005
N_2O_{eq}	**ton/year**	**0.0365**
CO_2 emission	kg CO_2/ ton sludge	1.65
CO_{2eq}	**ton/year**	**12.05**

Table 10.5 - GHG Drying Beds

CO_{2eq}		ton/year	12.05
N_2O_{eq}		ton/year	0.0365
CH_{4eq}		ton/year	0.730
CH_4	GWP	–	87
N_2O		–	273
CO_2		–	1
GHG		**ton/year**	**85.5**

10.1.3 Carbon Footprint of greenhouses

If the solar drying beds used for sludge drying are powered by photovoltaic panels, the indirect greenhouse gas emissions related to electricity consumption will be significantly reduced or even eliminated, as the electricity would be generated from a renewable source (photovoltaics). However, there will still be direct emissions from the sludge to consider, such as methane and nitrous oxide. To calculate the total emissions, it is necessary to distinguish between direct and indirect emissions:

- direct emissions from the sludge: emissions of gases such as methane and nitrous oxide produced during the drying process.
- indirect emissions related to energy: with the use of photovoltaic panels, the emissions associated with electricity consumption are zero.

The indirect emissions related to electricity consumption are assumed to be zero due to the use of solar panels. Methane emissions are 0.1 kg of CH_4 per ton of sludge, while nitrous oxide emissions are 0.005 kg of N_2O per ton of sludge. In Table 10.6 and Table 10.7 the calculated emissions and the GHG value are reported.

Table 10.6 - Emission for greenhouses

CH_4 emission	Kg CH_4/ton sludge	0.1
Total annual sludge	ton/year	7300
CH_{4eq}	**ton/year**	**0.73**
N_2O emission	Kg N_2O /ton sludge	0.005
N_2O_{eq}	**ton/year**	**0.0365**

Table 10.7 - GHG greenhouses

CO_{2eq}		ton/year	0
N_2O_{eq}		ton/year	0.0365
$CH_{4\,eq}$		ton/year	0.73
CH_4	GWP	–	87
N_2O		–	273
CO_2		–	1
GHG		**ton/year**	73.5

When a solar drying bed for sludge is powered by photovoltaic panels, the total greenhouse gas emissions are significantly reduced. Solar-powered drying beds therefore offer a considerably more environmentally friendly option compared to those powered by conventional energy sources.

10.2 Determination of GHG for the transport of dewatered sludge to landfill

To calculate the greenhouse gas (GHG) emissions associated with transporting dewatered sludge to a landfill, the following main factors need to be considered:

- transport distance (in km) from the sludge treatment facility to the landfill.
- weight of the transported sludge (in tons).
- type of vehicle used for transportation and its fuel consumption.
- emission factor of the fuel used (diesel), expressed in kg CO_2eq per liter or per kilometer traveled.

10.2.1 Emission transport for dewatering mechanical processes

For the calculation of emissions related to the transport of dewatered sludge from the generical dewatering machine to the landfill, the following considerations were made:

- it was assumed that 20 tons of sludge are transported per trip.
- the transport distance to the landfill is 100 km (round trip).
- the diesel vehicle's fuel consumption is assumed to be 35 liters per 100 km.
- the emission factor for diesel is approximately 2.64 kg CO_2eq per liter of fuel.

From this, it was possible to determine the fuel consumption per trip and the associated CO_2 emissions (Table 10.8).

Table 10.8 - Emissions transport

Fuel Consumption	l/trip	35
Trip Emissions	kg CO_2eq /trip	92.4
Emission	kg CO_2eq /tons	4.62

In Table 10.9 the GHG emission for transport has been reported.

Table 10.9 - Emission transport for dewatering mechanical processes

Final Weight of Dewatered Sludge	Kg/day	2857.14
Final Weight of Dewatered Sludge	tons/year	1042.85
GHG	**t CO_2eq /year**	**4.81**

10.2.2 Emission transport for drying beds

For calculating the emissions related to transporting sludge from the drying beds, the same considerations as in the previous case were made. The only

exception was the final moisture content of the sludge leaving the treatment, which is set at 75 %.
The specific emissions associated with transporting the sludge to the landfill are the same as those reported in Table 10.8.
In Table 10.10, the GHG value associated with transporting the sludge to the landfill is reported.

Table 10.10 - Emission transport for drying beds

Final Weight of De-watered Sludge	Kg/day	4000
Final Weight of De-watered Sludge	tons/year	1460
GHG	**t CO_2eq /year**	**6.74**

10.2.3 Emissions transport for solar greenhouse

The same reasoning was applied to calculate the emissions related to transporting dewatered sludge to the landfill from the solar drying beds. The only different data point is the final moisture content of the treated sludge, which is set at 5 %. The specific emissions associated with transporting the sludge to the landfill are the same as those reported in Table 10.8. The GHG value obtained is reported in Table 10.11.

Table 10.11 - Emissions transport for solar greenhouse

Final Weight of Dewatered Sludge	Kg/day	1052
Final Weight of Dewatered Sludge	tons/year	384.21
GHG	t CO_2eq /year	1.77

10.3 Total GHG

For each treatment technology, the total GHG values were calculated as the sum of the emissions related to the process and the transportation. The total values obtained are reported in Table 10.12.

Table 10.12 - Total GHG

Technology	GHG Process	GHG Transport	GHG Total
	t CO_2eq /year		
Dewatering machine	96.36	4.81	101.18
Drying Beds	85.52	6.74	92.26
Greenhouses	73.47	1.77	75.25

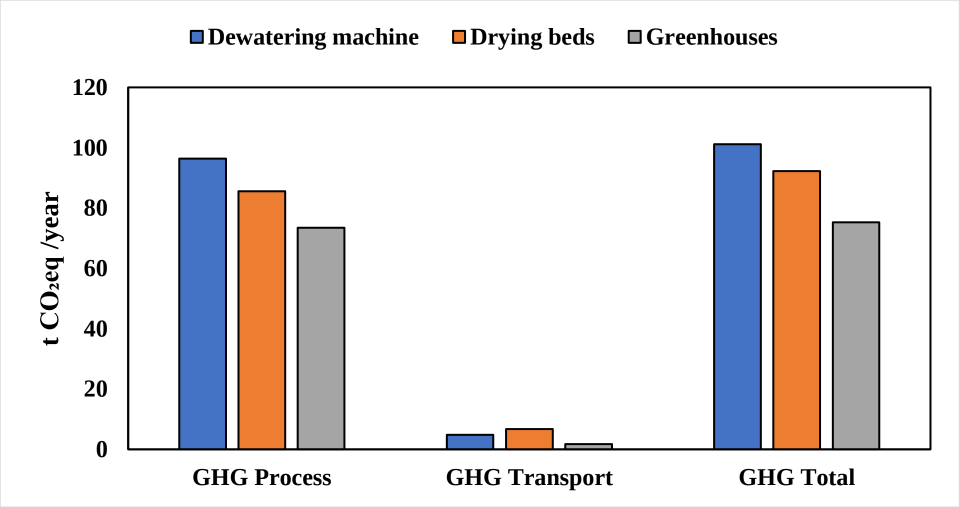

Figure 10.1 - Total GHG

From the figure (Figure 10.1), it can be observed that the GHG emissions related to the dewatering mechanical machine process and the drying beds are similar. The emissions from the dewatering machine are slightly higher due to the energy consumption required for its operation (higher indirect emissions). In the case of GHG emissions related to transportation, the dewatering machine shows a lower emission value compared to the drying beds, due to the lower weight of dewatered sludge that needs to be transported to the landfill.

Solar drying beds, on the other hand, have lower GHG emissions compared to the other two technologies. This is primarily due to two reasons: (1) indirect emissions related to energy consumption are zero because a renewable energy source is used, thanks to the presence of photovoltaic and solar panels; (2) emissions related to landfill transport are low due to the reduced weight of sludge to be disposed of, which results from the lower final moisture content achieved through this innovative technology.

11 Future Perspectives and Developments

The treatment of wastewater sludge through the use of solar greenhouses represents an innovative and sustainable technology that offers multiple environmental and economic advantages. However, despite the promising results obtained from this research, there are several areas in which the process can be further optimized and developed.

One of the main directions for future developments could be the expansion of the technology on an industrial scale. Although solar greenhouses have demonstrated high efficiency in prototypes and pilot-scale tests, their application in large-scale wastewater treatment plants requires a thorough evaluation of performance under varying conditions and in different contexts.

In particular, managing air flows and improving air distribution structures within the greenhouses could be optimized to maximize the efficiency of the dehydration process. Additionally, in the context of digital transition and circular economy, automation and remote monitoring of solar greenhouses are crucial aspects for more efficient management and for reducing operational costs. The use of advanced sensors, artificial intelligence, and remote monitoring systems could enable optimized control of environmental variables, such as temperature, humidity, and ventilation, further enhancing the reliability and profitability of the dehydration process.

Furthermore, future research should focus on the implementation of hybrid technologies that combine solar energy with other renewable sources, such as geothermal or wind energy, to improve the performance of greenhouses during less sunny periods or in winter seasons. This approach could ensure continuous operation, minimizing inefficiency periods.

The possibility of integrating the solar dehydration process with other treatment technologies or sludge minimization processes also represents an interesting area of research. Such combinations could lead to further improvements in sludge stabilization, potential energy production, and a reduction in the amount of sludge sent to landfills. This would make the process even more environmentally and economically advantageous.In conclusion, the adoption of solar greenhouses for sludge dehydration has the potential to revolutionize wastewater sludge treatment, significantly reducing costs and environmental impact. With further research and the implementation of these innovative solutions, sludge treatment could become an increasingly sustainable practice, integrated into waste management strategies.

12 Conclusions

This study aimed to develop solar greenhouse prototypes with an innovative technology for the dehydration of wastewater treatment sludge. The literature review allowed for a deeper understanding of the technologies currently used for sludge dewatering and their process efficiencies. Additionally, the study examined innovative technologies (solar greenhouses) used for minimizing the weight of sewage sludge. A solar greenhouse is an economically efficient and environmentally sustainable solution that reduces the water content in sludge by almost 90 %. Achieving a dry matter percentage of 80 -90 % results in a reduction of sludge volume and weight, which consequently minimizes disposal and transport costs. Furthermore, the dried sludge becomes odorless, biologically stable, and easy to store. Compared to traditional drying methods, solar greenhouses are much more cost-effective and provide a more appreciable final product.

The main goal of the work was to develop a solar drying system for sewage sludge to ensure an optimal environment for drying. In this system, the heat provided to the material to be dried is significantly higher than what would be available under natural environmental conditions. This increases the evaporation rate of water from the sludge due to the hot air heated by the solar panels.

The innovation of the process lies in introducing hot air directly beneath the sludge layer via an air distribution system. The study was conducted in several phases:

1. Design and execution of "bench tests" as a preliminary study before developing the solar greenhouse prototypes.
2. Design and construction of solar greenhouse prototypes at the Palermo wastewater treatment plant "Acqua dei Corsari."
3. Study of a full-scale solar greenhouse developed in collaboration with Caltaqua S.p.A at the Caltanissetta wastewater treatment plant.

Bench Tests were performed as a preliminary study on the dewatering process of sewage sludge to be carried out in the solar greenhouse prototypes. Specifically, at the end of the tests, the optimal sludge thickness for the greenhouses and the airflow rate to introduce into the system were determined. The drying process was studied within five cylinders replicating a typical drying bed, evaluating weight reduction and moisture content reduction at the end of the tests. Different sludge thicknesses and two airflow rates were used during the tests.

The highest weight reduction percentages were observed in the test conducted with a specific airflow rate (0.04 m^3/m^2xh). From this observation, it was concluded that, in addition to the thickness of the sludge, the airflow rate is another key design parameter for these systems. Therefore, as the sludge thickness increases (ranging from 20 - 28 cm), a greater reduction in sludge weight was observed. While lower airflow rates still led to increased sludge reduction with increasing thickness, the reductions remained lower compared to those achieved with higher airflow rates.

After the results from the bench tests, three solar greenhouse prototypes were designed and built. During the experimental period, seven tests were conducted, with varying configurations, including:

- Air input location: above, below, and mixed (above and below) the sludge layer.
- Airflow rate: varying between 2 and 28 m^3/m^2xh.

- Sludge thickness: varying between 18 and 28 cm.
- Season of testing.

The solar drying process was evaluated by determining:

- Sludge weight reduction.
- Moisture content change.
- Construction of drying curves and evaluation of process kinetics.
- Determination of the SSV/SST ratio of the sludge to assess the degree of stabilization at the end of the test.
- Recording of system temperatures using sensors.
- Recording of meteorological parameters via a meteorological station.

Results from the solar greenhouse prototypes suggested important considerations for the solar drying process. The solar greenhouse prototypes allowed for a weight reduction of 90-98 % (with final sludge moisture content between 5 % and 10 %) within 25-30 days, achieving a high final dry matter content and a low concentration of volatile solids in the sludge. The process efficiency varied depending on the air input type (above/below the sludge bed), airflow rate, sludge thickness, and the testing season. In general, the best performances were observed with prototypes where air was introduced from below the sludge layer. The optimal airflow rate range for weight reduction was between 3-6 m^3/m^2xh with a sludge thickness between 25 and 28 cm.

An additional phase of the research involved studying a full-scale solar greenhouse built in collaboration with Caltaqua S.p.A at the Caltanissetta wastewater treatment plant. One of the existing drying beds was converted into a solar greenhouse with air input below the sludge layer. The air distribution structures were inserted between the draining layer and the sludge layer, and continuous monitoring was carried out using a monitoring system developed by Caltaqua.

Two tests were conducted during the experimental period:

- Test 1: Conducted with one sludge load and one discharge, showing an 80% weight reduction, from 10,000 kg to 2,000 kg. The SSV/SST ratio of the sludge decreased from 78 % to 72 %.
- Test 2: Conducted with three sludge loads and one discharge at the end, to evaluate the influence of dehydrated sludge layers beneath the fresh sludge. The result was a 90 % weight reduction, from 30,000 kg to 3,000 kg. The SSV/SST ratio of the sludge changed from 36 % to 33 % due to the high content of inert solids.

The full-scale solar greenhouse built by Caltaqua achieved a weight reduction of 80-90 %. Traditional drying beds typically allow for a final sludge moisture content of around 60 %, while mechanical dewatering units reach about 70 %. These final moisture values are significantly higher than those achieved with solar greenhouses (5-10 %). Additionally, solar greenhouses have a reduced environmental impact due to lower energy consumption, as they use renewable energy sources (solar panels), which is not the case with mechanical sludge dewatering systems, which are generally energy intensive.

The solar greenhouse for sludge used in this experimental research has effectively met the criteria for a correct and efficient system, namely:

- Maximizing evaporation speed by optimizing the conversion of solar energy into thermal energy, heating both the sludge and the air above it.

- Managing the relative humidity of the air inside the greenhouse and controlling ventilation when necessary.
- Producing dried sludge suitable for further use.

Energy and environmental benefits of reducing water content in sludge include:

- Weight reduction of sludge by 3 to 4 times, reducing the impact of sludge transport.
- Potential for storing sludge before final disposal.
- Use of renewable energy (solar radiation).
- Low carbon footprint.
- Easy integration into the surrounding environment due to its greenhouse configuration.
- Effective odor control.
- Sludge sanitization and stabilization: the high temperature achieved through solar radiation ensures pathogen destruction and a significant reduction in moisture, preventing putrefaction.
- Dried sludge can have multiple uses, including being repurposed for quality compost production.
- Economic feasibility determined through a cost evaluation.

In conclusion, the results from this study demonstrate the effectiveness of the approach, system configuration, and operational methods employed. In 25-30 days, sludge moisture was reduced from 97 % to 4-5 %, resulting in a malleable and easily disposable product. Furthermore, the final weight reduction was 85-99 % compared to the initial weight, which is particularly significant when compared to conventional drying beds, where a final moisture content of no less than 55-60 % would be reached, and only after several months.

The high weight reduction, up to 99 %, achieved through solar drying leads to a reduction in sludge management costs. With moderate investment costs, low energy consumption thanks to solar energy, and low maintenance requirements, solar greenhouses represent a highly attractive technology for sludge drying in small-scale wastewater treatment plants. Through the economic evaluation, it was possible to assess the economic return on investment resulting from the construction of solar greenhouses. Based on the evaluation of the costs of solar greenhouse prototypes, referring to literature costs and performance achieved through experimental tests, it was possible to determine the investment costs of a full-scale greenhouse with a medium-small plant capacity. In particular, the net cash flow is due to a reduced amount of sludge to be disposed of in landfills compared to what would occur with conventional technologies. It has been demonstrated that, by the 6th year after the construction of the solar greenhouses, a positive cash flow can be achieved. Solar drying beds produce fewer greenhouse gas (GHG) emissions compared to the other traditional dewatering technologies. This can be attributed to two main factors: (1) indirect emissions from energy consumption are null, as the system relies on renewable energy sources, specifically through the use of photovoltaic and solar panels; and (2) emissions from transportation to landfills are minimized due to the reduced weight of the sludge, resulting from the lower moisture content achieved by this innovative drying method.

13 Bibliography

Adhikari, B., Howes, T., Bhandari, B. R., & Truong, V. (2001). Stickiness in foods: A review of mechanisms and test methods. *International Journal of Food Properties*, *4*(1), 1–33. https://doi.org/10.1081/JFP-100002186

Ali, I., Abdelkader, L., El Houssayne, B., Mohamed, K., & El Khadir, L. (2016). Solar convective drying in thin layers and modeling of municipal waste at three temperatures. *Applied Thermal Engineering*, *108*, 41–47. https://doi.org/10.1016/j.applthermaleng.2016.07.098

Ameri, B., Hanini, S., & Boumahdi, M. (2020). Influence of drying methods on the thermodynamic parameters, effective moisture diffusion and drying rate of wastewater sewage sludge. *Renewable Energy*, *147*, 1107–1119. https://doi.org/10.1016/j.renene.2019.09.072

An, X. (2017). Review on Sludge Drying Process and Dryer in Solar Energy. *American Journal of Energy Engineering*, *5*(5), 34. https://doi.org/10.11648/j.ajee.20170505.12

Badyda, K., & Krawczyk, P. (2008). *Research of heat and flow processes in a solar waste-water sludge dryer*. https://www.researchgate.net/publication/283795714

Bao, P., Du, C., Li, Y., Jiang, H., Zhou, L., Yu, G., Sun, S., Zhou, L., Li, X., Teng, J., Wang, X., & Wang, J. (2024). Application of skeleton builders to sludge dewatering and disposal: A critical review. In *Science of the Total Environment* (Vol. 906). Elsevier B.V. https://doi.org/10.1016/j.scitotenv.2023.167106

Bennamoun, L. (2012). Solar drying of wastewater sludge: A review. In *Renewable and Sustainable Energy Reviews* (Vol. 16, Issue 1, pp. 1061–1073). https://doi.org/10.1016/j.rser.2011.10.005

Boguniewicz-Zablocka, J., Klosok-Bazan, I., & Capodaglio, A. G. (2020). *Sustainable management of biological solids in small treatment plants: overview of strategies and reuse options for a solar drying facility in Poland*. https://doi.org/10.1007/s11356-020-10200-9/Published

Bunyawanichakul, P., Walker, G. J., Sargison, J. E., & Doe, P. E. (2007). Modelling and Simulation of Paddy Grain (Rice) Drying in a Simple Pneumatic Dryer. *Biosystems Engineering*, *96*(3), 335–344. https://doi.org/10.1016/j.biosystemseng.2006.11.004

Cai, L., Krafft, T., Chen, T. Bin, Gao, D., & Wang, L. (2016). Structure modification and extracellular polymeric substances conversion during sewage sludge biodrying process. *Bioresource Technology*, *216*, 414–421. https://doi.org/10.1016/j.biortech.2016.05.102

Canziani Roberto. (2016). I FANGHI, INEVITABILI PRODOTTI DELLA DEPURAZIONE DELLE ACQUE DI RIFIUTO. *Ingegneria Dell'ambiente*, *3*. http://ec.europa.eu/eurostat/statistics-explained/index.php/Water_statistics

Chang, H., Zhao, Y., Bisinella, V., Damgaard, A., & Christensen, T. H. (2023). Climate change impacts of conventional sewage sludge treatment and disposal. *Water Research*, *240*. https://doi.org/10.1016/j.watres.2023.120109

Cintoli, R., Tecnico, D., Barrella, C., & Tecnico, S. (2017). *Quadro di riferimento normativo*.

Collivignarelli, M. C., Abbà, A., Miino, M. C., & Torretta, V. (2019). What advanced treatments can be used to minimize the production of sewage sludge in WWTPs? In *Applied Sciences (Switzerland)* (Vol. 9, Issue 13). MDPI AG. https://doi.org/10.3390/app9132650

De Feo, G., De Gisi, Sabino., & Galasso, Maurizio. (2013). *Fanghi di depurazione : produzione, caratterizzazione e trattamento*. D. Flaccovio.

Defraeye, T. (2014). Advanced computational modelling for drying processes - A review. In *Applied Energy* (Vol. 131, pp. 323–344). Elsevier Ltd. https://doi.org/10.1016/j.apenergy.2014.06.027

Dellacqua Luisella, Z. M. (2020). *Caratterizzazione e valutazione sulla termovalorizzazione dei fanghi di depurazione*. Politecnico di Torino.

Deng, S., Wang, X., Tan, H., Mikulčić, H., Li, Z., Cao, R., Wang, Z., & Vujanović, M. (2015). Experimental and modeling study of the long cylindrical oily sludge drying process. *Applied Thermal Engineering*, *91*, 354–362. https://doi.org/10.1016/j.applthermaleng.2015.08.054

Dong, Y. J., Wang, Y. L., & Feng, J. (2011). Rheological and fractal characteristics of unconditioned and conditioned water treatment residuals. *Water Research*, *45*(13), 3871–3882. https://doi.org/10.1016/j.watres.2011.04.042

Enox SP. (2018). *Sludge Drying*.

Faragò, M., Damgaard, A., Madsen, J. A., Andersen, J. K., Thornberg, D., Andersen, M. H., & Rygaard, M. (2021). From wastewater treatment to water resource recovery: Environmental and economic impacts of full-scale implementation. *Water Research*, *204*. https://doi.org/10.1016/j.watres.2021.117554

Font, R., Gomez-Rico, M. F., & Fullana, A. (2011). Skin effect in the heat and mass transfer model for sewage sludge drying. *Separation and Purification Technology*, *77*(1), 146–161. https://doi.org/10.1016/j.seppur.2010.12.001

Gaspars-Wieloch, H. (2019). Project Net Present Value estimation under uncertainty. *Central European Journal of Operations Research*, *27*(1), 179–197. https://doi.org/10.1007/s10100-017-0500-0

Gomes, L. A. C. N., Gonçalves, R. F., Martins, M. F., & Sogari, C. N. (2023). Assessing the suitability of solar dryers applied to wastewater plants: A review. In *Journal of Environmental Management* (Vol. 326). Academic Press. https://doi.org/10.1016/j.jenvman.2022.116640

He, X., Wang, J., Guo, S., Zhang, J., Wei, B., Sun, J., & Shu, S. (2018). Ventilation optimization of solar greenhouse with removable back walls based on CFD. *Computers and Electronics in Agriculture*, *149*, 16–25. https://doi.org/10.1016/j.compag.2017.10.001

Huang, Y. W., Chen, M. Q., & Jia, L. (2016). Assessment on thermal behavior of municipal sewage sludge thin-layer during hot air forced convective drying. *Applied Thermal Engineering*, *96*, 209–216. https://doi.org/10.1016/j.applthermaleng.2015.11.090

ISPRA. (2023). *Rapporto Rifiuti Speciali*.

ISPRA. (2024). *Rapporto rifiuti speciali 2024*.

Iswa, B., Deak, B., Bernhard Matter, H., Alice Saabye, S., Ludivico Spinosa, D., Ådne Ø Utvik, I., Meozzi, P., & Manager, P. (1997). *Management Approaches and Experiences Sludge Treatment and Disposal*. www.eea.eu.int

Karakas, A., Tozum-Akgul, S., Komesli, O. T., & Kaplan-Bekaroglu, S. S. (2024). Carbon footprint analysis of advanced biological wastewater treatment plant. *Journal of Water Process Engineering*, *61*. https://doi.org/10.1016/j.jwpe.2024.105254

Kosse, P., Mikola, A., Lübken, M., Blomberg, K., Heinonen, M., Kuokkanen, A., Lange, R.-L., & Wichern, M. (2016). *Climate change and green-house gas emissions within the context of urban waste water management*. https://www.researchgate.net/publication/306119690

Kurt, M., Aksoy, A., & Sanin, F. D. (2015). Evaluation of solar sludge drying alternatives by costs and area requirements. *Water Research*, *82*, 47–57. https://doi.org/10.1016/j.watres.2015.04.043

Kusturin Mauro. (2007, September 24). *Fanghi di depurazione da letti di essiccamento: Quando sono rifiuti?* www.diritto dell'ambiente.com

Lei, Z., Dezhen, C., & Jinlong, X. (2009). Sewage sludge solar drying practise and characteristics study. *Asia-Pacific Power and Energy Engineering Conference, APPEEC*. https://doi.org/10.1109/APPEEC.2009.4918741

Ling, W., Xing, Y., Hong, C., Zhang, B., Hu, J., Zhao, C., Wang, Y., & Feng, L. (2022). Methods, mechanisms, models and tail gas emissions of convective drying in sludge: A review. In *Science of the Total Environment* (Vol. 845). Elsevier B.V. https://doi.org/10.1016/j.scitotenv.2022.157376

Mahmoud, A., Olivier, J., Vaxelaire, J., & Hoadley, A. F. A. (2011). Electro-dewatering of wastewater sludge: Influence of the operating conditions and their interactions effects. *Water Research*, *45*(9), 2795–2810. https://doi.org/10.1016/j.watres.2011.02.029

Marangoni Alessandro. (2021). La gestione sostenibile dei fanghi di depurazione - Serve una strategia nazionale. *SERVIZI A RETE*, 25–29.

Mortier, S. T. F. C., De Beer, T., Gernaey, K. V., Remon, J. P., Vervaet, C., & Nopens, I. (2011). Mechanistic modelling of fluidized bed drying processes of wet porous granules: A review. In *European Journal of Pharmaceutics and Biopharmaceutics* (Vol. 79, Issue 2, pp. 205–225). Elsevier B.V. https://doi.org/10.1016/j.ejpb.2011.05.013

Nayak, S., & Tiwari, G. N. (2008). Energy and exergy analysis of photovoltaic/thermal integrated with a solar greenhouse. *Energy and Buildings*, *40*(11), 2015–2021. https://doi.org/10.1016/j.enbuild.2008.05.007

Neri, A., Rizzuni, A., Garrone, P., & Cagno, E. (2024). Influence of policymakers and civil society stakeholders on sewage sludge management strategies: Empirical results from European utilities. *Journal of Environmental Management*, *364*. https://doi.org/10.1016/j.jenvman.2024.121396

Nivala, Jaime., Puigagut, Jaume., Von Sperling, Marcos., Dotro, Gabriela., Stein, Otto., Molle, Pascal., & Langergraber, Gپnter. (2017). *Treatment Wetlands*. IWA Publishing.

Nourhene Boudhrioua. (2004). *Etude des migrations de l'eau et du chlorire de sodium dans des gels alimentaires:influence de la composition du gel et du procede applique*. https://pastel.hal.science/pastel-00003704

Osvaldo Garanto. (2016). Solar Sludge Drying Technology and Dried Sludge as Renewable Energy—Closing the Loop. *Journal of Traffic and Transportation Engineering*, *4*(4). https://doi.org/10.17265/2328-2142/2016.04.005

Pan, Y., Li, P., Song, K., Liu, G., Li, L., Zhang, P., Gong, J., & Huang, Q. (2023). New model for evaluating greenhouse gas emissions from sludge treatment based on fossil and biogenic carbon migration. *Journal of Cleaner Production*, *425*. https://doi.org/10.1016/j.jclepro.2023.138845

Parravicini, V., Svardal, K., & Krampe, J. (2016). Greenhouse Gas Emissions from Wastewater Treatment Plants. *Energy Procedia*, *97*, 246–253. https://doi.org/10.1016/j.egypro.2016.10.067

Peeters, B., Dewil, R., Vernimmen, L., Van den Bogaert, B., & Smets, I. Y. (2013). Addition of polyaluminiumchloride (PACl) to waste activated sludge to mitigate the negative effects of its sticky phase in dewatering-drying operations. *Water Research*, *47*(11), 3600–3609. https://doi.org/10.1016/j.watres.2013.04.012

Piippo, S., Lauronen, M., & Postila, H. (2018). Greenhouse gas emissions from different sewage sludge treatment methods in north. *Journal of Cleaner Production*, *177*, 483–492. https://doi.org/10.1016/j.jclepro.2017.12.232

Ruiz, T., & Wisniewski, C. (2008). Correlation between dewatering and hydro-textural characteristics of sewage sludge during drying. *Separation and Purification Technology*, *61*(2), 204–210. https://doi.org/10.1016/j.seppur.2007.07.054

Sackey, L. N. A., Koomson, J., Kumi, R., Hayford, A. A., & Kayoung, P. (2023). Assessing the quality of sewage sludge: CASE study of the Kumasi wastewater treatment plant. *Heliyon*, *9*(9). https://doi.org/10.1016/j.heliyon.2023.e19550

Saveyn, H., Pauwels, G., Timmerman, R., & Van Der Meeren, P. (2005). Effect of polyelectrolyte conditioning on the enhanced dewatering of activated sludge by application of an electric field during the expression phase. *Water Research*, *39*(13), 3012–3020. https://doi.org/10.1016/j.watres.2005.05.002

Shahid, M. K., & Choi, Y. (2023). Comprehensive analysis of greenhouse gas emissions and emission factors in a Korean domestic wastewater treatment plant: Insights into mechanisms and pathways for climate change mitigation. *Journal of Water Process Engineering*, *56*. https://doi.org/10.1016/j.jwpe.2023.104476

Simone Visigalli, L. S. R. C. (2019, April). Tecnologie di disidratazione dei fanghi. *Ingegneria Dell'ambiente*, *6*, 241–268. https://doi.org/dx.doi.org/10.32024/ida.v6i4.235

Singh, P., Shrivastava, V., & Kumar, A. (2018). Recent developments in greenhouse solar drying: A review. In *Renewable and Sustainable Energy Reviews* (Vol. 82, pp. 3250–3262). Elsevier Ltd. https://doi.org/10.1016/j.rser.2017.10.020

Solarkup s.r.l. (2015). *Pannello SolarAir (Manuale Tecnico)*. WWW.SOLARKUP.COM

Sorrenti, A., Corsino, S. F., Traina, F., Viviani, G., & Torregrossa, M. (2022). Enhanced Sewage Sludge Drying with a Modified Solar Greenhouse. *Clean Technologies*, *4*(2), 407–419. https://doi.org/10.3390/cleantechnol4020025

Suez. (n.d.). *Natural sludge drying in green house*. Retrieved November 15, 2024, from https://www.suezwaterhandbook.com/content/download/5443/88563/version/5/file/Heliantis_P-B-015-EN-1604_v2.pdf

Vaxelaire, J., & Cézac, P. (2004). Moisture distribution in activated sludges: A review. In *Water Research* (Vol. 38, Issue 9, pp. 2215–2230). Elsevier Ltd. https://doi.org/10.1016/j.watres.2004.02.021

Viega Group. (2021). *World's largest solar-thermal sewage sludge drying system*.

Wu, B., Dai, X., & Chai, X. (2020). Critical review on dewatering of sewage sludge: Influential mechanism, conditioning technologies and implications to sludge re-utilizations. In *Water Research* (Vol. 180). Elsevier Ltd. https://doi.org/10.1016/j.watres.2020.115912

Wu, R. M., Lee, D. J., Wang, C. H., Chen, J. P., & Tan, R. B. H. (2001). RAPID COMMUNICATION NOVEL CAKE CHARACTERISTICS OF WASTE-ACTIVATED SLUDGE. In *Wat. Res* (Vol. 35, Issue 5).

Zhao, G., Yin, F., Liang, X., Yuan, D., Geng, W., Wang, L., & Sun, R. (2020). Drying Experiment and Drying Model Analysis of Dehydrated Sludge Particles. *IOP Conference Series: Materials Science and Engineering*, *768*(2). https://doi.org/10.1088/1757-899X/768/2/022031

Zheng, Q., Hu, Z., Li, P., Ni, L., Huang, G., Yao, Y., & Zhou, L. (2021a). Effects of air parameters on sewage sludge drying characteristics and regression analyses of drying model coefficients. *Applied Thermal Engineering*, *198*. https://doi.org/10.1016/j.applthermaleng.2021.117501

Zheng, Q., Hu, Z., Li, P., Ni, L., Huang, G., Yao, Y., & Zhou, L. (2021b). Effects of air parameters on sewage sludge drying characteristics and regression analyses of drying model coefficients. *Applied Thermal Engineering*, *198*. https://doi.org/10.1016/j.applthermaleng.2021.117501

Zhou, Y., & Jin, Y. (2016). Mathematical Modeling of Thin-layer Infrared Drying of Dewatered Municipal Sewage Sludge (DWMSS). *Procedia Environmental Sciences*, *31*, 758–766. https://doi.org/10.1016/j.proenv.2016.02.066

Zimmer, T., Rudi, A., Glöser-Chahoud, S., & Schultmann, F. (2022). Techno-Economic Analysis of Intermediate Pyrolysis with Solar Drying: A Chilean Case Study. *Energies*, *15*(6). https://doi.org/10.3390/en15062272

14 Webography

Feliciano, D. (1979). Wastewater Aerosols and Health Risks. Water Pollution Control Federation, 2573-2576. Wastewater Aerosols and Health Risks on JSTOR

Acquedotto Pugliese (2021). Linea Guida per la progettazione di sistemi d'abbattimento di emissioni odorigene negli impianti di depurazione. Microsoft Word - Linee Guida per la progettazione di Coperture per vasche negli Impianti di depurazione_2021.doc (aqp.it)

Sistema Nazionale per la Protezione Ambientale (SNPA). (2018). Metodologie per la valutazione delle emissioni odorigene - Documento di sintesi. Metodologie per la valutazione delle emissioni odorigene – SNPA – Sistema nazionale protezione ambiente (snpambiente.it)

Regione Puglia. (2018). Legge Regionale 16 luglio 2018 n. 32 - "Disciplina in materia di emissioni odorigene". Regione Puglia. (2018). Legge Regionale 16 luglio 2018 n. 32 - "Disciplina in materia di emissioni odorigene". - Cerca (bing.com)

Regione Lombardia. (2012). D.g.r. 15 febbraio 2012 - n. IX/3018_Determinazionei generali in merito alla caratterizzazione delle emissioni gassose in atmosfera derivanti da attività a forte impatto odorigeno. DGR+3018_2012.pdf (regione.lombardia.it)

How to Use Class A Biosolids Wastewater Digest https://www.wwdmag.com/sludge-and-biosolids/article/21062140/how-to-use-class-a-biosolids